Physics Reports 545 (2014) 125–195

Contents lists available at ScienceDirect

Physics Reports

journal homepage: www.elsevier.com/locate/physrep

Structure and dynamics of monohydroxy alcohols—Milestones towards their microscopic understanding, 100 years after Debye

Roland Böhmer [a], Catalin Gainaru [a], Ranko Richert [b]

[a] Fakultät Physik, Technische Universität Dortmund, 44221 Dortmund, Germany

[b] Department of Chemistry and Biochemistry, Arizona State University, Tempe, AZ 85287-1604, USA

ARTICLE INFO

Article history:
Accepted 31 July 2014
Available online 19 August 2014
editor: I. Procaccia

Keywords:
Monohydroxy alcohols
Structure and dynamics
Review

ABSTRACT

In 1913 Debye devised a relaxation model for application to the dielectric properties of water and alcohols. These hydrogen-bonded liquids continue to be studied extensively because they are vital for biophysical processes, of fundamental importance as solvents in industrial processes, and in every-day use. Nevertheless, the way to a microscopic understanding of their properties has been beset with apparently conflicting observations and conceptual difficulties. Much of this remains true for water, but fortunately the situation for monohydroxy alcohols is different. Here, with the experimental progress witnessed in recent years and with the growing recognition of the importance of specific supramolecular structures, a coherent microscopic understanding of the structure and dynamics of these hydrogen-bonded liquids is within reach.

Contents

http://dx.doi.org/10.1016/j.physrep.2014.07.005
0370-1573/

1. Scope

Hydrogen bonds with their ability to break and reform even under ambient conditions play an eminent role for countless physical, chemical, and biological processes. The consequent formation of supramolecular structures in, e.g., water, monohydroxy alcohols, and proteins as well as its impact on the dynamics of these substances are the subjects of scientific debate since long. In this review the focus is on monohydroxy alcohols whose properties are not as anomalous as those of water and yet not as complex as those of typical bio-macromolecules. Nevertheless, it may be hoped that microscopic insights into the physical mechanisms governing the macroscopic behavior of monohydroxy alcohols will facilitate to understand the behavior of other hydrogen bonded liquids as well.

A view on earlier studies of monohydroxy alcohols, see Section 2, demonstrates the lack of consensus on how their structure and in particular their dynamics are to be understood from a microscopic standpoint. One of the most prominent dynamic features that distinguishes monohydroxy alcohols (and water) from most other, even hydrogen bonded fluids is an enormously strong electrical absorption that appears in addition to the structural relaxation characterizing any liquid. For decades it was assumed that this additional feature, commonly referred to as Debye (-like) relaxation, is experimentally detectable only by dielectric spectroscopy and other techniques that are explicitly sensitive to charge fluctuations. With only a single experimental method considered useful to unravel the nature of a puzzling and seemingly exceptional phenomenon, in the past many scientific questions regarding monohydroxy alcohols had to remain without a commonly accepted resolution. However, in view of a number of recent experimental as well as computational advances, and taking into account some largely overlooked approaches, we are at the verge of seeing a change of this situation.

It seems that never before an attempt was made to provide a broad survey on the field of monohydroxy alcohol liquids. However, Böttcher's book from the 1970s gives a fairly extensive account of the dielectric work performed on these interesting substances up to that time [1]. The present review aims at summarizing the results from a wide range of theoretical and experimental techniques that have contributed to the current understanding of the structure and dynamics of (pure) monohydroxy alcohols. Next, in Section 2, we recapitulate some of the ups and downs encountered in the century long effort to rationalize the behavior of monohydroxy alcohols on a molecular basis. Section 3 then summarizes various approaches directed at resolving the supramolecular structure of monohydroxy alcohols. This section includes work from classical diffraction and inelastic X-ray techniques and it also gives a brief survey on some of the molecular dynamics and Monte Carlo simulations that have significantly contributed in this respect. Then, a number of macroscopic features of monohydroxy alcohol behavior is reviewed, e.g., with a focus on their thermodynamic (Section 4), dielectric (Section 5), molecular transport, and viscoelastic (Section 7) properties. Also optical techniques were particularly successfully exploited to unravel details related to, e.g., local bonding and molecular reorientation of monohydroxy alcohols (see Sections 6 and 9). The supramolecular behavior of monohydroxy alcohols is intimately connected to the structure at and the dynamics of the association mediating hydroxyl group. Therefore, techniques such as nuclear magnetic resonance (Section 8), vibrational spectroscopy (Section 9), as well as X-ray absorption and emission (Section 3.2) that allow one to probe this function selectively is also given particular attention.

It will become obvious that neat monohydroxy alcohols with their enormous molecular variability regarding length and branching of the alkyl chain, position of the structure inducing hydroxyl group, etc., represent a fertile testing ground for ideas directed at understanding their physical properties and of hydrogen bonded liquids in general. Mixing monohydroxy alcohols with other substances, while often highly relevant in technological applications and sometimes useful for suppressing the crystallization tendency of neat supercooled monohydroxy alcohols, typically introduces another level of complexity without necessarily helping to understand the pure substances better. Therefore, and in order to keep the present review focused, we will not explicitly deal with monohydroxy alcohol containing mixtures, unless data suitable to illustrate results of specific experimental techniques are not available for neat monohydroxy alcohols. Furthermore, many pure monohydroxy alcohols can already be supercooled with ease below their melting point and thus allow one to study their dynamics over particularly broad spectral ranges, a circumstance that often facilitates to unravel details of their behavior.

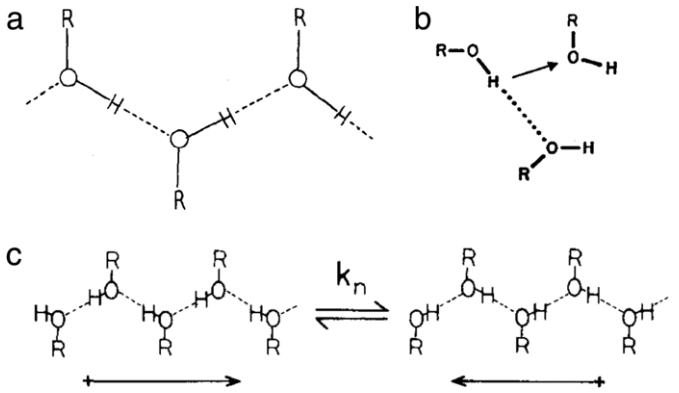

Fig. 1. (a) Polymer-like hydrogen bonding pattern of monohydroxy alcohol molecules as considered by Oster and Kirkwood. Reprinted with permission from Ref. [15]. Copyright 1943, AIP Publishing LLC. (b) The "switch" of a hydrogen bond between two monohydroxy alcohol molecules according to Sagal. Reprinted with permission from Ref. [16]. Copyright 1962, AIP Publishing LLC. (c) The "dipole inversion" mechanism was proposed by Minami et al. to explain process I in monohydroxy alcohols. In all cases R denotes the molecular alkyl rest.
Source: Reprinted with permission from Ref. [17].

Finally, in Section 10 we will briefly address the question whether or not the Debye-like process that appears in several other (hydrogen-bonded) liquids – including water and secondary amides as well as certain supramolecular polymers and amorphous pharmaceuticals – should be viewed in full analogy to that in monohydroxy alcohols.

2. Early models, measurements, and … misconceptions

The following is a brief collection of ideas that have guided (in some cases misguided) research on monohydroxy alcohols. It should be clear that we can focus attention here on only a small fraction of the work done in this area. The present Section 2 is not meant to provide a exhaustive historical survey but it tries to sketch what, in the author's subjective view, has been particularly remarkable for the development of the subject covered in the current article.

Most monohydroxy alcohols are strongly polar and excellent candidates for dielectric investigations. Therefore, after some early dielectric work on monohydroxy alcohols in the late 19th century [2], already in the mid-1920s their frequency dependent dispersion was studied more thoroughly using this technique [3–8]. In 1929 Peter Debye included the dielectric response of several monohydroxy alcohols in his famous book *Polar Molecules* [9] to test the theoretical description of polarization phenomena that he had developed in 1913 [10]. The Debye model considers liquids as an elastic continuum in which the dispersed molecules, for simplicity regarded as spheres, perform unrestricted isotropic Brownian reorientation all with the same time constant [10]. The Debye model, aiming at describing the structural relaxation in liquids, provided a good description of the main dielectric absorption, as demonstrated in 1929 for 1-propanol [9]. A few years later Girard found significantly larger dielectric constants of various primary alcohols than for their tertiary isomers and concluded that "one is forced to accept the existence of … association-complexes, especially in view of the fact that the numerical values of the elementary moments are the same" [11].

Peculiar structural correlations in monohydroxy alcohols were indeed then already known from Steward and Morrow's 1927 X-ray scattering experiments [12]. They identified two microscopic length scales in these liquids, one corresponding to the distance between adjacent molecules and the other associated with the separation between "planes containing the polar groups". From an analysis of the radial distribution function of several monohydroxy alcohols [13,14], it was soon thereafter concluded that the polar hydroxyl groups aggregate in linear structures in which "every hydroxyl group is linked to the hydroxyl groups of two neighboring molecules" [13]. Taking this insight one step further, Oster and Kirkwood realized that a strong orientational correlation among neighboring polar groups might explain the anomalously large dielectric constants of monohydroxy alcohols [15]. Using a model of freely rotating (infinitely long) chains of monohydroxy alcohol molecules these authors calculated the dielectric relaxation strength of these liquids. The polymer-like association which they assumed for the monohydroxy alcohols is sketched in Fig. 1(a). Since the estimated dielectric strength by Oster and Kirkwood was smaller than experimentally observed, they suggested that in monohydroxy alcohols "a residual correlation in the orientations of molecules in different chains" may exist [15].

In 1951, Davidson and Cole [18] noted that while the Debye model is able to describe the frequency dependent dielectric loss for monohydroxy alcohols it fails for poly-alcohols thereby confirming earlier observations [19]. Concerning the peculiar shape of the dielectric spectrum of propanol Davidson and Cole stated that "the existence of a single relaxation process for the low frequency dispersion in *n*-propanol implies that a single unit rather than a linear polymer with a variety of modes of reorientation is involved" [18]. In the same work Davidson and Cole estimated the hydrodynamic volumes for propanol,

propylene glycol, and glycerol. With the geometrical radii of the three molecules not differing much, propanol's hydrodynamic volume turned out to be more than 1000(!) times larger than for the poly-alcohols. This finding was in agreement with previous observations by Girard and Abadie who reported that "a value different from the real value to the radius of the molecule" is required to achieve agreement of the calculations using Debye's model with experimental results [20].

In the early 1970s it became clear that while the earliest experiments on monohydroxy alcohols seemed to substantiate Debye's relaxation model, in view of the general observation of an exponential polarization response in monohydroxy alcohols, this agreement was "fortuitous" [21]. Dannhauser and Flueckinger judged that the Debye model might not really be applicable for monohydroxy alcohols because "either unrealistic molecular radii or an empirical microviscosity had to be invoked to achieve agreement" [21]. Section 7.1 provides current views on 'microviscosity'.

In the footsteps of Girard [11] and in harmony with other observations [11,22], in the mid-1960s Dannhauser and Johari [23–28] and later Vij et al. [29,30] emphasized that the overall dielectric strength of monohydroxy alcohols depends strongly on the molecular branching and the positioning of the hydroxyl group. Dannhauser [23] distinguished two types of monohydroxy alcohol liquids: The first type of substances, with the OH group in a terminal position which favors large dielectric constants and that are thought to arise from chain-like molecular association. And the second type, for which the polar unit is located in a non-terminal, sterically screened molecular site. This situation can give rise to the formation ring-like structures with very small effective dipole moments.

Obviously, in a study on octanol, Girard and Abadie were the first to identify that in addition to the dominant dielectric dispersion a weak high-frequency shoulder shows up in monohydroxy alcohols [20]. Later, these two relaxations were baptized process I and process II [31], respectively, a terminology that will be frequently used in the following. Based on Perrin's extension [32] of the Debye model, the appearance of the two distinct relaxations was initially related to the ellipsoidal shape of the octanol molecule [20]. But Smyth pointed out that if this assumption were to hold then the strengths of the two dispersions should be comparable, at variance with experimental evidence [33].

In liquids the main dielectric absorption corresponds almost ubiquitously to the structural relaxation. The first indication that in monohydroxy alcohols the process I, the "Debye loss" as Magat has put it [34], might have a different microscopic origin was provided by Kauzmann in 1948 [35]. When comparing the calorimetric glass transition temperatures with the temperatures at which the polarization fluctuations of various supercooled liquids fall out of equilibrium he noted that "in all examples except possibly 1-propanol a reasonable extrapolation yields dielectric relaxation times of the order of a few minutes to an hour at the glass-transformation point". Later, it was suggested that process I and II are *both* involved in the structural relaxation [36]. But a direct comparison of dielectric with modulated heat capacity measurements indicated that the large dielectric Debye-like process "is not associated with calorimetric modes" [37] within the given experimental resolution.

Probably starting with the 1956 ultrasonic work of Litovitz [38,39] it was believed that (shear) mechanical and many other experimental techniques are unable to probe process I. That this process may not be governed by microscopic flow events was still essentially confirmed in 2008 [40], a contention that in view of recent experimental evidence may need revision [41,42]. Nuclear magnetic resonance (NMR) is another method that seemingly had little to say about process I. From the 1970s on NMR relaxometry was used to study the dynamics in monohydroxy alcohols [43,44], mostly focusing on aspects related to intramolecular flexibility, see the references in Section 8.2, while efforts to relate the time scales from NMR with those from dielectric spectroscopy were undertaken only much later [45,46]. Finally, for propanol the time constants measured via light scattering techniques were compared with those from dielectric spectroscopy [47]. But it was found that, "in contrast to typical α-processes", process I "possesses no counterpart signals in the quantities directly related to structural relaxation like viscosity and density fluctuations" and that process II is nothing else but the structural relaxation [47]. To "explain why the prominent dielectric peak possesses no mechanical or calorimetric counterpart" it was proposed that "proton conductivity within reverse micelles could also be made responsible for the dielectric 'amplification' or 'enhancement' based on the Maxwell–Wagner–Sillars theory of heterogeneous dielectrics" [48]. Here, reference was made to the earlier work of Floriano and Angell who pictured the clustering in monohydroxy alcohols as "an embryonic inverse micelle in the case of the n-alkyl alcohols" [49].

With the few electro-optical Kerr effect studies on monohydroxy alcohols largely overlooked [50,51] and the solvation technique applied to monohydroxy alcohols relatively recently [52], see also Section 6, the foregoing remarks show how the belief could be fueled for a long time that the techniques probing charge fluctuations, notably of course dielectric spectroscopy, are the only ones sensitive to process I. However, dielectric spectroscopy alone is usually not particularly well suited to provide detailed insights into the microscopic nature underlying the observed processes. With essentially just a single experimental method imposing constraints and telling us how we should think about the origins of the dynamical behavior of monohydroxy alcohols, it is no surprise that scientists have come up with a host of different, often mutually excluding molecular assignments of processes I and II. A few examples are given in the following.

In 1953, Hassion and Cole proposed that "the higher-frequency dispersion results from orientations of OR moments consistent with fixed intermolecular chain-bonding of the OH groups, and the lower from orientations of the OH groups as their bonding changes" [53]. At the same time the idea was advanced that process II is caused by rotation of free or single-bonded molecules [54]. Two years later an increase in the amplitude of process II upon cooling was reported for several monohydroxy alcohols, inconsistent with the "proposal that the second dispersion arises from reorientation of unbonded molecules, the number of which for any reasonable bond energy would decrease rapidly at the lower temperatures" [55]. Also in 1955, Dannhauser and Cole [22] modified the model of Oster and Kirkwood [15] by assuming that monohydroxy

alcohols are characterized by a temperature dependent distribution of chain lengths. But it was found difficult to rationalize the single exponential relaxation underlying process I given that "it would be expected that a wide range of complexes would occur, leading to a continuous distribution of relaxation times instead of one or two discrete ones" [56].

In 1962, Sagal discusses a possible mechanism for process I in which a hydrogen bond between two monohydroxy alcohol molecules breaks when another one approaches with its oxygen oriented favorably for a "switch", see Fig. 1(b) [16]. In a revived variant of this so-called wait-and-switch model the dielectric relaxation time of process I is conceived to be governed by a change in the orientation of the OH vector (see Fig. 4 of [57]), in other words it "is mainly determined by the period for which a dipolar molecule or group has to wait until favorable conditions for the reorientation exist" [57]. As an alternative, Minami et al. [17] proposed that process I stems from a dipolar inversion mechanism in which "each monomer can perform successive rotation of the OH group around the OC axis" and "after all the OH-groups changes their direction, then the overall dipole moment of the multimer changes its direction", see Fig. 1(c). A concerted motion was obviously not on the mind of Fragiadakis et al. who described the dynamics underlying process I as "being internal to the cluster, and thus not involving cooperative rearrangement of many molecules" with the internal motion suggested to be "the rotation of a molecule around its chain cluster axis, which would still change substantially the total dipole of the cluster" [58].

Yet another model based on fluctuations of the end-to-end vector of associated multimers is due to Levin and Feldman who proposed "that the rotation of molecules in the chain produces a change in the distance between its ends and hence in its dipole moment" and that their model "would be senseless if τ_H appeared smaller than τ" [59]. In their work τ_H and τ denote the hydrogen bond lifetime and the time constant of process I, respectively. Much earlier, Brot and Magat also suggested that "it is the breaking of an H bond that makes possible the orientation of the liberated dipoles", and consequently the characteristic time of process I should correspond to the lifetime of a hydrogen bond [60]. Accordingly, this process "does not present any distribution of relaxation times because the lifetime of the H bonds is roughly independent of the size of the polymer" [60]. In 1969 Bordewijk et al. mentioned with respect to process I that "the theory … which … states that breaking of the hydrogen bond is the rate determining step, must be rejected" since "the dielectric properties of the mixtures can (also)… be described by means of a single principal relaxation range" [61]. However, in 2000 Kalinovskaya and Vij argue that "the mechanism of process I is the breaking followed by dipolar reorientation and reforming of the H-bonds in the intermolecularly H-bonded structure, and process II is that of the orientation of the other dipolar groups, such as the —OR group" [62]. While their second statement was confirmed by NMR [63], regarding their first statement near infrared temperature-jump experiments on a monohydroxy alcohol indicated that close to the glass transition the effective hydrogen bond lifetime is similar to the time scale of process II and thus much shorter than the time scale of process I [64]. An intermediate time scale, between those of process I and II, was identified from the hydroxyl group dynamics as detected by NMR [65]. This time scale was attributed to the time a particular monohydroxy alcohol molecule is part of a transient hydrogen-bonded chain.

In view of cooperative effects in hydrogen bonding [66], which means that hydrogen bonds become stronger upon addition of molecules to an existing hydrogen bonded cluster, Gainaru et al. proposed a "transient chain model" [67]. In this approach the fluctuations of the end-to-end dipole moment correspond to a "snakelike motion induced by a successive loss (or gain) of segments at its one end and a gain (or loss) of segments at its other end" [65]. An analytical model in the spirit of the transient chain model was formulated recently [68], and molecular dynamics simulation provide a framework to refine some of the main ideas of this approach [69]. Based upon high-field dielectric measurements Singh and Richert [70] stated that a "rearrangement of the chain structure is observed to occur on the time scale of the Debye process, suggesting that the Debye peak of monohydroxy alcohols originates from a fluctuation of the net dipole moment … on a time scale that is largely controlled by viscosity". Their vision of the relevant fluctuations in monohydroxy alcohols is "similar to the model of sequential reorientations of molecules in chains developed by Levin and Feldman", however, "these chain structure changes may in part be promoted by chain scission and recombination of chain fragments" [70].

This collection of results demonstrates not only the recent upsurge of research activities in this field, but it also has made it possible to rule out some of the models and to confirm others so that the views of many scientists finally seem to convergence.

3. Structure determination

Scattering and simulation techniques are classical workhorses for the elucidation of structural characteristics of liquids and solids at the microscopic level. While the present article is mostly concerned with the properties of neat monohydroxy alcohol liquids, it is instructive to recall some structural features of *crystalline* monohydroxy alcohol solids that were extensively examined using X-ray and neutron diffraction techniques [71–77]. Quite generally, primary monohydroxy alcohols display a strong preference to form infinite hydrogen bonded chains, while in secondary monohydroxy alcohols chains as well as rings can form, and in tertiary monohydroxy alcohols even isolated OH···O bonds were reported if hydrogen bonds form at all [71]. For monohydroxy alcohols crystal formation including nucleation [78] and crystal growth attracted recent attention [79]. Also the discussion of polymorphism has been a major issue, e.g., for ethanol which apart from a glassy and an ordered crystalline state exhibits an orientationally disordered crystal phase. The relaxation dynamics in the latter phase is quite similar to that of *liquid* ethanol [80]. Polymorphism was also discussed for 1-butanol which was believed to form a second frozen liquid phase, the so called glacial state [81].

Let us now focus attention on liquid monohydroxy alcohols. First, in Section 3.1 a brief review of literature concerning the theoretical treatment of the structure of monohydroxy alcohols is given. It includes selected results mainly from molecular dynamics (MD) and Monte Carlo simulations. *Ab initio* techniques directed at modeling structural properties are mentioned in Section 3.1. But so far *ab initio* work has found more widespread application in studies of spectroscopic quantities. Therefore, results from quantum chemical calculations and computer simulations will also be discussed in subsequent chapters, e.g., on magnetic resonance (Section 8.1) or vibrational spectroscopy (Section 9.1).

After dealing with some theoretical aspects of structure determination in Section 3.1 experimental work is considered. Section 2 summarizes some of the progress that elastic neutron and elastic X-ray diffraction have made possible to elucidate the structural properties of monohydroxy alcohols. Recently, as we will review in Section 0, also *inelastic* scattering techniques, mostly using X-rays, has yielded a wealth of information regarding the hydrogen bonding and the supramolecular organization of monohydroxy alcohols. Results from inelastic X-ray and neutron scattering directed at studying diffusional properties (see Section 7.3) or vibrational properties (see Section 9.4) of monohydroxy alcohols are not dealt with in Chapter 3.

3.1. Computer simulations

Most of the MD work on monohydroxy alcohols was carried out using *classical* simulations. In particular, this requires to treat hydrogen bonding using phenomenological concepts. One should be aware, however, that the problems encountered here are only one facet of how to define hydrogen bonding with its fascinating complexities in general and to distinguish it from other types of bonding [82]. In classical computer simulations the covalent aspects of hydrogen bonding are neglected and replaced by empirical constraints that are considered useful to provide an approximate description [83]. Without going into detail regarding the role played by hybridization effects and oxygen's lone pairs in the formation of hydrogen bonds, let us just note that the use of geometrical constraints is most popular [84], e.g., one may assume that a hydrogen bond is formed when the O–H…O angle is within $\sim 35^\circ$ of being linear and the length of the O-to-O bonds does not exceed ~ 0.35 nm. The choice of the given numbers is to some extent arbitrary and differences in cluster sizes, topologies, etc. that have been reported from different MD simulations may in some cases simply result from different hydrogen bond definitions. As an alternative it was suggested to apply topological constraints [83] or constraints regarding the interaction energy of the potential hydrogen bonding partners [85]. However, a general consensus regarding an optimal criterion for judging when a hydrogen bond is to be considered closed does obviously not exist so far.

A number of empirical potentials were devised at different levels of coarse graining in order to be able to simulate large systems efficiently. Many MD investigations on monohydroxy alcohols were carried out using Jorgensen et al.'s OPLS (optimized potential for liquid simulations) force fields [86] in their all-atom or united-atom (UA) variants [87–97]. To model structural data TraPPE—UA (transferable potential for phase equilibria — united atom) and other force fields were used, mostly in conjunction with Monte Carlo simulations [98–103].

In an effort to overcome problems faced when trying to describe hydrogen bonding in monohydroxy alcohols properly *ab initio* approaches appear to be better suited. However, due to extensive computational demands only very small molecules are currently tractable with the inclusion of intramolecular flexibility presenting another complicating factor. Therefore, hybrid approaches are increasingly used in which quantum chemical strategies are combined with MD techniques [104–106].

Let us now briefly discuss the prototypic topologies and the typical sizes of the supramolecular clusters in monohydroxy alcohols that were identified from computer simulations. The basic association motifs are chain-like and ring-like structures, as depicted in Fig. 2(a) and (b), respectively [95]. A more visually appealing impression of chain-like clustering can be gained from Fig. 2(c) which represents a snapshot from MD simulations of 1-octanol [95]. Branching of hydrogen bonds, which can lead to lasso-like supramolecular patterns, is usually not considered to be particularly important. For linear alcohols larger than ethanol, MD simulations suggested that the fraction of three-coordinated molecules is $<5\%$ [94]. Furthermore, from an MD study of the radial distribution function, $g_{OO}(r)$, on 54 linear and branched alcohols the mean coordination number $Z_{OO} = 4\pi\rho \int g_{OO}(r) r^2 dr$ was calculated by integration over the first oxygen's coordination shell [96]. Here ρ is the liquid's molecular number density. All Z_{OO} values reported in [96] are slightly smaller than 2, indicating that the fraction of free, non-bonded molecules is small (if not compensated by the occurrence of branched bonds), but still leaving open the question whether linear or cyclic structures prevail.

It is generally found that the majority of molecules form chain-like aggregates and for liquid methanol it was suggested that adjacent chains even display a tendency for parallel arrangement [87]. But the percentage of molecules that are identified to occur in cyclic structures varies widely [98]. The reported fractions of ring-like aggregates range from some 10% (from 12% for ethanol to 27% for hexanol [100] or even larger [107,108]) to values less than 4% (from 0.3% for methanol to 3.6% for octanol [93]). Clearly, these numbers do not only depend on the size and branching of the monohydroxy alcohol's alkyl chain but also on modeling details and the hydrogen bond criteria used to analyze the simulations. Similarly, the length of the linear aggregates as estimated from different simulations also vary. Early MD simulations reported that typical hydrogen bonded chains comprise of the order of 10 molecules [84,87].

More recent studies often present histograms for the cluster size distributions of monohydroxy alcohols [94,98,100,101]. For different alkyl chain lengths and across different simulations by and large rather similar results for these distributions are obtained. An example for methanol and propanol for two different weightings is shown in Fig. 3. This plot gives the

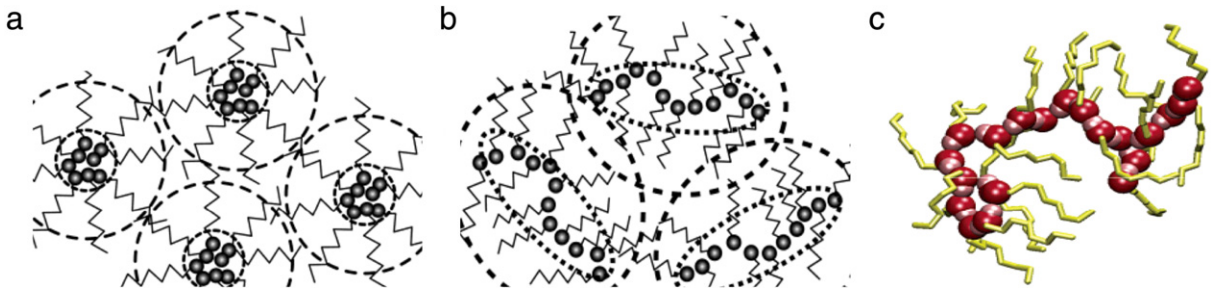

Fig. 2. Schematic representation of (a) ring-like and (b) chain-like association in models of monohydroxy alcohols. As highlighted by the dotted lines, the polar cores display (a) a more spherical or (b) a more prolate shape. The dashed lines indicate that the degree of interdigitation of the carbon chains is more pronounced when linear chains form. (c) Snapshots of a simulated hydrogen-bonded cluster of 1-octanol. The carbon chains are represented as yellow lines, the hydroxyl groups are colored in red. (For interpretation of the references to color in this figure legend, the reader is referred to the web version of this article.)
Source: Adapted with permission from Ref. [95].

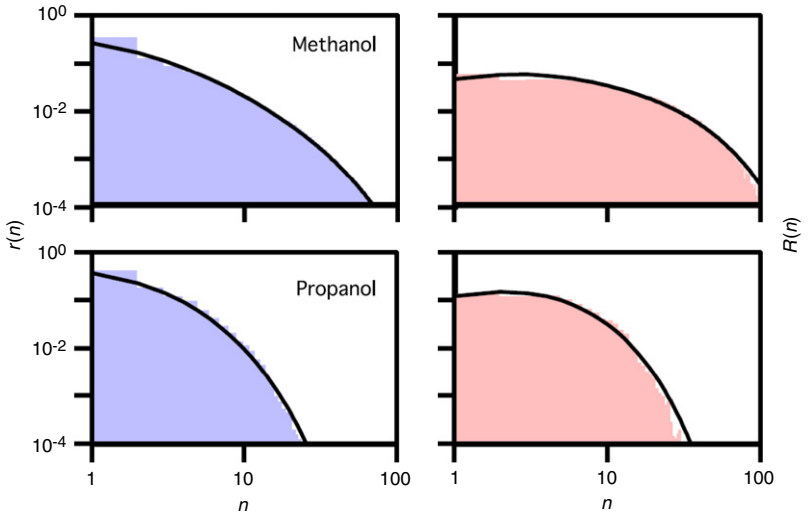

Fig. 3. The cluster size distributions $r(n)$, reflecting the probability that a randomly chosen cluster comprises n molecules, and $R(n)$, reflecting the probability that a randomly chosen molecule is part of a cluster formed by n monomers, are shown on the left and on the right, respectively.
Source: Adapted with permission from Ref. [101].

probability (i) that a randomly chosen cluster is formed by n molecules (on the left) or (ii) that a randomly chosen molecule is a member of a cluster formed by n monomers (on the right). One recognizes that both these distributions are very broad.

3.2. Static structure factors and prepeaks from diffraction experiments

There is a large number of X-ray diffraction studies dealing with monohydroxy alcohols, see, e.g., [12,14,100,109–116]. Of course, also neutron diffraction was extensively applied to study structural details of methanol [117–123], ethanol [93,124,125], propanol [126–130], and butanol [131–135]. Naturally, the prime goal of these studies on monohydroxy alcohols was to unravel the most likely intramolecular conformations, the intermolecular arrangements, coordination numbers, etc. Generally, the intermolecular O · · · O distances were found in the 2.7…2.8 Å range and an average number of up to two hydrogen bonds per molecule was reported, see, e.g., the compilations in [96,136].

Fig. 4 presents typical total scattering structure factors, $S(Q)$, for methanol, ethanol, and propanol covering a relatively large range of momentum transfers, Q. The experimental results are (a) from neutron or (b) from X-ray diffraction, see [151] and the references cited therein. At first glance, the neutron and X-ray data look very similar, despite the fact that fully deuterated alcohols were used in this neutron work while fully protonated species were employed for the barely proton-sensitive X-ray scattering.

In order to unravel structural details neutron diffraction has the major advantage that the (coherent as well as incoherent) scattering lengths of protons and deuteron are rather different. Therefore, in principle, all partial structure factors, $S_{XY}(Q)$, relating to two kinds of atoms X and Y, e.g., $S_{OH}(Q)$ and $S_{OO}(Q)$, and the associated partial radial distribution functions

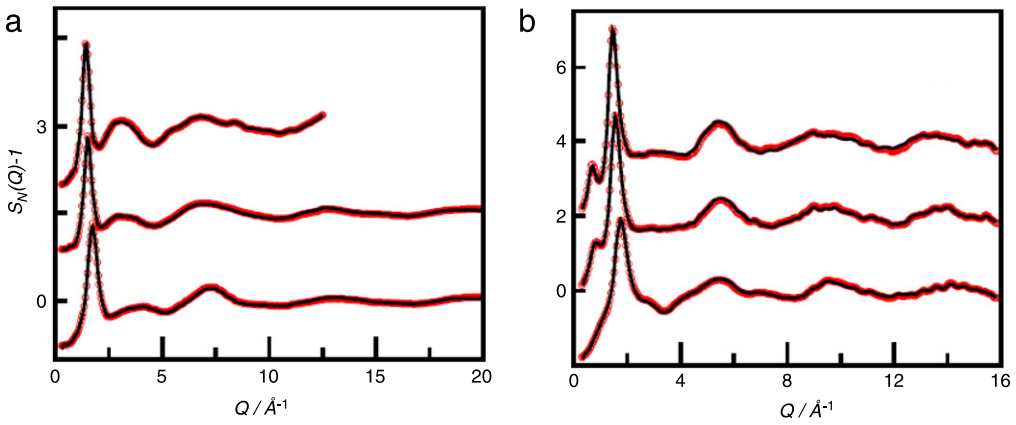

Fig. 4. Total scattering structure factor $S(Q)$ (a) from neutron diffraction and (b) from X-ray diffraction. Data are shown as circles for methanol (bottom curves), ethanol (middle curves), and propanol (top curves). The lines represent modeling via reverse Monte Carlo calculations. Some data are shifted vertically for visual clarity.
Source: Reproduced by permission of IOP Publishing from [151].

can be accessed experimentally. This approach was indeed applied to study up to 7 methanol isotopomers or isotopic mixtures, some of the latter chosen such that [137] they exhibit zero coherent scattering length with respect to specific atomic sites [118]. In a study dealing with liquid ethanol even up to 10 partial structure factors were measured [119]. On the one hand, it may be argued that not all of these partials may be needed to address a given question regarding the microscopic structure of monohydroxy alcohols. On the other hand, the isotope substitution approach has practical as well as fundamental limitations. On the practical side, 10 partial structure factors are required for a complete description of methanol, 21 for ethanol, and already 36 for propanol. This may rationalize why neutron diffraction was barely applied in studies of monohydroxy alcohols featuring more than four carbon atoms.

On the fundamental side, bond lengths, librational motions, and the hydrogen-bonded chain structure of monohydroxy alcohols (cf. Fig. 2) were found to change slightly upon H/D substitution [121]. For instance, for methanol the bond lengths were probed using X-ray [121,122] as well as using neutron scattering [138] and it turned out that the intramolecular C–O and O–H bonds shorten upon deuteration. For intramolecular distances the changes were found smaller (2%…5%) than at the intermolecular level (5%…8%) and effects up to 20% were reported to occur at ∼200 K [121]. It was suggested to represent some of these quantum effects by (phenomenological) temperature shifts. In view of the diminishing importance of isotope effects seen in the transport coefficients of alcohols with longer alkyl chains (see Section 7.3), one may expect that also the impact of these quantum effects on structure decreases when going from methanol to ethanol to propanol etc. In a *neutron* study on ethanol it was stated that "the magnitude of the quantum effects are assumed to be below the limit of the experimental error of the technique" [119].

Returning to Fig. 4 one recognizes that overall the interference patterns, in particular the main peak position near momentum transfers of $Q \approx 1.5 \ldots 2.0$ Å, depend somewhat on the alkyl chain length. But the most obvious difference concerns the so called prepeak appearing in some of the $S(Q)$ data at $Q < 1$ Å. It is clearly resolved in the X-ray profiles except for methanol, barely visible in the neutron data of Fig. 4, but present in other data sets [130]. The prepeak stems from suprastructure formation via the hydroxyl group. This was directly demonstrated by substituting the OH group in 2-propanol [127] for a halogen atom: In chloro- and bromo-propane a prepeak could not be discerned [139].

From detailed analyses, mainly based on comparisons of experiments with various kinds of simulations, see Section 3.1, it is clear that the intensity at the prepeak is mainly due to intermolecular O–O correlations. It was clearly stated that the prepeak "is bigger in the X-ray than in the neutron curves as the oxygen has a large electronic density around it and furthermore the local structure arises from oxygen atoms and their hydrogen bonds" [140]. Fig. 5(a) reproduces experimental data of 1-butanol along with simulations which demonstrate that the prepeak is mostly sensitive to the O–O correlations and that the main peak is dominated by C–C contributions, i.e., by the correlations between the hydrocarbon tails [100]. However, it was pointed out that even if a prepeak is absent (as, e.g., for tertiary butanol in nanoscopic confinement) O–O correlations may still exist [135].

An "inner" peak in the structure factor of liquids was probably first observed for monohydroxy alcohols [109], but its detection is by no means restricted to this class of substances. In the context of inorganic glass formers a prepeak is often called 'first sharp diffraction peak' [141] and has been taken to signify the existence of medium range order. Prepeaks were detected for numerous hydrogen bonded liquids [142–145] including water [146] and even for a van der Waals glass former [147]. Moreover, prepeaks were observed in polymers tending to display a phase separation (e.g., of a polar backbone from nonpolar side groups) on the local scale [148,149]. For monohydroxy alcohols, one may rather conceive a reverse organization of hydrogen bonded clusters featuring a hydrophilic (hydroxyl rich) core and a hydrophobic (alkyl rich)

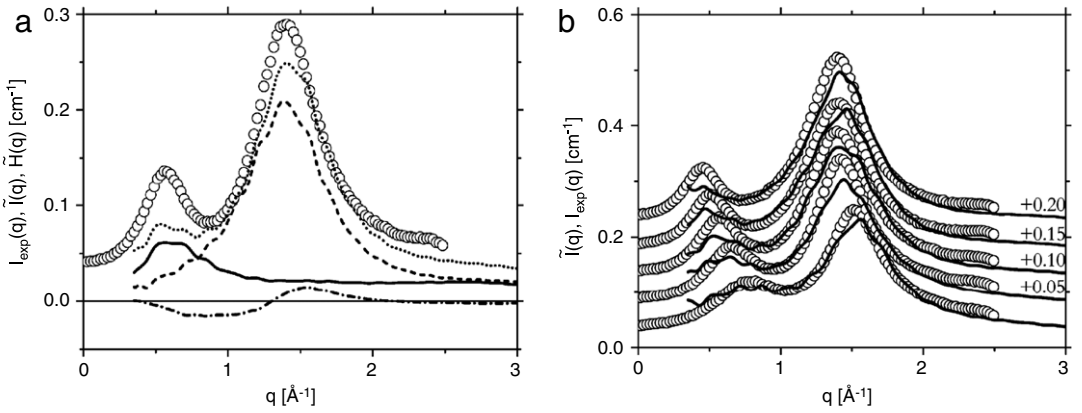

Fig. 5. (a) Experimental scattering intensity $I_{exp}(q)$ of 1-butanol (circles) compared with calculated contributions: $I_{CHx}(q)$ (alkyl–alkyl correlations, short dashed line), $I_o(q)$ (hydroxyl–hydroxyl correlations, solid line), and $H(q)$ (alkyl–hydroxyl cross term, short dash-dotted line). The dotted line represents the sum of all these partial contributions. (b) From bottom to top the symbols represent experimental scattering data of ethanol, 1-propanol, 1-butanol, 1-pentanol, and 1-hexanol, shifted upward for visual clarity as indicated. Calculations are shown as solid lines.
Source: Reprinted with permission from Ref. [100].

exterior, see, e.g., Fig. 2(b). In that sense the prepeak can be viewed to yield information on the intercluster correlations or the cluster–cluster segregation [134].

With increasing chain length the position of the prepeak, Q_{max}, shifts to lower momentum transfers, as clearly seen in Fig. 5(b). For linear alcohols larger than propanol an approximate linear relationship between $1/Q_{max}$ and the number of carbon atoms was found [109,114]. However, the position of the prepeak, relative to that of the main peak of the structure factor, depends also on the branching of the hydrocarbon chain and the position of the OH group. When calculating the effective chain lengths of monohydroxy alcohols [14] these isomeric effects have to be taken into account.

It is of considerable interest to learn more about the supramolecular structure of monohydroxy alcohols. Are rings, chains, or branched motifs prevalent; how large are these, etc.? But unfortunately, the determination of supramolecular structures from X-ray or neutron diffraction patterns is by no means unique, even if one combines results from both scattering techniques [150,151]. Leaving aside a discussion of the many experimental challenges one faces in this context, the residual ambiguity in superstructure determination mainly arises because modern interpretations of diffraction patterns require detailed comparisons with structural models. Yet, rather different structural models can yield essentially indistinguishable diffraction patterns. Furthermore, *a priori* it is not clear which kind of computational strategies are the most appropriate ones for structural modeling. For instance, is modeling in terms of reverse or configurational bias Monte Carlo techniques, or of effective potential structure refinement to be preferred? Do all-atom or united-atom approaches yield more reliable results? Should the analyses be combined with classical or with quantum mechanical MD simulations?…

So far, diffraction methods did not allow for an unambiguous resolution of the questions just raised regarding several aspects of supramolecular organization in monohydroxy alcohols. However, major steps forward in this directions have become possible using the inelastic X-ray scattering techniques that are dealt with next.

Hydrogen bonding and supramolecular structure probed by inelastic X-ray scattering

With the advent of highly brilliant synchrotron radiation sources inelastic X-ray scattering has become more or less routine [152]. Modern X-ray techniques are well suited to unravel structural changes taking place at the sites of the intermolecular hydrogen bond partners. Later in this section, we will review results that have been obtained using Compton scattering [153], but first techniques exploiting oxygen's K-edge will be dealt with. The K-edge of oxygen is highly sensitive to the local oxygen environment, i.e., just where needed to find out whether changes in hydrogen bond length, cooperative effects, or non-conventional phenomena such as bond bifurcations are at stake. It turns out that K edge spectroscopy of the oxygen-bonded carbon atom (or other carbons) is well suited to address these issues.

X-ray (near-edge) absorption spectroscopy (XAS or XANES, also termed EXAFS = extended X-ray absorption fine structure) involves (resonant) excitation near and up to about 20 eV above the absorption threshold in order to gather information regarding the *unoccupied* density of states (DOS) of those electrons involved in the absorbing atom's chemical bonds [154,155]. Using X-ray emission (or fluorescence) spectroscopy (XES), on the other hand, one is sensitive to the *occupied* electronic DOS of the atom's bonds [156,157]. With oxygen's K-edge located near energies of 530 eV [158] one operates in the regime of soft (<1 keV) X-rays that typically suffers from submicron path lengths. This problem can be circumvented by applying X-ray Raman scattering (XRS), a bulk sensitive method based on non-resonant inelastic X-ray scattering from core electrons [136].

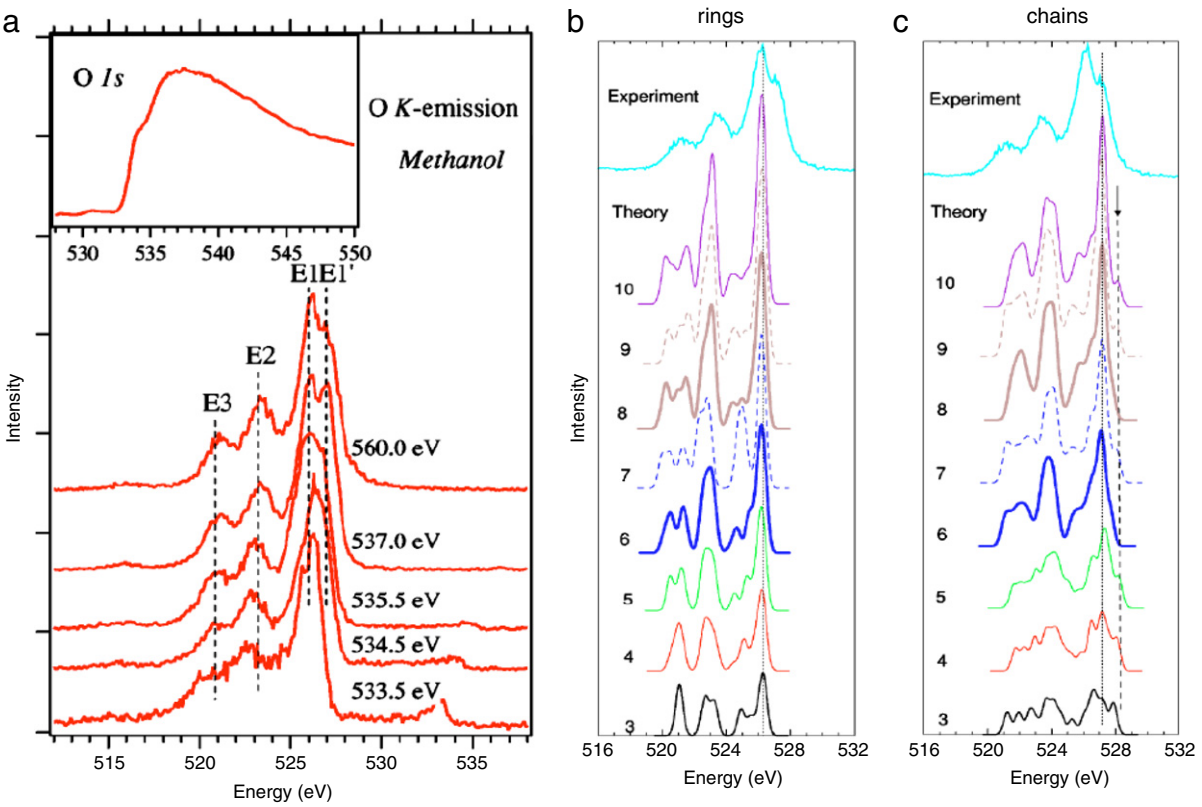

Fig. 6. (a) Resonant X-ray emission spectra of pure liquid methanol measured near the K-edge of oxygen for several incoming photon energies obtained from a tunable synchrotron source. The spectral changes, induced by using different photon energies, suggest that different mixtures of supramolecular conformations are selectively excited. The dashed lines highlight various emission lines. The corresponding absorption spectrum is shown in the inset. Calculated emission spectra of (b) ring and (c) chain structures of methanol clusters containing 3–10 molecules are compared with an experimental emission spectrum.
Source: Reprinted with permission from [156].

All of these methods can be combined with pump and probe schemes to enable the excitation (e.g., using mid-infrared to extreme ultra-violet laser pulses) and X-ray detection of dynamical processes with ultrafast (up to femtosecond) time resolution [159–161]. But we are not aware of the experimental application of such methods to monohydroxy alcohols. For a discussion of all-optical pump and probe experiments, see Section 9.5.

Let us first turn to soft X-ray experiments. In the inset of Fig. 6(a) we reproduce an absorption spectrum of liquid methanol which is assigned to electronic transitions from oxygen's 1s level to unoccupied states [156]. The emission spectra shown in the mainframe of Fig. 6(a) were recorded subsequent to excitation at the labeled photon energies. As detailed in [156,157] the emission lines (E1, E2, and E3) correspond to transitions from the occupied valence orbitals to the core vacancy and the line intensities reflect the local oxygen *p*-wave character of the occupied states.

It turns out that ring-like and chain-like structures yield different inelastic X-ray spectra. According to density functional calculations the most distinctive feature in the emission spectra is that ring structures yield an intensity maximum at an energy of 526 eV, while chain structures are characterized by a maximum at 527 eV [156,157]. Since the experimental emission spectra in Fig. 6 (stated resolution 0.2 eV) reflect a superposition of the various supramolecular aggregates, the double peak feature of the E1 line was interpreted to indicate a coexistence of ring- and chain-like structures [156,157].

To see how such superpositions come about in different kinds of structural motifs, let us look at simulations, now of *absorption* spectra which provide similar information than emission spectra. In particular, also *absorption* spectra are sensitive to the type of suprastructure, as confirmed by results of explicit calculations shown in Fig. 7(a) for the three molecules forming a methanol trimer. This figure, taken from [155], illustrates that in chain-type arrangements distinguishable spectra are obtained depending on whether the respective molecules donate hydrogen bonds (β), that they accept them (γ), or that they do both (δ). Furthermore, the spectra all differ from that of the free, monomeric species (α). Here the Greek letters refer to the nomenclature commonly used in the framework of vibrational spectroscopy, cf. Fig. 47 in Section 9.1, below. The calculated O orbitals of the molecules in a trimer, i.e., essentially the lowest unoccupied molecular orbitals (LUMO) of the various species are depicted in Fig. 7(c). Expectedly, in a ring-type cluster the X-ray absorption spectra are evidently all the same, see Fig. 7(b) [155]. In [156] the difference in the electronic structure of the chain versus ring

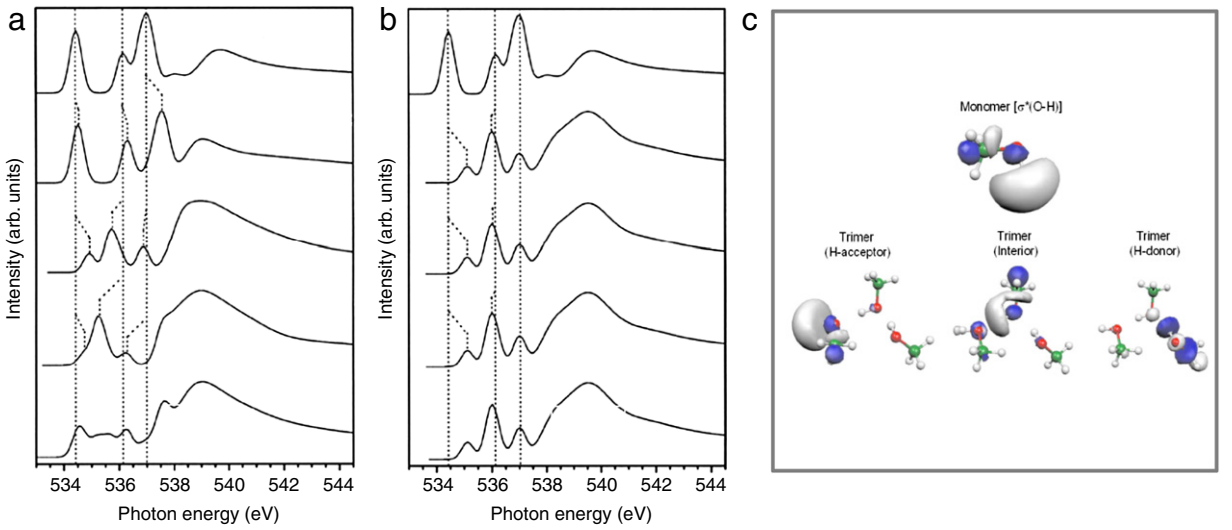

Fig. 7. Calculated X-ray oxygen near K-edge absorption spectra of methanol trimers in (a) chain and (b) ring conformations compared to the monomer spectrum (top). The spectra of each molecule and the superposed spectra (bottom) are also shown. The vertical lines mark peak positions in the monomer spectrum. Depending on the chemical state the first resonance peak near 534 eV undergoes major "chemical-shift" changes. This peak is predominantly due to the anti-bonding σ^*(O–H) orbital. (c) Visualization of the excited orbitals corresponding to the peak near 534 eV. The blue and gray shading indicates different lobes of the LUMO. From left to right the trimer molecules correspond to β, δ, and γ species in terms of the nomenclature common in vibrational spectroscopy. (For interpretation of the references to color in this figure legend, the reader is referred to the web version of this article.)
Source: Reprinted with permission from [155].

conformations was pinpointed by emphasizing that "the molecular orbitals of chains are strongly localized, whereas for the ring structures they show strong delocalization characteristics and behavior like covalent π orbitals in a conjugated system". Interestingly, as revealed by Fig. 6(b) and (c), the simulated emission spectra even depend sensitively on the *number* of molecules that form either ring- or chain-type structures and a similar sensitivity has been documented for near-edge *absorption* spectra [154].

When performing the Raman variant of these experiments, XRS, the incoming high-energy photons are inelastically scattered and only a small part of their energy excites an electron from an inner shell to an empty state. Using oxygen's K-edge, this again allows one to study the unoccupied electronic DOS and thus to unravel details of the chemical bonding of the hydroxyl group of monohydroxy alcohols. The rather low cross section for this scattering process (nowadays counterbalanced by virtue of intense synchrotron radiation sources) depends on the momentum transfer Q. Thus, by performing experiments at various Q, contributions to the DOS with different symmetries can be mapped out. It turns out that near the oxygen K edge, only s- and p-type partial densities of unoccupied states (s-DOS and p-DOS) are relevant [136]. It has been stated that near the edge the p-DOS is directly comparable to the X-ray absorption spectrum [136].

In Fig. 8(a) and (b) we show XRS spectra of methanol as measured at two different momentum transfers, $Q = 3.2$ Å^{-1} and $Q = 9.2$ Å^{-1}, respectively. Panel (c) shows the s-DOS and panel (d) the p-DOS calculated from these spectra. The main characteristics of the s-DOS is a single peak dominating the pre-edge feature in the high-Q spectrum, Fig. 8(b). The s-type contribution, which corresponds to the LUMO, is only weakly developed in the low-Q XRS spectrum which thus indeed looks very much like the p-DOS.

Similar observations were made for ethanol and various isomeric species of propanol and butanol [136]. When comparing the spectra of these monohydroxy alcohols with each other it was found that chemical differences are reflected more sensitively in the high-Q spectra [136].

Let us now turn to Compton scattering [162], a non-resonant X-ray scattering technique permitting one to resolve changes in (hydrogen) bonding geometries with sub-Angstrom resolution. The basic quantity measured using this technique is the Compton profile, $J(q)$, as a function of a momentum variable q. Taking into account the experimental parameters (i.e., the energy of the incident and of the scattered photons as well as the scattering angle) $J(q)$ is essentially given by the cross section for inelastic scattering of photons that transfer a large energy and momentum to the electrons of the target. For the isotropic systems that we deal with in the present context, the Compton profile, $J(q) = \int_{|q|}^{\infty} \int_{\Omega} \langle N(\vec{p}) \rangle \, d\Omega \, p \, dp$, is given by the time-averaged electronic momentum density of the liquid integrated over momentum p and the solid angle Ω. On the theoretical side, the normalized Compton profile ($\int_{-\infty}^{\infty} J(q) \, dq = Z$, with Z denoting the number of electrons in an alcohol molecule) can be computed by summing over the Fourier-transformed single-particle electron wave functions or, more precisely, the *occupied* ground-state orbitals. In the present context it is important to recognize that hydrogen bonding impacts on the distribution of electronic charges in the sample and thus on the corresponding wave functions and momentum densities of the bonded molecules [163]. Thus, variations in the intra- as well as in the intermolecular geometries

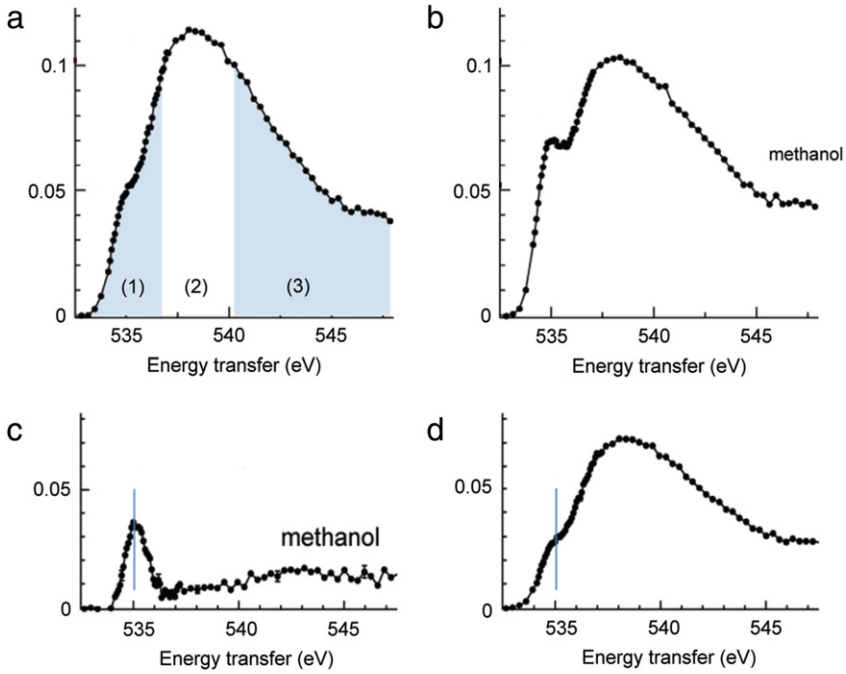

Fig. 8. Oxygen K edge XRS spectra of methanol measured near room temperature at (a) $Q = 3.2$ Å^{-1} and (b) $Q = 9.2$ Å^{-1}. For the experiments the analyzer energy was fixed at 9.68 keV and the incident photon energy was varied. Shaded areas in (a) mark (1) pre-edge, (2) main-edge, and (3) post-edge regions. (c) s-DOS and (d) p-DOS contribution extracted from the experimental spectra. Vertical lines mark the peak position of the non-dipole type (s-) DOS.
Source: Adapted with permission from [136].

of the bonding partners lead to changes in $J(q)$. On the practical side, it is often useful to consider differences in Compton profiles, $\Delta J(q)$, from spectra taken at different temperatures [164] or for different samples [165] under otherwise identical experimental conditions, with the goal to minimize systematic measuring errors.

To illustrate the kind of information that can be expected from $\Delta J(q)$, in Fig. 9 calculated difference Compton profiles are shown for a cluster in which an ethanol molecule is solvated by six water molecules [165]. Panel (a) reveals that an elongation of a single intramolecular O–H bond by 0.01 Å (i.e., on the 10^{-2} level) changes $\Delta J(q \to 0)/J(0)$ by about 10^{-4}. An elongation of an O–H bond can for instance be induced intermolecularly, if the hydrogen bond which the hydroxyl group may form is strengthened, e.g., by making the hydrogen bond more linear which in turn leads to an increase of the O $\cdots$ O distance. Thus, shortening this distance should reverse the sign of $\Delta J(q \to 0)$, an expectation which is confirmed by the calculations shown in Fig. 9(b) for an O $\cdots$ O contraction, again on the 10^{-2} level. The other piece of information obvious from $\Delta J(q)$ is the "wavelength" inferred from its q dependence. Due to the Fourier relationship noted above, a longer wavelength $\Delta J(q)$ signals a stronger spatial localization of the electronic charge density near the nuclei. The results are typically given on the atomic unit scale of momentum with 1 a.u. corresponding to $\hbar/a_0 \approx 2.0 \times 10^{-24}$ kg m/s and a_0 denoting Bohr's radius.

It was found experimentally that the $J(q)$ profiles of branched alcohols display a shorter-wavelength oscillation than the linear species [163]. From the results depicted in Fig. 9(b) a larger delocalization of the electronic charge for the branched alcohols was thus inferred and tentatively ascribed to increased intramolecular interactions with respect to the situation in linear alcohols [163]. An intermolecular origin of this effect was not found likely because density-functional calculations suggested that the narrowing of the Compton profile is independent of whether the branched alcohols are hydrogen bonded or not [163].

To conclude this chapter, let us point out that there is a formal relationship which connects the Compton profile via the expectation value of the kinetic electron energy to the configurational enthalpy, $H_{\mathrm{conf}} \approx 3 \int_0^\infty q^2 J(q)\, dq$ [164]. This equation has been exploited to estimate the configurational contribution to the heat capacity of hexagonal ice [164].

4. Thermodynamic aspects

In simple liquids, the calorimetric signature of the glass transition in a differential scanning calorimetry (DSC) experiment is a step from $C_{\mathrm{p}}^{\mathrm{glass}}$ to $C_{\mathrm{p}}^{\mathrm{liquid}}$, which usually amounts to a change by a factor of two, i.e., $C_{\mathrm{p}}^{\mathrm{liquid}} \approx 2C_{\mathrm{p}}^{\mathrm{glass}}$. The onset temperature of this increase defines the calorimetric glass transition temperature, $T_{\mathrm{g,cal}}$, if a standard heating rate, e.g., 20 K/min, is used. This value of $T_{\mathrm{g,cal}}$ is in most cases very close to the kinetic glass transition temperature, $T_{\mathrm{g,kin}}$, if defined by the kinetic

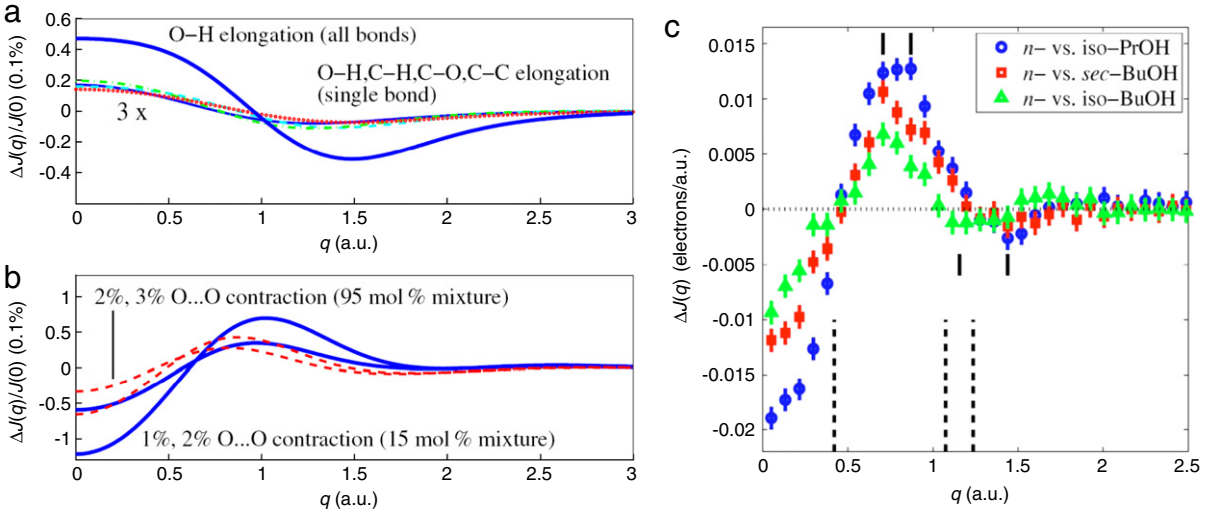

Fig. 9. Effects of (a) intramolecular and (b) intermolecular changes of bond lengths. Adapted from Ref. [165] with permission. Copyright 2011 by American Physical Society. (c) Measured Compton profile differences $\Delta J(q)$: $J_{n\text{-PrOH}}(q) - J_{\text{iso-PrOH}}(q)$, $J_{n\text{-BuOH}}(q) - J_{\text{sec-BuOH}}(q)$, and $J_{n\text{-BuOH}}(q) - J_{\text{iso-BuOH}}(q)$. Minima, maxima, and zero crossings, defining the "wavelength" of $\Delta J(q)$ are marked. The incident X-rays had an energy of 176 keV; the energy resolution was about 0.6 keV.
Source: Reprinted with permission from [163].

criterion $\tau_\alpha(T_{g,\text{kin}}) = 100$ s. In the case of monohydroxy alcohols, the C_p step height also amounts to a factor of about two. However, the coincidence of $T_{g,\text{cal}}$ and $T_{g,\text{kin}}$ is not observed for these alcohols, if the kinetic T_g is based upon the prominent dielectric polarization process. The first mention of this discrepancy may have been Kauzmann's review [35], see Section 2.

A systematic study of the comparison between calorimetric and kinetic glass transition temperature has been performed by Murthy [166], based upon the recognition of two dynamic processes (labeled 'I' and 'II' in the order of increasing peak frequency) that both follow a super-Arrhenius type temperature dependence typical of glass-forming liquids. The activation graphs for several monohydroxy alcohols suggest that the smaller and faster of the two modes, process II, is more similar in behavior to the α-process of non-associating liquids. Of the two kinetic processes involved, $T_{g,\text{kin-I}}$ and $T_{g,\text{kin-II}}$, the latter was found to be more consistent with the calorimetric counterpart, $T_{g,\text{cal}}$. A more recent analogous study on a series of isomeric octanols arrived at the same conclusion [167], based upon calorimetric T_g values which deviated from an earlier report [168]. The problem inherent in this comparison is that $T_{g,\text{kin-I}}$ and $T_{g,\text{kin-II}}$ are too close together relative to the uncertainties of the T_g values to generate a decisive result if only a single or very few monohydroxy alcohols are considered. On the other hand, the differences $T_{g,\text{cal}} - T_{g,\text{kin}}$ show different signs for process I and II in a very systematic manner [169]. This is depicted in Fig. 10 for a number of alcohols in comparison to other liquids. Pairs of calorimetric T_g's that were assumed to correlate with process I and II for five monohydroxy alcohols have been reported by Murthy and Nayak [36], but such a scenario had not been confirmed otherwise.

A different approach to assessing the kinetic glass transition of process II is through an analysis of the dynamics governing the DSC curve, $C_p(T)$, which, in principle, contains the information of the temperature dependent structural relaxation near T_g, as the enthalpy relaxation competes with the scan rate $q = dT/dt$. A common approach to analyzing such DSC curves is the Tool–Narayanaswamy–Moynihan (TNM) model [170]. Because a sample falls out of equilibrium during such a DSC scan, the enthalpy relaxation times depend on both temperature and structure (or fictive temperature), $\tau = \tau(T, T_f)$. In the TNM approach, the so-called non-linearity parameter, x, partitions the dependence of τ on T and T_f. As an adjustable parameter, x is a main source of uncertainty in applying this model. Examples of such calculations are given by Murthy and Tyagi [171] and later by Wang et al. [169], again indicating that process II is consistent with the enthalpy relaxation result of the DSC scan. The advantage of this method over comparing $T_{g,\text{kin}}$ and $T_{g,\text{cal}}$ values only is that also the relaxation time dispersions are involved, a quantity regarding which processes I and II differ considerably. While process I is of the Debye type with a stretching exponent $\beta > 0.95$, cf. Eq. (4), below, process II displays the dispersion typical of structural relaxation in viscous liquids, with $\beta \approx 0.5$. Accordingly, the TNM fits are seen to be more compatible with dispersive structural relaxation, and less consistent with a Debye type nature of the α-process. If the highest amplitude dielectric signal of these monohydroxy alcohols were regarded as a signature of structural relaxation, a Debye type character of the α-process would be expected.

A drawback of the above mentioned comparison of the calorimetric onset temperature with a kinetic criterion regarding dielectric relaxation is that the latter is an equilibrium measurement at a well defined temperature, while the former is not. A straightforward analysis of such data is possible only with a robust model of non-equilibrium relaxation behavior, which is not available. An added source of uncertainty in a $T_{g,\text{cal}}$ versus $T_{g,\text{kin}}$ study is the possibility of some alcohols changing supramolecular configurations with temperature, which affects a DSC trace and thus $T_{g,\text{cal}}$ but without a concomitant impact

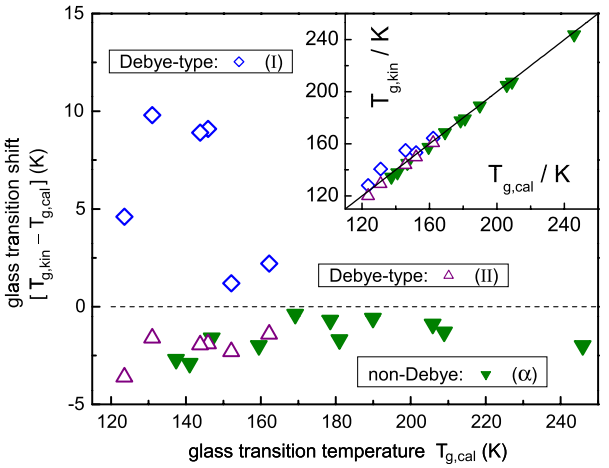

Fig. 10. The calorimetric and kinetic glass transition temperatures of generic (solid triangles) and Debye-type (α: open triangles, D: diamonds) liquids, shown as $T_{g,kin} - T_{g,cal}$ and $T_{g,kin}$ versus $T_{g,cal}$ in the main figure and inset, respectively. All $T_{g,cal}$'s are based on cooling/heating rates $q = -/+20$ K/min, and $T_{g\text{-}kin}$'s on isothermal dielectric measurements using $T_g = T(\tau_g = 100$ s). The generic liquids are: decalin, 2-ethylhexylamine, 3-methoxy-1-butanol, propylene carbonate, propylene glycol, di-*n*-butyl phthalate, decahydroisoquinoline, glycerol, 2,4-pentanediol, 2-ethyl-1,3-hexanediol and ortho-terphenyl. The Debye-type liquids are: 2-methyl-1-butanol, 2-ethyl-1-butanol, 3-methyl-2-pentanol, 2-ethyl-1-hexanol, 5-methyl-2-hexanol, and 4-methyl-3-heptanol. Both lists are given in the order of increasing $T_{g,cal}$.
Source: Adapted from [169].

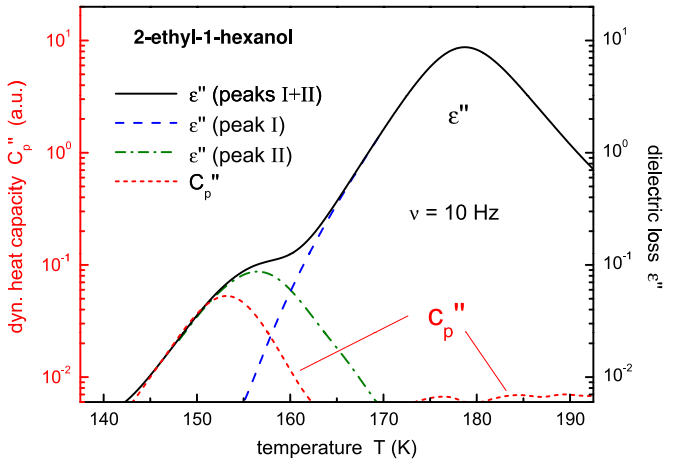

Fig. 11. Loss components ε'' and C_p'' for 2E1H versus temperature, both measured at a frequency of $\nu = 10$ Hz. The C_p'' curve is shifted arbitrarily along the ordinate scale. The dashed lines separate the dielectric signal into the Debye (I) and non-Debye (II) contributions.
Source: Adapted from [37].

on isothermal kinetics results [172]. As a consequence, a more meaningful comparison between enthalpy relaxation and dielectric polarization is obtained using dynamic heat capacity data, i.e., confined to the reversing contribution to heat capacity [173]. These issues are avoided in the measurements of $C_p'(\omega)$ and $C_p''(\omega)$ at a constant temperature T, which can be compared more directly with $\varepsilon'(\omega)$ and $\varepsilon''(\omega)$ at the same T, as both quantities are obtained in equilibrium. The result of such an experiment has been reported by Huth et al. [37] for 2-ethyl-1-hexanol.

The comparison of $C_p''(T)$ with $\varepsilon''(T)$, both recorded at the same frequency of $\nu = 10$ Hz, is reproduced in Fig. 11. Clearly, there is practically no contribution to $C_p''(T)$ in the temperature range from 165 to 190 K, in which the prominent dielectric Debye peak appears. However, the peak of $C_p''(T)$ does coincide with the $\varepsilon''(T)$ signature of process II, seen in the 145–155 K range. As a result, a model of this Debye process needs to be consistent with a heat capacity contribution at the Debye frequency that is negligible within the experimental resolution, see Fig. 11.

The exceptional behavior of supercooled monohydroxy alcohols is also manifested in experiments that can be viewed as 'reverse calorimetry' [174], where a relaxation process is initiated by the influx of energy via absorption from the external electric field, $E_0 \sin(\omega t)$. As in nonresonant dielectric hole burning [175–177], the power is spectrally selective, i.e., most pronounced for modes whose relaxation time constants τ match the frequency ω of the applied electric field ($\tau \approx 1/\omega$). The effect of the extra energy accumulated by these modes is a change in the fictive temperature T_f that can be calculated on

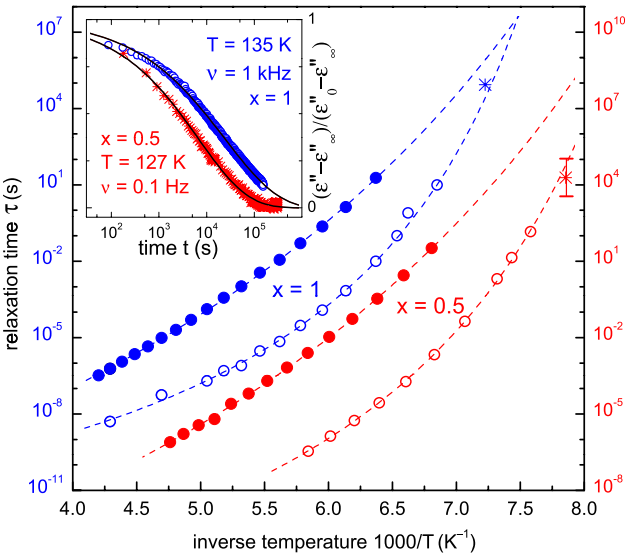

Fig. 12. Arrhenius plot of 2E1H (left ordinate axis) and of $(2E1H)_{0.5}(2E1Br)_{0.5}$ (right ordinate axis). The full and the open circles represent τ_D and τ_α, respectively, from dielectric equilibrium measurements. The lines are fits using the Vogel–Fulcher law, see Eq. (12), below. The stars represent time constants from aging, $\langle\tau_{age}\rangle$, determined from the isothermal dielectric loss curves shown in the inset. The error bar indicates the variation limits for $\langle\tau_{age}\rangle$ between the equilibrium (linear) relaxation times at the temperatures before and after the T-jump, $\tau_{initial}$ ($T = 129.5$ K) $< \langle\tau_{age}\rangle < \tau_{final}$ ($T = 127$ K).
Source: Reprinted with permission from [187].

the basis of the power ($\propto\varepsilon'' E_0^2$), the heat capacity, and the relaxation time τ [176,178,179]. As the change of T_f impacts the relaxation time constant τ, the result of energy absorption can be monitored via the concomitant change in the loss ε'' or dissipation factor $\tan\delta$. For simple, non-Debye type liquids, the hallmark of spectral selectivity and thus of the heterogeneous nature of the dynamics is the observation that the initial rate of change is proportional to the peak frequency of the mode that matches the frequency of the sinusoidal electric field. Experimental access to the time-resolved effects is accomplished by the application of a sinusoidal field which is subject to a considerable increase in amplitude at time zero. As a result, the power is negligible for time $t < 0$, and for $t > 0$ the value of $\tan\delta$ is obtained for each subsequent period separately by Fourier analysis [180,181]. In essence, this method is a measurement of the time scale of enthalpy relaxation (τ_T) associated with a mode of a certain dielectric relaxation time (τ_d), with the value of τ_d determining its rate of energy absorption via its spectral position relative to ω.

For simple, non-Debye type liquids, it has been observed repeatedly that the values of dielectric and enthalpy relaxation times are virtually identical, i.e., $\tau_d = \tau_T$ [182]. For monohydroxy alcohols, however, the change in $\tan\delta$ that is associated with τ_T is much faster than the dielectric time τ_d [181–183]. A typical example for this situation is depicted in Fig. 29, below, where the dashed line indicates the curve expected for $\tau_d = \tau_T$, whereas the data indicates $\tau_d \geq 100\tau_T$. As for the results based upon standard calorimetry, these high-field dielectric experiments confirm that structural relaxation is more consistent with the time scale of process II, instead of matching the value of τ_d of the Debye peak labeled process I.

It should be noted that high electric fields impact the configurational entropy of a liquid via $S_{cfg}(E) = S_{cfg}(0) + (\partial\varepsilon_s/\partial T)\, E^2\varepsilon_0/2$ [184], with the direction of field induced changes depending on the type of liquid (type I if $\partial\varepsilon_s/\partial T < 0$ and type II if $\partial\varepsilon_s/\partial T > 0$) [185]. For the majority of liquids including many alcohols, the property of $\partial\varepsilon_s/\partial T < 0$ results in a field induced reduction of S_{cfg}, and via the Adam–Gibbs relation [186], $\ln\tau = A + C/\left(S_{cfg}T\right)$, in an increase of relaxation times with A and C denoting phenomenological constants. The high-field dielectric experiments described in the present Section 4 consistently lead to reductions of relaxation times [183], suggesting that the field-induced increase in configurational temperature outweighs the decrease in entropy.

Another technique of monitoring genuine structural relaxation is by a physical aging experiment, regardless of which quantity is used to follow the progress of aging (e.g., volume, enthalpy, dielectric permittivity, mechanical properties, etc.). Provided that the time scales of peak I and II are sufficiently separated, one can discriminate which of the two processes is associated with the aging process and thus with structural relaxation.

The mixture of 2-ethyl-1-hexanol and 2-ethyl-hexylbromide is an ideal candidate for such an aging based experiment, as the peaks I and II display a pronounced spectral separation near T_g, with peak I being more intense and thus more clearly characterized than in the case of most pure monohydroxy alcohols. Fig. 12 demonstrates that the time scale of physical aging for this system coincides well with that of peak II, and this result is obtained without having to rely on a particular model of aging [187].

In summarizing the above results, it appears that peak II has significant spectral overlap with enthalpy relaxation modes and is thus a much more convincing candidate for a dielectric signature of structural relaxation than is peak I.

Supportive of this notion is that peak II (with the higher peak frequency and lower amplitude relative to peak I) falls with the typical correlation band of fragility in terms of steepness index m and relaxation time dispersion in terms of the Kohlrausch–Williams–Watts stretching exponent β [188]. The Debye process labeled 'I' would constitute an exceptional case as having super-Arrhenius behavior combined with a purely exponential correlation function, $\beta = 1$ [47,189].

5. Dielectric spectroscopy

5.1. Orientational correlation functions

In the present context, the dielectric properties of a material are usually characterized by permittivity ε, an intensive quantity that is defined by the constitutive equation that relates the dielectric displacement D to the electric field E, $D = \varepsilon\varepsilon_0 E$ [9]. As isotropic homogeneous samples are considered here, it is sufficient to focus on D, E, and ε as scalar quantities. The contribution of the material to the displacement is its polarization P, with $P = D - \varepsilon_0 E = (\varepsilon - 1)\,\varepsilon_0 E = \chi\,\varepsilon_0 E$ in the regime of linear response where the susceptibility χ is field invariant. For molecular liquids, there are two main sources of polarization, electronic polarizability, α_{el}, and orientational polarizability, α_{or}, of permanent dipole moments. To a good approximation, the electronic component is independent of the orientation of the molecule and its contribution to ε is practically frequency independent and equal to the square of the refractive index, $\varepsilon \approx n^2$. For the study of liquid dynamics, the polarization due to reorientation of permanent dipoles is the key quantity of interest. Apart from constant geometrical factors (surface area A and electrode distance d), polarization P, displacement D, and macroscopic dipole moment M are all variables that gauge the amount of charge on the surface of the sample, and their changes can be measured directly via the resulting current in the time or frequency domain.

Various experimental techniques exist that will characterize the two-time autocorrelation function of the macroscopic dipole moment,

$$\left\langle \vec{P}\,(0)\cdot\vec{P}\,(t)\right\rangle = \left\langle \left(\sum_{i=1}^{N}\vec{\mu}_i\,(0)\right)\cdot\left(\sum_{j=1}^{N}\vec{\mu}_j\,(t)\right)\right\rangle. \tag{1}$$

Due to interactions among the dipoles, there is no guarantee that the fluctuation of the macroscopic dipole is a true reflection of the fluctuation of molecular dipoles, i.e., the observable is a collective response [190]. In the absence of such interactions, the accessible decay would reflect the single particle autocorrelation function of molecular dipoles,

$$C_\mu\,(t) = \frac{1}{N\mu^2}\sum_{i=1}^{N}\langle\vec{\mu}_i\,(0)\cdot\vec{\mu}_i\,(t)\rangle = \frac{1}{\mu^2}\,\langle\vec{\mu}\,(0)\cdot\vec{\mu}\,(t)\rangle = \langle\cos\theta\,(0)\cos\theta\,(t)\rangle\,. \tag{2}$$

Only when the dipole is constant and fixed within the coordinates of the molecule, then one can derive the single particle orientation correlation function of molecules, a quantity that can be interpreted in a straightforward fashion. A useful indicator for the extent of orientational correlations is the Kirkwood correlation factor, $g_{\mathrm{K}} = 1 + z\,\langle\cos\theta\rangle$, where z is the number of coordinated molecules [191]. When g_{K} is found to be near unity, then the dynamics of $\varepsilon(t)$ reflect the single particle reorientation to a good approximation. In a homogeneous electric field, translational displacements of dipoles do not contribute directly to the overall polarization.

For the case of reorientation being governed entirely by diffusion, Debye's solution of the diffusion problem predicts that the correlation function associated with the projection of order ℓ, which involves the ℓth order Legendre polynomial $P_\ell\,(\cos\theta)$, decays exponentially as $\exp\left[-\ell\,(\ell+1)\,D_{\mathrm{rot}}t\right]$, where D_{rot} is the rotational diffusion constant. Dipole orientation corresponds to $\ell = 1$, whereas experiments such as NMR or optical depolarization are governed by the $\ell = 2$ projection, which leads to a three fold decrease of the decay time constant. For larger jump angles, the time scales of reorientation become more similar for the different orders ℓ.

In a time-domain–step-response type experiment, polarization of a material can be measured in various ways. In the 'constant voltage' case, i.e. when the voltage or field is independent of the progress of polarization, $P(t)$ is linearly related to the displacement $D(t)$ and thus to the permittivity $\varepsilon(t)$. This situation corresponds to the standard technique of applying a voltage step at time zero and recording the displacement of charge (or current) as a retardation function of time. An alternative is to apply a charge step at time zero and record the voltage relaxation versus time. In this 'constant charge' situation, polarization is linearly related to the field $E(t)$ and to the so-called electric modulus $M(t)$. This electric modulus characterizes the autocorrelation function of the (macroscopic) electric field. In the steady state, the complex quantities $\hat{M}$ and $\hat{\varepsilon}$ are related by the equality $\hat{M}\,(\omega) = 1/\hat{\varepsilon}\,(\omega)$. According to Fröhlich [184], an exponential retardation $\varepsilon(t)$ leads to and exponential relaxation $M(t)$, but the time constants τ_ε and τ_{M} are not identical. For the linearly averaged time constants, the following relation holds,

$$\bar{\tau}_M = \frac{\varepsilon_\infty}{\varepsilon_{\mathrm{s}}}\times\bar{\tau}_\varepsilon, \tag{3}$$

which implies that modulus relaxation is generally faster than its retardation counterpart [192].

In a typical liquid, the dielectric relaxation dynamics is found to be dispersive with respect to the time constants involved, i.e., the Debye theory does not account for the observed width and asymmetry of loss spectra. For the case of time domain data, the stretched exponential or Kohlrausch decay has found wide application,

$$\varepsilon(t) = \varepsilon_\infty + (\varepsilon_s - \varepsilon_\infty)\left[1 - e^{-(t/\tau_0)^\beta}\right], \tag{4}$$

where τ_0 is a characteristic time scale and β gauges the deviation from exponential correlation decay, with $\beta = 1$ restoring the Debye case. By virtue of the one-sided Fourier transform,

$$\hat{\varepsilon}(\omega) = \varepsilon_\infty + \int_0^\infty \frac{d\varepsilon(t)}{dt} e^{-i\omega t} dt \tag{5}$$

or approximations thereof, Williams and Watts have emphasized that the empirical Kohlrausch approach can also be applied successfully to frequency domain data [193,194].

The more common method of data reduction in frequency domain studies is based on empirical permittivity functions, many of which can be summarized by the Havriliak–Negami (HN) function [195],

$$\hat{\varepsilon}(\omega) = \varepsilon_\infty + \frac{\varepsilon_s - \varepsilon_\infty}{[1 + (i\omega\tau_{HN})^\alpha]^\gamma}. \tag{6}$$

Here, τ_{HN} sets a characteristic time scale, and the exponents α and γ with $(0 < \alpha, \alpha\gamma \leq 1)$ determine the extent of symmetric and asymmetric broadening, respectively. This expression has three well known special cases, the Debye limit with $\alpha = \gamma = 1$, the symmetric Cole–Cole function which has $\gamma = 1$, and the asymmetric Cole–Davidson case obtained for $\alpha = 1$, which has a Debye type low frequency slope [196].

For complex dynamics such as those found in monohydroxy alcohols, three distinct loss peaks and dc-conductivity need to be accounted for in order to provide a complete characterization of the dielectric loss spectra. In such a case, the superposition of the various contributions is a common fit function,

$$\hat{\varepsilon}(\omega) = \varepsilon_\infty + \sum_{k=1}^{3} \frac{\Delta\varepsilon_k}{[1 + (i\omega\tau_k)^{\alpha_k}]^{\gamma_k}} + \frac{\sigma_{dc}}{i\omega\varepsilon_0}, \tag{7}$$

where also contributions from dc conductivity, σ_{dc}, are included.

An equivalent approach to non-exponential dynamics is to consider a superposition of Debye processes, where the probability density function $g(\tau)$ determines the overall time or frequency dependence of the permittivity. The corresponding expressions are

$$\varepsilon(t) = \varepsilon_s - \Delta\varepsilon \int_0^\infty g_\varepsilon(\tau)\, e^{-t/\tau} d\tau, \tag{8a}$$

and

$$\hat{\varepsilon}(\omega) = \varepsilon_\infty + \Delta\varepsilon \times \int_0^\infty g_\varepsilon(\tau) \frac{1}{1 + i\omega\tau} d\tau. \tag{8b}$$

Here the subscript 'ε' indicates that the $g(\tau)$ are different for permittivity and modulus, i.e., $g_\varepsilon(\tau) \neq g_M(\tau)$. While the proper choice of $g_\varepsilon(\tau)$ can make this superposition approach mathematically identical to any of the above empirical functions, these latter expression are more adopted to the concept of heterogeneous dynamics. In this context, heterogeneity refers to the picture of a superposition of mutually independent Debye modes being at the source of overall dispersive relaxation [197–201]. For the extreme case of heterogeneity associated with local Debye type responses [202], $g_\varepsilon(\tau)d\tau$ can be interpreted as the volume fraction of modes associated with time constants in the range from τ to $\tau + d\tau$.

In the relations of Eq. (8), it is understood that the time constants τ are time invariant. If this were strictly true, then the system would not be ergodic, as ensemble and time averages would differ. In reality, the time constants can fluctuate on a relatively slow time scale, a process designated as rate exchange [203]. The basic idea behind such fluctuations is that the time constant of a particular molecule in a liquid is defined by its environment and the relevant interactions, and the fluctuations in the environment lead to changes in the value of τ [204]. A simple consequence of efficient environmental fluctuations is that any process that is much slower than the time scale of rate exchange will display Debye character, because that process will be subject to an averaged environment.

In addition to deriving the dynamics of a liquid from time or frequency dependent dielectric measurements, it is also important to rationalize the amplitudes of the signals, $\Delta\varepsilon = \varepsilon_s - \varepsilon_\infty$. Initially, measurements of dielectric constants were an important source of information concerning the structure of a molecule via knowledge of its permanent dipole moment μ. For dense dipolar liquids, Onsager has provided a link between dipole moment and dielectric constants under the assumption that short-ranged orientational correlations remain negligible [205],

$$\frac{(\varepsilon_s - \varepsilon_\infty)(2\varepsilon_s + \varepsilon_\infty)}{\varepsilon_s(\varepsilon_\infty + 2)^2} = \frac{\rho N_A}{9 k_B T \varepsilon_0 M} \mu^2. \tag{9}$$

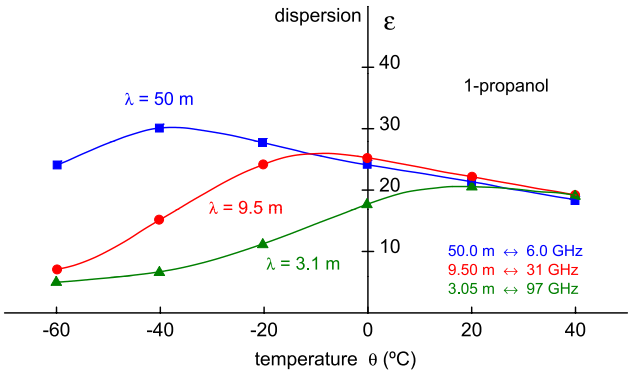

Fig. 13. Dielectric constant ε' versus temperature for 1-propanol for three different frequencies ν: 6.0 MHz (50 m), 31 MHz (9.5 m), and 97 MHz (3.1 m). The graph compares the data (symbols) taken by Mizushima [6] with the Debye theory (lines) for a given viscosity.
Source: Adapted from [9].

In this equation, N_A is Avogadro's constant, ρ is the density, M the molar mass, k_B is Boltzmann's constant, and ε_0 is the permittivity of vacuum. The generalization that includes orientational correlations is known as Kirkwood–Fröhlich equation, which is identical to Eq. (9), but with μ^2 replaced by $g_K\mu^2$, with g_K representing the Kirkwood correlation factor [1,184,191]. A value of $g_K > 1$ indicates preferred parallel orientations of dipoles, $g_K < 1$ suggests that anti-parallel alignment of dipoles is dominant, and $g_K = 1$ restores Onsager's relation and is commonly interpreted as the absence of such correlations. In a homogeneous single-component bulk liquid, the two typical reasons for g_K being close to unity are a small dipole density or the presence of quadrupoles which are capable of suppressing orientational correlations even at high dipole densities [206,207].

5.2. Spectral profiles

The most recurring observation regarding the dielectric relaxation features of monohydroxy alcohols is the Debye type nature of their prominent dielectric loss process. These loss profiles can be quantified by only two parameters, the time constant τ_D and the amplitude, $\Delta\varepsilon = \varepsilon_s - \varepsilon_\infty$. An important aspect of the Debye profile was the existence of a theory that predicts such a permittivity for a permanent dipole subject to rotational diffusive motion. An early example of validating the Debye type behavior was based upon the data obtained by Mizushima [3–7] for various alcohols, including methanol, ethanol, 1-propanol, 2-propanol and using wavelengths between $\lambda = 3$ and 50 m (corresponding to frequencies between $\nu = 6$ and 100 MHz). After comparing dispersion data with Debye's theory, Mizushima concludes: "It can now be admitted that Debye's theory holds in the first approximation for monovalent alcohols". [6], while recognizing that the approach fails for glycerol. A graphical comparison is shown in Debye's monograph on polar molecules, see Fig. 13.

When the frequency range coverage was widened to several decades, deviations from the Debye profile at high frequencies became obvious, as in the example of unusually large deviations of that kind shown in Fig. 14. Because the analysis of the frequency dependent permittivity was limited to a superposition of Debye processes (rather than Cole–Cole or Cole–Davidson type peaks), the extra high-frequency loss was described with two additional Debye peaks [208] in order to account for the dispersive nature of that high-frequency excess loss.

The shape of the prominent process of monohydroxy alcohols can be checked by graphical means on the basis of the following relation,

$$\left[\varepsilon'(\omega) - \left(\frac{\varepsilon_s + \varepsilon_\infty}{2}\right)\right]^2 + \left[\varepsilon''(\omega)\right]^2 = \left[\frac{\varepsilon_s - \varepsilon_\infty}{2}\right]^2, \tag{10}$$

which states that a Debye type permittivity will generate a semicircle in an ε'' versus ε' plot with radius $(\varepsilon_s - \varepsilon_\infty)/2$ and center at $\varepsilon' = (\varepsilon_s + \varepsilon_\infty)/2$ and $\varepsilon'' = 0$. For 2-methyl-1-butanol, such a Cole–Cole type graph (analogous to a Nyquist plot) is depicted in Fig. 15.

A closer inspection of such semicircles (see inset of Fig. 15) reveals the existence of minute additional processes at higher frequencies, covering the range of $2.0 < \varepsilon' < 2.8$ [48]. For many monohydroxy alcohols, the Debye peak is the most prominent and lowest frequency process within the spectrum and it accounts for 90% or more of the entire relaxation amplitude $\Delta\varepsilon$. Fits based upon the more general Havriliak–Negami expression, Eq. (6), yield exponents α and γ that indicate logarithmic slopes $|d\lg\varepsilon''/d\lg\omega| > 0.95$, i.e., only minor deviations from the Debye shape are observed near the peak. Towards lower frequencies, $\omega\tau_D \ll 1$, the power law behavior, $\varepsilon'' \propto \omega^\alpha$ with $\alpha \approx 1$, usually continues until the loss is taken over by dc-conductivity. The levels of dc-conductivity are usually small and possibly governed by impurity ions. For 2-ethyl-1-hexanol, the conductivity relaxation time, $\tau_\sigma = \varepsilon_0\varepsilon_s/\sigma_{dc}$, is more than six orders of magnitude larger than the average time constant of the primary structural relaxation. Significantly higher levels of dc-conductivity are required in order for the ions to impact the spectral position and amplitude of the Debye process [209].

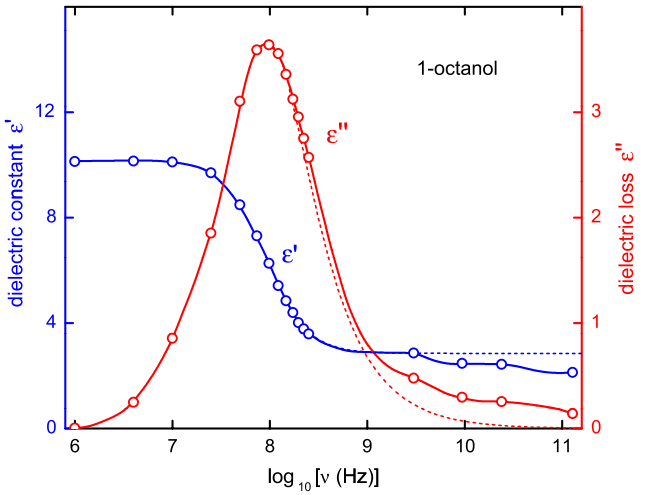

Fig. 14. Real (ε') and imaginary (ε'') components of permittivity for 1-octanol at ambient temperature and a Debye fit (dashed line). Deviations from Debye's theory for frequencies in excess of ν_{max} are clearly identified.
Source: Adapted from [208].

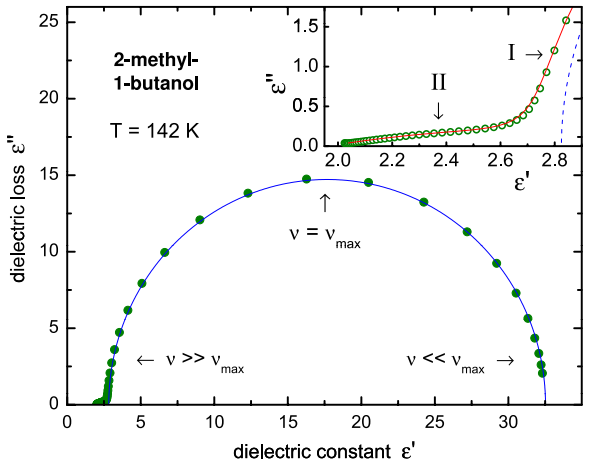

Fig. 15. Cole–Cole representation, $\varepsilon''(\omega)$ versus $\varepsilon'(\omega)$, of the dielectric response of 2-methyl-1- butanol at $T = 142$ K. The symbols are the experimental results in the frequency range 40 mHz–2 MHz. The inset displays the high frequency range, 6 Hz–2 MHz. In each panel, the solid line represents a fit to the Debye-peak and α-relaxation with $\varepsilon_\infty = 1.96$, $\Delta\varepsilon_D = 29.7$, $\tau_D = 0.23$ s, $\Delta\varepsilon_\alpha = 0.87$, $\tau_\alpha = 0.77$ ms, $\alpha = 0.57$, and $\gamma = 0.52$. The dashed line shows the Debye component of the fit.
Source: Adapted from [48].

That the Debye process is detectable also in the absence of external electrical fields has been demonstrated unambiguously by Schildmann et al. for 2-ethyl-1-hexanol [210]. This is achieved by measuring the voltage noise and deriving its spectral density $S_V(\omega)$. A comparison with the concomitant relaxation experiment in terms of the voltage correlation decay $C_V(t)$ with $C_V(t) = P(t)/P(0)$ is based upon the Wiener–Khinchin theorem,

$$S_V(\omega) = \int_{-\infty}^{\infty} C_V(t)\, e^{-i\omega t} dt. \tag{11}$$

The occurrence of the Debye peak in $S_V(\omega)$ and thus in the absence of an external electrical field is shown in Fig. 16.

The additional features on the high frequency side, $\omega\tau_D \gg 1$, are commonly described by two extra processes, and a survey of the literature could be interpreted as indicating the existence of a total of three distinct relaxation processes across the entire liquid range. An early example for the use of three peaks to fit each of ten different normal alcohols is reported by Garg and Smyth [208]. From today's point of view, this analysis is biased by the fact that only Debye type peaks were considered for the superposition that represents the entire loss profile, whereas a single Cole–Cole or Cole–Davidson function could be appropriate for describing the loss that is in excess of the prominent Debye peak [166]. Particularly for temperatures at which the Debye peak enters the GHz regime, a total of three distinct peaks may be required to capture the dielectric behavior of monohydroxy alcohols [211–213]. For those substances that are capable of entering the supercooled

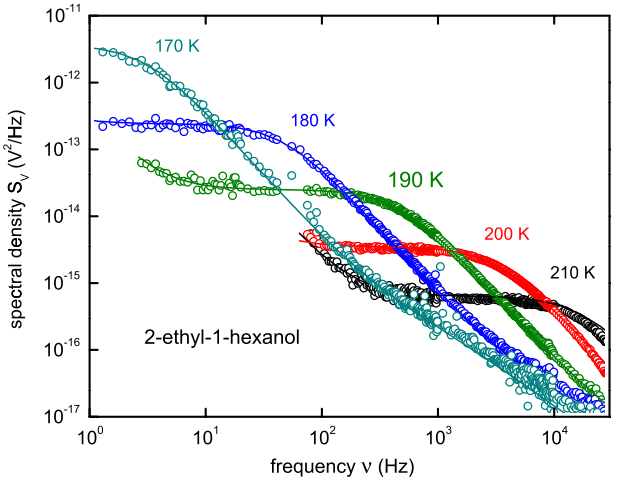

Fig. 16. Power spectra of the voltage noise measured for 2-ethyl-1-hexanol at several temperatures as indicated in the legend. The lines are calculated on the basis of conventional dielectric measurements and demonstrate the correspondence of noise and relaxation measurements.
Source: Reprinted with permission from Ref. [210].

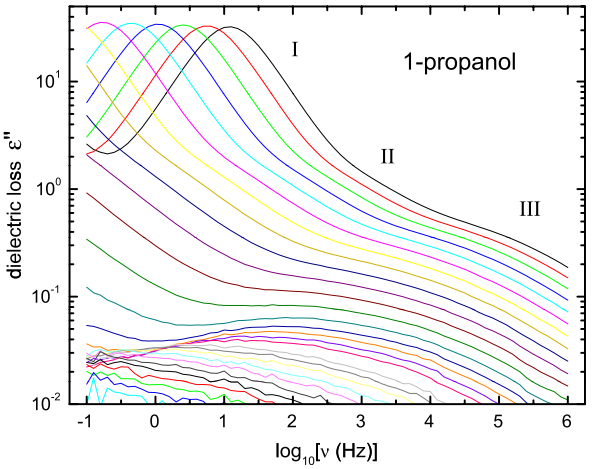

Fig. 17. Experimental dielectric loss ε'' results for 1-propanol in the temperature range 120.8 K $\geq T \geq$ 64.8 K in steps of 2 K and in the order from upper to lower curves. Three distinct contributions, I, II, and III, are observed, where only peak I resembles a Debye type process.
Source: Adapted from [47].

regime ($T_g < T < T_m$) with higher viscosities, spectra with one Debye and one dispersive loss peak are seen only for sufficiently high temperatures, where peaks are positioned at frequencies higher than about 1 MHz [166].

At lower temperatures and higher viscosities, a third relaxation process appears at the high-frequency side of the former two. Fig. 17 displays the resulting occurrence of a total of three peaks for viscous 1-propanol [47]. The highest frequency peak displays the symmetry of a Cole–Cole profile, amplitudes that increase with temperature, and it remains active below T_g, where the remaining dynamics are frozen in. Accordingly, this third peak has the typical characteristics of a Johari–Goldstein (JG) type [214] secondary or slow β-relaxation. As these secondary JG processes are known to merge with the primary or α-relaxation near T_c (the critical temperature of the idealized mode-coupling theory), the occurrence of three distinct peaks for many supercooled monohydroxy alcohols is limited to the temperature range from T_g to T_c.

Of the two dispersive peaks that are both faster than the Debye process, the slower one (peak II in the notation of Fig. 17) is clearly broadened compared with the Debye case, but its symmetry is ambiguous. Both Cole–Cole and Cole–Davidson type fit functions have been used with success to describe this peak, with the uncertainty originating from the overlap with the typically much more intense Debye process on the low-frequency side of peak II. Considerable increases in the peak II amplitudes can be obtained by mixing with a bromide analogue of the alcohol (e.g., 2-ethyl-1-hexanol/2-ethyl-hexylbromide [187]) or by substitution within the alkane tail towards an increased dipole moment (e.g., 3-methylthio-1-hexanol [215]). In both cases, the Debye character of the prominent low-frequency process I is preserved. An interesting observation regarding the width of peak II is that it aligns well with the typical correlation of fragility m and stretching

exponent β observed for numerous glass forming materials, $m = 250\ (\pm 30) - 320\beta$ [47,188]. By contrast, the Debye peak with $\beta = 1$ falls significantly outside this correlation between extent of non-exponential relaxation (β) and deviation from Arrhenius behavior in terms of fragility m.

There are exceptions to the correlation between the monohydroxy character of the alcohol and the occurrence of the prominent dielectric Debye peak. The dynamics of polyols such as glycerol or propylene glycol do not display a Debye type process that is slower than the structural relaxation [216]. Generally, diols do not show a Debye process unless the hydroxyl groups are mutually independent enough, which was observed for a series of pentanediols. According to Davidson [217], the dielectric behavior of 1,5-pentanediol is reminiscent of monohydroxy alcohols, whereas the other isomers (1,2-, 1,4-, 2,3-, 2,4-pentanediol) do not share this property. This exceptional feature of the 1,5-pentanediol isomer is also revealed in depolarized light scattering studies [218].

It is also important to realize that not all monohydroxy alcohols are associated with a prominent Debye peak. Examples for compounds with little or no Debye peak are 2-phenyl-1-ethanol, 1-phenyl-1-propanol, and 1-phenyl-2-propanol [219]. Particularly instructive in this context is the isomeric series of octyl alcohols, 3-methyl-3-heptanol (3M3H), 4-methyl-3-heptanol (4M3H), 5-methyl-3-heptanol (5M3H), and 6-methyl-3-heptanol (6M3H) [24]. The interesting feature of this series is that only a change in the methyl-group position is needed to gradually shift the behavior from a pronounced Debye peak (6M3H) to the absence of such a process (3M3H), as shown in Fig. 18 [24,167]. The intermediate case of 4M3H does display a Debye peak, but it is only somewhat larger than peak II, with the amplitude of peak I depending on the particular diastereomer of 4M3H [220].

It has been found for the longer branched monohydroxy alcohols, specifically 2-butyl-1-octanol and 2-hexyl-1-decanol, that what is otherwise reminiscent of the Debye peak develops considerable asymmetric broadening [221,222] An analysis of fit residuals shows that Cole–Davidson type profiles with γ as low as 0.5 are needed to account for the lowest frequency loss process of these materials. As shown in Fig. 19, this effect becomes more pronounced the smaller the peak amplitude ratio $\Delta\varepsilon_D/\Delta\varepsilon_\alpha$ is.

In recent years, 2-ethyl-1-hexanol has received considerable attention due to several advantageous features: this liquid has a relatively high glass transition temperature of $T_g = 146$ K, it is a good glass former with little tendency to crystallize, and, most importantly, it displays the very large spectral separation of peak I and II by a factor of $\nu_{max,II}/\nu_{max,I} = 2000$ [48,171,210]. The value of 1600 reported for 1-propanol by Litovitz and McDuffie [39] should have read 160. A broadband assessment of the loss profiles of 2E1H has been published by Gainaru et al. [64], showing the pronounced spectral separation of peaks I and II at low temperatures, see Fig. 20.

In conclusion, monohydroxy alcohols display loss spectra that are reminiscent of those of non-associating liquids, but with the Debye peak representing an additional polarization fluctuation on the low-frequency side. However, peaks II and III only will not account for the relaxation amplitude expected on the basis of the permanent dipole moment of the isolated molecule.

5.3. Relaxation amplitudes

As outlined in Section 5.1, Onsager's theory provides a link between dipole density and dielectric constant ε_s or relaxation amplitude $\Delta\varepsilon$ for dense dipolar liquids. For many molecular liquids, particularly those that also possess molecular quadrupoles, Onsager's relation, Eq. (9), has been checked by experiment via knowledge of the molecular dipole μ determined in the gas-phase. For liquids whose molecular constituents are characterized by pure dipolar charge distributions or other intermolecular interactions that promote short range orientational correlations (such as hydrogen bonds or covalent bonds), significant deviations from the dielectric constant expected on the basis of Onsager's relation can be found. As mentioned in Section 5.1, these deviations can be translated into a numerical value for the Kirkwood correlation factor, g_K, and this has been done extensively for monohydroxy alcohols. The main motivation for focusing on g_K is its interpretation in terms of the orientation correlation, $g_K = 1 + z\,\langle\cos\theta\rangle$, where $\cos\theta$ measures the angle between dipole vectors, averaged over the coordination shell with z molecules.

Kirkwood factor data is available for a large number of monohydroxy alcohols, and the values of g_K can span the range from 0.1 to 4 depending on the compound [196]. These severe deviations from unity are mostly found for temperatures below ambient, while the data approaches $g_K = 1$ for elevated temperatures [23,223], see for example Fig. 21. The straightforward interpretation with hydrogen bonding liquids is that $g_K > 1$ is indicative of parallel alignment of hydroxyl dipoles due to chain-like structures connected by hydrogen bonds. The opposite case, $g_K < 1$, is then understood to reflect a preference for anti-parallel orientation, as would be realized by ring-like structures held together by hydrogen bonding. The general trend of approaching $g_K \approx 1$ at higher temperatures is often associated with the thermally activated breaking of hydrogen bonds, resulting in un-bound and thus orientationally un-correlated individual molecules. If the $g_K(T)$ curves cut through the $g_K = 1$ level (see 5M3H near 200 K in Fig. 21), the interpretation has to be a different one: these situations have been explained by a balance of different hydrogen bonded structures that are characterized by $g_K > 1$ and $g_K < 1$, such that the net macroscopic average for g_K becomes unity [23].

The obvious advantageous feature of a Kirkwood correlation analysis is the access to structural information on the basis of steady state dielectric measurements [224]. However, a recent critical assessment of the use of the Kirkwood–Fröhlich equation has raised the following issues [167]. The value obtained for g_K is very sensitive to the choice of ε_∞, for which values between the permittivity observed at high frequencies and n^2 have been employed [225]. This sensitivity becomes

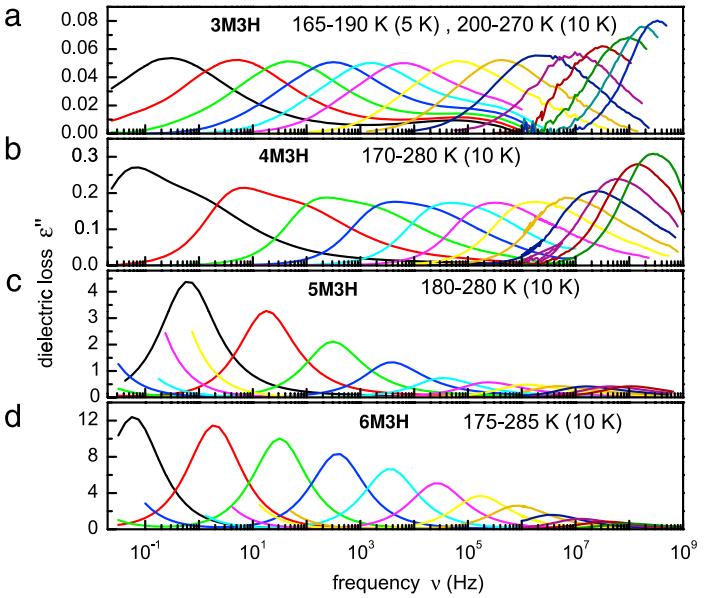

Fig. 18. Dielectric loss spectra of four isomeric octyl alcohols for the temperatures indicated: (a) 3M3H, (b) 4M3H, (c) 5M3H, and (d) 6M3H.
Source: Adapted from [167].

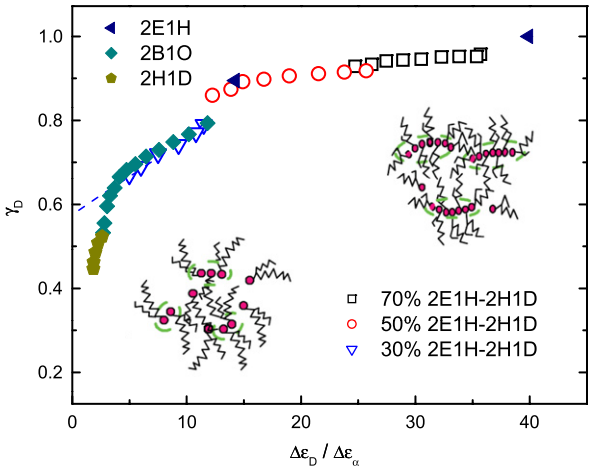

Fig. 19. Dependence of the Cole–Davidson parameter, γ_D, characterizing the Debye-like relaxation (peak I) on the relaxation strength ratio of relaxations I (D) and II (α), $\Delta\varepsilon_D/\Delta\varepsilon_\alpha$, in various glass-forming liquids: 2-ethyl-1-hexanol (2E1H), 2-butyl-1-octanol (2B1O), 2-hexyl-1-decanol (2H1D), and mixtures thereof with the mole fraction of 2E1H indicated in the legend. The inset pictures indicate the possible change in structure when γ_D changes from ≈1 (top right) to ≈0.5 (bottom left).
Source: Adapted from [221]. Courtesy of L.M. Wang.

more pronounced for lower values of the static dielectric constant ε_s, i.e., at elevated temperatures. Moreover, the typical derivation of g_K assumes that the orientational correlation is the same for all modes that are active between the levels of ε_∞ and ε_s, i.e., identical for processes I, II, and III. As process II and III occur on very different time scales relative to the Debye peak, it is likely that the reorientation associated with these modes is not subject to the same g_K. Accounting for $g_K = 1$ for these two fast modes, II and III, can be accomplished by employing the value of $\varepsilon_\infty + \Delta\varepsilon_\alpha + \Delta\varepsilon_\beta$ instead of ε_∞ in the Kirkwood–Fröhlich equation. The resulting effect on $g_K(T)$ for some isomeric octyl alcohols is included in Fig. 21, indicating considerable changes in g_K at the higher temperatures and concomitant differences in the structures derived from these values. An approach that seems more consistent with the multi peaked spectra of alcohols would involve a frequency dependent 'correlation spectrum' $g_K(\omega)$.

In practice, the Kirkwood factor analysis casts $\varepsilon_s(T)$ data into a $g_K(T)$ representation, thereby removing the Boltzmann population effect on the temperature dependence and leaving the non-trivial changes in the structure. Examples for such changes in supramolecular structures are the equilibria of more open and more compact hydrogen bonded structures as discussed by Dannhauser [24]. Provided that a realistic model for the kinetics is available [226,227], $g_K(T)$ data can be used

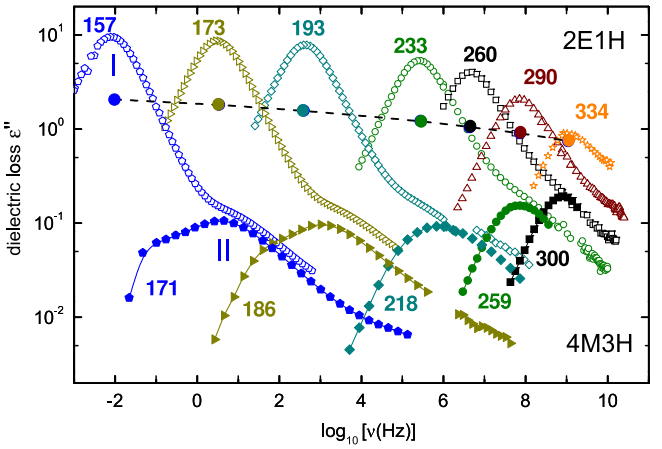

Fig. 20. Compilation of dielectric loss spectra for 2E1H (open symbols, taken from [64]) and 4M3H (filled symbols and lines, taken from [228]) at several temperatures indicated in Kelvin. The similarities between the spectral contribution of process II for the two systems indicate that its amplitude does not depend much on the steric hindrance of the polar group. The dots represent the maximum values for a Debye-like loss with orientational correlations neglected ($g_K = 1$), calculated via Eqs. (6) and (9) using $\rho_{2E1H} = 0.833$ g/cm^3, $M = 130.23$ g/mol, $\mu = 1.7$ D, $\varepsilon_\infty = 2$, and the temperatures that correspond to the 2E1H spectra. The dashed line is a guide for the eye.

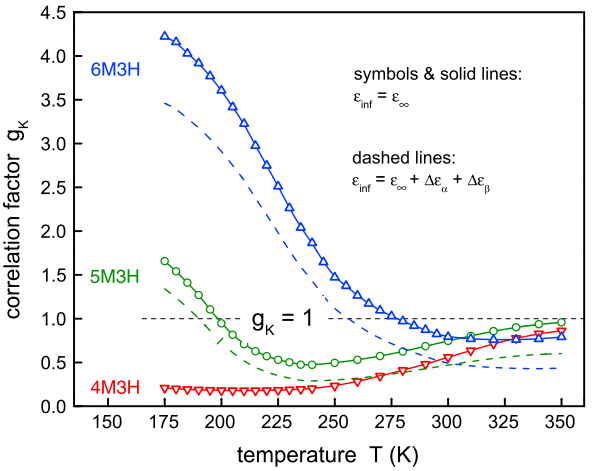

Fig. 21. Kirkwood correlation factors, g_K, versus temperature for the three isomeric octyl alcohols, 4M3H, 5M3H, and 6M3H, as indicated. Symbols and solid lines are based upon using ε_∞ as 'infinite frequency' permittivity (ε_{inf}) within the Kirkwood–Fröhlich relation. Dashed lines refer to the calculation using $\varepsilon_{inf} = \varepsilon_\infty + \Delta\varepsilon_\alpha + \Delta\varepsilon_\beta$.
Source: Adapted from [167].

to derive enthalpies and entropies involved in hydrogen bond formation [23,185], see also Section 4. Such models also yield estimates for the g_K limit for infinitely long chains, which agree with observed values and turn out to settle near 4 for many systems [1,23]. An anomaly near $T = 250$ K of the dielectric constant versus temperature of monohydroxy alcohols has been discussed by Bauer et al. [228], which should also leave a signature in $g_K(T)$ curves.

The pressure dependence of g_K has also been studied, albeit not as extensively as the effect of temperature. Chen et al. have demonstrated that the pressure dependence of the dielectric constant in alcohols is generally dominated by pressure induced changes in the Kirkwood correlation factor, whereas changes in density and molecular dipole moment play minor roles [26,28]. Regarding the magnitude of g_K, it has been observed that g_K increases with pressure p when the ambient value $g_K(p = 100$ kPa) was near unity, but decreases when $g_K(p = 100$ kPa) was closer to its maximum of around 4. This trend appears to be confirmed for a variety of different mono-alcohols in the survey compiled by Böttcher [1], and also for a series of isomeric heptanols [29]. On the basis of the standard assignment of g_K to the various hydrogen-bonded structures (chain multimers when $g_K > 1$, ring multimers when $g_K < 1$, monomers when $g_K = 1$), this systematic pressure dependence suggests the following inequality for the molar volume for a given configuration: $V_{ring} > V_{chain} > V_{monomer}$. As in the case of (hexagonal) ice and water, the development of hydrogen bonded structures reduces the efficiency of dense molecular packing [229].

As for the smaller and higher frequency peak labeled II, Johari and Dannhauser have noted that pressure enhances the amplitude of peak II for a series of isomeric octanols [230]. For pressures $p \leq 400$ MPa, this study revealed that $\Delta\varepsilon_I/\Delta\varepsilon_{II}$,

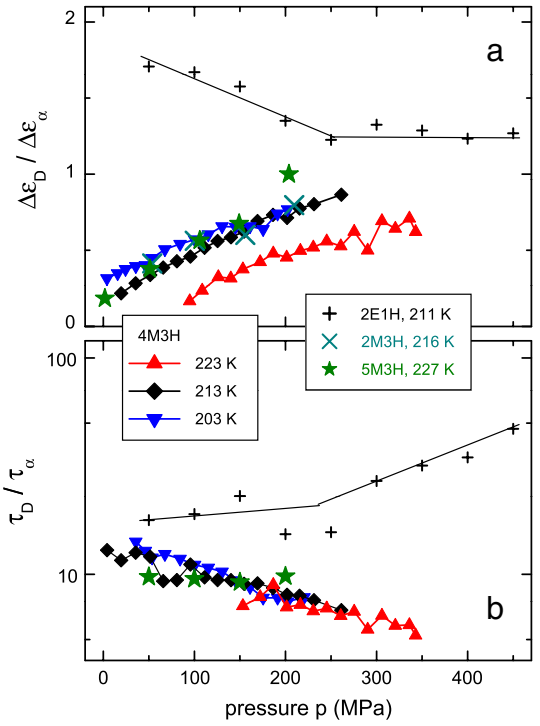

Fig. 22. (a) Pressure dependence of $\Delta\varepsilon_D/\Delta\varepsilon_\alpha$ for 4M3H and for 2E1H reflecting their opposite trends also under isothermal conditions. For comparison, 2M3H and 5M3H data from [230] are also included. To emphasize common trends, $\Delta\varepsilon_D/\Delta\varepsilon_\alpha$ for 2E1H and 2M3H were divided by a factor of 4 and for 5M3H by a factor of 20. Frame (b) displays the pressure dependences of the τ_D/τ_α ratio demonstrating that opposing behaviors are found for the two alcohols 4M3H and 2E1H not only by monitoring static but also dynamic quantities. The temperature independent τ_D/τ_α ratio observed for 5M3H marks an intermediate situation.
Source: Reprinted with permission from [231].

decreases mildly or increases more strongly, depending on whether the magnitude of $\Delta\varepsilon_I/\Delta\varepsilon_{II}$ at ambient pressure is higher or lower, respectively. Based upon measurements of different octanols, a study by Pawlus et al. suggests that the amplitude ratio of peak I and II, $\Delta\varepsilon_D/\Delta\varepsilon_\alpha$, approaches unity when increasing pressure, from below if $g_K(p = 100\ \text{kPa}) < 1$ or from above if $g_K(p = 100\ \text{kPa}) > 1$ [231]. The results demonstrating this qualitatively different behavior of 4M3H and 2E1H is depicted in Fig. 22.

5.4. Temperature dependence of dynamics

In early studies of the effect of temperature on the dielectric relaxation time, the focus was mostly on the prominent Debye peak [3–5,18,232]. Debye's hydrodynamic approach provided a link between viscosity and dielectric relaxation time, $\tau \propto \eta/T$, which has been validated as a crude approximation if the value of the hydrodynamic volume is disregarded [6,7]. Realizing the existence of significant deviations from the hydrodynamic behavior was promoted by data becoming available for the supercooled and very viscous regime, where broadband dielectric measurement accommodated the changes in viscosity by many orders of magnitude.

On the basis of the work of Vogel [233], and the extension into the supercooled regime by Fulcher [234], and Tammann and Hesse [235] (VFT), it was quite expected that the activation map for supercooled alcohols displayed a curvature that suggested a relaxation time divergence at a finite temperature according to the VFT relation,

$$\log \tau\ (T) = A + B/(T - T_0). \tag{12}$$

This super-Arrhenius type behavior was clearly observed not only for non-associating liquids but also for alcohols regarding their prominent Debye peak [232]. A comparison of loss spectra derived from simultaneous dielectric and depolarized photon correlation spectroscopy (PCS) light-scattering measurements confirmed indications that structural relaxation occurs on the time scale of peak II rather than the Debye peak I [47]. This separation of time scales has also been confirmed by Brillouin scattering [236], see also Section 7.1. With the emerging recognition of the relevance of process II for the glass transition phenomenology, more systematic studies of the temperature dependence of all three processes were conducted [47,166,237]. Based on the activation graphs alone, it appears that the temperature dependent time constants of monohydroxy alcohols reflect the canonical behavior of other glass-forming liquids, provided that only process II and III

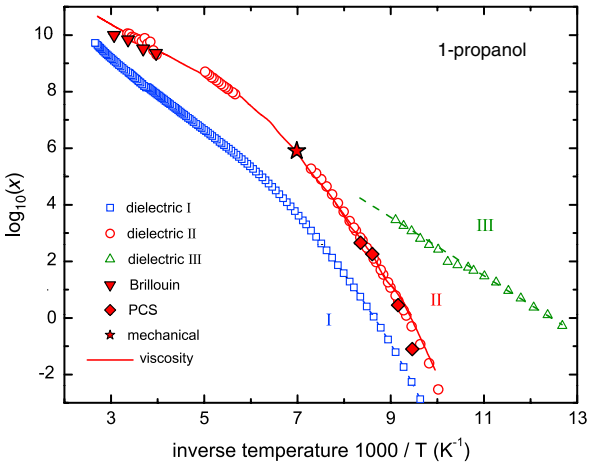

Fig. 23. Temperature dependence of the peak frequency ν_{max} for 1-propanol, defined by the condition $\chi''(\nu_{max}) = \chi''_{max}$, and of the viscosity η. The open symbols refer to the dielectric results ($x = \nu_{max}/\mathrm{Hz}$) for peak I (□), peak II (◯), and peak III (△). The dashed line is an Arrhenius fit to the peak III relaxation data, $\log_{10}(\nu_{max}/\mathrm{Hz}) = 12.9 - 1032\ \mathrm{K/T}$. The solid symbols refer to light scattering data ($x = \nu_{max}/\mathrm{Hz}$), PCS data (diamonds), and Brillouin results (triangles down). The solid line following $\nu_{max}(T)$ of peak II indicates the temperature dependent inverse viscosity ($x = 10^{8.3}\ \eta^{-1}/\mathrm{P}^{-1}$) of 1-propanol taken from literature results, where $\eta^{-1}(T)$ is shifted by 8.3 decades to match the mechanical retardation data point (+).
Source: Adapted from [47].

are considered. For 1-propanol, this behavior is shown in Fig. 23, which includes dielectric relaxation data as well as other indicators of structural relaxation (light scattering, mechanical, viscosity). A more extensive compilation of time scales for 1-propanol with a focus on the high-temperature regime was recently given in [238].

The similarity of peaks II and III to non-associating cases is based upon the correlation of fragility and stretching exponent [47,189], the merging behavior of processes II and III [47,166], as well as the correlation of peak II with enthalpy and dominant mechanical dynamics, see Sections 4 and 7.1. Building on the ideas of Kauzmann's kinetic approach to dielectric relaxation [239] and the environmental fluctuation of Anderson and Ullman [204], such a decoupling of 'dipolar reorientation' from the faster structural relaxation was already noted by Johari and Dannhauser [230]. Note, however, that the amplitude of peak II is much below the value expected for the complete orientational correlation decay of the molecular dipole [47,219]. As a result, peak II should be viewed as a signature of the dynamics of structural relaxation, with the degrees of freedom of molecular motion being constrained by the involvement of the OH dipole in hydrogen-bonded multimers.

In some instances, it seems that the Debye process (peak I) would trace the temperature dependence of peak II (and thus of structural relaxation) with a temperature invariant offset. A survey of many monohydroxy alcohols indicates that this is generally not the case. The separation between peak I (τ_D) and peak II (τ_α) displays a variety of behaviors as a function of temperature, and a tendency towards a uniform ratio of $\tau_D/\tau_\alpha \approx 100$ has been suggested [48]. As evident from Fig. 24, more recent data is consistent with a further approach to $\tau_D \approx \tau_\alpha$, but uncertainties in delineating the spectral position of peak II at these conditions can be high [238].

In any case, the activation trace of the Debye peak, $\log\tau_D$ versus $1/T$, displays an inflection point in the range of nanosecond dynamics [63], as shown in Fig. 25. For a given compound, it is observed that the peak separation in terms of τ_D/τ_α increases with a decreasing amplitude ratio $\Delta\varepsilon_D/\Delta\varepsilon_\alpha$, regardless of whether temperature [64], pressure [231], or steric hindrance [228] is at the source of modifying the ratio. Comparing τ_D/τ_α ratios for different alcohols, a trend of large spectral separation for the higher g_K systems has been reported [167].

5.5. Pressure dependence of dynamics

For five different octanols, Johari and Dannhauser have characterized the pressure dependence of the dynamics in the range $p \leq 400$ MPa for various temperatures, with the Debye peak time constant varying between 10^{-8} and 10^{-3} s [230]. For each compound the variation of $\ln\tau_D$ with T or p was approximated by an activation energy and an activation volume, respectively. Isochronal graphs of T versus p yield practically the same slopes for all systems, consistent with pressure shifts of kinetically defined transition temperatures around $dT_g/dp = 100$ K/GPa. Molar activation volumes for processes I and II are similar and range from about 20 to 60 cm^3. The large activation volumes led the authors to conclude on the highly cooperative nature of reorientation associated with the Debye process.

The effect of changing temperature on the position of $\ln\tau$ versus g_K isotherms divides the alcohols into the low g_K and high g_K classes. This has been demonstrated convincingly by Vij, Scaife, and Calderwood, providing the data for the Debye type peaks compiled in Fig. 26 [30]. Each set of curves associated with one letter is for one compound, and changes in τ and g_K within a curve originate from pressure variations. In the majority of cases, elevated temperatures shift the isotherm towards a decreased $\ln\tau$ and increased g_K position for low g_K materials, while the directions of changes are opposite for

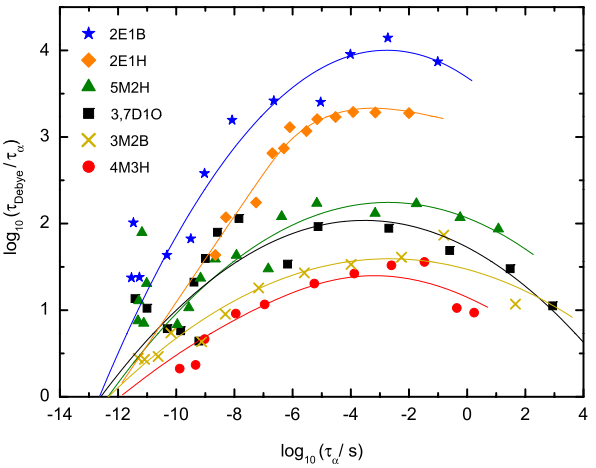

Fig. 24. The logarithmic time scale decoupling ratio $\log_{10}(\tau_D/\tau_\alpha)$ is plotted versus the structural relaxation time, $\log_{10}(\tau_\alpha/\mathrm{s})$. Here data for 2-ethyl-1-butanol, (2E1B), 2-ethyl-1-hexanol (2E1H), 5-methyl-2-hexanol (5M2H), 3,7-dimethyl-1-octanol (3, 7D1O), 3-methyl-2-butanol (3M2B), and 4-methyl-3-heptanol (4M3H) are included. For each substance, the decoupling is maximum when $\tau_\alpha \approx 10^{-4}$ s. An extraordinarily large maximum ratio of about 10^4 is exhibited by 2E1B. The solid lines are meant as guides only.
Source: Reprinted with permission from [228].

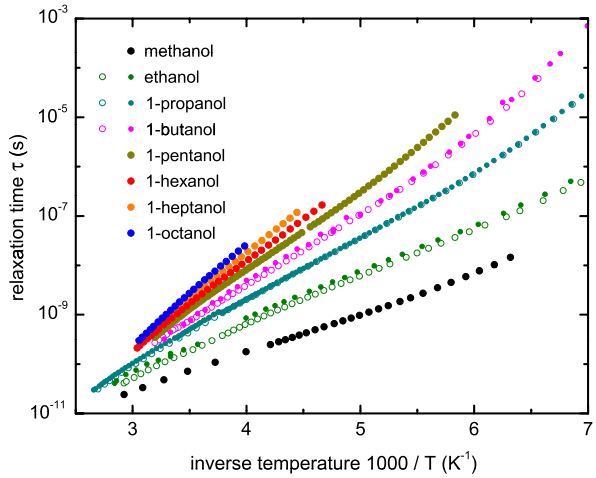

Fig. 25. Arrhenius plot for the Debye relaxation times of various monohydroxy alcohols published previously. At the highest temperatures all log τ_D versus $1/T$ curves exhibit an inflection point.
Source: Based upon the data cited in [63] from which this figure was adapted.

the higher g_K systems. The positive $\ln\tau$ vs. g_K correlation observed for each curve has been understood as reflecting Debye's model, $\tau = 4\pi a^3\eta/kT$, cf. Section 7.3, with both the hydrodynamic volume ($\propto a^3$) and the correlation factor g_K increasing with number n of correlated (i.e., hydrogen bonded) monomers.

More recent pressure studies have looked into the relation of peaks I and II as a function of pressure. For 2-ethyl-1-hexanol (2E1H), Fragiadakis and coworkers have reported that the relaxation times and intensities of peaks I and II become more equal with increasing pressure [58]. A detailed assessment of the same alcohol by Reiser et al. has shown that isochronal scaling is violated, i.e., the position of one peak does not determine the shape of the entire loss spectrum [240]. The authors concluded on a pressure induced transition to shorter linear chains and further to individual molecules. Another study of 2E1H observed that $\tau_D(T)$ approaches the fragility of $\tau_\alpha(T)$ with increasing pressure, and that the Debye peak widens [241]. Similar behavior is found for 5-methyl-2-hexanol according to Pawlus et al.: the Debye peak widens from 1.14 decades at 0.1 MPa to 1.3 decades at 780 MPa, $\tau_D(T)$ becomes more curved with increasing pressure, and peaks I and II are being merged into one dominant process for $p > 500$ MPa [242].

In a recent pressure investigation of alcohols conducted by Pawlus et al., the spectral separation of peaks I and II, τ_D/τ_α, has been confirmed yet another quantity that separates alcohols into low and high g_K classes [231]. The ratio τ_D/τ_α was found to decrease from above 10 to about 5 with increasing p (0.1–350 MPa) for 4M3H at the temperatures $T = 203$, 213, and 223 K. By contrast, 2E1H at $T = 211$ K is subject to an increase in τ_D/τ_α from approximately 20 to 70 when pressure is

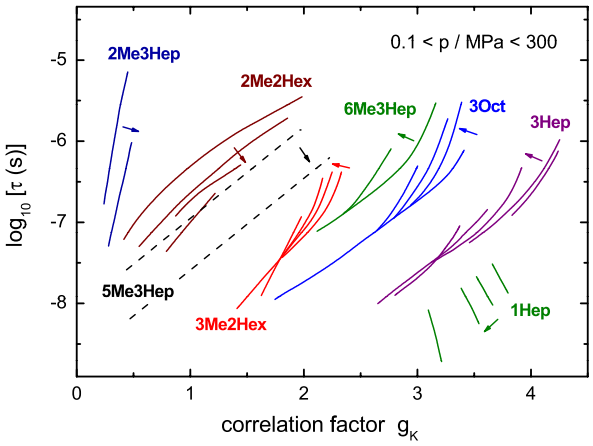

Fig. 26. Isotherms of Debye time constants in terms of the logarithm of τ versus Kirkwood correlation factor g_K for a variety of heptanol and octanol isomers. Arrows indicate shifts of the isotherms resulting from an increase in temperature. Changes within a curve are the result of pressure variations in the range 0.1–300 MPa. Temperatures increase in the direction of the arrows. For compounds and temperatures see the original publication.
Source: Adapted from [30].

changed from 50 to 550 MPa. These effects are included in Fig. 22. The intermediate high-pressure behavior of 5M3H was re-examined recently [243].

5.6. Nonlinear techniques

Early studies of nonlinear dielectric effects (NDE) of alcohols have been conducted by Małecki [244,245] and by Piekara [246]. At the time, reductions in permittivity or polarization were termed 'negative saturation', while field induced increases were referred to as 'positive saturation'. Later Małecki [247] assigned the labels 'Langevin' and 'chemical' effects to these features, respectively. In the context of pure alcohols, Piekara interpreted the increase of $\Delta\varepsilon$ as field induced proton shift of alcohol dimers (a shift of the proton along the O–H $\cdots$ O bond, equivalent to the occurrence of a large polarizability), where the high field is understood to change the equilibrium constant towards the proton shifted dimers with higher dipole moment [246].

More recently, high-field impedance spectroscopy on monohydroxy alcohols revealed a similar 'chemical effect', i.e., a field induced increase of the dielectric constant [70]. For 5-methyl-3-heptanol (5M3H) at temperatures around 200 K, it was found that a sinusoidal field with peak amplitude $E_0 = 170$ kV/cm raised ε_s by several percent. The compound 5M3H was chosen for this study because its Kirkwood correlation factor changes from 1.6 to 0.4 when the temperature is increased from 185 K to 215 K. This unusual temperature sensitivity of g_K was reported by Dannhauser and explained by a shift in the equilibrium constant, $K_{r/c}$, that governs the balance between compact ring-like structures with $g_K \approx 0$ and more open chain-like structures with $g_K \gg 1$ [23]. The $g_K \approx 1$ situation for 5M3H near $T = 200$ K suggests comparable free energies for the two species involved, leading to the expectation of a considerable field dependence of $K_{r/c}$ via a field induced change in the free energy of the polar chain-like species, while the free energy of the nonpolar rings remains field invariant.

An important feature of the high-field impedance spectroscopy NDE study on 5-methyl-3-heptanol is the broadband character of the experiment ranging from 0.1 Hz to 50 kHz. As depicted in Fig. 27, the relative increase in the field dependent permittivity, $(\varepsilon'_{hi} - \varepsilon'_{lo})/(\varepsilon'_{lo} - \varepsilon_\infty)$, is practically frequency independent for frequencies below the loss peak value of the (linear response) Debye process. The observation suggests that the field induced conversion from ring- to chain-like structures occurs on the time scale of the Debye process, instead of this change of the equilibrium constant proceeding at a slower rate.

Subsequent high field experiments have supported this interpretation of the field induced shift of $K_{r/c}$ by assessing the sensitivity of ε_s to the field as a matter of the g_K of the liquid [167]. It turned out that the highest field driven increases of the dielectric constant are obtained for alcohols with a correlation factor near unity. For other cases displaying $g_K \ll 1$ or $g_K \gg 1$, the sensitivity of ε_s to the large-amplitude excitation was reduced, consistent with the field induced change in the free energy of chain-like structures having little effect when $K_{r/c}$ is much above or below unity. In all cases, the midpoint of the decrease of the field induced effect (see Fig. 27) occurred at a frequency $\omega = 2/\tau_D$, where τ_D is the time constant of the Debye peak.

A very different type of non-linear dielectric experiment is based upon the energy that is transferred irreversibly from an electric field of sufficient amplitude to a sample. For a given applied field, $E(t) = E_0 \sin(\omega t)$, the power density absorbed by the material is $p = \varepsilon_0 E_0^2 \omega \varepsilon''(\omega)/2$, with the absorbance quantified by the dielectric loss ε'' at the frequency of the external field [183]. In non-associating liquids, the resulting non-linear dielectric effects have been modeled successfully by assuming that the absorbed energy increases the configurational temperature, T_{cfg}, to a steady state value determined by $T_{cfg} = T + \varepsilon_0 E_0^2 \Delta\varepsilon / (2\rho \Delta C_p)$. Via the apparent activation energy of the overall dynamics, E_A, the increase in T_{cfg} results

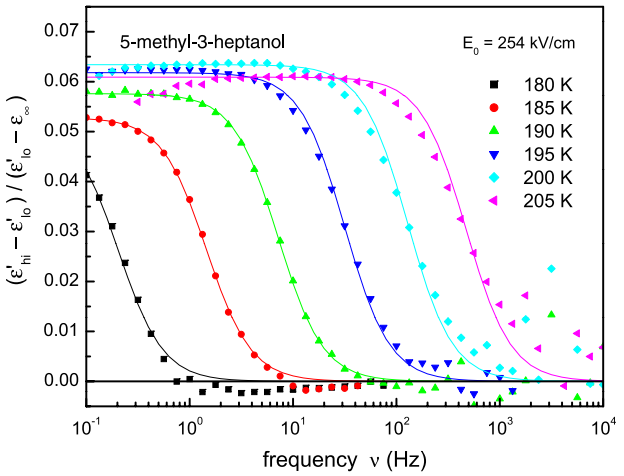

Fig. 27. Field induced relative increase of the non-instantaneous contribution to the permittivity versus frequency, calculated as $(\varepsilon'_{\rm hi} - \varepsilon'_{\rm lo})/(\varepsilon'_{\rm lo} - \varepsilon_\infty)$ for 5M3H. Here, 'hi' and 'lo' refer to a field of $E_0 = 254$ kV/cm and $E_0 = 14$ kV/cm, respectively. Different curves are for different temperatures as indicated. Lines are fits according to a Debye type frequency dependence.
Source: Adapted from [167].

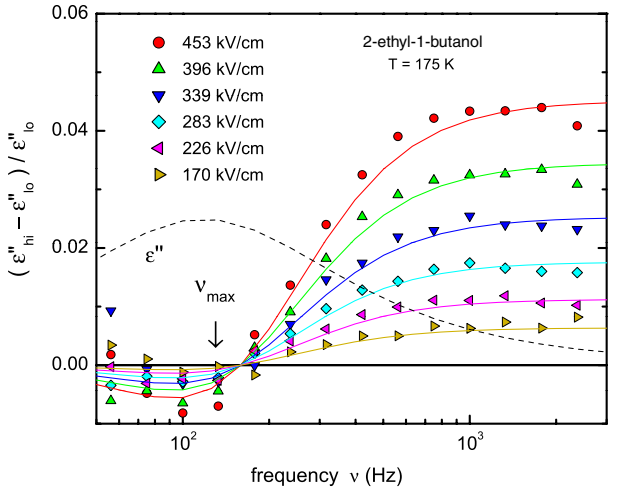

Fig. 28. Experimental results (symbols) for the field induced relative change of the loss, $\Delta \ln \varepsilon''$, versus frequency ν for 2-ethyl-1-butanol at $T = 175$ K. The curves are recorded at different fields E_0 as indicated, and evaluated relative to a low-field reference using $E_0 = 14$ kV/cm. The dashed line indicates the loss profile ε'' using arbitrary units, the arrow marks the position $\nu_{\rm max}$ of the loss peak. The lines are calculations using Eq. (13) with $t \to \infty$.
Source: Adapted from [183].

in a reduction of the relaxation time constants, which in turn modifies the dielectric loss at a given frequency. For a typical high $g_{\rm K}$ type alcohol, the prominent Debye peak dominates the dielectric behavior and the field induced change can be approximated by

$$\frac{\varepsilon''_{\rm hi} - \varepsilon''_{\rm lo}}{\varepsilon''_{\rm lo}} = \frac{E_{\rm A}}{k_{\rm B}T^2}\,\frac{\varepsilon_0 E_0^2 \Delta\varepsilon}{2\rho\Delta C_p}\,\frac{\tau_T}{\tau_{\rm D}}\,\frac{\omega^4\tau_{\rm D}^4 - \omega^2\tau_{\rm D}^2}{\left(1+\omega^2\tau_{\rm D}^2\right)^2} \times \left(1 - e^{-\frac{t}{\tau_T}}\right), \tag{13}$$

where subscripts 'hi' and 'lo' refer to the high-field amplitude E_0 and the zero-field limit, respectively. In this equation, $\Delta C_{\rm p}$ is the (glass to liquid) step in the configurational heat capacity, ρ is the density, $\tau_{\rm D}$ is the Debye dielectric time constant, and $\tau_{\rm T}$ is the 'thermal relaxation time' [180]. The latter time constant represents the dynamics of approaching the new equilibrium, which is offset from its linear response counterpart by the continuous flow of energy from the slow degrees of freedom to the phonon bath. Because internal energy flow is reversed compared with a standard calorimetry experiment, this technique has been coined reverse calorimetry [174,248]. The meaning of $\tau_{\rm T}$ is very similar to a time constant gauging enthalpy relaxation, physical aging, or true structural relaxation [249], but it is obtained at a constant sample temperature [250].

Steady state spectra of the field induced relative increase of ε'' are compiled graphically in Fig. 28, and the curves are well approximated by Eq. (13) in the limit of $t \to \infty$. Similar spectra have been reported for 1-propanol, but for a much wider range of frequencies that includes the alpha and beta peaks [251]. Expectedly, the magnitude of the effect is linear

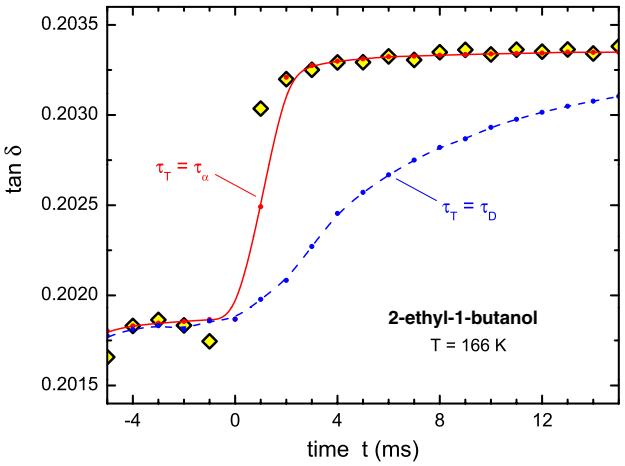

Fig. 29. Experimental results (symbols) for the time resolved loss factor, $\tan\delta$, measured at $\nu = 1$ kHz for the transition from a low (91 kV/cm) to a high (453 kV/cm) field for 2-ethyl-1-butanol at a temperature of $T = 166$ K, where $\nu_{\max} = 20$ Hz. The duration for the low and high fields is 8 and 16 periods, respectively. The sample was equilibrated at zero field for times $t < -8$ ms. The solid and dashed lines are model calculations assuming a thermal relaxation time that is much faster and matching the dielectric Debye time scale, respectively.
Source: Adapted from [183].

in the energy, i.e., quadratic in the external electric field. Time resolved high-field impedance measurements can probe the equilibration process that follows $\left(1 - e^{-t/\tau_T}\right)$, the time dependent term in Eq. (13), by evaluating the dielectric properties for each period prior and subsequent to a change in the field amplitude at time $t = 0$ [182]. An example of the result of such an experiment is depicted in Fig. 29 for 2-ethyl-1-butanol at $T = 166$ and 172 K, showing that the steady state high-field plateau of $\tan\delta$ is reached after about 3 periods only. Assuming that the relevant 'thermal' relaxation (τ_T) occurs on the Debye time scale leads to the dashed lines in Fig. 29, which clearly equilibrates much too slow compared with the observed data for both temperatures and the resulting peak frequencies, $\nu_{\max} = 20$ and 100 Hz. However, if the configurational temperature is assumed to approach its steady state value on the time scale of peak II, then model and observation agree as indicated by the solid lines in Fig. 29. While these experiments do not provide a quantitative answer regarding the spectral separation of τ_D and τ_α, they deliver yet another piece of evidence for structural relaxation being much faster than the time constant of the prominent Debye peak in monohydroxy alcohols.

6. Optical methods probing supramolecular relaxations

There are numerous optical methods capable of probing liquid dynamics, with Brillouin light scattering, photon correlation spectroscopy (PCS), optical depolarization, dipolar and mechanical solvation dynamics, and Kerr effect studies being a few examples. In the present section we will discuss only those methods that have been demonstrated to probe the supramolecular relaxation involved in alcohol dynamics: dipolar solvation dynamics and electro optical Kerr effect experiments. While PCS has the potential to detect the Debye-like relaxations, see Section 10, for monohydroxy alcohols the signal associated with this mode may be insufficient for its straightforward detection, and no PCS signature of the Debye peak in monohydroxy alcohols has been reported to date.

6.1. Dipolar solvation dynamics

In optical spectroscopy, the Stokes shift refers to the spectral separation of absorption and emission energy levels, which are determined by the extent of solvation of the ground and excited electronic states involved. For dipolar solvation (opposed to ion or mechanical solvation, see Section 7.2), the decisive quantities are the electrostatic interactions between the permanent dipoles of the solute in the ground (μ_G) and excited (μ_E) state with the polar solvent, characterized by its wavevector and frequency dependent permittivity $\varepsilon(\vec{k}, \omega)$ [252]. In response to an instantaneous excitation of the solute, the transition $\mu_G \rightarrow \mu_E$ will alter the local field of the solute dipole, initiating a polarization response in the solvent and thus a dynamical aspect to the Stokes shift. By recording the emission spectra as a function of time, the time dependent characteristic wavenumber, $\langle\bar{\nu}(t)\rangle$, as well as its limiting values for $t \rightarrow 0$ and $t \rightarrow \infty$ are derived, leading to the so-called Stokes-shift correlation function,

$$C(t) = \frac{\langle\bar{\nu}(t)\rangle - \langle\bar{\nu}(\infty)\rangle}{\langle\bar{\nu}(0)\rangle - \langle\bar{\nu}(\infty)\rangle}. \tag{14}$$

This dynamical aspect of the Stokes shift indicates how solvent polarity evolves with time after excitation. One can also think of this experiment as an optically detected dielectric polarization experiment, but with two main differences compared

with the macroscopic capacitor counterpart: First, the electric field is that of a local dipole instead of being macroscopically homogeneous, which requires accounting for the wavevector dependence $\varepsilon\left(\vec{k}, \omega\right)$ rather than the macroscopic limit, $\vec{k} \to 0$. Second, the charge distribution on the solute is largely independent of the progress of polarization, and the observed quantity is linearly related to the change of the local field, $\Delta \langle \bar{\nu}(t) \rangle \propto \vec{\mu} \Delta \vec{E}(t)$. As a result, the Stokes shift correlation function $C(t)$ is more akin to the dielectric modulus $M(t)$ that it is to $\varepsilon(t)$ [253].

Monohydroxy alcohols have been common solvents in the study of solvation dynamics using fluorescent probes whose excited state lifetimes limit the observation time window to several nanoseconds [52,254,255]. Compared with non-associating liquids, the energy levels in alcohols are offset from the typical correlation of solvent polarity (as obtained by optical probes) and estimates of the solvation free energy based on dielectric continuum models. This is assumed to reflect hydrogen bonding as additional source of solvation [52]. However, the magnitude of the dynamical Stokes shift aligns well with the dielectric continuum expectations [52].

Regarding the solvation time scales, alcohols did not display unexpected deviations from their aprotic counterparts when comparing solvation dynamics and dielectric time scales based upon the prominent Debye peak I [52]. However, the solvation times in normal alcohols were reported to be exceptionally slow compared to those of polar aprotic liquids when compared relative to probe rotation times that sense local viscosities [256], another manifestation of the spectral separation of peaks I and II.

Solvation dynamics of supercooled alcohols can be studied using longer lived triplet probes [257,258]. As in the case of fast dynamics, the magnitude of the dynamical Stokes shift, $\langle \bar{\nu}(0) \rangle - \langle \bar{\nu}(\infty) \rangle$, is similar for alcohols and polar aprotic liquids of comparable dielectric constants. Accordingly, the amplitudes of only peaks II and III would fail to explain the large solvation shifts observed for monohydroxy alcohols. As expected for the viscous state of glass-forming monohydroxy alcohols near T_g, the separation of the solvation time scale from structural relaxation is much more pronounced. In fact, as elaborated upon in Section 7.2, the spectral separation of mechanical and dipolar solvation matches the factor of 25 derived for the time scale ratio of peak I and II in terms of the modulus, $M''(\omega)$, of 1-propanol [259]. Another interesting feature of that study is that the stretching exponents β were practically the same for mechanical and dipolar solvation, whereas the Debye nature of peak I would let one expect a less dispersive Stokes-shift correlation function for the dipolar solvation that senses the electrostatic interactions. An example based on quinoxaline as probe in 2-ethyl-1-hexanol is shown in Fig. 30, which compares solvation dynamics in terms of $C(t)$ with the single-particle probe rotation correlation function, $r(t)/r_0$. This probe rotation result is derived from optical depolarization data of the chromophore quinoxaline, measured simultaneously with the solvation dynamics [258]. Both decays are separated only by a factor of five on the time scale, but recall that $C(t)$ is closer to $M(t)$ than $\varepsilon(t)$, with the latter decays differing by another factor of about ten. Interestingly, the stretching exponents of the Kohlrausch fits are equal, $\beta = 0.58$, for both the solvation and rotation decays. The difference in the $C(t)$ curves as a matter of polarization angle provides evidence of dynamic heterogeneity and a local correlation between solvation and probe rotation times. This observation suggests that the process responsible for the prominent polarization with Debye character in monohydroxy alcohols is not a single exponential response if probed on a molecular level.

6.2. Electro-optical Kerr effect

The Kerr effect is based upon the generation of optical birefringence as a result of anisotropic orientation of molecules with respect to their electronic polarizabilities. For the optical Kerr effect (OKE) or derivatives thereof, see Section 9.4, it is an intense light source that induces birefringence that facilitates the measurement of the correlation decay of polarizability anisotropy [260]. By contrast, it is an externally applied electric field E that creates refractive index anisotropy in case of the electro-optical Kerr effect (EOKE). For moderate field amplitudes E, typically $E \leq 100$ kV/cm, the induced average orientation is proportional to the field, $\langle \cos\theta \rangle \propto E$, for liquids that possess inversion symmetry in the absence of an external field. The relevant projection for a change, Δn, in the refractive index is the second-order Legendre polynomial, $P_2(\cos\theta) = \frac{1}{2}\left(3\cos^2\theta - 1\right)$, resulting in an overall quadratic field dependence of the EOKE, $\Delta n \propto E^2$ [51].

Experimental results based on the EOKE in monohydroxy alcohols have been reported for 2-ethyl-1-hexanol by Coelho and Manh [50] and for 6-methyl-3-heptanol by Crossley and Williams [51]. In both cases, a comparison with the dielectric relaxation time of peak I is made, and the rise and fall times of the optical birefringence coincide with the dielectric Debye time of the alcohol. Although both dielectric and optical time scales reflect collective dynamics, their coincidence is not trivial and it may reflect that the optical anisotropy is largely linked to the orientation of the OH bond [261,262]. The case of 2-ethyl-1-hexanol is outlined in Fig. 31 in terms of a relaxation map, and the Kerr effect is clearly governed by the Debye time scale. If all processes involved were diffusive, the Kerr time scales (rank $\ell = 2$) would be expected to be a factor of three faster than the dielectric (rank $\ell = 1$) polarization times, but this does not seem to be the case.

7. Viscoelasticity and molecular transport

7.1. Mechanical relaxation

There is a host of techniques that allows one to explore the mechanical relaxation of monohydroxy alcohols in a broad range of frequencies. Experiments on liquid monohydroxy alcohols were performed using shear relaxation methods for

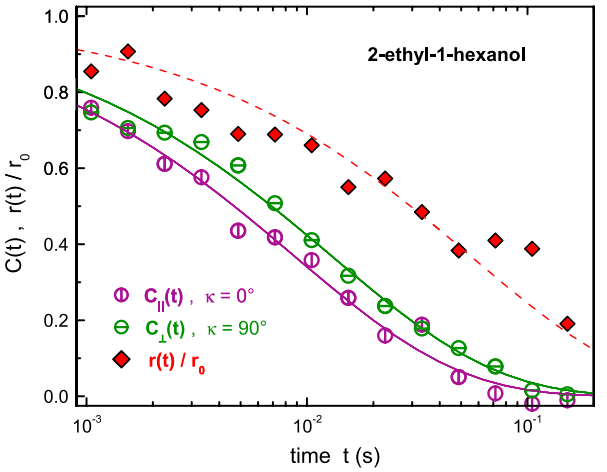

Fig. 30. Solvation and probe rotation dynamics of quinoxaline (QX) in 2-ethyl-1-hexanol (2E1H), measured simultaneously at $T = 160.0$ K using a 308 nm excitation source. Open symbols refer to the Stokes shift correlation function $C(t)$ measured at the angles $\kappa = 0^\circ$ and $\kappa = 90^\circ$ as indicated. Solid diamonds refer to the probe rotation correlation function $g_2(t) = r(t)/r_0$ as derived from the solvation data. The lines are stretched exponential ($\beta = 0.58$) fits with $\tau_{sol} = 8.8$ ms for $C(t)$ with $\kappa = 0^\circ$, $\tau_{sol} = 13$ ms for $C(t)$ with $\kappa = 90^\circ$, and $\tau_{rot} = 56$ ms for $r(t)/r_0$.
Source: Adapted from [258].

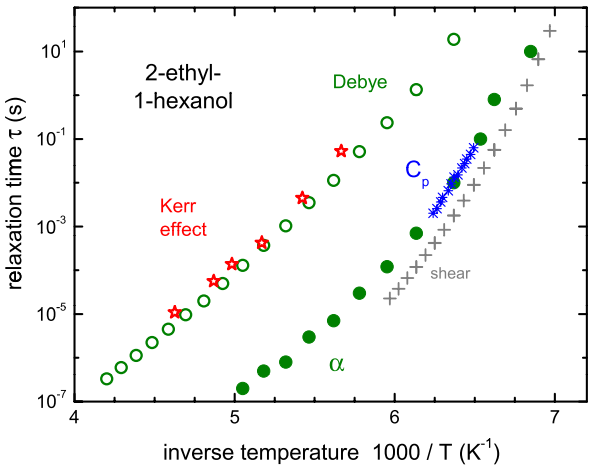

Fig. 31. Relaxation time map for 2-ethyl-1-hexanol including dielectric relaxation times for peak I (open circles) and peak II (solid circles), electro-optical Kerr effect data (stars) [50], dynamic heat capacity time scales (crosses) [37], and shear modulus times (plus signs) [40].
Source: Adapted from [210].

$\nu < 1$ MHz [40] and ultrasonic measurements in the MHz to GHz range [38,39,41,263–265]. Brillouin scattering and other light scattering techniques [47,236,266–271] as well as inelastic neutron scattering [272,273] and inelastic X-ray scattering [274] were employed in this context at typically still higher frequencies.

The frequency dependent mechanical relaxation of monohydroxy alcohols was in the scientific focus early on. This is exemplified by a 1956 ultrasonic study of 1-propanol [38]. It covered almost 2 decades (from 1 to 82 megacycles) and the temperature range from 0 to −155 °C and was motivated by the prior finding that the dielectric relaxation of this monohydroxy alcohol is single exponential [18]. However, the measurement of the mechanical modulus showed convincingly that a proper description of the data requires the assumption of a broad distribution of relaxation times. Interestingly, the authors of the 1956 ultrasonic work noted that the theoretical expression used for describing their data was "nearly identical in form with the distribution calculated … from the stress relaxation data on polymers".

The finding of a non-exponential main mechanical relaxation in the supercooled liquid state was later confirmed by several authors [40,263,275]. However, the idea that the existence of hydrogen-bonded supramolecular structures could enhance the mechanical rigidity of monohydroxy alcohols was obviously dismissed for a long time. Another remarkable finding was that the time scale of the most prominent dielectric response is much slower than the mechanical relaxation [39]. As a recent example, in Fig. 32 we show a shear mechanical loss spectrum $G''(\omega)$ of 2E1H recorded at 160 K [40] and compare it with corresponding dielectric data in the susceptibility format as well as in modulus form [276].

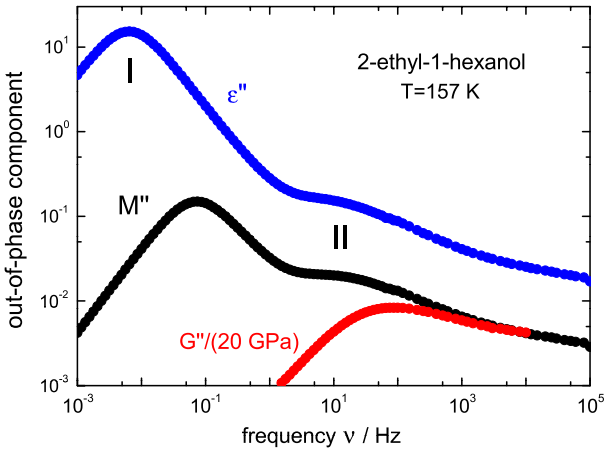

Fig. 32. Frequency dependent loss components of the shear mechanical modulus G'' compared with those of the dielectric modulus, $M'' = \varepsilon''^2/(\varepsilon'^2+\varepsilon''^2)$ and of the dielectric permittivity ε''. All results refer to 2E1H and 157 K.
Source: Data were taken or calculated from the work of Jakobsen et al. [40].

The mechanical data clearly reveal the structural relaxation, but no peak is seen in the $G''(\omega)$ spectra at frequencies corresponding to that of the dielectric Debye peak. In the words of Jakobsen et al. [40] "a shear-mechanical relaxation process corresponding to the Debye-type process in the dielectrics must have a relaxation strength below 5 MPa (corresponding to at most 1% of the full relaxation strength) if it exists". Such an additional shear mechanical feature was certainly expected to show up on the low-frequency side of the main peak in the shear mechanical spectra.

In fact, near ambient temperatures an additional low-frequency feature was identified in a broadband (0.3 to 3000 MHz) ultrasonic relaxation study of several monohydroxy alcohols [41]. As an example, Fig. 33(a) shows a spectrum of the acoustical excess absorption, $\alpha_{\rm exc}\lambda$, for 1-dodecanol at 25 °C. "Excess" means that the trivial background absorption ($\propto \nu^2$) was already accounted for. The variable λ denotes the acoustical wavelength within the sample [277]. The main peak appearing at frequencies of a few GHz was attributed to collective modes that stem from the isomerization of the alkyl chain [41]. The assignment of the high-frequency process in Fig. 33(a) was motivated by the expectation that in 1-dodecane and other alkanes trans-gauche isomerization processes will contribute to the acoustical absorption [278,279]. 1-dodecane data are included in Fig. 33(a) as well and confirm this expectation. Interestingly, on the low-frequency flank of the acoustical excess absorption spectrum of 1-dodecanol another process can be resolved [280]. This relaxation which is ∼7 times slower and ∼10 times weaker than that leading to the main peak was assumed to reflect chiefly the rate at which an equilibrium is established within the liquid between alcohol molecules existing as monomers and those in hydrogen bonded clusters. Ultrasonic absorption spectra featuring two relaxation processes near room temperature were reported for a range of other branched and unbranched monohydroxy alcohols [41].

Very recently, related low-temperature observations were made in the sub-kHz frequency range for various branched alcohols [42,243]: In Fig. 34(b) we show data on 2E1H, 5M3H, and 4M3H in terms of the frequency dependent viscosity $\eta'(\nu) = G''(\nu)/(2\pi\nu)$. In order to compare with liquids devoid of a dielectric Debye process we scaled that data using η_α. Here, the index α refers to process II, cf. Fig. 32. According to the Maxwell relation $\eta_\alpha = G_\infty/(2\pi\nu_\alpha)$ is given by the peak frequency ν_α of the mechanical loss spectrum and by the high-frequency shear modulus G_∞. In the plot of $2\pi\nu_\alpha\eta'(\nu)/G_\infty$ vs. ν shown in Fig. 34(b) a two-step behavior is clearly resolved. For 2E1H the enhancement of the shear viscosity is about tenfold for temperatures near 160 K [42]. This enhancement is slightly larger than the one noted when comparing the low- and high-frequency shear viscosities, denoted $\eta_{\rm s0}$ and $\eta_{\rm s\infty}$, respectively, near room temperature [41]. For several branched and unbranched monohydroxy alcohols $\eta_{\rm s0}$ and $\eta_{\rm s\infty}$, are reproduced from [41] in Fig. 34(a) as a function of the number n of carbon atoms in the alkyl chain. While $\eta_{\rm s0}$ displays a systematic increase with n, known from previous studies [281], $\eta_{\rm s\infty}$ is essentially independent of the length of the alkyl chain. Correspondingly, very small differences of $\eta_{\rm s0}$ and $\eta_{\rm s\infty}$ are expected to show up also for short-chain alcohols. Indeed, a close inspection of the master plot for 1-propanol (see Fig. 6 in [38]) reveals a small kink on the low-frequency side of its $M''(\omega)$ peak.

Regarding the interpretation of the low-frequency mechanical response of monohydroxy alcohols it was suggested that it reflects fluctuations of hydrogen bonded clusters, along the lines mentioned above [41]. More recently, the pronounced increase of the viscosity towards low frequencies seen in Fig. 34(b) was found suggestive of supramolecular polymeric behavior, at least in 2E1H [42]. Supramolecular polymers are an exciting class of materials held together by weak to intermediately strong intermolecular forces such as mediated by metal coordination, by π–π interactions, and, particularly relevant in the present context, by hydrogen bonding [282]. Depending on the details of that bonding the formation of mesoscopic (∼μm sized) structures has been reported that in many cases are stable near room temperature [283,284]. Analogies to monohydroxy alcohols were stressed in a study of a triply hydrogen bonded supramolecular polymer, which also features a strong mono-exponential dielectric relaxation [285]. It appears that monohydroxy alcohols are member of

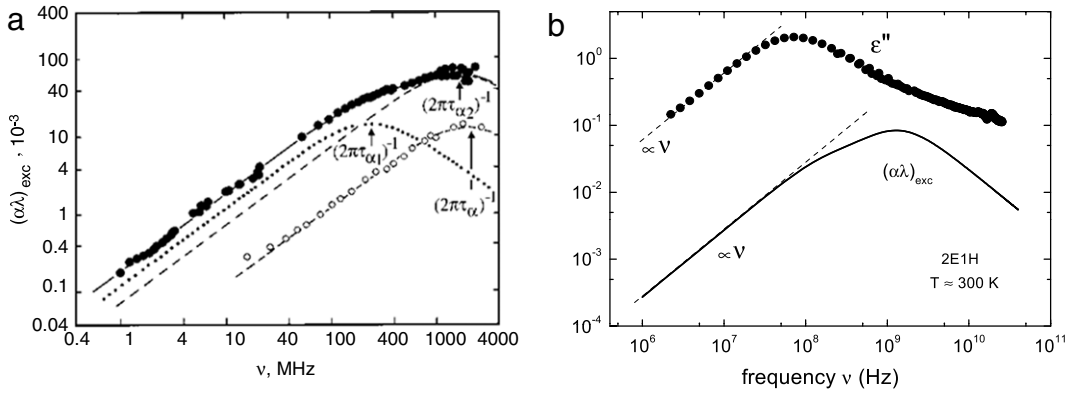

Fig. 33. (a) Ultrasonic excess absorption spectra of 1-dodecanol and 1-dodecane measured at 25 °C. (b) Comparison of dielectric loss (symbols [64]) and acoustical spectra (solid line [41]) of 2E1H, both recorded near room temperature.
Source: Reprinted with permission from Ref. [41].
© 2001, American Chemical Society.

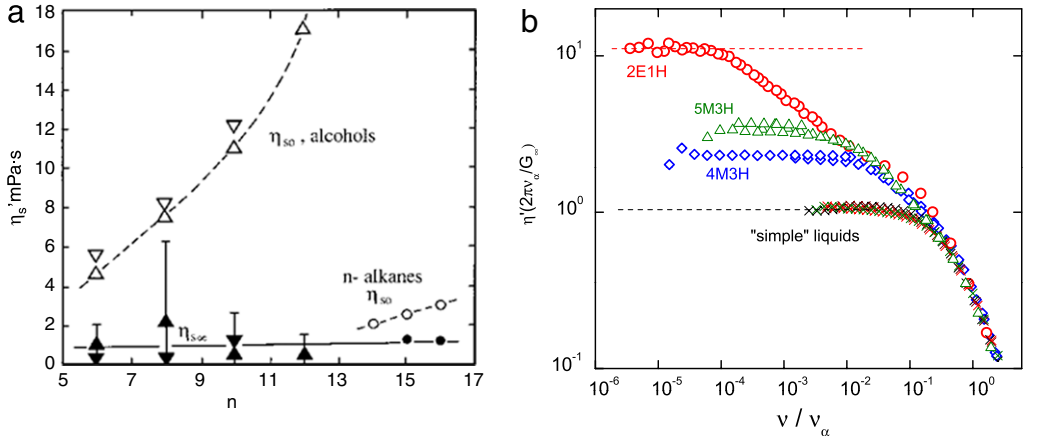

Fig. 34. (a) Comparison of static shear viscosity η_{so} (open symbols) and high-frequency shear viscosity $\eta_{s\infty}$ (closed symbols, $\nu > 5$ GHz) for alcohols featuring n carbon atoms per molecule. For $n \geq 13$ the viscosities refer to alkanes. Frame (b) shows the scaled viscosity $\eta(\omega)/\eta_\alpha$ of 4M3H, 5M3H, and 2E1H as compared to the same quantities measured for liquids devoid of a dielectric Debye process. For details see [42,243].
Source: Reprinted with permission from Ref. [41].
© 2001, American Chemical Society.

a big family of substances [42] for which various theoretical concepts are available [286–288] that may need, however, adaptation to singly hydrogen bonded patterns and relatively small supramolecular length scales. Using approaches applied in polymer science [289,290], such as the Rouse model, it was estimated that about ten 2E1H molecules might temporarily assemble into a supramolecular hydrogen bonded structure [42]. Consideration of the analogy to the mechanical behavior of reverse micelles may also turn out fruitful, see, e.g., [288].

Which additional insights into the supramolecular relaxation of monohydroxy alcohols did other mechanical probes yield so far? Owing to the relatively small optical anisotropy of the OH group, photon correlation spectroscopy was rarely applied to monohydroxy alcohols [47] and, for 1-propanol, provided evidence for process II (the α-relaxation) only. Brillouin scattering was able to resolve the trans-gauche isomerization of a long-chain alcohol [291] but obviously does not detect relaxation processes on the time scale of the dielectric Debye process. Furthermore, the assignment of the slowest process (time scale τ_B) that was resolved using this technique, e.g., for 1-propanol is not straightforward. In any such comparisons one faces the difficulty that, due to the small relaxation strength of process II, the determination of associated dielectric relaxation times is not very reliable near room temperature [238]. When comparing τ_B from Brillouin scattering with mechanical time scales determined from the Maxwell relationship, $\tau_M = \eta/G_\infty$, for 1-propanol it appears that τ_B is larger than τ_M [47,238,265]. It is obvious that the broad rheological response of monohydroxy alcohols does not comply with a model which involves only a single time constant [292]. Based on the experimental observation of their two-step viscosity profile, one may consider that, similar to polymers [293], in monohydroxy alcohols the stress relaxes over a broad range of time scales embracing the ones characterizing the local rearrangements and the suprastructural relaxation. In this context, the assignment of a unique mechanical time scale for monohydroxy alcohols is not fully justified. For practical reasons, however, since the overall (normalized) shear modulus response function $\Phi(t)$ of monohydroxy alcohols is dominated

by the "segmental" contribution [42], the Maxwell relation should provide a time scale that roughly corresponds to that of the microscopic fluctuations, $\tau_M = \eta/G_\infty = \int_0^\infty G(t)/G_\infty\, dt = \int_0^\infty \Phi(t)\, dt \approx \tau_\alpha$. On the other hand, if, $G_{\infty,\mathrm{pol}}$, the "instantaneous" shear modulus associated with only the supramolecular, polymer-like modes is used instead of G_∞ [294], then the estimated mechanical time scale would be much longer and will approach the Debye relaxation time τ_D [243].

Clearly, a quantitative assessment of the relationship of the two time scales deserves further study. Elastic constants and related quantities can also be determined from coherent inelastic neutron scattering experiments. However, from such a study on methanol it was found difficult "to derive a sound velocity from this kind of measurements" [272].

Insights into the hydrogen bonding in monohydroxy alcohols are available from studies in which these liquids are subjected to large mechanical shear stresses. Using non-equilibrium molecular dynamics simulations the viscosity of methanol [295] and ethanol [296] was studied for various shear rates. Shear thinning was found to occur and because the hydrogen-bonded chains formed by the molecules become shorter they align with the direction of shear, and the lifetime of the hydrogen bonds decreases.

Let us now compare the mechanical response of monohydroxy alcohols with dielectric results. To this end in Fig. 33(b) we plot the dielectric loss of 2E1H recorded near room temperature [64] and its acoustical absorption spectrum calculated from the parameters given in [41] for 25 °C. The ultrasonic spectrum shows a bend close to the frequency at which the dielectric Debye process displays a maximum loss. The low-frequency bend and the peak in the mechanical spectrum are separated by about 0.85 decades near 300 K while near 160 K the separation has increased to about 4 decades [42]. Hence, at high temperatures a parameterization of the spectrum in terms of two relaxation processes is possible. However, this approach fails to describe the low-temperature data.

Mechanical low-frequency modes are not only observed in some monohydroxy alcohols (cf. Fig. 33) but are a well-known feature of polymers [297] and they lead to an effective two-step behavior of the viscosity. An example for monohydroxy alcohols is shown in Fig. 34(b). Using conventional viscosity experiments, on the one hand, the static "macroscopic" shear viscosity (above denoted η_{so}) is measured. On the other hand, the concept of a "micro-viscosity" [21], in the context of Fig. 34(b) denoted high-frequency shear viscosity $\eta_{s\infty}$, was variously referred to. However, it appears that it has not been thoroughly explored how for monohydroxy alcohols this concept relates to that of the monomeric friction coefficient, well known from the field of polymer science [289].

Already in Debye's book (macroscopic) viscosities and dielectric relaxation times were compared in order to estimate the effective molecular radius of monohydroxy alcohol molecules [9]. Not taking into account possible effects of a micro-viscosity such comparisons have repeatedly reported to fail [298]. More on this issue can be found in Section 7.3.

Section 7.1 shows that it was long believed that viscoelastic measurements provide little insight into the nature of the Debye (-like) relaxation of monohydroxy alcohols. However, recent results demonstrate that their mechanical properties can provide important information regarding this supramolecular relaxational feature.

7.2. Mechanical solvation

The optical technique of solvation dynamics also provides a means of comparing dielectric with mechanical relaxation, but on a more local level. The technique requires the addition of chromophores at a very low concentration level, and these probe molecules are excited selectively by a short laser pulse. By recording their emission spectra as a function of time, one can obtain the temporal change of the average energy levels that are involved in the relevant optical transition [299]. One basis for the change of these energy levels is that electronic excitation of the chromophore leads to a change in its dipole moment, which persists for the lifetime of the excited state. Analogous to a dielectric relaxation experiment, the solvent dipoles will reorient towards minimizing the energy levels in the new electric field generated by the excited probe, and this polarization is observed as a change in the average emission wavenumber versus time, $\langle\bar{\nu}(t)\rangle$, cf. Section 6.1. The dynamics of the process is reflected in the Stokes shift correlation function $C(t)$, defined in Eq. (14) as $C(t) = [\langle\bar{\nu}(t)\rangle - \langle\bar{\nu}(\infty)\rangle]/[\langle\bar{\nu}(0)\rangle - \langle\bar{\nu}(\infty)\rangle]$.

Because the solutes charge distribution remains virtually constant while the solvent is polarized locally, the decay of $C(t)$ is more related to the electric modulus $M(t)$ than to the permittivity $\varepsilon(t)$ [252]. In order for this method to reveal the slow dynamics (10 s to 10 μs) of supercooled liquids near their glass transition, probe molecules with long lived triplet states are used [257], while shorter lived fluorescent solutes are appropriate for measuring solvent relaxation time below 10 ns. By combining different probe molecules, the time scale of $C(t)$ has been shown to trace that of dielectric relaxation across the picoseconds to seconds time range [300].

For probe molecules for which the electronic excitation does not alter the dipole moment, or when the solvent is non-polar, the lack of any significant electrostatic interaction between solute and solvent can lead to the expectation that no solvation dynamics should occur. In reality, dynamic solvation is observed for systems for which electrostatic interactions should be negligibly small [301]. The explanation is that a molecule changes its net volume upon electronic excitation, and the response of the solvent is the equivalent of shear stress relaxation [302,303]. Hence, this type of solvation dynamics is termed 'mechanical' solvation. A comparative study exploiting the difference between mechanical and dielectric solvation has been performed on 1-propanol. The dielectric solvation has been measured with quinoxaline (QX) as probe, which is subject to a dipole moment change of about 1.3 Debye upon excitation. The mechanical counterpart employed naphthalene (NA) as chromophore which lacks any change in dipole moment due to symmetry. The result of the respective Stokes-shift

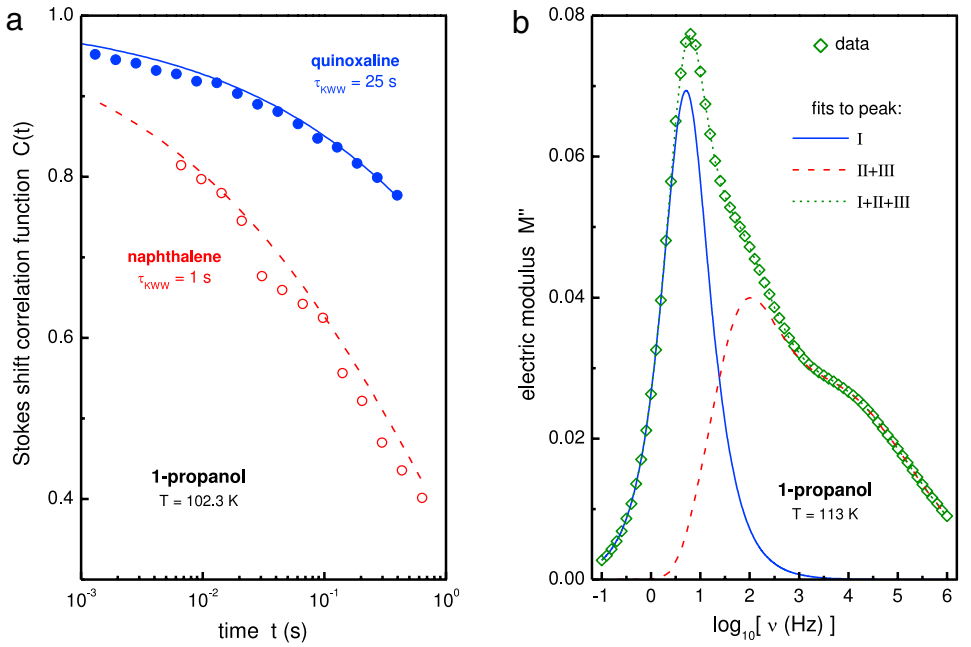

Fig. 35. (a) Stokes-shift correlation function $C(t)$ for the probes naphthalene (NA, open symbols) and quinoxaline (QX, solid symbols) in 1-propanol at $T = 102.3$K. The dashed and solid lines are stretched exponential fits, $C(t) = \exp[-(t/\tau)^{\beta}]$, differing only in the value of τ which is 1 s for NA and 25 s for QX. (b) Experimental results for the imaginary part of the electric modulus $M''(\omega)$ versus $\log_{10}(\nu/\text{Hz})$ for 1-propanol at $T = 113$K (symbols). The lines show the fit and decomposition of the $M''(\omega)$ trace into the dominant Debye-type dielectric peak (I) at $\log_{10}(\nu/\text{Hz}) = 0.70$ and the remaining profile associated with the structural relaxation (II+III) peaking at $\log_{10}(\nu/\text{Hz}) = 2.03$.
Source: Adapted from [259].

correlation functions is depicted in Fig. 35. It is noteworthy that the mechanical $C(t)$ decay is a factor of 25 faster than the dielectric $C(t)$ [259].

The above factor of 25 that separates the time constants of dielectric and mechanical solvation turns out to coincide with the spectral separation of the two slowest peaks of the dielectric modulus of *n*-propanol in terms of $M''(\omega)$. Consistent with the macroscopic mechanical results, the conclusion of this solvation study [259] is that the mechanical response of the alcohol occurs on the time scale of the smaller and faster process (II), and that no mechanical solvation modes have been resolved to date that match the time scale of the dielectric Debye process.

7.3. Self-diffusion and effective molecular radii

It is interesting to find out whether and to which extent the transport properties in monohydroxy alcohols are affected by their supramolecular relaxation: Do the supramolecular entities diffuse as a whole? Does proton hopping, e.g., in the form of a Grotthus-type mechanism, play a significant role? Are collective transport processes relevant? Since, the electrical properties are often considered in relation with monohydroxy alcohols, it is also interesting to ask about the electrical conduction of (intrinsic vs. impurity) mobile ions in monohydroxy alcohols. Since conductivity is very briefly dealt with in connection with dielectric spectroscopy, Section 5.2, here the focus is more on the molecular transport that is accessible via techniques such as molecular dynamics simulations [93,304,305], field gradient NMR, and incoherent quasi-elastic neutron scattering. The latter method, though, was rarely used to study diffusion in monohydroxy alcohols [306–308]. Therefore, in the following we will deal mainly with NMR based self-diffusion studies. Translational self diffusion coefficients, D_t, for 1-alcohols such as methanol, ethanol, propanol, etc. are available for relatively wide ranges of temperature and pressure [63,309–319]. As a function of chain length it was of course found that monohydroxy alcohols with bulkier alkyl tails diffuse slower, see, e.g., [281,305].

Before entering into a discussion of the diffusional properties of monohydroxy alcohols, let us briefly recall that such diffusion data are typically analyzed using the classical Stokes–Einstein equation [320]

$$D_t = \frac{k_B T}{p\,\pi\,\eta\,R}. \tag{15}$$

This equation was derived for a macroscopic sphere of radius R in a medium of viscosity η assuming either stick ($p = 6$) or slip ($p = 4$) boundary conditions. Nevertheless, this equation is often applied to microscopic, typically flexible, non-spherical objects (=molecules) by assigning an effective hydrodynamic radius R_H to them. For ideas on how these and other boundary conditions may arise on the molecular level see [321].

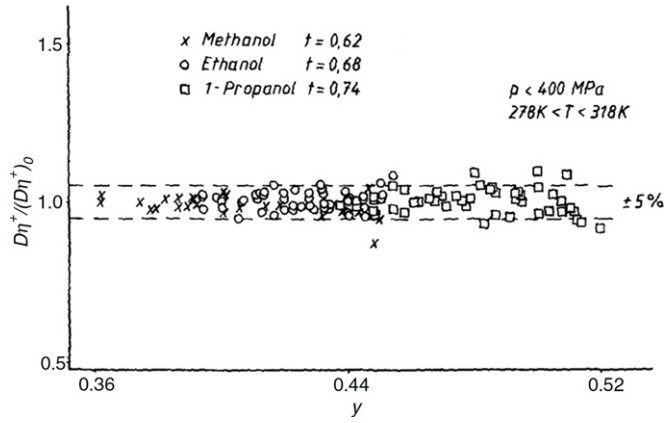

Fig. 36. Plot showing that the fractional Stokes–Einstein equation, $D_t\eta^{\xi} = \text{const.}$, is obeyed for a range of effective packing fractions y (adjusted experimentally by varying pressure and temperature in the indicated range).
Source: This plot is taken with permission from Ref. [314] and includes methanol data from [309].

For the rotational diffusion of a sticky sphere of radius R_D one likewise obtains the rotational diffusion coefficient [9]

$$D_{\text{rot}} = \frac{k_B T}{8\pi\eta R_D^3} = \frac{1}{\ell(\ell+1)\tau_\ell}. \tag{16}$$

D_{rot} can be related to a reorientational time constants τ_λ by solving the rotational diffusion equation in terms of the Legendre polynomials of rank λ. In practical terms $\lambda = 1$ applies if one considers reorientations of vector-like objects (e.g., of dipole moments in dielectric spectroscopy) or $\lambda = 2$ when dealing with rotational properties of second-rank tensorial quantities that are typically relevant when analyzing NMR and light scattering experiments, cf. Section 5.1 for some general remarks.

Identifying R_D with R (and with R_H) and combining Eq. (15) with Eq. (16) the viscosity can be eliminated yielding the rotational correlation time

$$\tau_\ell = \frac{8\pi R^3}{\ell(\ell+1)k_B T}\eta = \frac{6V}{\ell(\ell+1)k_B T}\eta = \frac{4}{3\ell(\ell+1)}\frac{R^2}{D_t}, \tag{17}$$

if one defines the "molecular volume" as $V = 4\pi R^3/3$. It has been noted that the application of Eq. (17) for the macroscopic viscosity, η, and the dielectric relaxation time, τ_D, of the main peak of monohydroxy alcohols yields molecular volumes that are too large [20,298] when compared to simple estimates based on the so called van der Waals radius R_{vdW} [322].

It is also well known that in viscous supercooled liquids the relation between diffusion coefficient, D_t, and macroscopic viscosity, η, cannot be described by the Stokes–Einstein relation, Eq. (15), if a constant hydrodynamic radius is assumed, i.e., if R is taken to be independent of pressure or temperature [323,324]. In a number of instances, the so called fractional Stokes–Einstein equation, $D_t\eta^{\xi} = \text{const.}$, with an exponent $\xi < 1$ was found to provide a basis for a satisfactory description of various supercooled liquids [198,325,326]. As shown in Fig. 36 this fractional relation is fulfilled for methanol, ethanol, and propanol in a range of effective packing fractions [314]. The fractional exponent was found material dependent, but constant for each monohydroxy alcohol with numerical values ξ in the range 0.62…0.74, similar to observations made for other supercooled liquids [326,327].

Often times translational diffusion coefficients are not available but rotational diffusion data, as estimated, e.g., from dielectric spectroscopy using Eq. (16). By assuming equality of R_D with R, as indicated above, from the resulting Debye–Stokes–Einstein relation, Eq. (17), proportionality of τ and η is suggested. Recent work on 2E1H, see Fig. 37(a), documents a breakdown of this relation, at least above a pressure of about 550 MPa [328]. By plotting the data in the pressure range from 0.6 to 1.5 GPa the fractional exponent describing the decoupling of dielectric relaxation and mechanical relaxation is directly obtained from $\tau_{\text{diel}} \propto \eta^{0.75}$, see Fig. 37(b).

Other attempts to "rescue" the Stokes–Einstein equation relax the condition that the hydrodynamic molecular radius should be independent of temperature, pressure, etc. As an example for this kind of analysis, the diffusion coefficient D_t of 1-butanol is shown in Fig. 38 [63,370]. One aspect addressed in these studies was whether the molecules diffuse as a whole or whether the OH group displays a particular behavior (e.g., based on a Grotthus type mechanism). When using isotope labeling either for the alkyl or for the hydroxyl part of the molecule virtually identical diffusion coefficients were obtained, see Fig. 38(a). This result confirms diffusion coefficient determinations exploiting chemical-shift resolution [63] which enables selective probing of various groups within a molecule (cf. Section 8.1) and is in harmony with earlier results on 2-propanol [329].

The data in Fig. 38(a) suggest that a dynamic isotope effect does not exist for 1-butanol. This result is in accord with previous D_t data on a series of monohydroxy alcohols. For methanol it was found that $D_t(CH_3OH)/D_t(CH_3OD)$, being ∼1

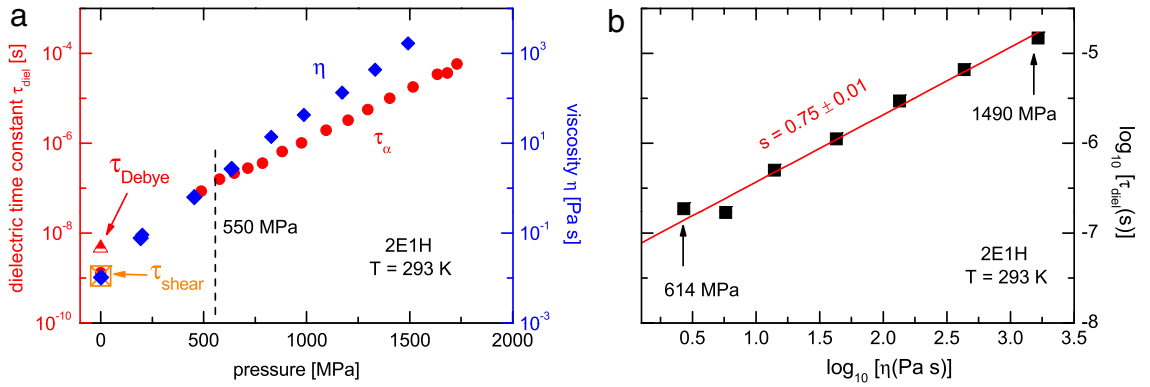

Fig. 37. (a) Dielectric relaxation time τ and viscosity η of 2E1H as measured at 293 K. The dashed line emphasizes that significant decoupling between these two quantities occurs above pressures of about 550 MPa. (b) Plot showing how the fractional exponent describing this decoupling can be determined. *Source:* Adapted with permission from Ref. [328].

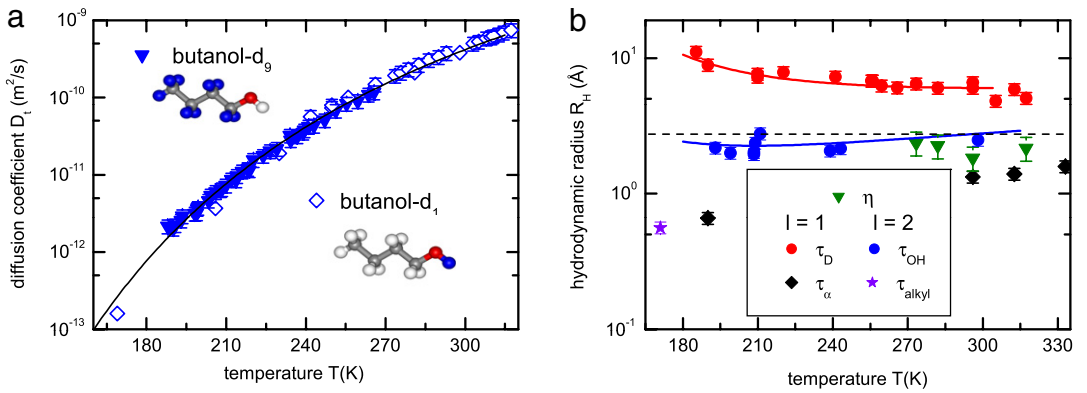

Fig. 38. (a) Temperature dependent diffusion coefficients of various isotopomers of 1-butanol. The solid line represents a Vogel–Fulcher law, $D = 2.4 \times 10^{-6}$ m^2/s exp[-2461 K/$(T - 15$ K)], cf. Eq. (18), and provides a good description of the data [63,370]. (b) Temperature dependence of the effective hydrodynamic radius R_H of 1-butanol as calculated on the basis of viscosity [331] and the diffusion coefficients from Eq. (15). Other determinations of R involve Eq. (16) and rotational correlation times using τ_D and τ_α from dielectric spectroscopy as well as τ_{OH} and τ_{alkyl} from NMR. The solid lines in frame (b) are calculated from Vogel–Fulcher fits to the τ or η or D_t versus T data as shown for an example in frame (a). The dashed line marks the calculated van der Waals radius of butanol, $R_{vdW} = 2.75$ Å [322]. For details see [63,370].

above room temperature, increases to about 1.4 near 150 K [315]. For propanol the corresponding ratio turned out to be significantly smaller (1.2 for 1-propanol and 1.1 for 2-propanol, both near 210 K) [316]. For 1-, 2-, and 3-pentanol no isotope effect could be detected [317]. Liquid water, like the small-molecule monohydroxy alcohols, does show a dynamic isotope effect that was assigned to the formation of more and stronger hydrogen bonds in D_2O as compared to H_2O [330].

Returning to monohydroxy alcohols, in Fig. 38(b) we present effective molecular radii estimated for 1-butanol by employing Eqs. (15) to (17). Using the macroscopic viscosity [331] and assuming stick boundary conditions, Eq. (15) with $p = 6$, yields an effective molecular radius which, given the considerable experimental uncertainty obvious from Fig. 38(b), is compatible with the computed van der Waals radius R_{vdW}. Compatibility is also achieved when starting from rotational correlation times determined at the OH group using NMR [65] in conjunction with Eq. (17). The physical implications of this finding with respect to the mechanisms of the supramolecular relaxation is discussed in [210]. Here it may suffice to note that in the expression for τ_ℓ, on the right hand side of Eq. (17), viscosity does not enter explicitly.

Determinations using τ_α (exploiting NMR or dielectric spectroscopy) or τ_D on the basis of Eq. (17) give molecular radii much different than R_{vdW}, see Fig. 38(b), if the macroscopic viscosity η is used. Similar results were found for the branched alcohol 2E1H [210]. As far as we know, analyses based on "micro-viscosities" were not carried out for monohydroxy alcohols so far. In any case it was found that hydrogen bonding can lead to a strong reduction of the translational mobility which is most pronounced at low temperatures [320]. This statement is confirmed by computer simulations which investigate the degree of hydrogen bonding by changing the effective charge of the OH group and find that "fine-tuning the partial charges of the hydroxyl group by 3.2% changed the simulated diffusion coefficient of aliphatic alcohols by 30%, while the density was changed by less than 1%" [305].

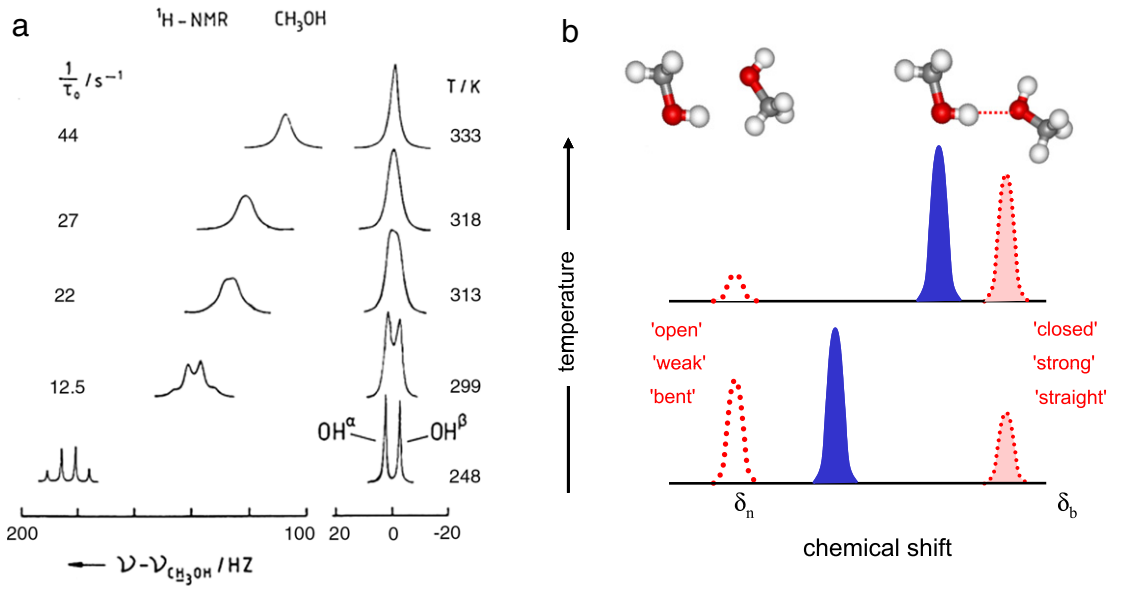

Fig. 39. (a) High-resolution ^{1}H spectra of methanol. The resonance of the CH_3 group was utilized as internal standard, therefore the corresponding spectra appear near $\Delta\nu = 0$. The position of the OH group displays a strong variation with temperature. The pseudo first-order self-exchange rate constants, i.e., the inverse proton lifetimes $1/\tau_0$ derived from these spectra are also given. The fine structure of the lines is due to the through-molecule coupling of the nuclear spins (the so called J coupling). Taken from [334]. Courtesy of H.H. Limbach. (b) Schematic illustration how the temperature dependence of the proton chemical shift arises as a consequence of a thermally driven re-population of open and closed hydrogen bonds that is fast on the time scale set by the inverse line splitting of the (unobserved) lines at δ_n and δ_b, respectively. Other attributes in the literature used for "open" and "closed" hydrogen bonds are given as well.

8. Nuclear magnetic resonance

Magnetic resonance techniques are well suited to identify molecular structures and to map out the dynamics of different parts of a molecule within a monohydroxy alcohol liquid. By spectroscopic separation of the various sites or by suitable ^{1}H, ^{2}H, or ^{17}O isotope labeling the hydroxyl group dynamics can be distinguished from that of the carbohydrate remainder. In this section we will deal exclusively with NMR since only very little electron spin resonance data is available for monohydroxy alcohols [332].

8.1. Chemical shifts and proton exchange dynamics

Ethanol is the classical example for the demonstration of the chemical shift [333]. This property allows one to resolve the proton resonances (or those of other nuclei) and is routinely exploited to study molecular structures of liquid-like and solid-like samples. In this most simple application of NMR one relies on the fact that the electron distribution near a specific molecular group produces a characteristic shielding of the external magnetic field at the nuclear probe. The method owes its usefulness also to the finding that typically this shielding is virtually temperature insensitive. The proton resonance associated with the OH group, however, represents an interesting exception. In Fig. 39(a) we show the relevant parts of the ^{1}H spectrum of pure methanol as an example [334]. It is seen that the OH resonance (on the left) experiences a pronounced temperature dependent frequency shift $\Delta\nu(T) = \nu(T) - \nu_{\rm ref}$ with respect to the methyl protons (on the right) that acts as a reference [335,336]. This shift and the corresponding one in $\delta(T) = \Delta\nu(T)/\nu_{\rm ref}$ arises from a dynamic equilibrium among different OH protons. For simplicity, these will be referred to as protons in hydrogen bonded (b) or non-bonded (n) situations as illustrated in Fig. 39(b). In these two situations the chemical shifts of the OH protons can be significantly different with $\Delta\delta_{\rm OH} = \delta_n - \delta_b$ of the order of at least 5 ppm, see, e.g., [337,338].

Let us now define the fraction f_n of open hydrogen bonds and of closed hydrogen bonds, $f_b = 1 - f_n$. Then, if temperature changes, one would naively expect separate proton resonances at δ_n and at δ_b, characterized by relative strengths f_n and $1 - f_n$, respectively. Experimentally, separate peaks are not resolved as long as sufficiently fast hydrogen bond switching occurs which leads to a motional narrowing of the corresponding NMR lines. This fast-exchange limit requires that the exchange rates, $1/\tau_{\rm ex}$, are larger than the chemical shift difference, $|\Delta\delta_{\rm OH}|$. Proton exchange rates can directly be obtained from high-resolution spectra such as those reproduced in Fig. 39(a) [334]. There, one recognizes that the resonance lines display a multiplet structure arising from the mutual coupling of the protons on the methanol molecule. However, with increasing temperature, this fine structure gets blurred, a manifestation of another motional narrowing phenomenon, which the authors of [334] relate to an *inter*molecular proton exchange between the alcohol molecules. By comparison with simulated line shapes, the effective exchange rate characterizing the fast single proton transfer processes of methanol was

found to be of the order of 10^9 s^{-1} near room temperature. This rate is smaller than the dielectric relaxation rate of about 2×10^{10} s^{-1} [339] and can be expected to slow down with temperature. Therefore, the condition $1/\tau_{ex} \gg |\Delta\delta_{OH}|$ is fulfilled not only in the equilibrium liquid state but more or less in the entire supercooled regime. Then, the motionally averaged NMR line shows up at a chemical shift of $\bar{\delta}_{OH}(T) = f_n\delta_n + f_b\delta_b$. Recording the frequency position $\bar{\delta}_{OH}$ as a function of temperature thus provides experimental access to the fraction of open (or closed) hydrogen bonds. This phenomenon was exploited for various monohydroxy alcohols in the highly fluid [337] and down to the moderately viscous regime.

The thermal evolution of the chemical shift at the OH group can be tracked in a straightforward manner down to temperatures at which the proton exchange rates are of the order of about microseconds. If the dynamics slows down much more, the NMR lines will broaden, e.g., due to magnetic dipole ^{1}H–^{1}H interactions. This will eventually lead to a spectral overlap of the resonances of the OH protons with the carbon bonded ones, an effect that could be circumvented, e.g., by selectively deuterating the alkyl chain. More seriously, if the spectral width arising from dipolar or other broadening mechanisms exceeds $|\Delta\delta_{OH}|$, then line narrowing techniques such as magic-angle spinning are required to restore spectral resolution as a prerequisite to studying exchange processes.

NMR investigations on monohydroxy alcohols carried out with the goal to monitor the slow re-equilibration of hydrogen bond populations using this approach are not known to us, but other techniques were exploited in this context [64], see Section 9.2. Furthermore, NMR studies of the OH bond may be difficult because any distributions of OH bond lengths lead to an additional broadening of the corresponding proton and oxygen lines. Studies of exchange processes involving NH bonds, on the other hand, are available [340], but have yet to be applied to systems featuring a dielectric Debye process such as the secondary amides.

Chemical shifts and parameters such as quadrupole coupling constants for deuterium nuclei were calculated for several monohydroxy alcohols using quantum chemical approaches [341–346]. Most of these results were obtained using small molecules such as methanol [343] and ethanol [344,345], but also a nonanol species (3-ethyl-2,2-dimethyl-3-pentanol = 2, 2-dimethyl-3-ethyl-3-pentanol, DMEP) was investigated using density functional calculations in combination with a quantum cluster equilibrium (QCE) model [341,342]. Using this approach the impact of cooperative effects caused by hydrogen bonding is automatically taken into account.

In Fig. 40 we reproduce results for the chemical shift of methanol's hydroxyl proton [343]. Interestingly, the shifts depend on the assumed suprastructure and furthermore the cooperative effects saturate for cluster sizes larger than about 5. For ethanol similar results were obtained and the temperature dependence of the calculated isotropic chemical shift of its hydroxyl ^{1}H and ^{17}O nuclei was reported and compared with experimental results [344,347]. These computations and experiments were carried out down to temperatures near 250 K and yielded evidence for a predominance of pentameric clusters. Similar investigations for DMEP revealed that only dimers should be stable at these temperatures [341,342] and that trimers are avoided for enthalpic reasons. Currently, some effort is expounded in order to calculate chemical shifts of monohydroxy alcohols using *ab initio* methods. However, due to the difficulty of properly incorporating the internal flexibility already for relatively small molecules into the computations, *ab initio* methods obviously do not yet yield reliable results for the chemical shifts in liquid monohydroxy alcohols [345,348].

8.2. Fast dynamics probed by nuclear spin relaxation

The access to molecular correlation times on the nanosecond scale is most efficiently provided by spin relaxation experiments. Here, a radio-frequency pulse creates non-equilibrium magnetization. Its subsequent re-equilibration is driven by fluctuations of the NMR frequency experienced at the site of the probe nuclei. Molecular motions can lead to such frequency fluctuations if, e.g., reorientational motions modulate the anisotropic chemical shift. Apart from chemical shift interaction, other interactions may need to be considered and their relative importance needs to be assessed in each specific case. However, spin relaxation is only efficient, i.e., transitions between the Zeeman-split nuclear energy levels can only occur if the molecular fluctuation rate κ is sufficiently close to the Larmor frequency ω_L. Denoting the fluctuation probability at a given frequency ω as the spectral density, $J(\omega)$, in the simplest case of an overall isotropic molecular motion, the spin–lattice relaxation rate arising from fluctuations in the chemical shift anisotropy is given by

$$1/T_1 = \Delta K\, J(\omega). \tag{18}$$

Here $\omega = \omega_L$ and ΔK is related to the squared fluctuation amplitude in frequency space. For other relaxation mechanisms or for anisotropic motions more complicated expressions will arise [349,350]. Furthermore, chemical shift interactions usually probe purely intramolecular motions, while by a suitable combination of, e.g., ^{1}H and ^{2}H data inter- and intramolecular spin-relaxation rates can be separated. The explicit form of the spectral density function, $J(\omega)$, depends on the shape of the underlying effective distribution of molecular correlation times [351]. Spin–spin relaxation measurements, if probing molecular motions in a constant magnetic field, can often be analyzed using an expression similar Eq. (18) but for $1/T_2$ and with ω replaced by the frequency width of the NMR absorption spectrum.

Small-molecule monohydroxy alcohols such as methanol, ethanol, propanol, or butanol were often dealt with in magnetic resonance studies using various nuclear isotopes, see, e.g., [43,44,46,329,352–356]. However, low-temperature NMR experiments on longer chain or branched alcohols seem to be scarce [210,220]. As a representative example of measurements on monohydroxy alcohols in Fig. 41 we show temperature dependent ^{1}H NMR spin–lattice relaxation times measured for C_2D_5OH, CD_3CH_2OD, and CH_3CD_2OD, i.e., for differently isotope labeled ethanol species [357]. It is clearly seen

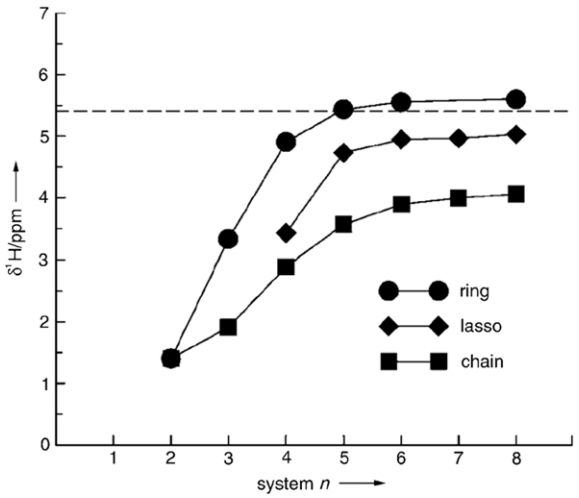

Fig. 40. Isotropic proton chemical shift at the hydroxyl site calculated for methanol clusters displaying ring-, lasso-, or chain-like structures involving up to n molecules. The dotted line represents the experimentally determined chemical shift for liquid CH_3OH at 298 K.
Source: Taken with permission from [343].

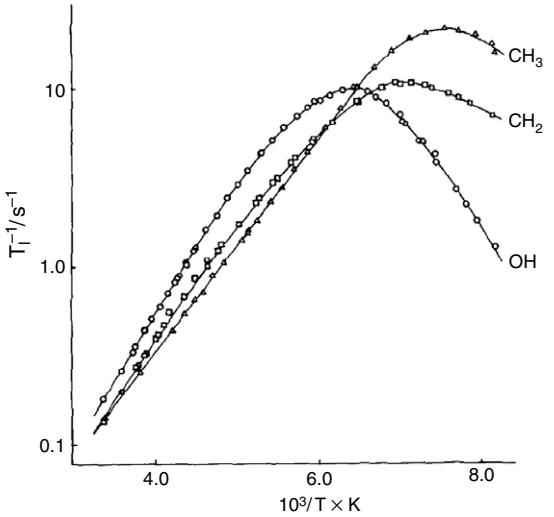

Fig. 41. Proton spin–lattice relaxation rates, T_1^{-1}, of the ethanol isotopomers C_2D_5OH, CD_3CH_2OD, and CH_3CD_2OD. The motion of the hydroxyl group freezes in on the time scale of the inverse Larmor frequency (with $\omega_L/2\pi = 30$ MHz [358]) at the largest temperature, indicating a relatively slow OH group dynamics. The methyl group, on the other hand, displays a much faster dynamics.
Source: Reprinted from [357].

that the T_1^{-1} rates measured for the different molecular sites deviate significantly from each other. The rate maximum for the OH group appears at the highest temperature, hence the OH motion is slowest. The slow-down of the methyl group appears at the lowest temperatures and hence this group moves fastest. From site-selective studies of monohydroxy alcohols, a number of authors found that the dynamics is slowest if measured closest to the hydroxyl group [63,355–357].

In early analyses of results such as those shown in Fig. 41 it became clear that locally anisotropic motions need to be invoked [352] suggesting that different intramolecular degrees of freedom dominate the behavior of monohydroxy alcohols. Difficulties were encountered to interpret the experimental results in terms of a single-molecule picture, so that with respect to CH_3OH Hertz stated that "the system of the H-bonded OH groups constitutes 'the molecule' for methanol which may be dimers or trimers or whatever" [357]. Furthermore, a description in terms of intramolecular motions was not considered satisfactory [359]. As far as we can see, Hertz and colleagues never attempted to compare their NMR results with those from dielectric spectroscopy. This was done later [360] by considering the ratio of time scales, τ_{DS}/τ_{NMR}, from NMR and from dielectric spectroscopy (DS). For the series from methanol to hexanol this ratio (denoted τ_D/τ_c) was found to be about 10

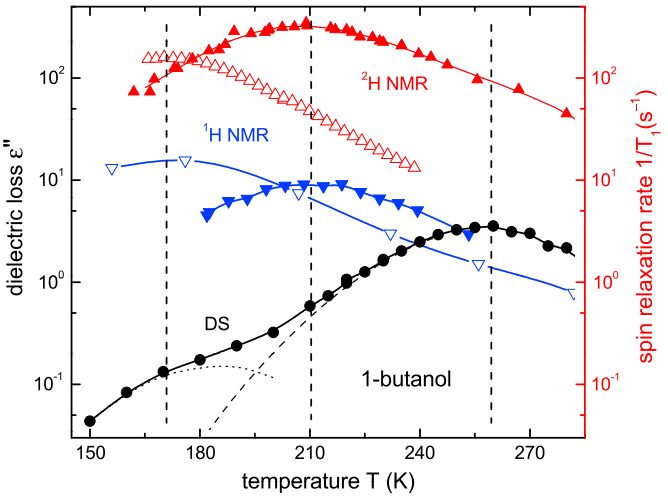

Fig. 42. Proton and deuteron spin–lattice relaxation rates (triangles) and dielectric loss (circles) of 1-butanol, all measured at frequencies close to 50 MHz. The closed triangles refer to measurements at the hydroxyl group, the open triangles to those at the alkyl part of butanol. According to Eqs. (18) and (19) ε'' and $1/T_1$ probe similar spectral densities. The solid lines guide the eye, the dashed line marks the contribution of the Debye relaxation, and the dashed curve corresponds to the α process. From left to right the vertical lines mark τ_α, τ_{OH}, and τ_D.
Source: Adapted from [65].

and thus more than 3 times larger than the expectations expressed in [360]. In that work, τ_{DS} (or τ_D) refers to the Debye process because the correct assignment of the structural relaxation was achieved only later [47].

For an efficient comparison of dielectric loss curves, from which contributions due to the α relaxation (=process II) and Debye process can be distinguished, with spin–lattice relaxation times, it useful to exploit a variant of the fluctuation dissipation theorem [361]. According to this theorem, the fluctuation rate is related to the absorptive part, χ'', of the corresponding (e.g., dielectric) susceptibility so that

$$\frac{1}{T_1^{\chi}(\omega, T)} = \frac{\chi''(\omega, T)}{\omega \Delta\chi(T)}. \tag{19}$$

Here $\Delta\chi$ denotes the static susceptibility. Keeping in mind that dielectric and NMR quantities refer to molecular correlation functions with different rank ℓ (cf. Section 5.1), Eq. (19) provides a framework to facilitate a direct comparison of the results from the two techniques.

An example is given in Fig. 42 which summarizes NMR and dielectric data for 1-butanol measured for frequencies close to 50 MHz [65]. From the dielectric loss the Debye process and the α-relaxation can be clearly resolved. The $1/T_1$ maxima from ^{1}H-NMR of C_4H_9OD or from ^{2}H-NMR of C_4D_9OH correspond well to the dielectric loss peak that refers to the α-process. Hence, this process can be ascribed to the motion of the alkyl chains, a finding confirmed by ^{13}C-NMR [63]. When probing the dynamics of the hydroxyl group, e.g., by performing ^{2}H-NMR on C_4H_9OD or ^{1}H-NMR on C_4D_9OH it is clear from Fig. 42 that spin–lattice relaxation measurements are unable to detect the Debye process directly. However, in harmony with results on other monohydroxy alcohols, see, e.g., Fig. 41, a maximum in the spin–lattice relaxation rate is obtained which has no dielectric analogue.

With the problems in mind that were previously encountered when interpreting T_1 measured for the hydroxyl group, a model of transient, hydrogen bonded chains has been suggested [65]. Within this approach, the rate maximum showing up in Fig. 42 near 210 K defines a new time scale, τ_{OH}, as a measure for the mean time an monohydroxy alcohol molecule is part of an hydrogen bonded cluster. The assignment of the time scale which is intermediate between those characterizing the structural and the Debye process, was recently confirmed by neutron scattering experiments [238].

The relationship of the three time scales, τ_α, τ_{OH}, and τ_D, was established for a wide temperature interval by varying the Larmor frequency of the spin–lattice relaxation experiments in a range extending over more than 3 orders of magnitude [65]. A determination of $1/T_1(\omega)$ over such a broad frequency range becomes possible by exploiting the recently reviewed fast field cycling technique [362].

Using Eq. (19) we just demonstrated how the (temperature dependent) dielectric loss can be compared directly to $1/T_1(T)$. Conversely, Eq. (19) also enables one to transform the T_1^{-1} data to the susceptibility format via $\chi''(\omega_L, T) = \Delta k\, \omega/T_1(\omega_L, T)$. Here Δk is a coefficient proportional to ΔK, cf. Eq. (18).

In Fig. 43(b) we replotted the $1/T_1(\omega)$ data from [65] in the susceptibility format as small symbols. These data, enable one to determine correlation times from spin–lattice relaxation rates recorded at a single Larmor frequency. In Fig. 43(a) we show such data, i.e., ^{1}H-T_1 times on C_4D_9OH and scaled ^{2}H-T_1 times on C_4H_9OD as a function of temperature [65]. On the basis of the results in Fig. 43(a), an essentially model free determination of correlation times is only possible by analyzing the $1/T_1$

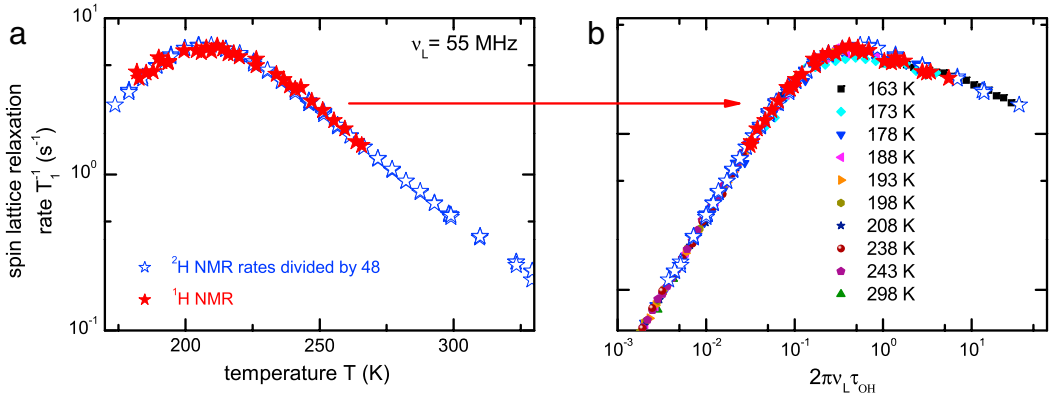

Fig. 43. (a) Proton and deuteron spin–lattice relaxation rates of 1-butanol, both measured for a Larmor frequency of 55 MHz at the hydrogen position of the hydroxyl group. After dividing the ^{2}H-T_1^{-1} rates by a factor of 48 (which roughly corresponds to the ratio of the squared gyromagnetic ratios of the ^{1}H and ^{2}H nuclear probes) the two sets of $T_1(T)$ data are seen to coincide. (b) Small symbols represent the spin–lattice relaxation rates, $1/T_1(\omega)$, from field-cycling relaxometry plotted in the susceptibility format [65]. The time scale axis in frame (b) is "calibrated" by comparing the rate maxima of the curves in both frames at which $\omega_L\tau_{OH} \approx 1$. For temperatures away from the rate maximum the single-frequency data in panel (a) are "shifted" onto the susceptibility curve in panel (b), thus enabling one to determine how much the OH time scale is different from that inferred at the rate maximum.

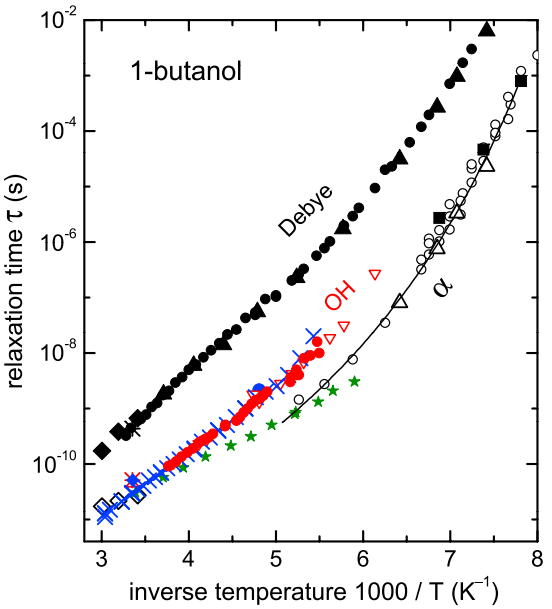

Fig. 44. Arrhenius plot of 1-butanol based on [65] and including time constants from dielectric spectroscopy and from NMR. Additionally, correlation times measured using ^{13}C-NMR at the α-carbon (green stars [63]) and those determined on the basis of Fig. 43 from the ^{1}H-T_1 data (red dots) and ^{2}H-T_1 data (blue crosses) are included. The solid line represents an interpolation with a Vogel–Fulcher function, Eq. (12), $\tau_\alpha = 10^{13}$ s $\times$ exp[950 K/(T − 86 K)], of dielectric time constants for the α-process, cf. [63].

curve at its maximum at which $\omega_L\tau_{OH} \approx 1$ [363]. However, using the data in Fig. 43(b), correlation times can be determined in the entire temperature range covered in Fig. 43(a) from the horizontal "shift" required to map the single-frequency $1/T_1$ data onto the susceptibility master curve. Here, this procedure yields τ_{OH} in the range from $\sim 10^{-11}$ to $\sim 10^{-8}$ s. Ultimately, the long-time limit of this kind of analysis is set by the condition that $1/\tau_{OH}$ should be significantly smaller than the low-temperature line width of the nuclear probe.

The τ_{OH} time constants determined from this shift analysis, illustrated in Fig. 43, are included in Fig. 44, an Arrhenius plot which also contains the structural relaxation time τ_α (from dielectric spectroscopy and from ^{13}C-NMR) and the dielectric Debye time, τ_D, for 1-butanol. Fig. 43 demonstrates that the time scales τ_α and τ_{OH} differ considerably, yielding a τ_{OH}/τ_α ratio of about 5…10, in harmony with findings on other lower alcohols [44,329,355–359] and on the octanol 2E1H [210]. This time scale ratio translates into a considerable difference in the temperatures at which the alkyl versus the hydroxyl motion slows down, i.e., in the temperatures at which the maxima in T_1^{-1} show up. For 2E1H this temperature difference is about 20 K [210], see the solid lines in Fig. 45, a typical value for a number of alcohols [44,355–359].

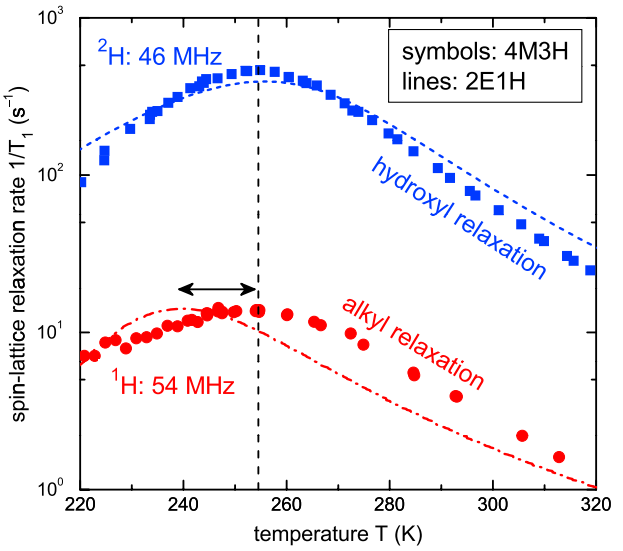

Fig. 45. The squares and circles represent spin–lattice relaxation rates probing the dynamics of the alkyl part and of the hydroxyl group, respectively, of 4M3H. Both sets of data were recorded at Larmor frequencies near 50 MHz, display $1/T_1$ maxima at $T \approx 254$ K, and show that the dynamics of the OD group is very similar to that of the overall molecular motion. The dashed and dash-dotted lines reflect measurements of the spin–lattice relaxation rates of 2E1H. The arrow highlights that for 2E1H the temperatures at which the alkyl- and the hydroxyl-related rate maxima appear differ by about 20 K.
Source: Adapted from [220].

Rather than interpreting these observations in terms of intramolecular flexibility which was attempted for the lower alcohols but was not found satisfactory [357], in [65] the observed τ_{OH}/τ_α ratio of about 5…10 for 1-butanol was linked to the average size of the transient end-to-end chain of alcohol molecules. The same interpretation was given for the branched octanol 2E1H [210] while on the basis of nuclear Overhauser enhancements measured for the unbranched monohydroxy alcohol 1-octanol an aggregation in the form of a reverse micelle-like or worm-like structures was suggested [364]. A significant time scale separation of the alkyl versus the hydroxyl group is typical for monohydroxy alcohols exhibiting a large dielectric Debye process. However, such a separation does not appear in systems displaying only a weak Debye-like process. This is illustrated for 4M3H, an alcohol with a sterically screened OH group, see the symbols in Fig. 45. Here the T_1^{-1} maxima reflecting the freezing of the alkyl and of the hydroxyl group dynamics appear at virtually the same temperature, in contrast to the behavior of 2E1H and many other monohydroxy alcohols.

8.3. Slow motions and dynamic exchange

Slow molecular motions in the range from $\sim 10^{-4}$ s up to ~ 1 s and in favorable cases also beyond are accessible using NMR line shape analyses and two-dimensional exchange techniques [365]. Two-time stimulated deuteron echo experiments were recently carried out for various monohydroxy alcohols as a function of the mixing time t_m, a time interval during which molecular dynamics can take place. All results obtained so far [210,220] yield stretched exponential orientational correlation functions that resemble the behavior of typical supercooled organic liquids [366]. This means that in monohydroxy alcohols these experiments also detect only the α process (or faster processes) but no slower relaxations. Furthermore, in solid-echo spectra features peculiar for monohydroxy alcohols could not be identified to date. Therefore, there is no need to review these experiments here in detail. The failure of the echo experiments to detect motions slower than the α-response was previously rationalized as follows [210]: The α-process leads to an effective isotropization of the molecular orientations and consequently to a complete decay of the two-time echo amplitude, $F_2(t_m)$, thus precluding a detection of slower motions. Spin relaxometry, on the other hand, involves rate averaging for sufficiently fast dynamics and thus does not suffer from this drawback. Any line narrowing effects on solid-echo spectra specific to monohydroxy alcohols may be minute and thus be hard to detect.

Dynamical processes slower than the α relaxation were previously studied for supercooled liquids using reduced four-dimensional NMR [367] or four-time correlation functions. These allow for a detection of dynamic exchange processes, for a review see [366]. Four-time echo functions, $F_4(t_{m1}, t_{m2}, t_{m3})$, involving three different mixing times, were recently recorded for monohydroxy alcohols to study a peculiarity which has been noted for a range of neat monohydroxy alcohols [228,368] and concerns the symmetric broadening of process II, i.e., the dielectrically detected α-relaxation peak. This symmetrical shape, particularly evident from the dielectric loss spectra of diluted monohydroxy alcohols [187,369], is different from that of typical glass formers. For latter the asymmetric shape of the corresponding loss peaks is thought to arise from dynamical exchange processes taking place on time scales not much slower than that of the mean structural relaxation time [367].

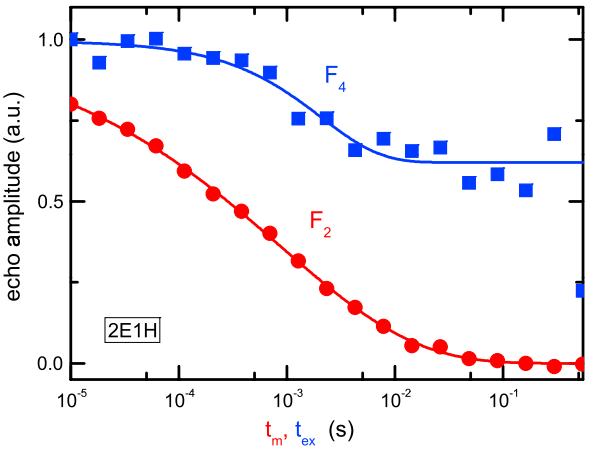

Fig. 46. Two-time echo function $F_2(t_m)$ and four-time echo function $F_4(t_{\text{filter}}, t_{\text{ex}}, t_{\text{filter}})$, both recorded for 2E1H at an evolution time of 15 μs and corrected for spin–lattice relaxation. Solid lines are fits using stretched exponential functions.
Source: From [371].

Thus, one may suspect that in monohydroxy alcohols the symmetric spectral shape hints at a relatively slow dynamical exchange process, a conjecture recently tested by virtue of four-time correlation functions [370].

Corresponding experimental data recorded at 160 K at which $\tau_D/\tau_\alpha \approx 1700$ are shown for 2E1H in Fig. 46 together with fits using stretched exponential functions. These data are corrected for spin–lattice relaxation. For the $F_4(t_{m1}, t_{m2}, t_{m3})$ function filter time $t_{\text{filter}} = t_{m1} = t_{m2} = 0.2$ ms was chosen, resulting in a filter efficiency $FE = 1 - F_2(t_{m1}) = 0.48$, and the exchange time t_{m2} was varied. However, the ratio of experimentally determined decay times τ_4 and τ_2, referring to the decay of the F_4 and the F_2 functions, respectively, is that expected on the basis of the non-exponentiality of the F_2 functions [202]. This demonstrates that the α-relaxation in 2E1H is dynamically heterogeneous, but indications of an unusual dynamic exchange are not evident.

With respect to 2E1H it may be argued that the α process is partially submerged under the large Debye peak and thus it may be questioned whether the relevant distribution of correlation times describing the structural relaxation is indeed symmetrical. Such issues are not a concern in suitably chosen mixtures of 1-butanol (BuOH) with 1-bromobutane (BuBr) for which the symmetric shape of a dielectrically fully resolved process II is evident [369]. Multiple-time stimulated-echo experiments obtained for $(\text{BuOH})_{0.52}(\text{BuBr})_{0.48}$ near 116 and 111 K [370,371] strengthen the conclusion drawn already for 2E1H: A particularly slow dynamic exchange is not detectable for monohydroxy alcohols, still leaving open the question regarding the origin of the spectral shape of process II in these substances.

9. Vibrational spectroscopy

Infrared (IR) and Raman techniques are sensitive to OH stretching vibrations and thus can yield detailed information on the extent and kind of hydrogen bonding in monohydroxy alcohols. In liquids the two methods yield similar information [372], however, when a hydrogen bond is formed the IR absorption typically increases much stronger (in some cases by a factor of ∼20 [373]) than the Raman scattering intensity. The pending studies can be carried out in a wide spectral range that is usually sub-sectioned into the far-infrared (FIR, $\bar{\nu} < 400$ cm^{-1}), mid-infrared (MIR, 400 to 4000 cm^{-1}), and near-infrared (NIR, 4000–14000 cm^{-1}) regimes. In this chapter, wavenumber $\bar{\nu} = \nu/c$ and frequency ν are occasionally used interchangeably.

In Section 9.1 we will start reviewing recent findings for the fundamental modes of the OH stretching vibrations which essentially probe localized properties [374]. In Section 9.2 we will discuss aspects of overtone spectra and Section 9.3 is devoted to a discussion of experimental measures of anharmonicity and hydrogen bond cooperativity. The FIR or terahertz response which is particularly sensitive to detect intermolecular degrees of freedom is dealt with in Section 9.4. Finally, in Section 9.5 some recent developments in the field of pico- and femtosecond vibrational spectroscopy with its ability to study ultrafast chemical exchange processes are mentioned.

9.1. Fundamental OH stretching vibrations

Various aspects of the stretching vibrations of hydroxyl groups in monohydroxy alcohols, e.g., with a focus on alcohol clusters in the gas phase, from matrix isolation studies, or in the liquid state with emphasis on certain analyses were reviewed recently [375–377]. IR spectroscopy on liquid monohydroxy alcohols has a long history, see, e.g., [378,379] for classical accounts. There are numerous studies on methanol [380–388], ethanol [344,383,388–390], propanol [388,391,392],

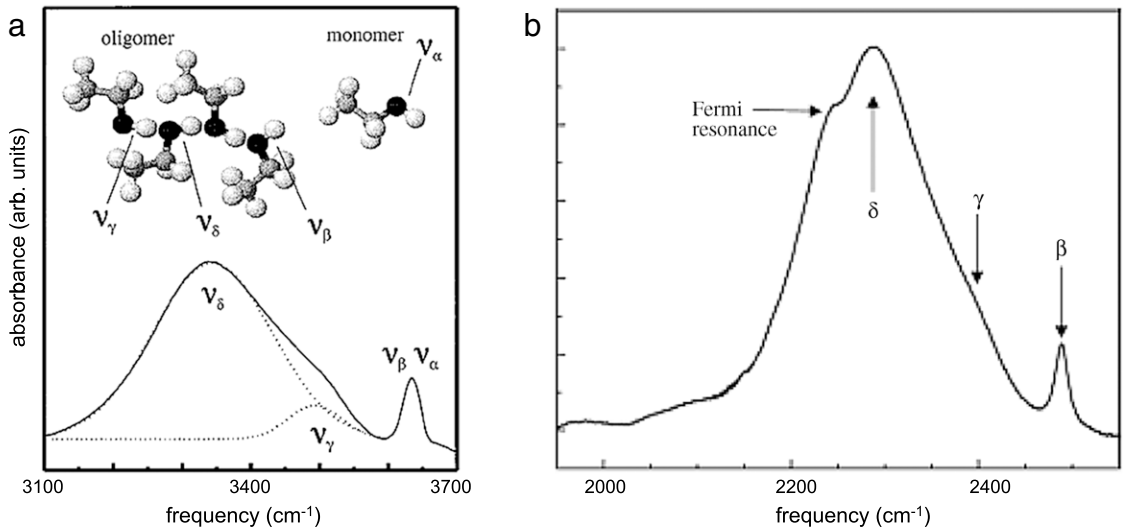

Fig. 47. (a) MIR absorption spectrum of a 1.5 mol/l solution of C_2H_5OH in CCl_4 recorded at room temperature. Typical bonding situations are shown. β molecules donate and γ molecules accept hydrogen bonds, δ species do both and α species are free. Adapted from [424]. Copyright 1997, AIP Publishing LLC. (b) MIR absorption spectrum of hydroxyl deuterated methanol, CH_3OD, diluted in CCl_4. Note that H/D exchange in the hydroxyl group shifts the α to δ bands down in frequency.
Source: Adapted from [427].

1-butanol [132,373,393–396], *tert*-butanol [134,397–399], and various isomeric species of octanol [228,319,397,398,400–406], as well as other monohydroxy alcohols [341,407–411]. This compilation of articles is far from being exhaustive, but it documents the continuing activity in the field. The more recent progress achieved in the interpretation of conventionally recorded IR spectra is mostly due to the increased availability of quantum chemical calculations which specifically compute vibrational spectra for these substances, see, e.g., [412–421]. In the following, we will focus on aspects that we feel are important for the current discussion of the microscopic understanding in relation to the dielectric Debye process. Fluorinated monohydroxy alcohols [422] and thiols [423] will not be considered explicitly.

As an example for the unique potential of IR spectroscopy to provide details regarding the hydrogen bonding in monohydroxy alcohols, in Fig. 47(a) we reproduce an MIR spectrum of ethanol, C_2H_5OH, diluted in CCl_4 [424]. Various bands are labeled in that figure according to the nomenclature by Graener et al. [425]: δ refers to hydroxyl groups that donate *and* accept hydrogen bonds. Thus, molecules that are simultaneously proton acceptor and donor are located in the "middle" of a supramolecular structure. The terminal positions are marked by either β, referring to molecules that accept but do not donate, or by γ, referring to molecules that donate but do not accept hydrogen bonds; and isolated monomeric molecules are designated as α species [426]. Their vibrational frequency is typically very close to that of the β OH group. Thus, in accord with Badger's rule, stronger hydrogen bonds lead to more red shifted frequency positions. The given nomenclature does not specify the *intra*molecular conformation of monohydroxy alcohols which anyway is usually hard to resolve in the liquids state.

In Fig. 47(b) we show a spectrum of OD deuterated methanol diluted in a 10% CCl_4 solution [427]. The frequency of the stretching vibration of the hydroxyl group depends on its effective mass and thus is subject to an isotope shift of about $\sqrt{2}$ [428], but overall both spectra in Fig. 47 look very similar. The α to δ nomenclature is commonly applied also to the deuterated species. Nevertheless, one has to bear in mind that this way of classifying bands of hydroxyl groups represents a considerable simplification. A more detailed speciation is possible on the basis of density functional calculations, see, e.g., [418]. In the cited work fully protonated methanol was studied, hence, the stretching vibration frequencies appear in the ∼3000 to ∼3600 cm^{-1} range. Methanol clusters involving up to $n = 7$ molecules were taken into account and a few examples from [418] are collected in Fig. 48. In addition to what is illustrated in Fig. 47 also branched hydrogen bonds were considered. The density functional calculations yielded optimal geometries, vibrational frequencies, and the total hydrogen bond energy, $\Delta E_{\rm hb}$, as well as the average energy, $\Delta\bar{E}_{\rm hb}$, per hydrogen bond. In [418] these energies were defined as $\Delta E_{\rm hb} = nE(\text{monomer}) - E(n\text{-mer})$ and $\Delta\bar{E}_{\rm hb} = \Delta E_{\rm hb}/m$ with m denoting the number of hydrogen bonds in a cluster. In Fig. 48 the average energies per hydrogen bond, given for a few n-meric structures, were found in the range of $\Delta\bar{E}_{\rm hb} = 20\ldots30$ kJ/mol. A metric was identified in [418] that could explain the trend in the OH bond energies by considering how an OH···O donor–acceptor group bonds to the nearest and to the next nearest neighbors. Furthermore, a linear relationship was established between the length of a covalent OH bond and its vibrational frequency $\nu_{\rm OH}$. This relationship was found to be valid no matter whether so-called coupled or uncoupled modes were considered. In [418] $\nu_{\rm OH}$ was computed for CH_3OH, contained in clusters otherwise made up of only CH_3OH molecules (coupled case), or of CH_3OD molecules (uncoupled case). The alternative situation, $\nu_{\rm OD}$ computed for CH_3OD diluted in CH_3OD (coupled) or in CH_3OH

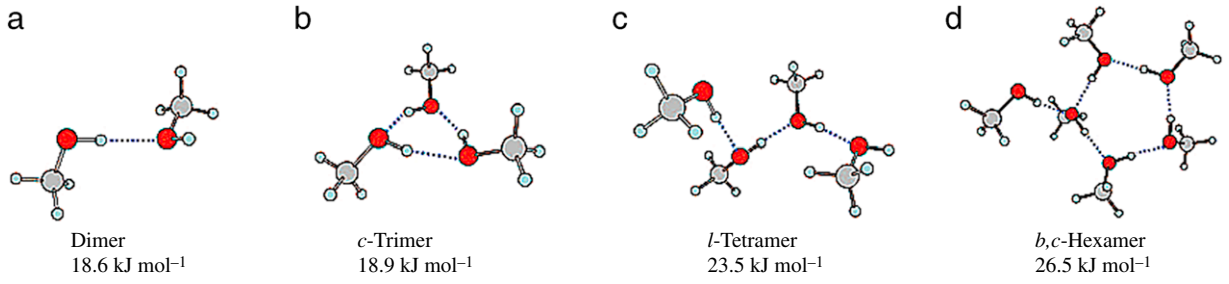

Fig. 48. Examples of $(CH_3OH)_n$ clusters and their average energy $\Delta\bar{E}_{hb}$ per hydrogen bond according to quantum chemical calculations. Cyclic (c), linear (l), and branched (b) n-mers are shown. The energy of the dimer is relatively low because cooperative effects are absent and that of the trimer is low because the hydrogen bonds in this configuration are significantly strained. The energies for the tetramer and the hexamer clusters are in the range typically found in experiments.
Source: Adapted with permission from Ref. [418] from which gives energies for many more clusters.

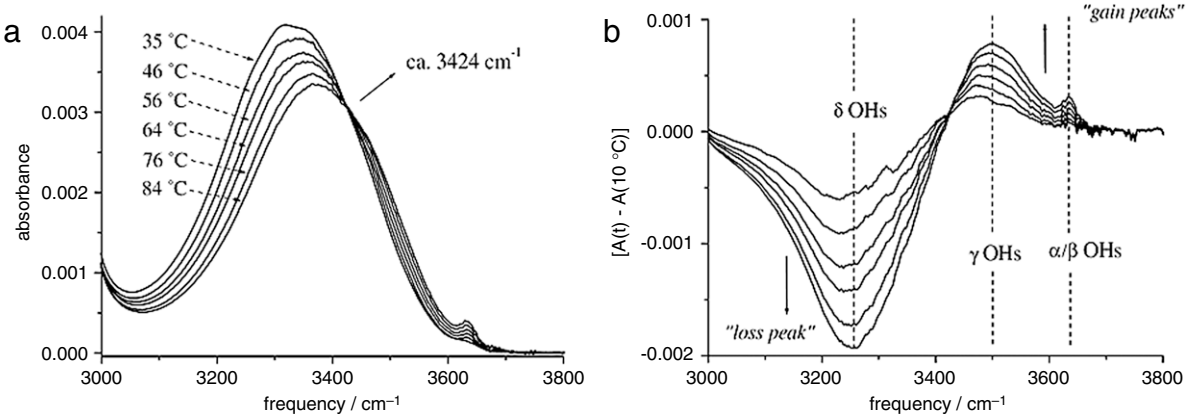

Fig. 49. (a) MIR absorption spectra of 1-octanol focusing on the range of the OH stretching vibration. (b) Difference spectra, $A^d(\bar{\nu}, T_{ref})$, generated using the data in frame (a) for a reference temperature of $t_{ref} = 10$ °C, showing gain and loss peaks. The wavenumbers $\bar{\nu}_{\alpha/\beta}$, $\bar{\nu}_\gamma$, and $\bar{\nu}_\delta$ corresponding to the various bands are marked.
Source: Adapted from [405].

(uncoupled) was not explicitly considered. So far detailed quantum calculations of vibrational properties focused mostly on clusters of small molecules.

The existence of hydrogen bond cooperativity is also well known from vibrational experiments. As a recent example, in Fig. 49(a) temperature dependent MIR spectra of 1-octanol are shown focusing again on the spectral region of the OH stretching vibration. The main peak of the IR absorbance $A(\nu)$ and also of the Raman intensity $I(\nu)$, see [403], which is dominated by the δ-band (sometimes called polymer band) undergoes a significant blue shift as temperature is increased. The position of the α/β-band, stemming from non bonded or weakly bonded hydroxyl groups, on the other hand, varies only little with temperature. The corresponding changes are more readily grasped from difference spectra, A^d, such as the ones shown in Fig. 49(b). Here, $A^d(\nu, T_{ref}) = A(\nu, T) - A(\nu, T_{ref})$ is plotted with T_{ref} denoting an arbitrarily chosen reference temperature. Not only changes in the α/β- and in the δ-band, but also in the γ-band, hard to recognize from Fig. 49(a), are now immediately obvious from so-called gain and loss peaks. The arrow in Fig. 49(a) hints at a so-called isosbestic point which arises in the presence (not only) of a two-state equilibrium. Various other scenarios can also lead to the occurrence of quasi-isosbestic points [429].

There are numerous ways to highlight spectral changes that appear as a function of temperature (or of other variables such as pressure, composition, etc.). Apart from simply providing fit parameters from a line shape analysis (which we will not focus upon here), let us discuss two approaches, (i) a derivative analysis as summarized in the following and (ii) two-dimensional (2D) correlation analysis as outlined in Section 9.2.

In the frame work of the derivative analysis, a wavenumber dependent effective energy $E(\nu) = -R\,\partial \ln I(\nu)/\partial(1/T)$ [430] is calculated from the absolute Raman intensity, $I(\nu)$, [403] or similarly from the IR absorbance, $A(\nu)$ [405]; here R is the gas constant. $E(\nu)$ as determined from the 1-octanol spectra in Fig. 49(a) is shown in Fig. 50. The condition $\partial E(\nu)/\partial\nu \to 0$ indicates the presence of the various OH oscillator states highlighted by the vertical lines in Fig. 49(b). The energies corresponding to the δ, γ, and α/β bands can directly be read off from the horizontal bars in Fig. 50. The authors of [405] emphasize that for 1-octanol the energy difference $E(\nu_{\alpha/\beta}, \nu_\delta) = E(\nu_{\alpha/\beta}) - E(\nu_\delta)$ is about 27 kJ/mol and that for

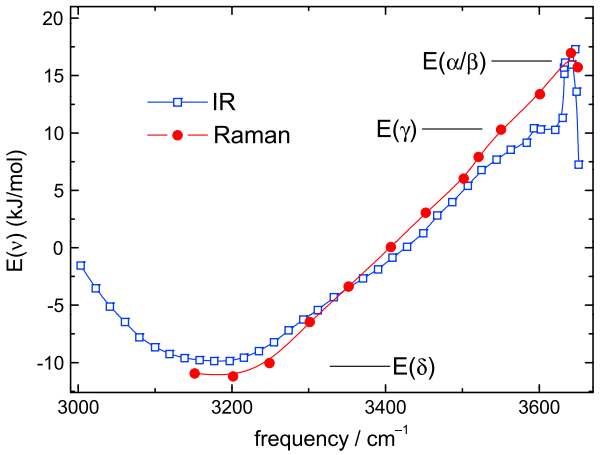

Fig. 50. Dispersion of the effective energy $E(\nu) \propto \ln X(\nu)/\partial(1/T)$ calculated [403] from the data shown in Fig. 49. Here $X(\nu)$ denotes either the MIR absorbance, $A(\nu)$, or the Raman intensity, $I(\nu)$. Horizontal bars are drawn at $E(\nu_\delta) = -10$ kJ/mol, $E(\nu_\gamma) = +10$ kJ/mol, and $E(\nu_{\alpha/\beta}) = +17$ kJ/mol.
Source: Redrawn from [403].

many alcohols this is a typical maximum hydrogen bonding energy. The energy of a terminal hydrogen bond, $E(\nu_{\alpha/\beta}, \nu_\gamma)$, was estimated from $E(\nu_{\alpha/\beta}, \nu_\delta) - E(\nu_\gamma, \nu_\delta)$ and found to be only about 7 kJ/mol, thus much smaller than $E(\nu_{\alpha/\beta}, \nu_\delta)$. The cooperative energy itself was identified with $E(\nu_\gamma, \nu_\delta)$ and turned out to be ∼3 times larger than the energy of a terminal hydrogen bond, see also [431].

Fig. 50 includes results from vertical–vertical (VV) polarized Raman spectra. In this context it is worthwhile to mention that depolarized (horizontal–vertical, HV) Raman and polarized scattering do not yield identical results. Merely, the wavenumber $\bar{\nu}_{\rm iso}$ from the δ peak of the isotropic Raman profiles, $I_{\rm iso}(\nu) = I_{\rm VV}(\nu) - (4/3)I_{\rm VH}(\nu)$, differs from the wavenumber $\bar{\nu}_{\rm aniso}$ at which the anisotropic profile, $I_{\rm VH}(\nu)$, is peaked. For 1-octanol at 10 °C this "non-coincidence effect" is evident from a 90 cm^{-1} red shift of the VV peak with respect to the HV peak [403]. In [403] the peak at $\nu_{\rm iso}$ was assigned to the in-phase collective mode of δ hydroxyl groups efficiently stabilized by specific cooperative effects. These can arise from directly hydrogen bonded OH pairs aligned in a way so that a resonant energy transfer among them becomes likely. The peak at $\bar{\nu}_{\rm aniso}$ was ascribed to δ OHs performing either anti-phase collective vibrations or else uncorrelated vibrations. The latter decoupled scenario can arise, e.g., from a wavenumber mismatch of the corresponding δ OH groups that in turn is, for instance, caused by a distribution of inter-oscillator angles and distances. Conventional IR spectroscopy, with $\bar{\nu}_{\rm aniso} > \bar{\nu}_{\rm IR} > \bar{\nu}_{\rm iso}$, is unable to distinguish isotropic from anisotropic contributions.

The examples presented here render it obvious that Raman and IR methods are not only powerful tools to selectively study the properties of the molecular group that is held responsible for the generation of the monohydroxy alcohols' supramolecular behavior. Merely, vibrational spectroscopy is indispensable when striving for detailed insights into the cooperative nature of hydrogen bonding, to quantify hydrogen bond populations, as well as to monitoring their thermally driven equilibration or the time evolution of its establishment subsequent to external perturbations. Several applications along these lines as well as some developments pushed forward (e.g., with the goal to enhance spectral resolution) will therefore be reviewed in the following subsections.

9.2. Vibrational overtones and hydrogen bond equilibria

Due to the anharmonicity of the vibrational potential, overtones are allowed, with the first hydroxyl overtones typically appearing in the NIR spectral range. As an example, in Fig. 51 spectra of diluted 1-pentanol are compared to that of 1-pentane [409]. Due to the existence of various overtone and combination bands the NIR range is relatively crowded and thus for a band assignment it may be useful to consult compilations of spectra, e.g., [432]. To some extent an overlap of different vibrational components is also present in the range of the first OH stretch overtone. But fortunately the overlaying first overtones of the CH stretches can often be disentangle by comparison, e.g., with spectra of similar molecules devoid of hydroxyl groups (here 1-pentane) or by analyzing difference spectra. In order to resolve spectra further, various statistical techniques have been exploited [409]. Also, the 2D correlation analysis mentioned in Section 9.1 was applied in this context.

To perform a 2D correlation analysis, a set of s difference spectra, for suitably chosen reference temperatures also termed dynamic spectra [375], $A_j^d(\nu)$ with $j = 1$ to s is required. In the spirit of ideas developed for the analysis of time series, it turned out useful to construct so called synchronous spectra, $\Phi(\nu_1, \nu_2)$, and asynchronous spectra, $\Psi(\nu_1, \nu_2)$. These are defined according to [375,433]

$$\Phi(\nu_1, \nu_2) = \frac{1}{s-1}\sum_{j=1}^{s} A_j^d(\nu_1)A_j^d(\nu_2) \quad \text{and} \quad \Psi(\nu_1, \nu_2) = \frac{1}{s-1}\sum_{j=1}^{s} A_j^d(\nu_1)\sum_{k=1}^{s} H_{jk}A_k^d(\nu_2), \tag{20}$$

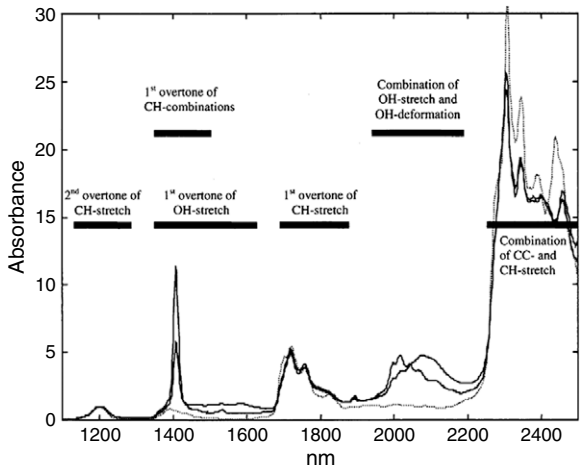

Fig. 51. NIR spectra of 0.1 and 0.5 M 1-pentanol in CCl_4 (solid lines) and 1-pentane (dotted line). The spectra are normalized to the intensity of the band at 1200 nm.
Source: Adapted with permission from [409].

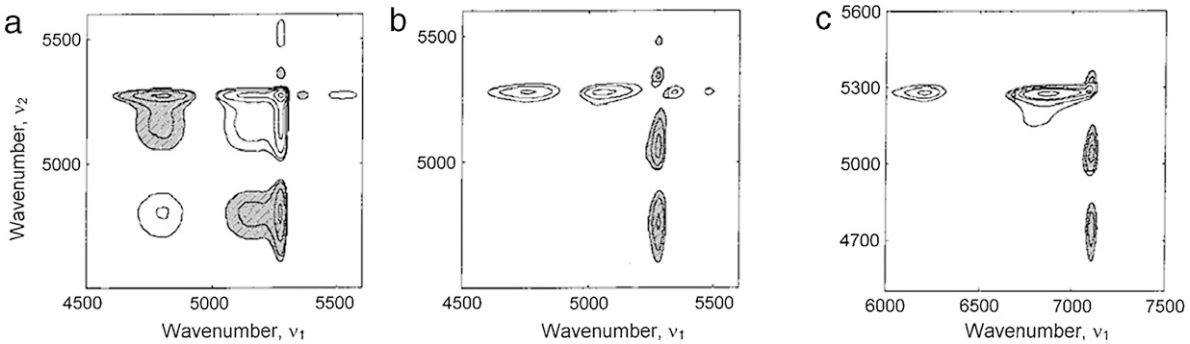

Fig. 52. Examples for results of 2D correlation analyses. (a) Synchronous and (b) asynchronous NIR correlation spectra of hydroxyl deuterated 1-butanol-d_1 constructed on the basis of spectra recorded in the temperature range from 20 to 85 °C. (c) Asynchronous spectra of fully protonated 1-butanol on the ν_1 axis versus 1-butanol-d_1, on the ν_2 axis, calculated from absorbance data in the same temperature range. Negative peaks are hatched.
Source: Reprinted with permission from [394].

on the basis of the difference spectra. The H_{jk} matrix mediates a Hilbert transform. Off-diagonal intensity arises in 2D spectra, constructed according to Eq. (20), if features in the corresponding dynamic spectra evolve differently as a function of the external parameter (here: temperature). In Fig. 52(a) and (b) we reproduce synchronous and asynchronous spectra, respectively, of hydroxyl deuterated 1-butanol-d_1 [394]. Prominent OD stretching overtones appear near 5270 cm^{-1} (monomer band) and near 4800 cm^{-1} (polymer band) and their "auto" peaks show up on the diagonal in Fig. 52(a). The intense "cross" peaks between them are negative (indicated by gray hatching) implying that temperature variations change the intensity of the polymer versus monomer band in opposite directions. The asynchronous spectrum, Fig. 52(b), reveals that the intensity change near 5270 cm^{-1} proceeds at a rate smaller than intensity changes at any other wavenumber. From this observation it was concluded that the thermal dissociation of the polymers into the monomers proceeds through intermediate species [394]. The heterospectral 2D plot reproduced in Fig. 52(c), based on an analysis involving hydroxyl protonated *and* hydroxyl deuterated 1-butanol, looks very similar to that shown in Fig. 52(b). Thus, despite their vastly different stretching frequencies the bands of both isotopomers exhibit the same temperature trends.

Generally, it was found that this kind of analysis can help in enhancing the effective resolution and in securing the assignment of IR spectra, e.g., when trying to disentangle nearby bands that can appear in the presence of rotational isomerism [393] or in the context of chiral discrimination [400]. Isotopic dilution is usually not helpful in this respect, because it was noted that it does not reduce the line width significantly if it is due to the disorder inherent in the liquid [434]. Furthermore, 2D correlation analysis also allows one to combine spectral information from NIR and MIR or from IR and Raman spectroscopies. Of course, due to the involved processing of the raw data particular caution and experience is required to interpret the resulting 2D spectra properly [375,433,435]. It is noted that 2D correlation analyses were recently carried out also in the fields of dielectric [436] and mechanical spectroscopy [437].

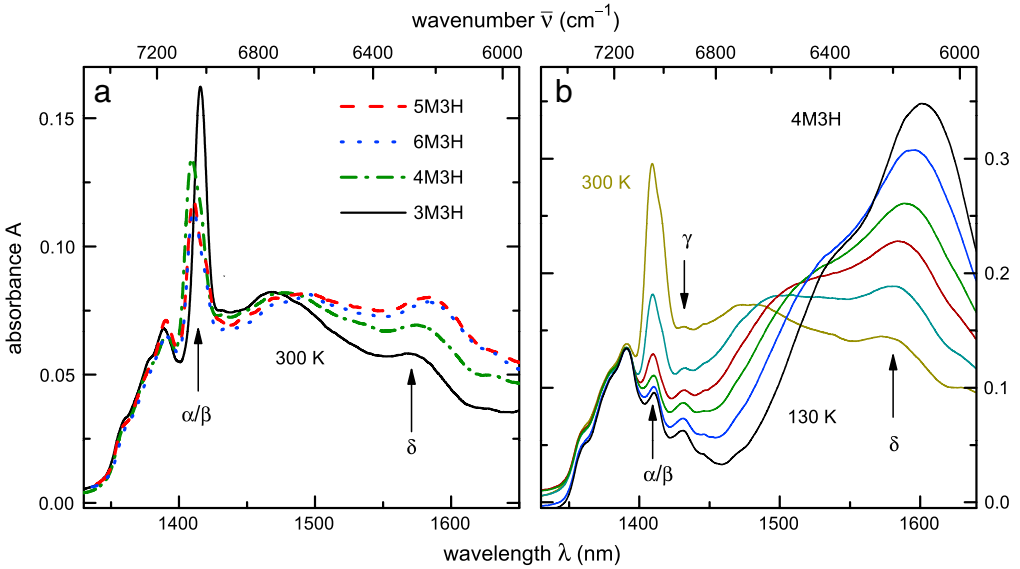

Fig. 53. (a) Room temperature NIR spectra focusing on the spectral range of the first OH stretching overtone for the octanols 3M3H, 4M3H, 5M3H, and 6M3H measured for a 1 mm path length [438]. (b) Temperature dependent spectra of 4M3H (measured for a 2 mm path length) reprinted with permission from [228]. Copyright 2013 AIP Publishing LLC. The α/β, γ, and δ bands are highlighted by arrows.

Let us now examine effects of molecular branching on the NIR absorption. In Fig. 53(a) spectra for various octanol isomers are shown. One recognizes that the strength of the bands depends sensitively on the molecular structure and in particular on the position of the methyl group in the series of j-methyl-3-heptanol (jM3H) molecules with $j = 3$, 4, 5, and 6. The monomer band is larger if the hydroxyl group is sterically shielded more efficiently. At 300 K at which these spectra were recorded the other (γ and δ) bands are quite broad. However, this situation changes if temperature is lowered. In Fig. 53(b) spectra for 4M3H are shown that reveal a decrease of the α/β band and an increase of the δ band upon cooling [228]. Furthermore, the peak showing up near 1470 nm at 300 K that might be due to (cyclic) oligomers [402] seems to shift to longer wavelengths as T is reduced. A red-shift also of the δ band is observed from Fig. 53(b) as well as for other monohydroxy alcohols [228]. Typically this red-shift is interpreted to indicate a strengthening of the hydrogen bonds in which the δ OH groups participate. This strengthening of the O $\cdots$ H bond destabilizes the covalent O–H bond thereby reducing the frequency of the associated stretching vibration.

An analysis of the temperature dependent absorbance spectra is often performed using van't Hoff plots. An example is shown in Fig. 54(a) which includes absorbance ratios for a number of monohydroxy alcohols with different alkyl chain length and molecular branching. An equilibrium constant K and a reaction enthalpy ΔH is estimated from this kind of representation according to the van't Hoff equation, written here as

$$\log_{10} K \propto \log_{10} \frac{A(\lambda_{\alpha/\beta})}{A(\lambda_{\delta})} = -\frac{\Delta H}{R \ln(10)} \cdot \frac{1}{T} + \text{const.} \tag{21}$$

Eq. (21) assumes that a description in terms of a two-state equilibrium (here involving the α/β and the δ species) is appropriate, that the number of participating species is properly reflected by the absorbances, and that their variation is indeed dominated by changes of these numbers (and not, e.g., by changes of the anharmonicity, cf. Section 9.3).

Even without taking for granted that the absorbance variations reflect only population changes, from Fig. 54(a) it is obvious that for many monohydroxy alcohols a change of behavior occurs for temperatures near 250 K. Similar nontrivial temperature dependences are reflected also in other static quantities, such as the dielectric constant or the proton chemical shift for a large number of monohydroxy alcohols [228], see Fig. 55(a) for an example, as well as in dynamic quantities (such as the dielectric Debye relaxation time τ_D [63], see Fig. 25). A Raman scattering study of 1-butanol also identified particular behavior near 250 K and 3330 cm^{-1} [132]. On the other hand, from a van't Hoff plot for 1-octanol Raman [403] and IR spectroscopy [405] (not extending to below 10 °C) a hint was obtained that a change in the hydrogen bonding energies occurs at ∼320 K.

The enthalpy ΔH, can be calculated from the data shown in Fig. 54(a) by taking the derivative $R \ln(10) \partial \ln[A(\lambda_{\alpha/\beta})/A(\lambda_{\delta})] / \partial(1/T)$, see Fig. 54(b). For $T > 220$ K the effective enthalpies are seen to increase with increasing temperature, at the highest temperature accessible in [438] reaching $\Delta H \approx 25$ kJ/mol a value very similar to that discussed in the context of Fig. 49(c). In various NIR studies on (also other) hydrogen bonded systems only temperatures lower than ambient were covered, see, e.g., [228,439,440] and enthalpies smaller than 25 kJ/mol were reported. For $T < 220$ K enthalpy values of just a few kJ/mol are found for all monohydroxy alcohols represented in Fig. 54(b). On the basis of only a subset of the substances compiled in Fig. 54(b), the finding of this small ΔH was interpreted to hint at a population equilibrium involving different

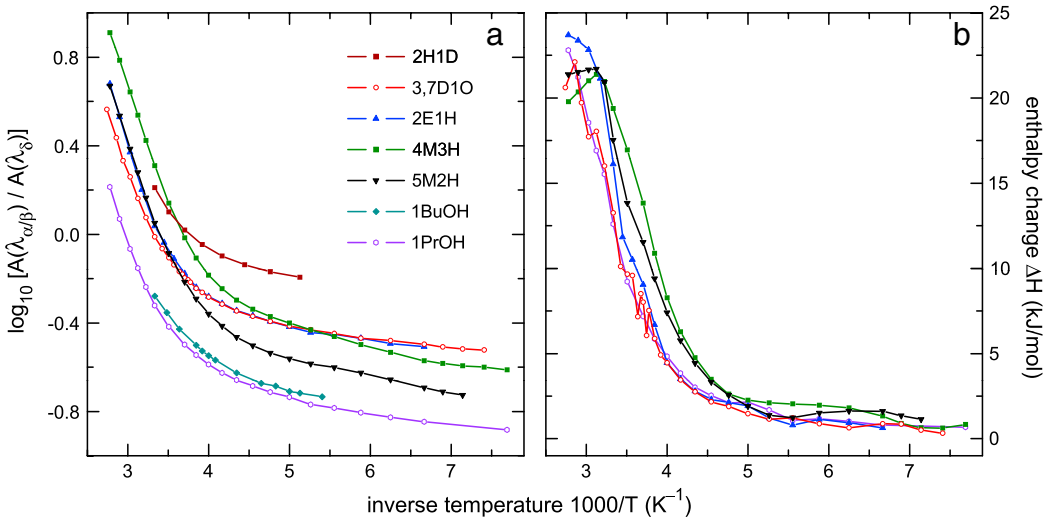

Fig. 54. (a) Van't Hoff plot for the absorbance ratio of monomer and polymer bands for 2-hexyl-1-decanol (2H1D), 3, 7-dimethyl-1-octanol (3, 7D1O), 2E1H, 4M3H, 5-methyl-2-hexanol (5M2H), 1-butanol (1BuOH), and 1-propanol (1PrOH) with data taken from [228,238,370]. Overall $A(\lambda_{\alpha/\beta})/A(\lambda_\delta)$ increases with increasing alkyl chain length because at stronger "dilution" of the hydroxyl group the probability of finding hydrogen bonding partners is reduced. (b) Reaction enthalpies ΔH obtained from the derivative $R\ln(10)\partial\ln[A(\lambda_{\alpha/\beta})/A(\lambda_\delta)]/\partial(1/T)$ of the data shown in frame (a). One recognizes clearly that ΔH increases from just a few kJ/mol at low temperatures to ∼25 kJ/mol at $T = 360$ K.

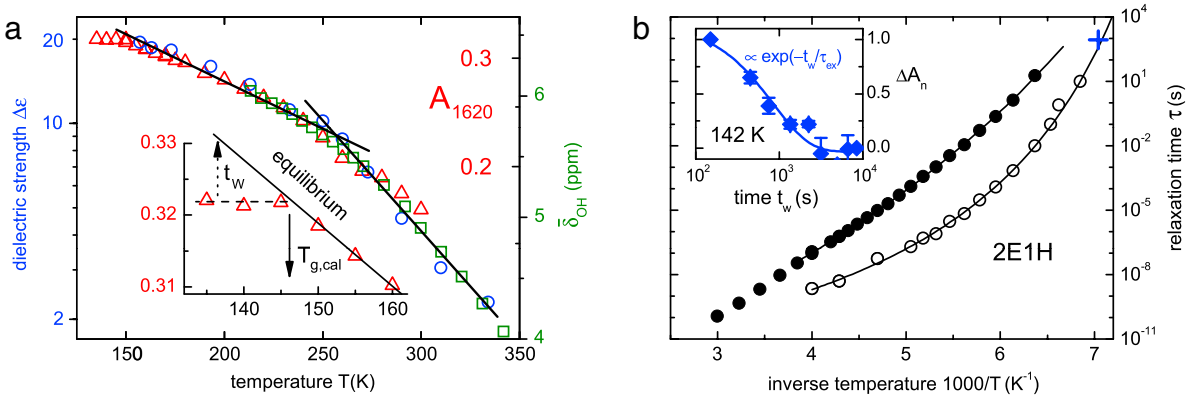

Fig. 55. (a) Temperature dependence of several static quantities measured for 2E1H. Changes are observed near 250 K in the dielectric strength, $\Delta\varepsilon_D$ (circles), in the absorbance maximum near 1620 nm, and in the chemical shift, $\bar{\delta}_{OH}(T)$, of the hydroxyl proton. The inset demonstrates that near T_g the absorbance $A_{1620}(T)$ is "frozen in" on the time scale of the experiment. The dashed arrow indicates that for long waiting times t_w the peak absorbance returns to its extrapolated equilibrium value. (b) Temperature dependent dielectric relaxation times for the Debye process (closed circles) and for the α-process (open circles). The solid lines are fits using the Vogel–Fulcher equation, (12). The cross marks the time constant τ_{ex} governing the equilibration of the time resolved NIR spectra. The inset shows the time dependence of the NIR absorbance at 142 K together with an exponential fit (dashed line).
Source: Adapted from [64].

(e.g., chain-like and ring-type) supramolecular hydrogen bonded structures that are energetically almost equivalent [228]. While ΔH shows little variation when comparing different monohydroxy alcohols, from Fig. 54(a) it is obvious that in the low-temperature regime, by and large, the absorbance ratio does increase with increasing overall molecule size. In other words, the density of the non- or weakly bonded OH groups relative to that of the bonded ones increases. This is plausible because if the alkyl chain becomes bulkier and bulkier, then it will become more and more difficult to find a hydrogen bonding partner. This notion is indirectly confirmed by a recent dielectric study which shows that for a monohydroxy alcohol with 24 carbon atoms, supramolecular association is suppressed to an extent that not even a small Debye process can be detected [222].

For many monohydroxy alcohols the temperature dependent absorbance ratio does change slope not only near 250 K. Also the glass transition temperature typically marks itself as a change of absorbance properties in monohydroxy alcohols [64] as well as in other glass formers [238,440,441]. In Fig. 55(a) absorbance data for 2E1H are shown (similar plots for several other monohydroxy alcohols are presented in [228]). In the inset of Fig. 55(a) one recognizes that a break in slope occurs near the calorimetric glass transition temperature [64]. This result suggests that the time scale which governs

the establishment of the hydrogen bond population in 2E1H is given by the structural relaxation time, τ_α, and not by the time scale of the dielectric Debye process, τ_D, which at $T_{g,cal}$ is ∼3 orders of magnitude longer than τ_α [228].

The equilibration of the hydrogen bond distribution and thus the time scale of the "chemical exchange" among different bonding states of the hydroxyl group can be monitored more directly by recording the time resolved absorbance subsequent to an external perturbation induced, e.g., by a jump [442,443] or by a (harmonic) variation [444] in pressure or temperature. The inset of Fig. 55(b) shows the time evolution of the normalized absorbance $\Delta A_n(t)$ of 2E1H that was initiated by a 3 K downward jump in temperature. The exchange time scale τ_{ex} extracted from the data in this inset can then directly be compared with τ_D and τ_α, see the Arrhenius plot, Fig. 55(b), confirming the above conjecture that τ_{ex} and τ_α virtually coincide.

Chemical exchange cannot only be monitored by vibrational spectroscopy on ultraslow time scales, but certainly also with microsecond time resolution (and subsequent to an electrical field perturbation [445], not applied to monohydroxy alcohols so far), and even in the sub-picosecond regime, see Section 9.5.

9.3. Anharmonicity and hydrogen bond cooperativity

How much of the (temperature dependent) intensity change of the overtone bands seen, e.g., in Fig. 53(b), is due to a variation of anharmonicity effects? The answer is: Apparently very little! Let us give some background [372,434,446] to justify this answer properly. In a Morse potential the lowest-order anharmonic oscillator frequencies are $\nu_\upsilon = \upsilon_i\nu_0 + \upsilon_i(\upsilon_i+1)X$ or $\nu_\upsilon = \upsilon_i\nu_0\,[1-x_e(\upsilon_i+1)]$. Here, ν_0 is the harmonic frequency, $\upsilon_i = 0, 1, 2, \ldots$ vibrational quantum numbers, and $x_e > 0$ the dimensionless anharmonicity constant. Often the anharmonicity constant also is given in wavenumber units as $X = -\nu_0 x_e$. Using these notations, the fundamental vibration ($\upsilon_i = 1 \rightarrow 0$ or $|1\rangle \rightarrow |0\rangle$ transition) appears at $\nu_1 = \nu_0\,(1-2x_e) = \nu_0 + 2X$ and the first overtone ($|2\rangle \rightarrow |0\rangle$ transition) at $\nu_2 = 2\nu_0 + 6X$ or $\nu_2 = 2\nu_1\,(1-3x_e)/(1-2x_e) \approx 2\nu_1\,(1 - x_e - 2x_e^2) < 2\nu_1$. The latter approximation is valid for small x_e (which typically is of the order of a few percent). The anharmonicity $\nu_0 x_e$ of the OH stretching vibration was related to the O···O distance [447]. While we deal here solely with the first OH overtone, in general it may be useful to consider higher overtones as well [389].

Regarding the origin of the anharmonicity [434,446], one often distinguishes two types (i) the mechanical anharmonicity, due to the non-harmonic terms of the vibrational potential, and (ii) the electrical anharmonicity. The latter generally arises if the transition dipole moment $\mu(Q)$ depends on the normal coordinate Q describing the vibration. One way to handle this situation, is to expand $\mu(Q)$ in terms of a Taylor series with coefficients $\mu_n = (d^n\mu/dQ^n)/n!$ [434]. Mechanical anharmonicity is then needed to give μ_1 appreciable weight. Another way is to consider (smooth) dipole moment functions $\mu(Q)$. This allows one to calculate the vibrational frequencies, ν_υ, and also their integrated band intensities, A_υ. Based on plausible assumptions for $\mu(Q)$, for uncoupled vibrations from [448] the relative intensity of the first overtone band can be estimated as $A_2/A_1 \approx 4x_e\,(1-5x_e)/(1-3x_e)^2 \approx 4x_e\,(1+x_e)$. Within this small x_e approximation the overtone is proportional to x_e (and to the intensity of the fundamental band). It is noted, however, that in the frame work of other approaches and for specific choices of μ_1 and μ_2 even opposing trends can arise for A_1 versus A_2 [434].

Let us now discuss experimental determinations of anharmonicity constants for monohydroxy alcohols. When only considering the fundamental and first overtone band in wavenumber units one often writes $X_{12} = \tilde{\nu}_2/2 - \tilde{\nu}_1$ (<0). The anharmonicity constant for the monomer band of methanol, CH_3OH, was found to be $X_{12} = -80\ cm^{-1}$ and for the polymer band $-94\ cm^{-1}$ (in dilute solution at −190 °C) or $-115\ cm^{-1}$ (in the pure liquid at room temperature) [449]. For the temperature dependence $dX_{12}/dT = 0.2 \ldots 0.3\ cm^{-1}/K$, was reported for several protonated monohydroxy alcohols, implying that the anharmonicity is smaller for lower temperature [450]. This could indicate that the O–H···O bond becomes more symmetric upon cooling. The anharmonicity of methanol displays an isotope effect expressed as $X_{12}(OH)/X_{12}(OD) \approx 0.6 \ldots 0.7$. For several deuterated monohydroxy alcohols one finds $dX_{12}/dT = 0.1 \ldots 0.2\ cm^{-1}/K$ [450].

Let us now discuss the concept of hydrogen bond cooperativity [66] which is well established and, as already emphasized, backed up by a host of experimental observations and computations. In this context it is worthwhile to mention Car–Parrinello molecular dynamics simulations which found that the electrical dipole moment μ of methanol depends on the number of hydrogen bonds it forms [104]: Values for μ of 2.06, 2.24, 2.71, and 2.99 D were reported as the number of hydrogen bonds per molecule increases from zero to three.

In the following we recapitulate an approach that allows one to quantify hydrogen bond cooperativity using vibrational spectroscopy, by means other than already discussed in the present Section 9. It has been suggested that *simultaneous* photon absorption of monohydroxy alcohol molecules that are in close spatial proximity can quantify cooperativity [451]. It is well known that adjacent molecules can absorb a single photon simultaneously and "share" its energy so that *all* of these molecules become vibrationally excited at the same time. The experimental approach presented in [451] is based on using isotopically enriched $(CD_3OH)_x(CD_3OD)_{1-x}$ mixtures, so that the concentration of neighboring OH···OH pairs can be tuned experimentally if the CD_3OH mole fractions x is sufficiently small. In Fig. 56(a) normalized NIR spectra are shown in the OH overtone region for $x = 0.05$, 0.1, 0.2, and 0.3 from which the absorbance of neat CD_3OD was already subtracted. The overtone intensity (at $2 \times 3343\ cm^{-1}$) was found proportional to x, as expected for absorption by single molecules [451]. The simultaneous absorbance intensity, on the other hand, was shown to display an x^2 dependence. This quadratic effect demonstrates that near $6720\ cm^{-1}$ (adjacent) *pairs* of hydrogen bonded hydroxyl groups are the absorbing species.

By suitably subtracting the overtone contributions from the spectra shown in Fig. 56(a) a "simultaneous absorption band" is obtained, see Fig. 56(b). Interestingly, its intensity maximum shows up at a frequency *larger* than corresponding to the

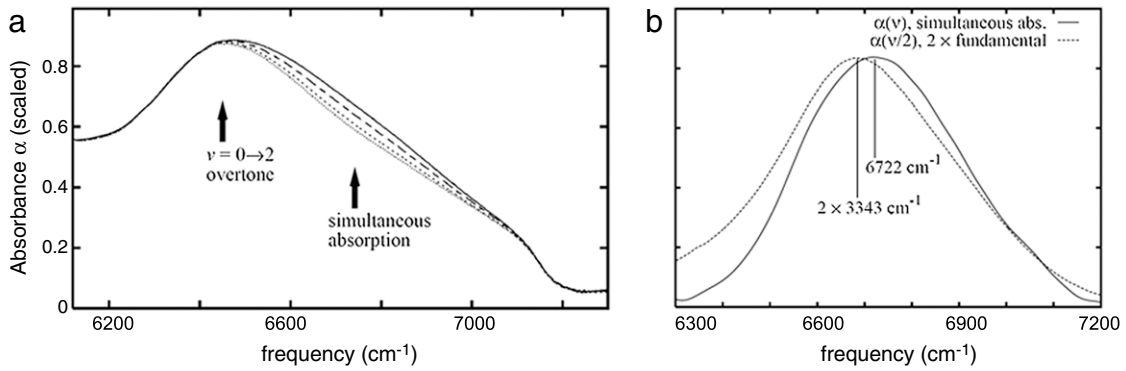

Fig. 56. (a) Absorbance of $(CD_3OH)_x(CD_3OD)_{1-x}$ mixtures for $x = 0.05$, 0.1, 0.2, and 0.3. The simultaneous absorption increases with increasing x after scaling the spectra at 6300 cm^{-1}, which is slightly below the OH stretch overtone maximum. (b) The solid curve represents the "simultaneous absorption band" as obtained by subtracting the absorption from a sample with $x = 0.05$ from one with $x = 0.2$. The dashed curve represents the fundamental MIR spectrum corresponding to the OH stretching vibration, but with the frequency axis multiplied by a factor of 2. The maximum of the simultaneous absorption occurs at a frequency that is 36 cm^{-1} higher than twice that of the fundamental frequency.
Source: Reprinted with permission from Ref. [451].

sum of the fundamental frequencies of each molecule in the simultaneously absorbing pair [452]. The positive frequency shift of 36 cm^{-1} is thus interpreted as a measure of the interaction strength between the vibrationally coupled OH bonds.

All mechanisms that conceivably mediate an interaction among the simultaneously absorbing species are short ranged: Dipolar couplings decay as d^{-6}, with d measuring the distance between the hydroxyl groups; other couplings would imply an even stronger dependence on d. Therefore, in dilute solutions only OH bond pairs have been argued to be relevant in rationalizing the effect. It was pointed out in [451] that the observed frequency shift of the simultaneous photon absorption is about two times smaller than the shift determined from the Raman non-coincidence effect (see the discussion below Fig. 49) in (isotopically pure) methanol. This observation was rationalized by noting that in the neat liquid, each OH group can interact with *at least* two OH groups. Thus simultaneous absorption as well as the Raman non-coincidence effect, can yield the coupling strength of vibrations that share similar frequencies [451]. Two-dimensional vibrational spectroscopy, on the other hand, see Section 9.5, is only suited for this purpose if the corresponding vibration frequencies are sufficiently well separated.

9.4. Terahertz dynamics

The FIR or (sub-) millimeter regime, nowadays usually called THz spectral range, was long deemed experimentally hardly accessible. Nevertheless, the dielectric response can be probed in this range using classical techniques [392,453,454] and using more recent (typically time-domain) methods [455–464]. For a short survey on some of them see [465,466]. When comparing different techniques it is useful to keep in mind that 30 GHz, 1 cm^{-1}, and 0.124 meV refer to the same "frequency".

Apart from absorption based spectroscopies, THz dynamics is also accessible via incoherent inelastic neutron scattering [467–470] and using low-frequency Raman techniques. Here one usually monitors the relaxation of the anisotropic component of the polarizability either as depolarized light scattering in the frequency domain [266,463,471,472] or in the time as pulse response function via the Raman-induced optical heterodyne-detected optical Kerr effect (OHD-OKE) [260,473–476]. While the *electro-optical* Kerr effect *is* sensitive to the dynamics of the Debye process, see Section 6.2, OKE obviously is *not*, as will become clear in the following.

Let us therefore compare the collective anisotropic polarizability fluctuations [477] with those of the electrical dipole moment for the example of methanol at 25 °C, see Fig. 57 [463]. Here the FIR absorption [more precisely the dielectric loss $\varepsilon''(\nu)$] is shown together with the depolarized (VH) Raman scattering. To facilitate a comparison of the results from the two techniques, the low-frequency Raman intensity, $I(\nu)$, is transformed to the imaginary part of the complex dynamic susceptibility, $\chi''(\nu) = I(\nu)/[b(\nu) + 1]$, using the Bose population factor, $b(\nu)$ [463]. The intermolecular vibration and libration bands, visible in the Raman spectrum, could be described by a superposition of exponential relaxation processes and damped oscillator modes as indicated in Fig. 57 [463].

Fig. 57 documents that, apart from the τ_1 contribution which is missing in the Raman spectrum, the other processes show similar characteristic frequencies suggesting that the dielectric and the Raman relaxation modes reflect a common molecular dynamics. When it is recognized that here a rank $\ell = 1$ technique (see Section 5.1), dielectric spectroscopy, is compared with Raman scattering for which $\ell = 2$, it becomes clear why the time scales of the various processes agree within a factor of ≤ 3. A ratio of $\tau_{\ell=1}/\tau_{\ell=2} = 3$ is expected for rotational diffusion processes according to Eq. (17) and many reasons are known that can render this ratio closer to 1, see, e.g., [478]. Most importantly, however, it was found that the cooperative dielectric Debye process (time scale 51.8 ps) is not Raman active [463]. Similar observations were made for water in that reference.

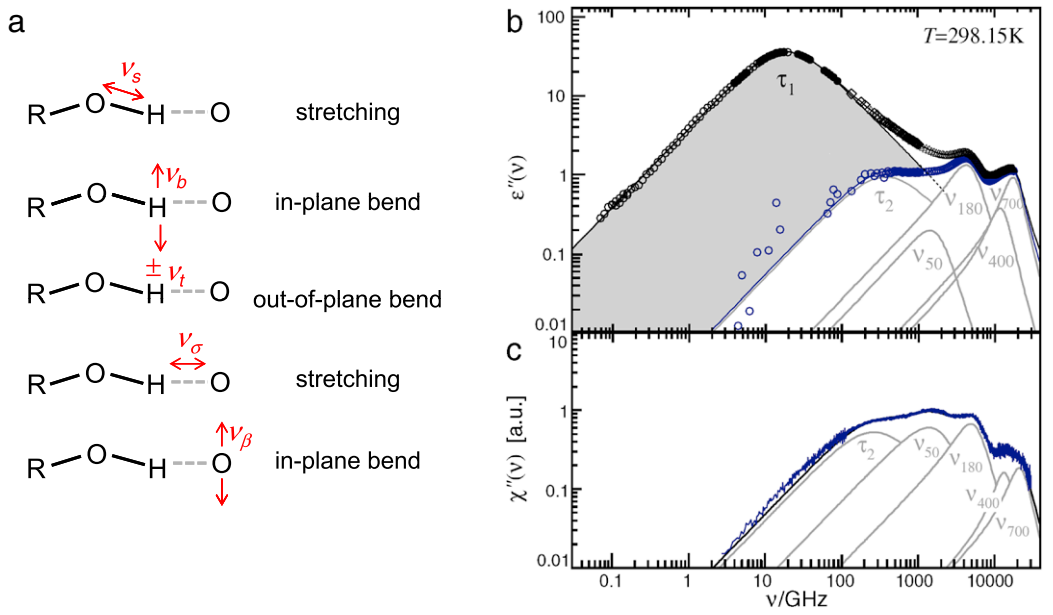

Fig. 57. (a) Illustration of low-frequency vibrational and librational modes adapted from [453]. (b) Dielectric loss of methanol (black symbols) decomposed into five different relaxation modes. After subtracting the τ_1 contribution, corresponding to the dielectric Debye process (and highlighted by the shading), a residual is obtained (blue symbols) that strongly resembles the Raman susceptibility shown in panel (c). (For interpretation of the references to color in this figure legend, the reader is referred to the web version of this article.)
Source: Adapted with permission from [464].
© 2010, American Physical Society.

Little seems to be known with certainty regarding the proper assignment of hydroxyl group related modes in monohydroxy alcohols [453] also since FIR vibrational frequencies are typically calculated in the gas phase [479]. As sketched in Fig. 57 intermolecular O · · · H stretching frequencies ν_σ are typically found in the 100 . . . 200 cm^{-1} range (corresponding to wavelengths of 100…50 μm) and torsional or out-of-plane bending modes typically appear at $\nu_t \sim 650$ cm^{-1}.

Terahertz time domain spectroscopy covering the range from 0.2 to 2.5 THz was performed for a host of other alcohols [455]. A broad vibrational mode around 1.2 THz (40 cm^{-1}) was identified as the so called Boson peak [460]. This low-energy excitation is also well-known from Raman and neutron scattering, e.g., in methanol [469] or ethanol [467]. It identifies itself as a broad feature in the 5…10 meV range. Density functional calculations suggest that in methanol oscillations of methyl groups around the OH · · · O segments of hydrogen-bonded chains also contribute in the frequency range up to about 50 cm^{-1} [470]. In the older dielectric literature the term Poley absorption was often used for features in this spectral range (smaller than ∼100 cm^{-1}) and understood to stem from molecular librations in a potential well that arise from inelastic molecular collisions of dipolar molecules [454]. For a recent discussion of this absorption and other low-energy excitations dealing, however, not explicitly with monohydroxy alcohols, see [480].

Vij et al. [456] studied various neat 1-alcohols and for the O · · · H stretching vibrations these authors report resonance frequencies ν_σ ranging from 110 cm^{-1} (ethanol) to 160 cm^{-1} (hexanol). For the 100–250 cm^{-1} range methyl rotations about C–O bonds coupled with translational and librational modes were suggested to play a role in methanol [470]. For larger monohydroxy alcohols, in the 220 to 250 cm^{-1} range, the O · · · H stretching vibrations were conjectured to interfere with CH_3 torsion modes [456]. For methanol, calculations indicate that low-lying modes (200 cm^{-1}) are hardly affected by deuterating the hydroxyl group unlike what is observed for the out-of-plane bending which then shifts to $\nu_t \sim 650$ cm^{-1}, see Fig. 3 in [85]. Interestingly, also various pure heptanol isomers were examined [456] and for the sterically hindered 4-heptanol, a "closed *n*-mer liquid lattice mode" was assigned to an absorption feature near 360 cm^{-1}.

Many more FIR data are available on monohydroxy alcohols in solutions of, e.g., alkanes, than in the pure liquid state. However, inferences from dilute solution studies are not always simple because even for long-chain alkanes (larger than *n*-butane) a weak FIR absorption exists. This absorption hints at a small (permanent or induced) dipole moment of ∼0.1 D the existence of which still lacks an unambiguous microscopic explanation [481,482].

9.5. Ultra-fast relaxation and two-dimensional chemical exchange

Unlike the 2D analyses reviewed in Section 9.2, the 2D spectra discussed here are based on the creation and detection of coherent quantum mechanical states, for reviews see, e.g., [483–486]. While we focus here on spectroscopy of the hydroxyl group, it is noted that the C–O stretching vibration has also received attention [487,488]. Before dealing with the 2D experiments, let us briefly discuss one of their predecessors, IR hole burning spectroscopy. A typical experimental scheme is

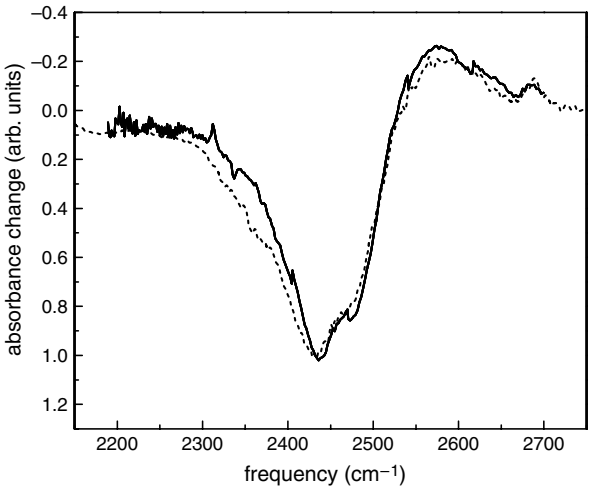

Fig. 58. A pump-probe spectrum of 10 mol% CH_3OD in CCl_4 (solid line) is compared with a temperature difference spectrum of 26 mol% CH_3OD in CCl_4 (dashed line). For the latter a 294 K spectrum was subtracted from a 301 K spectrum which changes the absorbance of the δ band (near 2500 cm^{-1}) by -0.045. After normalizing the spectra to maximum amplitude, they are virtually identical. The small differences between the pump–probe spectrum and the temperature difference spectrum reflects the use of different samples.
Source: Adapted from [427]. Courtesy of M. D. Fayer.

that first, using an intense narrowband (picosecond) pump beam, a given spectral position, e.g., in the OH stretching region, is excited. After a waiting time, the entire spectrum is probed using a broad-band (femtosecond) optical pulse (for a brief discussion of pump–probe experiments combining optical excitation with soft X-ray detection, see Section 0).

Results of a pump–probe experiment on CH_3OD diluted in CCl_4 are shown in Fig. 58 (solid line) as the difference signal of the absorbance before and 30 ps after a pump pulse [427]. It has been emphasized that the interpretation of the spectral changes is not at all unique, an ambiguity that can, however, be removed using 2D spectroscopy. Anticipating the result [427], it can be said that the feature near 2440 cm^{-1} is due to hydrogen bond breaking. After the pump the δ band is depleted, in Fig. 58 represented by the downward going absorbance change, and the γ band gains intensity, as can be seen from the upward going feature near 2600 cm^{-1}. Phenomenologically, these changes are similar to those effected by an increase of the sample temperature.

Indeed, the temperature difference spectrum (with $\Delta T = 9$ K) [494] shown in Fig. 58 matches the pump–probe spectrum in that figure after appropriate amplitude scaling [and resembles the one presented in Fig. 49(b)]. The estimated temperature increase of ≈ 0.01 K [494] induced via energy deposition during the laser pulse is much too small to explain the effects seen in the pump–probe spectrum. By increasing the waiting time between pump and probe pulses and recording the time dependent re-equilibration of the spectra this technique was exploited to study vibrational relaxation times and, by additionally analyzing perpendicular and parallel polarizations between pump and probe beams, also the orientational relaxation becomes accessible [425,424,489–494]. Transient IR spectroscopy was applied to ethanol for which several dilute CCl_4 solutions and also the neat liquid was studied [495]. Under the assumption that the chain-like clusters are formed for pure C_2H_5OH it was estimated that they contain 11–16 molecules.

In order to study exchange processes in the present context, conceptually the simplest approach is again to use hole burning laser spectroscopy. The full 2D information can in principle be gained by varying the frequency of the pump beam step by step across the entire vibrational band, so that one pumps one mode at a time and probes the response of any other mode. With the advent of techniques allowing to shape ultra-short laser pulses properly [496], this kind of information can be obtained much more elegantly using vibrational three-pulse stimulated-echo techniques. These methods were applied to study the hydrogen bond breaking for methanol diluted in CCl_4 [424,497,498].

Before discussing the results let us briefly outline the measuring principle by means of Fig. 59 [499]. A short pump pulse creates a coherent superposition (represented by dashed arrows) of the vibrational ground state $|0\rangle$ and first excited state $|1\rangle$ of the tagged hydroxyl stretching mode. After a pulse delay τ_1 a second pulse converts this coherence into population state (solid arrow). The dynamics under study can then take place during a long waiting time τ_2 (or T_w), here illustrated by a shift in the $|1\rangle$ level. After the third pulse, vibrational echo emission (wavy arrow) can occur during a time τ_3. By taking the Fourier transform of the emission signal (and down-conversion using a local oscillator signal) the spectra on the "direct" frequency axis (usually denoted as $\omega_3 = \omega_{\text{Probe}} = \omega_m$) are obtained. The "indirect" frequency axis ($\omega_1 = \omega_{\text{Pump}} = \omega_\tau$) can be accessed by incrementing τ_1 and carrying out another Fourier transform. If the $|1\rangle$ level is the same before and after the T_W, the vibrational frequency denoted here ω_A and ω_B, respectively, are the same and a diagonal peak will occur in the 2D spectrum. If changes have occurred, then off-diagonal peaks will show up. Generally, these so called cross peaks indicate that energy or coherence transfer, chemical exchange or other kinds of exchange have happened during T_w. Chemical exchange

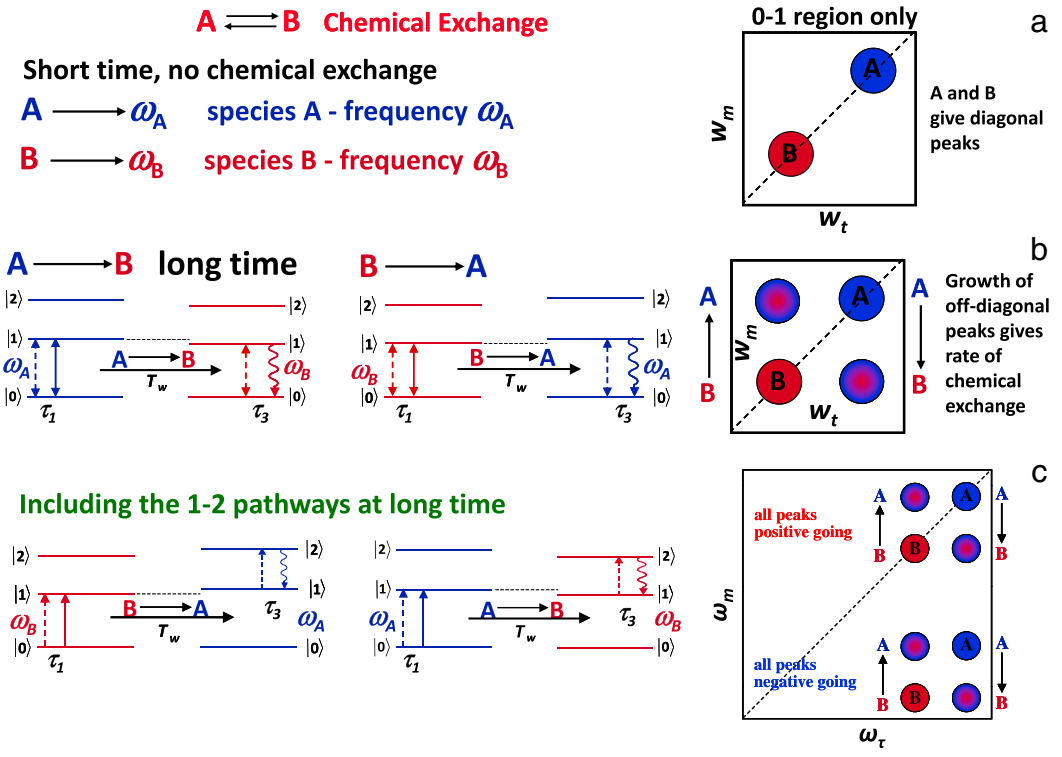

Fig. 59. Illustration of 2D spectra used to track chemical exchange between two states *A* and *B*, e.g., referring to differently hydrogen bonded species. (a) If no exchange has taken place on short time scales T_w only a diagonal spectrum is observed with one peak for each species. (b) During sufficiently long T_w times state *A* can transform into *B* and vice versa so that off-diagonal peaks develop. The three-pulse vibrational stimulated-echo sequence is schematically depicted using an energy level diagram focusing on the $|0\rangle \rightarrow |1\rangle$ absorption transition. The dashed arrows symbolize pulses that convert population into coherence states; the solid arrow symbolizes a pulse that converts coherence into population. The wavy arrows represent vibrational emissions. (c) Similar to (b) but now including the $|2\rangle \rightarrow |1\rangle$ pathway which gives rise to red-shifted (negative) emission peaks.
Source: Adapted from [499]. Courtesy of M. D. Fayer.

rates can be determined by measuring the time-dependent increase of the off-diagonal intensity, if peak attenuation due to vibrational lifetime and other relaxation process are properly accounted for.

Apart from stimulated absorption (positive peaks) also excited-state echo emission (negative peaks) can appear; in Fig. 59(c) this is indicated by the $|2\rangle \rightarrow |1\rangle$ transition. Then, the emission peaks are red-shifted along the ω_m axis by the amount of the vibrational anharmonicity which here is chosen such that the $|0\rangle \rightarrow |1\rangle$ and the $|2\rangle \rightarrow |1\rangle$ peaks do not overlap. The shift to lower frequency occurs because in the excited state the OH bond is slightly elongated. Generally, the sign of the cross peaks depends on whether the fluctuations of the transition frequencies ω_A and ω_B are positively or negatively correlated with each other.

In Fig. 60 we reproduce 2D exchange spectra that were recorded for mixing times (a) smaller and (b) larger than the chemical exchange time τ_{ex} [424]. By analyzing spectra for a large number of T_W, the exchange process can be monitored via the growth of the cross peak at ($\omega_1 = \omega_\tau \approx 2500\ \mathrm{cm}^{-1}$, $\omega_3 = \omega_m \approx 2600\ \mathrm{cm}^{-1}$). These two wavenumbers refer to the δ and the γ band, respectively, hence this cross peak indicates the dissociation of a hydrogen bond. Several bond breaking mechanisms were considered in [424]. A detailed analysis revealed preferred breaking of strongest hydrogen bonds (i.e., of those on the low frequency side of the δ band) [424]. This at first surprising feature that the strongest bonds break first was further examined theoretically [105,500,501].

The results in this section show that, due to their special supramolecular behavior, monohydroxy alcohols are not only fascinating liquids to study but merely that in many instances their particular properties have made them an ideal testing ground for the development of novel experimental techniques with the vibrational methods discussed here constituting formidable examples.

10. Variations on a theme? — Debye-like relaxations in other (viscous) liquids

Are there molecular functionalities other than, e.g., the well polarizable hydroxyl group that are giving rise to Debye-like behavior? And to render this question well defined: what should be considered as Debye-like relaxation? In a first step one may be tempted to state that the defining property of a Debye (-like) process is its single exponential appearance in the time domain. However, it is clear that this "definition" by itself is insufficient because it would for instance apply to single-particle

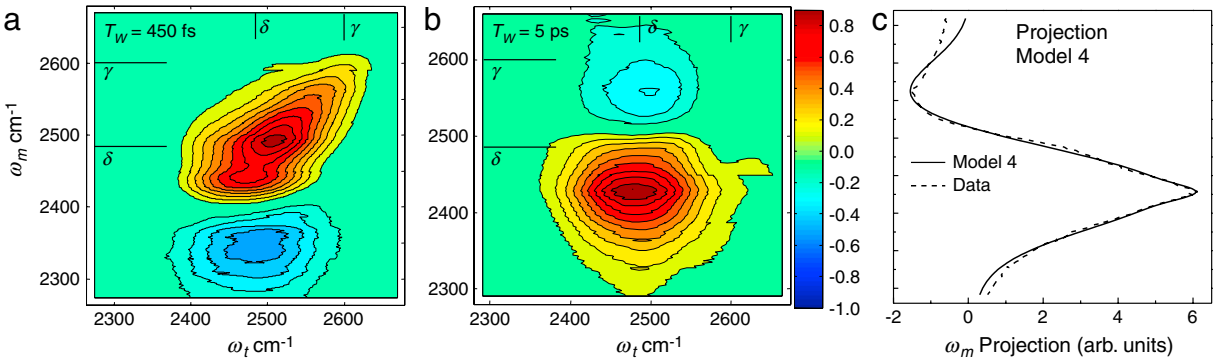

Fig. 60. 2D exchange spectra of 10 mol% CH_3OD in CCl_4 recorded for (a) small and (b) large waiting times T_w. The intensities of the contour plots in (a) and (b) are normalized separately and thus cannot be compared directly. (a) At $T_w = 450$ fs one recognizes positive (red) diagonal intensity from the $|0\rangle \rightarrow |1\rangle$ transitions of the δ and γ bands. The negative (blue) off-diagonal peak stems from the $|2\rangle \rightarrow |1\rangle$ band, downshifted with respect to the $|0\rangle \rightarrow |1\rangle$ band by ~ 150 cm^{-1} due to vibrational anharmonicity. (b) At $T_w = 5$ ps the main band on the diagonal has changed its shape and most importantly a new negative off-diagonal peak appears indicating a δ to γ transition. (c) Projection of the integrated intensities onto the ω_m axis for the 5 ps spectrum (dashed line). The solid line represents results from model calculations. (For interpretation of the references to color in this figure legend, the reader is referred to the web version of this article.)
Source: Adapted from [427]. Courtesy of M. D. Fayer.

phenomena in orientational crystals [502]. Hence, one may require that additional conditions be fulfilled: For instance that the Debye process should be slower than the calorimetrically active (structural) relaxation, but the δ-mode in some liquid crystals do also comply with this requirement [503].

Is the involvement of hydrogen bonds mandatory in generating a genuine Debye (-like) process? This can be doubted: In [187] the possibility was raised that also the strongly electronegative halogens with their ability to facilitate intermolecular association [504,505] could give rise to Debye-like features, albeit not particularly intense, in suitable liquids. For ethylhexylamine, a substance featuring an NH_2 group, a weak Debye-like feature has been spotted as well [506]. Furthermore, Debye processes were reported to occur in amorphous pharmaceuticals like acetaminophen [507] and ibuprofen [508]. Ibuprofen has been studied quite thoroughly: But MD simulations [509] and IR studies [510] suggest that the Debye process is essentially related to an (intramolecular) conformational change at the site of ibuprofen's carboxyl group. Furthermore, a mechanical signature of the Debye-like dielectric process similar to that observed for monohydroxy alcohols [42] was so far not detected for ibuprofen [511] suggesting that a mechanism different from that in monohydroxy alcohols may be at work in this pharmaceutical substance.

For some substances featuring a peptide group the existence of a Debye-type process was reported. Among them are the secondary amides like, e.g., the N-alkylacetamides (sum formula R_1–CO–NH–R_2, with $R_{1,2}$ denoting for instance H, CH_3, or C_2H_5) which typically show a rather strong dielectric Debye peak [512–516]. Results from techniques such as NMR [517] and vibrational spectroscopy [518–521] have indicated the occurrence of chain structures (for a sketch see Fig. 61) that were directly confirmed using X-ray and neutron diffraction [522] as well as by quantum chemical calculations [523,524]. The analogies between the amides and the monohydroxy alcohols may indeed be far reaching because it has been stated that it "is well known that amides develop transient hydrogen-bonded chains in the liquid state" [525]. And Wassink and Bordewijk [526] even remark that it is "plausible that the mechanism of the dielectric relaxation in the monohydric alcohols and the amides is the same". The extent to which this time honored statement is justified has to await more critical tests.

Peptide groups are also a feature of certain supramolecular polymers [285] that display a strong dielectric Debye peak as well as a mechanical signature similar to that of monohydroxy alcohols [42]. An example is shown in Fig. 62: Panel (a) presents the dielectric loss of a supramolecular polymer and panel (b) depicts the molecular structure of its self-complementary monomer unit [285]. Using the same nomenclature as for the alcohols, the time scale separation of the two processes was reported to reach ratios up to $\tau_D/\tau_\alpha \approx 50$. From the rheological behavior of the triply hydrogen bonded material referred to in Fig. 62 a polymer-like behavior was identified and assuming that a Rouse-like description applies an average supramolecular chain length of $\sim$10 was estimated [285]. For the substance depicted in Fig. 62(b) acid–base pairing leads to supramolecular behavior. But it may be conceived that other non-covalent interactions such as, for instance, mediated by metal–ligand coordination or π–π attraction can lead to similar results.

So far, as briefly mentioned in Section 6, dynamic light scattering (DLS) has not allowed one to detect the Debye process in monohydroxy alcohols. However, in view of the relatively small optical anisotropy of the hydroxyl group, one may suspect that this shortcoming may be a mere sensitivity issue. In this context, recent measurements using photon correlation spectroscopy (PCS) and tandem Fabry–Perot interferometry on substances involving N $\cdots$ H bonds are revealing and indeed may "provide the missing evidence of the slow, Debye-like relaxation in DLS" [527]. In Fig. 63 we reproduce depolarized PCS data on 2-ethyl-4-methylimidazole, a liquid that can form intermolecular N $\cdots$ H hydrogen bonds and thus give rise to chain-like supramolecular structures as sketched in the inset of Fig. 63. The lines in the mainframe of Fig. 63 represent a slower Debye-like contribution (mirrored by a Debye-like dielectric analogue) and a faster more stretched relaxation. Mechanical measurements confirmed that the latter feature corresponds to the structural relaxation [527].

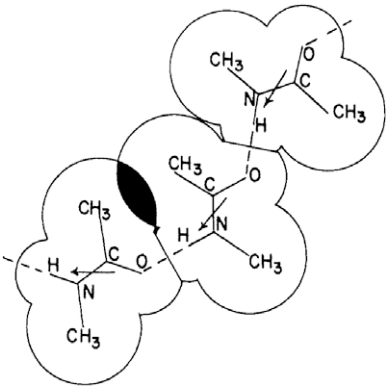

Fig. 61. Sketch of a chain fragment formed by hydrogen-bonded N-methylacetamide molecules. The arrows indicate the molecular dipole moment ($\mu \approx 4D$) of N-methylacetamide and the dashed lines mark hydrogen bonds. With the van der Waals radii drawn to scale, steric hindrance against molecular reorientation is expected as suggested by the shaded area.
Source: Reprinted with permission from Ref. [513].

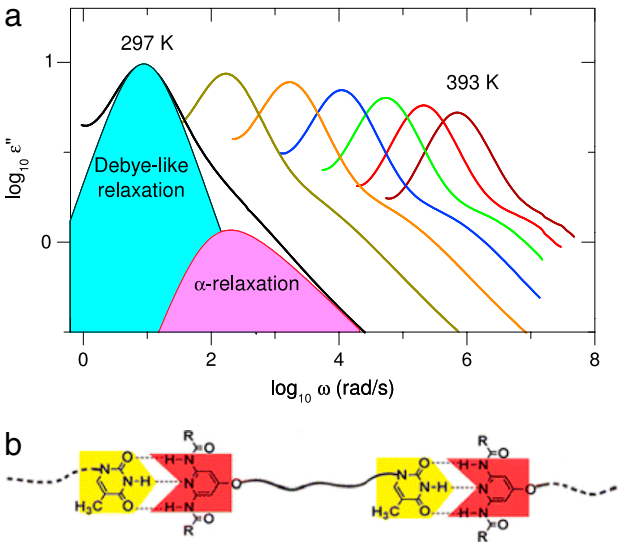

Fig. 62. (a) Dielectric loss spectra of a supramolecular polymer measured from 297 to 393 K in steps of 16 K. The different contributions to the dielectric loss are marked for the lowest temperature. (b) Schematic illustration of the covalently bonded thymine and diamidopyridine groups highlighted by yellow and red shading, respectively, that form the supramolecular polymer. Triple hydrogen bonds connecting the monomeric units are indicated by the dashed lines. The diamidopyridine group was augmented by nonyl rests, $R = -(CH_2)_8CH_3$, in order to increase the freezing temperature of this supramolecular system. (For interpretation of the references to color in this figure legend, the reader is referred to the web version of this article.)
Source: Adapted with permission from [285]. Courtesy of A. P. Sokolov.

Also using DLS a related observation was made on methyltrioctylammonium bis-(trifluoromethylsulfonyl)imide, an ionic liquid featuring relatively long side chains [528]. In this ionic liquid which involves hydrophobically aggregated alkyl tails a Debye-like process was found that is more than 2 orders of magnitude slower than the structural relaxation. The occurrence of the slow, Debye-like relaxation was tentatively attributed to the reorientational motion of relatively long-lived, aggregates of alkyl nanodomains.

This collection of recent experimental results exemplifies that Debye-like relaxation may be much more common than previously thought. It will remain interesting to examine the microscopic basis of this phenomenon for each class of substance in order to learn about the conditions that are minimally required to generate Debye-like relaxation in liquids.

Finally, let us turn to water, another hydrogen-bonded liquid that displays a relatively strong dielectric Debye process. In Fig. 64(a) we reproduce a comparison of the dielectric loss spectra of H_2O and ethanol, both recorded near room temperature [57]. The spectral shapes of the two liquids are very similar, including not only the intense Debye-type relaxation but also the faint feature on the high-frequency side of the main peak. The relaxation rate of liquid ethanol is expectedly somewhat smaller than that of water. A consistent trend concerning the Debye relaxation times, $\tau_D = \tau_1$, is observed when

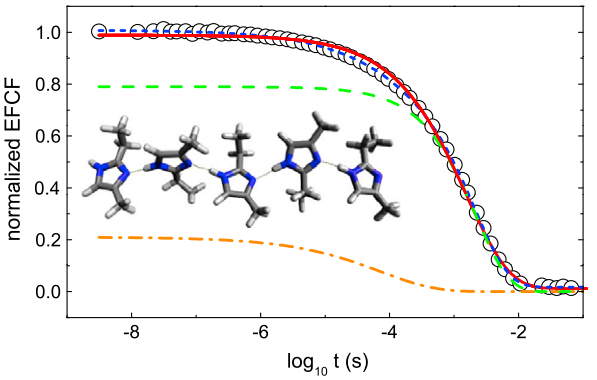

Fig. 63. The electric field correlation function (EFCF) obtained for the hydrogen bonded liquid 2-ethyl-4-methylimidazole from depolarized PCS at 260 K is represented by the symbols. A fit using a single stretched exponential function (red solid line) deviates systematically from the experimental data. The sum of a slow Debye-like relaxation (green dashed line) and an approximately 1.5 decades slower structural relaxation (orange dash–dot line) provides a much better description as can be seen from the sum of the two contributions (blue short-dashed line). The inset shows a sketch of a chain of hydrogen bonded 2-ethyl-4-methylimidazole molecules. The dotted lines represent intermolecular N · · · H bonds. (For interpretation of the references to color in this figure legend, the reader is referred to the web version of this article.)
Source: Adapted from [527]. Courtesy of A. P. Sokolov.

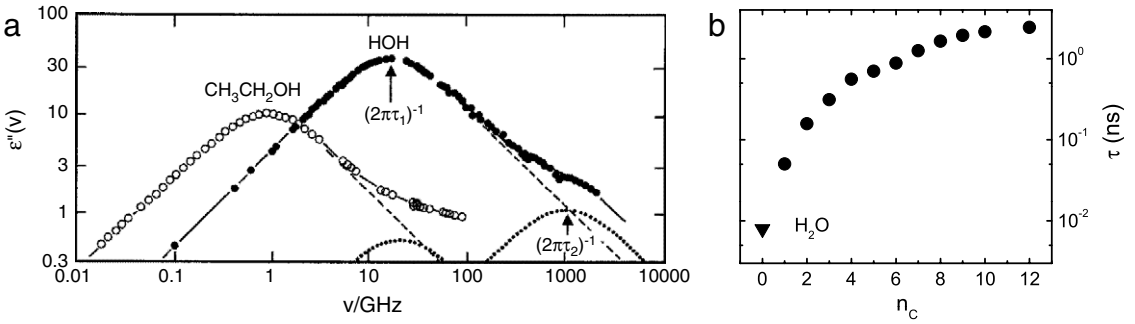

Fig. 64. (a) Dielectric loss spectra of ethanol (measured at 20 °C) and of water (measured at 19 °C). The dashed lines represent the low-frequency Debye relaxation and the dotted lines the high-frequency contribution. Reprinted from Ref. [57], Copyright 2002, with permission from Elsevier. (b) Relaxation times of the low-frequency process as a function of the number of carbon atoms of 1-monohydroxy alcohols (circles) are compared with that of water (triangle). These data, assessed in the 20–25 °C range, show that the behavior of water is in line with that of the monohydroxy alcohols.
Source: Adapted from Ref. [57].

taking also longer chain alcohols into account, see Fig. 64(b) [57]. In view of these similarities shared by water and alcohols it may be asked whether the mechanism underlying their dielectric Debye process is similar or not. In order to address this question, let us briefly examine a few more common features as well as some differences among these substances.

Apart from the trends regarding the dielectric relaxation times [529], near ambient temperature also the relaxation strengths of the normal alcohols vary systematically with the alkyl chain length. This was demonstrated in [530] in terms of the Kirkwood factor g_K which furthermore extrapolates satisfactorily to that of water. At 293 K and ambient pressure the Kirkwood factor of water was reported to range from 2.7 [15] to 3.5 [531], depending on the choice of the high-frequency dielectric constant ε_∞, see the discussion Section 5.2.

Another observation underscoring the analogous behavior of water and several normal alcohols is their (almost) ideal mixing [532]. On the one hand, in [532] it was emphasized that H_2O can significantly perturb the winding chain structure of, e.g., ethanol, and thus increase the number of monohydroxy alcohol molecules located near the chain ends [533]. On the other hand, with respect to the dielectric Debye process it was noted that for this "low-frequency relaxation … the contributions of alcohol and water cannot be distinguished" [532]. Furthermore, for monohydroxy alcohols (see Section 9.2) *and* for water the relaxation time τ_D read off from the dielectric Debye peak is significantly longer than the hydrogen bond lifetime. For water τ_D is 9.6 ps at 20 °C [534] but near this temperature depolarized Rayleigh scattering has found a relatively short hydrogen bond lifetime of < 1 ps [535,536], for further references and a recent discussion see [537]. Furthermore, and in analogy to the behavior of monohydroxy alcohols, see Section 7.1, also for water the (mechanical) Maxwell relaxation time $\tau_\eta = G_\infty/\eta$ is significantly shorter than τ_D: Estimating water's Maxwell time from the instantaneous shear modulus $G_\infty = 2.44$ GPa [538] and the viscosity $\eta = 10^{-3}$ Pa s one obtains ≈ 0.4 ps, a time scale much shorter than τ_D. These considerations are in accord with many estimates that find that the structural relaxation time of water is roughly 10 times shorter than the relaxation time corresponding to its Debye peak [181,539,540].

Thus, water and monohydroxy alcohols display many similarities regarding their dynamical behavior. On the other hand, it is well known that their microscopic structures differ substantially. For water, scattering experiments indicate a local tetrahedral arrangement and thus, unlike monohydroxy alcohols, water has to be considered a network liquid [541,542]. Nevertheless, like the monohydroxy alcohols (see Section 3.2) also water displays a prepeak in its static structure factor [543], albeit obviously for different reasons [146]. The question why, in spite of their significant structural differences, the dynamical properties of these hydrogen bonded liquids appear to be so closely related will be interesting to explore for many years to come.

11. Concluding remarks

Upon completing this review our impression fortified that the study of monohydroxy alcohols does not only constitute a long standing scientific challenge but one that has recently seen an upsurge of activities leading to major steps forward in our understanding of these fascinating liquids. It is particularly reassuring to observe that so many novel experimental and computational methods were recently applied with the goal to unravel the structure and dynamics of monohydroxy alcohols at the microscopic level. While it was long believed that by and large dielectric spectroscopy only can teach us a great deal on the nature of the Debye peak, it is now evident that monohydroxy alcohols can be considered a prime example that solely from a combination of methods major new insights should be expected. Particularly useful are those combinations of techniques that aim at interrelating structural and dynamical properties at the molecular scale. We have touched upon some of these efforts in the present review, but much of the potential of other "mixed" methods is yet to be exploited. Here one may think of, for instance, optical pump and soft X-ray probe schemes or mutual combinations of dielectric spectroscopy, rheology, calorimetry, NMR, etc.

To some extent motivated by the scientific background of the current authors, the selection of the material presented in this review is leaning more to the experimental rather than to the theoretical side. Nevertheless, it is hoped that it has become clear that much of the substantial progress seen in this field was achieved by an interplay of theoretical and experimental approaches. One example that we have given in this context concerns the combination of quantum chemical with X-ray absorption methods in order to unravel details of the supramolecular monohydroxy alcohol association. Developments that will advance the field further can be expected with respect to *ab initio* treatments of structural (and eventually also of dynamical) properties of (larger) clusters of not just the smallest monohydroxy alcohol molecules taking into account their internal flexibility. Also molecular dynamics simulations regarding the *dynamics* of liquid monohydroxy alcohols are still somewhat scarce [69], particularly when it comes to taking the covalent aspects of hydrogen bonding into account so that the computations reflect the cooperative nature of these bonds properly. Any major progress of the theoretical methodology in the monohydroxy alcohol field, dealing with molecules of limited complexity, should be useful also when quantum mechanically realistic simulations of biomacromolecules with their mesoscopic scale structuring driven functionality are a concern.

An optimistic view is warranted here because fluid monohydroxy alcohols constitute some of the simplest and relatively well studied examples for (transient) structure formation in liquids. But the general circumstances under which such structures form in liquids devoid of hydroxyl groups and then whether such structures may or may not give rise to a pronounced (e.g., electrical) Debye-like extra absorption are largely unexplored. Furthermore, many potential analogies of the processes I and II in monohydroxy alcohol to the normal and segmental modes in covalently polymers and possibly to other structured fluids like supramolecular and living polymers, micellar and ionic liquid systems, amides and so on are worthwhile to pursue from theoretical and experimental perspectives in future studies.

For alcohols containing several nearby hydroxyl groups it is generally agreed upon that a three-dimensionally cross-linked hydrogen bond network forms so that the Debye-like absorption that characterizes the monohydroxy alcohols should not occur, a conjecture that is in accord with experimental findings for, e.g., glycerol and many of its relatives. The exception to this expectation is – and one is tempted to say: like always – water. Despite of its predominantly three-dimensional network topology, water does display a Debye-like dielectric loss and presents many further phenomenological similarities to monohydroxy alcohols. But in the previous section we also mentioned several important differences which suggest that there is still a long way to go in order to understand this most important liquid on earth. In any case, we are convinced that in this respect monohydroxy alcohols will play an essential role.

Mainly for reasons of space, in this review we focused almost exclusively on the properties of pure monohydroxy alcohol liquids. A very large body of interesting work is already available for monohydroxy alcohol containing mixtures which are attractive from technological as well as from scientific standpoints. Taking, like everywhere else in this review, the latter perspective, a major advantage of suitable monohydroxy alcohol mixtures is that it has allowed one, for instance, to separate relaxations I and II to an extent that is larger than for most neat alcohols. The selective study of these processes, which incidentally is still to be achieved for the secondary amides, has surfaced a number of new insights. Nevertheless, a range of fundamental issues concerning monohydroxy alcohol mixtures await general answers: How and to which extent does the supramolecular association change upon dilution of and by monohydroxy alcohols? What is the impact of polar (aqueous and nonaqueous) and less polar solvents via a change of the overall structural architecture on the dynamical properties of the alcohols? Under which general conditions does microphase separation [544] play a major role in addition to the nanoscopic hydroxyl vs. alkyl segregation that characterizes many pure monohydroxy alcohols? These few questions may suffice to

illustrate that many rewarding scientific challenges remain to be tackled even more intensively in the future not only for pure but also for mixed monohydroxy alcohols.

Acknowledgments

We thank the numerous scientists whom we had or have the pleasure to work with on monohydroxy alcohols. These include Stefan Bauer, S. Peter Bierwirth, Thomas Büning, Burkhard Geil, Tarek El Goresy, Christina Lederle, Wolf Hiller, Sebastian Schildmann, Christian Sternemann, Hans-Jürgen Weber, Hendrik Wittkamp, Metin Tolan, and Eugen Vynokur from Dortmund; as well as Thorleif Berger, Christian Hansen, Wei Huang, Subarna Samanta, Lokendra P. Singh, Li-Min Wang, and Hauke Wendt from Tempe/Mainz. Herbert Zimmermann from the Max Planck Institute for Medical Research in Heidelberg is cordially thanked for providing isotope labeled substances. This project benefited much also from productive cooperation and discussions with Christiane Alba-Simionesco, Jeppe Dyre, Tina Hecksher, Hans-Heinrich Limbach, Peter Lunkenheimer, Alois Loidl, Aleksandar Matic, Johan Mattsson, Stefan Pawlus, Marian Paluch, Andreas Reiser, Ernst Rössler, Christoph Schick, Per Sillrén, Michael Vogel, Li-Min Wang, Herman Weingärtner, and Manfred Wilhelm. Furthermore, numerous colleagues are thanked for sending us high-quality figures from their work for reproduction in this article. Work done in Dortmund is generously supported by the Deutsche Forschungsgemeinschaft under Grant Nos. BO1301/8-1 and BO1301/8-2 which is gratefully acknowledged. The material based upon work at Tempe is supported by the National Science Foundation under Grant No. CHE 1026124 (International Collaboration in Chemistry).

References

[1] C.J.F. Böttcher, Theory of Electric Polarization, vol. 1, Elsevier, Amsterdam, 1973.
[2] See G. Potapenko, Die Elektrischen Absorptions- und Dispersionsspektren von Methyl- und Äthylalkohol im Bereiche von 30 bis 90 cm Wellenlänge, Z. Phys. A 20 (1923) 21–35. and the earlier dielectric work on monohydroxy alcohols which is quoted in that article.
[3] S. Mizushima, On the anomalous dispersion and absorption of electric waves. I, Bull. Chem. Soc. Jpn. 1 (1926) 47–53.
[4] S. Mizushima, On the anomalous dispersion and absorption of electric waves. II, Bull. Chem. Soc. Jpn. 1 (1926) 83–89.
[5] S. Mizushima, On the anomalous dispersion and absorption of electric waves. III, Bull. Chem. Soc. Jpn. 1 (1926) 115–123.
[6] S. Mizushima, On the anomalous dispersion and absorption of electric waves. IV. Anomalous dispersion and Debye's dipole theory, Bull. Chem. Soc. Jpn. 1 (1926) 143–145.
[7] S. Mizushima, On the anomalous dispersion and absorption of electric waves. V. Anomalous dispersion and Debye's dipole theory (continued), Bull. Chem. Soc. Jpn. 1 (1926) 163–168.
[8] S. Mizushima, Anomale Dispersion und Absorption elektrischer Wellen, Phys. Z. 28 (1927) 418–421.
[9] P. Debye, Polar Molecules, Chemical Catalog Company, New York, 1929.
[10] P. Debije, Zur Theorie der anomalen Dispersion im Gebiete der langwelligen elektrischen Strahlung, Verh. Dtsch. Phys. Ges. 15 (1913) 777–793.
[11] P. Girard, Dipole association in pure liquids, Trans. Faraday Soc. 30 (1934) 763–772.
[12] G.W. Steward, R.M. Morrow, X-ray diffraction in liquids: primary normal alcohols, Phys. Rev. 30 (1927) 232–244.
[13] W.H. Zachariasen, The liquid "structure" of methyl alcohol, J. Chem. Phys. 3 (1935) 158–161.
[14] W.C. Pierce, D.P. MacMillan, X-ray studies on liquids: The inner peak for alcohols and acids, J. Am. Chem. Soc. 60 (1938) 779–783.
[15] G. Oster, J.G. Kirkwood, The influence of hindered molecular rotation on the dielectric constants of water, alcohols, and other polar liquids, J. Chem. Phys. 11 (1943) 175–178.
[16] M.W. Sagal, Dielectric relaxation in liquid alcohols and diols, J. Chem. Phys. 36 (1962) 2437–2442.
[17] R. Minami, K. Itoh, H. Takahashi, K. Higasi, A theoretical approach to the dielectric relaxation of liquid alcohols, J. Chem. Phys. 73 (1980) 3396–3397.
[18] D.W. Davidson, R.H. Cole, Dielectric relaxation in glycerol, propylene glycol, and *n*-propanol, J. Chem. Phys. 19 (1951) 1484–1490.
[19] R. Bock, Über die Dielektrizitätskonstante und den Absorptionskoeffizienten von Glycerin, Z. Phys. 31 (1925) 534–543.
[20] P. Girard, P. Abadie, B. Theory of relaxation times. Experimental curves of losses and of anomalous dispersion as a basis of a spectral method, Trans. Faraday Soc. 42 (1946) 40–47.
[21] W. Dannhauser, A.F. Flueckinger, Liquid structure and dielectric relaxation of some isomeric methylheptanols, Phys. Chem. Liq. 2 (1970) 37–44.
[22] W. Dannhauser, R.H. Cole, Dielectric properties of liquid butyl alcohols, J. Chem. Phys. 23 (1955) 1762–1766.
[23] W. Dannhauser, Dielectric study of intermolecular association in isomeric octyl alcohols, J. Chem. Phys. 48 (1968) 1911–1917.
[24] W. Dannhauser, Dielectric relaxation in isomeric octyl alcohols, J. Chem. Phys. 48 (1968) 1918–1923.
[25] G.P. Johari, W. Dannhauser, Evidence for structural transformation in liquid octyl alcohols from PVT studies, J. Chem. Phys. 48 (1968) 3407–3408.
[26] G.P. Johari, W. Dannhauser, Dielectric study of the pressure dependence of intermolecular association in isomeric octyl alcohols, J. Chem. Phys. 48 (1968) 5114–5122.
[27] G.P. Johari, W. Dannhauser, Dielectric study of intermolecular association in sterically hindered octanol isomers, J. Phys. Chem. 72 (1968) 3273–3276.
[28] T. Chen, W. Dannhauser, G.P. Johari, Study of the pressure dependence of dielectric polarization, J. Chem. Phys. 50 (1969) 2046–2052.
[29] J.K. Vij, W.G. Scaife, J.H. Calderwood, The pressure and temperature dependence of the static permittivity and density of heptanol isomers, J. Phys. D: Appl. Phys. 11 (1978) 545–559.
[30] J.K. Vij, W.G. Scaife, J.H. Calderwood, The pressure and temperature dependence of the complex permittivity of heptanol isomers, J. Phys. D: Appl. Phys. 14 (1981) 733–746.
[31] R.H. Cole, D.W. Davidson, High frequency dispersion in *n*-propanol, J. Chem. Phys. 20 (1952) 1389–1391.
[32] F. Perrin, Movement Brownien d'un Ellipsoide. I. Dispersion Diélectrique pour des Molecules Ellipsoidales, J. Phys. Radium 5 (1934) 497–511.
[33] C.P. Smyth, Dielectric Behavior and Structure, McGraw-Hill, New York, 1955, p. 105.
[34] See the general discussion in F.C. Frank, C.G. Garton, M. Magat, D.H. Whiffen, S. Whitehead, Trans. Faraday Soc. 42 (1946) A075–A078.
[35] W. Kauzmann, The nature of the glassy state and the behavior of liquids at low temperatures, Chem. Rev. 43 (1948) 219–256.
[36] S.S.N. Murthy, S.K. Nayak, Experimental study of the nature of the glass transition process in monohydroxy alcohols, J. Chem. Phys. 99 (1993) 5362–5368.
[37] H. Huth, L.-M. Wang, C. Schick, R. Richert, Comparing calorimetric and dielectric polarization modes in viscous 2-ethyl-1-hexanol, J. Chem. Phys. 126 (2007) 104503.
[38] T. Lyon, T.A. Litovitz, Ultrasonic relaxation in normal propyl alcohol, J. Appl. Phys. 27 (1956) 179–187.
[39] T.A. Litovitz, G.E. McDuffie, Comparison of dielectric and mechanical relaxation in associated liquids, J. Chem. Phys. 39 (1963) 729–734.
[40] B. Jakobsen, C. Maggi, T. Christensen, J.C. Dyre, Investigation of the shear mechanical and dielectric relaxation processes in two monoalcohols close to the glass transition, J. Chem. Phys. 129 (2008) 184502.

[41] R. Behrends, U. Kaatze, Hydrogen bonding and chain conformational isomerization of alcohols probed by ultrasonic absorption and shear impedance spectrometry, J. Phys. Chem. A 105 (2001) 5829–5835.
[42] C. Gainaru, R. Figuli, T. Hecksher, B. Jakobsen, J.C. Dyre, M. Wilhelm, R. Böhmer, Shear-modulus investigations of monohydroxy alcohols: evidence for a short-chain-polymer rheological response, Phys. Rev. Lett. 112 (2014) 098301.
[43] B.M. Fung, T.W. McGaughy, Molecular motions in liquid. I. Rotation of water and small alcohols studied by deuteron relaxation, J. Chem. Phys. 65 (1976) 2970–2976.
[44] H. Versmold, NMR studies of reorientational motion in ethanol and ethanol glycerol mixtures, Ber. Bunsenges. Phys. Chem. 78 (1974) 1318–1327.
[45] R. Ludwig, M.D. Zeidler, T.C. Farrar, Molecular dynamics in lower alcohols, Z. Phys. Chem. 189 (1995) 19–27.
[46] H. Nadolny, A. Volmari, H. Weingärtner, Orientational dynamics of hydrogen-bonded liquids — a comparative study of dielectric and nuclear magnetic relaxation in n-butanol-tetrachloromethane mixtures, Ber. Bunsenges. Phys. Chem. 102 (1998) 866–871.
[47] C. Hansen, F. Stickel, T. Berger, R. Richert, E.W. Fischer, Dynamics of glass-forming liquids. III. Comparing the dielectric α- and β-relaxation of 1-propanol and o-terphenyl, J. Chem. Phys. 107 (1997) 1086–1093.
[48] L.-M. Wang, R. Richert, Dynamics of glass-forming liquids. IX. Structural versus dielectric relaxation in monohydroxy alcohols, J. Chem. Phys. 121 (2004) 11170–11176.
[49] M.A. Floriano, C.A. Angell, On the relaxation between Debye and nonexponential relaxation in supercooled monohydric alcohols and water: a solution study, J. Chem. Phys. 91 (1989) 2537–2543.
[50] R. Coelho, D. Khac Manh, Utilisation de la Biréfringence Électro-optique pour l'Étude de la Relaxation Dipolaire dans les Liquides Polaires Faiblement Conducteurs, C. R. Acad. Sci., Paris C 264 (1967) 641–644.
[51] J. Crossley, G. Williams, Relaxation in hydrogen-bonded liquids studied by dielectric and Kerr-effect techniques, J. Chem. Soc. Faraday Trans. 273 (1977) 1906–1917.
[52] M. Maroncelli, G.R. Fleming, Picosecond solvation dynamics of coumarin 153: The importance of molecular aspects of solvation, J. Chem. Phys. 86 (1987) 6221–6239.
[53] F.X. Hassion, R.H. Cole, Dielectric relaxation processes in ethanol, Nature 172 (1953) 212–213.
[54] C. Brot, M. Magat, L. Reinisch, Sur la Dispersion Diélectrique dans le Domaine Décimétrique et Centimétrique, Kolloidn. Zh. 134 (1953) 101–134.
[55] F.X. Hassion, R.H. Cole, Dielectric properties of liquid ethanol and 2-propanol, J. Chem. Phys. 23 (1955) 1756–1761.
[56] J.A. Saxton, R.A. Bond, G.T. Coats, R.M. Dickinson, Dispersion at millimeter wavelengths in methyl and ethyl alcohols, J. Chem. Phys. 37 (1962) 2132–2138.
[57] U. Kaatze, R. Behrends, R. Pottel, Hydrogen network fluctuations and dielectric spectrometry of liquids, J. Non-Cryst. Solids 305 (2002) 19–28.
[58] D. Fragiadakis, C.M. Roland, R. Casalini, Insights on the origin of the Debye process in monoalcohols from dielectric spectroscopy under extreme pressure conditions, J. Chem. Phys. 132 (2010) 144505.
[59] V.V. Levin, Y.D. Feldman, Dipole relaxation in normal aliphatic alcohols, Chem. Phys. Lett. 87 (1982) 162–164.
[60] C. Brot, M. Magat, Comment on "dispersion at millimeter wavelengths in methyl and ethyl alcohols", J. Chem. Phys. 39 (1963) 841–842.
[61] P. Bordewijk, F. Gransch, C.J.F. Böttcher, The dielectric behavior of mixtures of heptanol-1 and heptanol-4 and the fluid structure of the monoalcohols, J. Phys. Chem. 73 (1969) 3255–3258.
[62] O.E. Kalinovskaya, J.K. Vij, The exponential dielectric relaxation dynamics in a secondary alcohol's supercooled liquid and glassy states, J. Chem. Phys. 112 (2000) 3262–3266.
[63] C. Lederle, W. Hiller, C. Gainaru, R. Böhmer, Diluting the hydrogen bonds in viscous solutions of n-butanol with n-bromobutane: II. A comparison of rotational and translational motions, J. Chem. Phys. 134 (2011) 064512.
[64] C. Gainaru, S. Kastner, F. Mayr, P. Lunkenheimer, S. Schildmann, H.J. Weber, W. Hiller, A. Loidl, R. Böhmer, Hydrogen-bond equilibria and life times in a monohydroxy alcohol, Phys. Rev. Lett. 107 (2011) 118304.
[65] C. Gainaru, R. Meier, S. Schildmann, C. Lederle, W. Hiller, E.A. Rössler, R. Böhmer, Nuclear magnetic resonance measurements reveal the origin of the Debye process in monohydroxy alcohols, Phys. Rev. Lett. 105 (2010) 258303.
[66] A. Karpfen, Cooperative effects in hydrogen bonding, Adv. Chem. Phys. 123 (2002) 469–510.
[67] C. Gainaru, R. Meier, S. Schildmann, C. Lederle, E.A. Rössler, R. Böhmer, La Ola Mexicana (the wave) tumbling in a drop of alcohol: News about Debye's process, Talk presented in the Session on Biological Materials II of the 6th International Conference on Broadband Dielectric Spectroscopy, Madrid, September 07, 2010.
[68] P. Sillrén, A. Matic, Queuing Theory Unravels the Transient H-Bonded Chain Dynamics in Liquid Alcohols (unpublished), see also P. Sillrén, Trees, queues and alcohols (Ph.D. thesis), Chalmers University of Technology, 2013.
[69] P. Wieth, M. Vogel, Dynamical and structural properties of monohydroxy alcohols exhibiting a Debye process, J. Chem. Phys. 140 (2014) 144507.
[70] L.P. Singh, R. Richert, Watching hydrogen-bonded structures in an alcohol convert from rings to chains, Phys. Rev. Lett. 109 (2012) 167802.
[71] R. Taylor, C.F. Macrae, Rules governing the crystal packing of mono- and dialcohols, Acta Crystallogr. B57 (2001) 815–827.
[72] L. Ventolà, M. Ramírez, T. Calvet, X. Solans, M.A. Cuevas-Diarte, P. Negrier, D. Mondieig, J.C. van Miltenburg, H.A.J. Oonk, Polymorphism of n-alkanols: 1-heptadecanol, 1-octadecanol, 1-nonadecanol, and 1-eicosanol, Chem. Mater. 14 (2002) 508–517.
[73] M. Ramírez-Cardona, L. Ventolà, T. Calvet, M.A. Cuevas-Diarte, J. Rius, J.M. Amigó, M.M. Reventós, Crystal structure determination of 1-pentanol from low-temperature powder diffraction data by Patterson search methods, Powder Diffr. 20 (2005) 311–315.
[74] M. Ramírez-Cardona, J.C. Escamilla-Casas, M.A. Cuevas-Diarte, I. Barajas-Rosales, Structure determination of 1-pentanol ($C_5H_{12}O$) at 183 K, Z. Kristallogr. Suppl. 23 (2006) 601–606.
[75] H.A. Shallard-Brown, D.J. Watkin, A.R. Cowley, n-octanol, Acta Crystallogr. E 61 (2005) o213–o214.
[76] I.M. Shmyt'ko, R.J. Jiménez-Riobóo, M. Hassaine, M.A. Ramos, Structural and thermodynamic studies of n-butanol, J. Phys.: Condens. Matter 22 (2010) 195102.
[77] C. Talón, F.J. Bermejo, C. Cabrillo, G.J. Cuello, M.A. Gonzáles, J.W. Richardson, Jr, A. Criado, M.A. Ramos, S. Vieira, F.L. Cumbrera, L.M. González, Chemical isomerism as a key to explore free-energy landscapes in disordered matter, Phys. Rev. Lett. 88 (2002) 115506.
[78] A.A. Manka, J. Wedekind, D. Ghosh, K. Höhler, J. Wölk, R. Strey, Nucleation of ethanol, propanol, butanol, and pentanol: a systematic experimental study along the homologous series, J. Chem. Phys. 137 (2012) 054316.
[79] A. Sanz, A. Nogales, I. Puente-Orench, M. Jiménez-Ruiz, T.A. Ezquerra, Detection of early stage precursor during formation of plastic crystal ethanol from the supercooled liquid state: a simultaneous dielectric spectroscopy with neutron diffraction study, Phys. Rev. Lett. 107 (2011) 025502 and references cited therein.
[80] S. Benkhof, A. Kudlik, T. Blochowicz, E. Rössler, Two glass transitions in ethanol: a comparative dielectric relaxation study of the supercooled liquid and the plastic crystal, J. Phys.: Condens. Matter 10 (1998) 8155–8171.
[81] In Ref. [76] it was found that the 'glacial state' of butanol is merely an assembly of nanocrystallites embedded in a disordered matrix.
[82] E. Arunan, G.R. Desiraju, R.A. Klein, J. Sadlej, S. Scheiner, I. Alkorta, D.C. Clary, R.H. Crabtree, J.J. Dannenberg, P. Hobza, H.G. Kjaergaard, A.C. Legon, B. Mennucci, D.J. Nesbitt, Defining the hydrogen bond: an account (IUPAC technical report), Pure Appl. Chem. 83 (2011) 1619–1636. Definition of the Hydrogen Bond (IUPAC Recommendations 2011), Pure Appl. Chem. 83 (2011) 1637–1641.
[83] See D. Prada-Gracia, R. Shevchuk, F. Rao, The quest for self-consistency in hydrogen bond definitions, J. Chem. Phys. 139 (2013) 084501 and references cited therein.
[84] M. Haughney, M. Ferrario, I.R. McDonald, Molecular-dynamics simulation of liquid methanol, J. Phys. Chem. 91 (1987) 4934–4940.
[85] B.M. Ladanyi, M.S. Skaf, Computer simulations of hydrogen-bonding liquids, Annu. Rev. Phys. Chem. 44 (1993) 335–368.
[86] W.L. Jorgensen, Optimized intermolecular potential functions for liquid alcohols, J. Phys. Chem. 90 (1986) 1276–1284.
[87] G. Pálinkás, E. Hawlicka, K. Heinzinger, A molecular dynamics study of liquid methanol with a flexible three-site model, J. Phys. Chem. 91 (1987) 4334–4341.
[88] I.M. Svishchev, P.G. Kusalik, Structure in liquid methanol from spatial distribution functions, J. Chem. Phys. 100 (1994) 5165–5171.

[89] M.S. Skaf, T. Fonseca, B.M. Ladanyi, Wave vector dependent dielectric relaxation in hydrogen-bonding liquids: a molecular dynamics study of methanol, J. Chem. Phys. 98 (1993) 8929–8945.
[90] L. Zoranić, F. Sokolić, A. Perera, Microstructure of neat alcohols: a molecular dynamics study, J. Chem. Phys. 127 (2007) 024502.
[91] W.L. Jorgensen, D.S. Maxwell, J. Tirado-Rives, Development and testing of the opls all-atom force field on conformational energetics and properties of organic liquids, J. Am. Chem. Soc. 118 (1996) 11225–11236.
[92] S.L. Wallen, B.J. Palmer, B.C. Garrett, C.R. Yonker, Density and temperature effects on the hydrogen bond structure of liquid methanol, J. Phys. Chem. 100 (1996) 3959–3964.
[93] C.J. Benmore, Y.L. Loh, The structure of liquid ethanol: a neutron diffraction and molecular dynamics study, J. Chem. Phys. 112 (2000) 5877–5883.
[94] J. Lehtola, M. Hakala, K. Hämäläinen, Structure of liquid linear alcohols, J. Phys. Chem. B 114 (2010) 6426–6436.
[95] J.L. MacCallum, D.P. Tieleman, Structures of neat and hydrated 1-octanol from computer simulations, J. Am. Chem. Soc. 124 (2002) 15085–15093.
[96] S.K. Stephenson, R.D. Offeman, G.H. Robertson, W.J. Orts, Hydrogen-bond networks in linear, branched and tertiary alcohols, Chem. Eng. Sci. 62 (2007) 3019–3031.
[97] A.A. Vartia, K.R. Mitchell-Koch, G. Stirnemann, D. Laage, W.H. Thompson, On the reorientation and hydrogen-bond dynamics of alcohols, J. Phys. Chem. B 115 (2011) 12173–12178.
[98] P. Gómez-Álvarez, L. Romaní, D. González-Salgado, Association effects in pure methanol via monte carlo simulations. I. structure, J. Chem. Phys. 138 (2013) 044509.
[99] B. Chen, J.J. Potoff, J.I. Siepmann, Monte Carlo calculations for alcohols and their mixtures with alkanes. Transferable potentials for phase equilibria. 5. United-atom description of primary, secondary, and tertiary alcohols, J. Phys. Chem. B 105 (2001) 3093–3104.
[100] M. Tomšič, A. Jamnik, G. Fritz-Popovski, O. Glatter, L. Vlček, Structural properties of pure simple alcohols from ethanol, propanol, butanol, pentanol, to hexanol: comparing Monte Carlo simulations with experimental SAXS data, J. Phys. Chem. B 111 (2007) 1738–1751.
[101] P. Sillrén, J. Bielecki, J. Mattsson, L. Börjesson, A. Matic, A statistical model of hydrogen bond networks in liquid alcohols, J. Chem. Phys. 136 (2012) 094514.
[102] M. Tomšič, G. Fritz-Popovski, L. Vlček, A. Jamnik, Calculating small-angle X-ray scattering intensities from monte carlo results: exploring different approaches on the example of primary alcohols, Acta Chim. Slovaca 54 (2007) 484–491.
[103] J. Pérez-Pellitero, E. Bourasseau, I. Demachy, J. Ridard, P. Ungerer, A.D. Mackie, Anisotropic united-atoms (aua) potential for alcohols, J. Phys. Chem. B 112 (2008) 9853–9863.
[104] M. Pagliai, G. Cardini, R. Righini, V. Schettino, Hydrogen bond dynamics in liquid methanol, J. Chem. Phys. 119 (2003) 6655–6662.
[105] K. Kwac, E. Geva, Mixed quantum–classical molecular dynamics study of the hydroxyl stretch in methanol/carbon-tetrachloride mixtures II: excited state hydrogen bonding structure and dynamics, infrared emission spectrum, and excited state lifetime, J. Phys. Chem. B 116 (2012) 2856–2866.
[106] M.J. McGrath, I.F.W. Kuo, J.I. Siepmann, Liquid structures of water, methanol, and hydrogen fluoride at ambient conditions from first principles molecular dynamics simulations with a dispersion corrected density functional, Phys. Chem. Chem. Phys. 13 (2011) 19943–19950.
[107] A. Vrhovšek, O. Gereben, A. Jamnik, L. Pusztai, Hydrogen bonding and molecular aggregates in liquid methanol, ethanol, and 1-propanol, J. Phys. Chem. B 115 (2011) 13473–13488.
[108] G. Matisz, A.-M. Kelterer, W.M.F. Fabian, S. Kunsági-Máté, Application of the quantum cluster equilibrium (qce) model for the liquid phase of primary alcohols using B3LYP and B3LYP-D DFT methods, J. Phys. Chem. B 115 (2011) 3936–3941.
[109] I. Akiyama, M. Ogawa, K. Takase, T. Takamuku, T. Yamaguchi, N. Ohtori, Liquid structure of 1-propanol by molecular dynamics simulation and X-ray scattering, J. Solut. Chem. 33 (2004) 797–809.
[110] M. Magini, G. Paschina, G. Piccaluga, On the structure of methyl alcohol at room temperature, J. Chem. Phys. 77 (1982) 2051–2056.
[111] A.H. Narten, S.I. Sandler, X-ray diffraction study of liquid tertiary butyl alcohol at 26°C, J. Chem. Phys. 71 (1979) 2069;
A.H. Narten, S.I. Sandler, T.A. Rensi, X-ray diffraction study of liquid neopentane and tertiary butyl alcohol, Faraday Discuss. Chem. Soc. 66 (1978) 39–47.
[112] A. Mikusinska-Planner, X-ray diffraction study of the structure of 1-propanol at −25°C, Acta Crystallogr. A33 (1977) 433–437.
[113] N.P. Franks, M.H. Abraham, W.R. Lieb, Molecular organization of liquid n-octanol: an X-ray diffraction analysis, J. Pharm. Sci. 82 (1993) 466–470.
[114] K.S. Vahvaselkä, R. Serimaa, M. Torkkeli, Determination of liquid structures of the primary alcohols methanol, ethanol, 1-propanol, 1-butanol and 1-octanol by X-ray scattering, J. Appl. Crystallogr. 28 (1995) 189–195.
[115] A.H. Narten, A. Habenschuss, Hydrogen bonding in liquid methanol and ethanol determined by X-ray diffraction, J. Chem. Phys. 80 (1984) 3387–3391.
[116] T. Fukasawa, T. Sato, Versatile application of indirect Fourier transformation to structure factor analysis: from X-ray diffraction of molecular liquids to small angle scattering of protein solutions, Phys. Chem. Chem. Phys. 13 (2011) 3187–3196.
[117] Y. Tanaka, N. Ohtomo, K. Arakawa, The structure of liquid alcohols by neutron and X-ray diffraction. III. Liquid structure of methanol, Bull. Chem. Soc. Jpn. 58 (1985) 270–276.
[118] T. Weitkamp, J. Neuefeind, H.E. Fischer, M.D. Zeidler, Hydrogen bonding in liquid methanol at ambient conditions and at high pressure, Mol. Phys. 98 (2000) 125–134.
[119] T. Yamaguchi, C.J. Benmore, A.K. Soper, The structure of subcritical and supercritical methanol by neutron diffraction, empirical potential structure refinement, and spherical harmonic analysis, J. Chem. Phys. 112 (2000) 8976–8987.
[120] D.G. Montague, I.P. Gibson, J.C. Dore, Structural studies of liquid alcohols by neutron diffraction I. Deuterated methyl alcohol CD_3OD, Mol. Phys. 44 (1981) 1355–1367;
D.G. Montague, J.C. Dore, S. Cummings, Structural studies of liquid alcohols by neutron diffraction III. CD_3OH, CD_3OD, and CD_3OH/D mixtures, Mol. Phys. 53 (1984) 1049–1066;
D.G. Montague, J.C. Dore, Structural studies of liquid alcohols by neutron diffraction IV. CD_3OH and CD_3OD at various temperatures, Mol. Phys. 57 (1986) 1035–1047.
[121] B. Tomberli, P.A. Egelstaff, C.J. Benmore, J. Neuefeind, Isotopic effects in the structure of liquid methanol: II. Experimental data in Fourier space, J. Phys.: Condens. Matter 13 (2001) 11421–11434.
[122] B. Tomberli, C.J. Benmore, P.A. Egelstaff, J. Neuefeind, V. Honkimäki, Temperature dependence of structural quantum effects in liquid methanol, Europhys. Lett. 55 (2001) 341–347.
[123] T. Yamaguchi, K. Hidaka, A.K. Soper, The structure of liquid methanol revisited: a neutron diffraction experiment at −80 °C and +25 °C, Mol. Phys. 96 (1999) 1159–1168;
T. Yamaguchi, K. Hidaka, A.K. Soper, The structure of liquid methanol revisited: a neutron diffraction experiment at −80 °C and +25 °C, Mol. Phys. 97 (1999) 603–605 (erratum).
[124] D.G. Montague, I.P. Gibson, J.C. Dore, Structural studies of liquid alcohols by neutron diffraction II. deuterated ethyl alcohol C_2D_5OD, Mol. Phys. 47 (1982) 1405–1416.
[125] I. Bakó, T. Radnai, M.C. Bellisent-Funel, Investigation of structure of liquid 2,2,2 trifluoroethanol: neutron diffraction, molecular dynamics, and ab initio quantum chemical study, J. Chem. Phys. 121 (2004) 12472.
[126] P. Zetterstrom, U. Dahlborg, R.G. Delaplane, W.S. Howells, Neutron diffraction studies of liquid iso-propanol, Phys. Scr. 44 (1991) 56–62.
[127] P. Zetterström, U. Dahlborg, W.S. Howells, A systematic study of the structure of liquid iso-propanol by time-of-flight neutron diffraction, Mol. Phys. 81 (1994) 1187–1204.
[128] A. Sahoo, S. Sarkar, V. Bhagat, R.N. Joarder, The probable molecular association in liquid d-1-propanol through neutron diffraction, J. Phys. Chem. A 113 (2009) 5160–5162.
[129] G.J. Cuello, C. Talón, F.J. Bermejo, C. Cabrillo, Chemical isomeric effects on propanol glassy structures, Appl. Phys. A 74 (2002) S552–S554.
[130] P. Sillrén, J. Swenson, J. Mattsson, D. Bowron, A. Matic, The temperature dependent structure of liquid 1-propanol as studied by neutron diffraction and epsr simulations, J. Chem. Phys. 138 (2013) 214501.

[131] P.P. Nath, S. Sarkar, P.S.R. Krishna, R.N. Joarder, Intermolecular structure of liquid D-*tert*-Butanol by neutron-diffraction data, Appl. Phys. A 74 (2002) S348–S351.
[132] D.T. Bowron, J.L. Finney, A.K. Soper, The structure of pure tertiary butanol, Mol. Phys. 93 (1998) 531–543;
D.T. Bowron, J.L. Finney, A.K. Soper, The structure of pure tertiary butanol, Mol. Phys. 94 (1998) 249–251 (erratum).
[133] A. Hédoux, Y. Guinet, L. Paccou, P. Derollez, F. Danède, Vibrational and structural properties of amorphous n-butanol: a complementary raman spectroscopy and X-ray diffraction study, J. Chem. Phys. 138 (2013) 214506.
[134] A.R. Abdel Hamid, R. Lefort, Y. Lechaux, A. Moréac, A. Ghoufi, C. Alba-Simionesco, D. Morineau, Solvation effects on self-association and segregation processes in tert-butanol-aprotic solvent binary mixtures, J. Phys. Chem. B 117 (2013) 10221–10230.
[135] A. Ghoufi, I. Hureau, R. Lefort, D. Morineau, Hydrogen-bond-induced supermolecular assemblies in a nanoconfined tertiary alcohol, J. Phys. Chem. C 115 (2011) 17761–17767.
[136] T. Pylkkänen, J. Lehtola, M. Hakala, A. Sakko, G. Monaco, S. Huotari, K. Hämäläinen, Universal signature of hydrogen bonding in the oxygen k-edge spectrum of alcohols, J. Phys. Chem. B 114 (2010) 13076–13083.
[137] Here one exploits the negative coherent scattering length of the proton.
[138] C.J. Benmore, B. Tomberli, J. Neuefeind, P.A. Egelstaff, Isotopic quantum correction to liquid methanol at −30°C, Appl. Phys. A 74 (2002) S1670–S1672.
[139] P. Zetterström, U. Dahlborg, A. Wannberg, Structural studies of liquid 2-bromopropane and 2-chloropropane by neutron diffraction, Mol. Phys. 83 (1994) 971–981.
[140] P.A. Artola, A. Raihane, C. Crauste-Thibierge, D. Merlet, M. Emo, C. Alba-Simionesco, B. Rousseau, Limit of miscibility and nanophase separation in associated mixtures, J. Phys. Chem. B 117 (2013) 9718–9727.
[141] S.R. Elliot, Origin of the first sharp diffraction peak in the structure factor of covalent glasses, Phys. Rev. Lett. 67 (1991) 711–714.
[142] M. Descamps, V. Legrand, Y. Cuinet, A. Amazzal, C. Alba, J. Dore, "Pre-peak" in the structure factor of simple molecular glass formers, Progr. Theoret. Phys. Suppl. 126 (1997) 207–212.
[143] D. Morineau, C. Alba-Simionesco, M.-C. Bellissent-Funel, M.-F. Lauthié, Experimental indication of structural heterogeneities in fragile hydrogen-bonded liquids, Europhys. Lett. 43 (1998) 195–200.
[144] D. Morineau, C. Alba-Simionesco, Hydrogen-bond-induced clustering in the fragile glass-forming liquid m-toluidine: Experiments and simulations, J. Chem. Phys. 109 (1998) 8494–8503.
[145] For glycerol a prepeak is detected by some studies R. Busselez, R. Lefort, A. Ghoufi, B. Beuneu, B. Frick, F. Affouard, D. Morineau, The non-Gaussian dynamics of glycerol, J. Phys.: Condens. Matter 23 (2011) 505102. but not by others;
see M. Soltwisch, B. Steffen, The X-ray structure factor of liquid glycerol, Z. Naturf. a 36 (1981) 1045–1051.
[146] D.R. Barker, M. Wilson, P.A. Madden, N.N. Medvedev, A. Geiger, Voids in the H-bonded network of water and their manifestation in the structure factor, Phys. Rev. E 62 (2000) 1427–1430. This article states that in liquid water the prepeak "position is determined by the nearest-neighbor separation of voids in the spatial distribution of oxygen atoms".
[147] See Fig. 13 in: A. Tölle, Neutron scattering studies of the model glass former ortho-terphenyl, Rep. Progr. Phys. 64 (2001) 1473–1532.
[148] M. Wind, R. Graf, S. Renker, H.W. Spiess, W. Steffen, Structure of amorphous poly-(ethylmethacrylate): A wide-angle X-ray scattering study, J. Chem. Phys. 122 (2005) 014906.
[149] S. Hiller, O. Pascui, H. Budde, O. Kabisch, D. Reichert, M. Beiner, Nanophase separation in side chain polymers: new evidence from structure and dynamics, New J. Phys. 6 (2004) 10–16. Fig. 6 shows data for n-butyl methacrylate for various degrees of polymerization P. Already for $P = 6$ a sizeable prepeak was found.
[150] I. Bakó, P. Jedlovszky, G. Pálinkás, Molecular clusters in liquid methanol: a reverse Monte Carlo study, J. Mol. Liq. 87 (2000) 243–254.
[151] A. Vrhovšek, O. Gereben, S. Pothoczki, M. Tomšič, A. Jamnik, S. Kohara, L. Pusztai, An approach towards understanding the structure of complex molecular systems: the case of lower aliphatic alcohols, J. Phys.: Condens. Matter 22 (2010) 404214.
[152] For a general introduction see, e.g. W. Schülke, Electron Dynamics by Inelastic X-ray Scattering, Oxford University Press, Oxford, 2007.
[153] Compton profiles are also accessible using deep inelastic scattering of epithermal neutrons, see C. Andreani, D. Colognesi, J. Mayers, G.F. Reiter, R. Senesi, Measurement of momentum distribution of light atoms and molecules in condensed matter systems using inelastic neutron scattering, Adv. Phys. 54 (2005) 377–469. We are not aware of corresponding experiments on monohydroxy alcohols.
[154] K.R. Wilson, M. Cavalleri, B.S. Rude, R.D. Schaller, T. Catalano, A. Nilsson, R.J. Saykally, L.G.M. Pettersson, X-ray absorption spectroscopy of liquid methanol microjets: bulk electronic structure and hydrogen bonding network, J. Phys. Chem. B 109 (2005) 10194–10203.
[155] Y. Tamenori, K. Okada, O. Takahashi, S. Arakawa, K. Tabayashi, A. Hiraya, T. Gejo, K. Honma, Hydrogen bonding in methanol clusters probed by inner-shell photoabsorption spectroscopy in the carbon and oxygen K-edge regions, J. Chem. Phys. 128 (2008) 124321.
[156] S. Kashtanov, A. Augustson, J.-E. Rubensson, J. Nordgren, H. Agren, J.-H. Guo, Y. Luo, Chemical and electronic structures of liquid methanol from X-ray emission spectroscopy and density functional theory, Phys. Rev. B 71 (2005) 104205.
[157] J.-H. Guo, Y. Luo, A. Augustsson, S. Kashtanov, J.-E. Rubensson, D. Shuh, H. Agren, J. Nordgren, Molecular structure of alcohol-water mixtures, Phys. Rev. Lett. 91 (2003) 157401.
[158] For a compilation of the energies of various X-ray absorption edges as a function of the atomic number, see, e.g., Fig. 2 of L.J.P. Ament, M. van Veenendaal, T.P. Devereaux, J.P. Hill, J. van den Brink, Resonant inelastic X-ray scattering studies of elementary excitations, Rev. Modern Phys. 83 (2011) 705–767.
[159] R.K. Pandey, S. Mukamel, Simulation of X-ray absorption near-edge spectra and X-ray fluorescence spectra of optically excited molecules, J. Chem. Phys. 124 (2006) 094106.
[160] N. Huse, H. Wen, D. Nordlund, E. Szilagyi, D. Daranciang, T.A. Miller, A. Nilsson, R.W. Schoenlein, A.M. Lindenberg, Probing the hydrogen-bond network of water via time-resolved soft X-ray spectroscopy, Phys. Chem. Chem. Phys. 11 (2009) 3951–3957.
[161] K. Kunnus, I. Rajkovic, S. Schreck, W. Quevedo, S. Eckert, M. Beye, E. Suljoti, C. Weniger, C. Kalus, S. Grübel, M. Scholz, D. Nordlund, W. Zhang, R.W. Hartsock, K.J. Gaffney, W.F. Schlotter, J.J. Turner, B. Kennedy, F. Hennies, S. Techert, P. Wernet, A. Föhlisch, A setup for resonant inelastic soft X-ray scattering on liquids at free electron laser light sources, Rev. Sci. Instrum. 83 (2012) 123109.
[162] M.J. Cooper, P.E. Mijnarends, N. Shiotani, N. Sakai, A. Bansil, X-ray Compton Scattering, Oxford University Press, New York, 2004.
[163] M. Hakala, K. Nygård, J. Vaara, M. Itou, Y. Sakurai, K. Hämäläinen, Charge localization in alcohol isomers studied by Compton scattering, J. Chem. Phys. 130 (2009) 034506.
[164] K. Nygård, M. Hakala, S. Manninen, M. Itou, Y. Sakurai, K. Hämäläinen, Configurational energetics in ice ih probed by compton scattering, Phys. Rev. Lett. 99 (2007) 197401.
[165] I. Juurinen, K. Nakahara, N. Ando, T. Nishiumi, H. Seta, N. Yoshida, T. Morinaga, M. Itou, T. Ninomiya, Y. Sakurai, E. Salonen, K. Nordlund, K. Hämäläinen, M. Hakala, Measurement of two solvation regimes in water ethanol mixtures using X-ray Compton scattering, Phys. Rev. Lett. 107 (2011) 197401.
[166] S.S.N. Murthy, The nature of glass transition process in alcohols, J. Mol. Liq. 40 (1989) 261–276.
[167] L.P. Singh, C. Alba-Simionesco, R. Richert, Dynamics of glass-forming liquids. XVII. Dielectric relaxation and intermolecular association in a series of isomeric octyl alcohols, J. Chem. Phys. 139 (2013) 144503.
[168] G. Sartor, K. Hofer, G.P. Johari, Structural relaxation and H bonding in isomeric octanols and their LiCl solutions by calorimetry, J. Phys. Chem. 100 (1996) 6801–6807.
[169] L.-M. Wang, Y. Tian, R. Liu, R. Richert, Calorimetric versus kinetic glass transitions in viscous monohydroxy alcohols, J. Chem. Phys. 128 (2008) 084503.
[170] I.M. Hodge, Enthalpy relaxation and recovery in amorphous materials, J. Non-Cryst. Solids 169 (1994) 211–266.
[171] S.S.N. Murthy, M. Tyagi, Experimental study of the high frequency relaxation process in monohydroxy alcohols, J. Chem. Phys. 117 (2002) 3837–3847.
[172] E. Tombari, C. Ferrari, G. Salvetti, G.P. Johari, Specific heat relaxation of an alcohol and implications for dielectric comparison, J. Chem. Phys. 130 (2009) 124505.

[173] M. Pyda, B. Wunderlich, Reversing and nonreversing heat capacity of poly(lactic acid) in the glass transition region by TMDSC, Macromolecules 38 (2005) 10472–10479.
[174] R. Richert, Reverse calorimetry of a supercooled liquid: Propylene carbonate, Thermochim. Acta 522 (2011) 28–35.
[175] B. Schiener, R. Böhmer, A. Loidl, R.V. Chamberlin, Nonresonant spectral hole burning in the slow dielectric response of supercooled liquids, Science 274 (1996) 752–754.
[176] B. Schiener, R.V. Chamberlin, G. Diezemann, R. Böhmer, Dielectric hole burning spectroscopy of supercooled liquids, J. Chem. Phys. 107 (1997) 7746–7761.
[177] K. Duvvuri, R. Richert, Dielectric hole burning in the high frequency wing of supercooled glycerol, J. Chem. Phys. 118 (2003) 1356–1363.
[178] R.V. Chamberlin, B. Schiener, R. Böhmer, Slow dielectric relaxation of supercooled liquids investigated by nonresonant spectral hole burning, Mat. Res. Soc. Symp. Proc. 455 (1997) 117–125.
[179] R. Richert, S. Weinstein, Nonlinear dielectric response and thermodynamic heterogeneity in liquids, Phys. Rev. Lett. 97 (2006) 095703.
[180] L.-M. Wang, R. Richert, Measuring the configurational heat capacity of liquids, Phys. Rev. Lett. 99 (2007) 185701.
[181] W. Huang, R. Richert, The physics of heating by time-dependent fields: Microwaves and water revisited, J. Phys. Chem. B 112 (2008) 9909–9913.
[182] R. Richert, Calorimetry based on energy absorbed from time-dependent fields, J. Non-Cryst. Solids 357 (2011) 726–730.
[183] W. Huang, R. Richert, Dynamics of glass-forming liquids. XIII. Microwave heating in slow motion, J. Chem. Phys. 130 (2009) 194509.
[184] H. Fröhlich, Theory of Dielectrics, second ed., Oxford University Press, Oxford, 1958.
[185] G.P. Johari, Effects of electric field on the entropy, viscosity, relaxation time, and glass-formation, J. Chem. Phys. 138 (2013) 154503.
[186] G. Adam, J.H. Gibbs, On the temperature dependence of cooperative relaxation properties in glass-forming liquids, J. Chem. Phys. 43 (1965) 139–146.
[187] M. Preuß, C. Gainaru, T. Hecksher, S. Bauer, J.C. Dyre, R. Richert, R. Böhmer, Experimental studies of Debye-like process and structural relaxation in mixtures of 2-ethyl-1-hexanol and 2-ethyl-1-hexyl bromide, J. Chem. Phys. 137 (2012) 144502.
[188] R. Böhmer, K.L. Ngai, C.A. Angell, D.J. Plazek, Non-exponential relaxations in strong and fragile glass formers, J. Chem. Phys. 99 (1993) 4201–4209.
[189] S.S.N. Murthy, Dielectric relaxation in monohydroxy alcohols and its connection to the glass transition process, J. Phys. Chem. 100 (1996) 8508–8517.
[190] G. Williams, The use of the dipole correlation function in dielectric relaxation, Chem. Rev. 72 (1972) 55–69.
[191] J.G. Kirkwood, The dielectric polarization of polar liquids, J. Chem. Phys. 7 (1939) 911–919.
[192] J. Jäckle, R. Richert, Why retardation takes more time than relaxation in a linear system, Phys. Rev. E 77 (2008) 031201.
[193] G. Williams, D.C. Watts, Non-symmetrical dielectric relaxation behaviour arising from a simple empirical decay function, Trans. Faraday Soc. 66 (1970) 80–85.
[194] C.P. Lindsey, G.D. Patterson, Detailed comparison of the Williams-Watts and Cole–Davidson functions, J. Chem. Phys. 73 (1980) 3348–3357.
[195] S. Havriliak, S. Negami, A complex plane representation of dielectric and mechanical relaxation processes in some polymers, Polymer 8 (1967) 161–210.
[196] C.J.F. Böttcher, P. Bordewijk, Theory of Electric Polarization, vol. 2, Elsevier, Amsterdam, 1978.
[197] R. Böhmer, Nanoscale heterogeneity in glass-forming liquids: Experimental advances, Curr. Opin. Solid State Mater. Sci. 3 (1998) 378–385.
[198] H. Sillescu, Heterogeneity at the glass transition: A review, J. Non-Cryst. Solids 243 (1999) 81–108.
[199] M.D. Ediger, Spatially heterogeneous dynamics in supercooled liquids, Annu. Rev. Phys. Chem. 51 (2000) 99–128.
[200] R. Richert, Heterogeneous dynamics in liquids: Fluctuations in space and time, J. Phys.: Condens. Matter 14 (2002) R703–R738.
[201] L. Berthier, G. Biroli, J.-P. Bouchaud, L. Cipelletti, in: W. van Saarloos (Ed.), Dynamical Heterogeneities in Glasses, Colloids, and Granular Media, Oxford University Press, Oxford, 2011.
[202] R. Böhmer, R.V. Chamberlin, G. Diezemann, B. Geil, A. Heuer, G. Hinze, S.C. Kuebler, R. Richert, B. Schiener, H. Sillescu, H.W. Spiess, U. Tracht, M. Wilhelm, Nature of the non-exponential primary relaxation in structural glass-formers probed by dynamically selective experiments, J. Non-Cryst. Solids 235–237 (1998) 1–9.
[203] A. Heuer, Information content of multitime correlation functions for the interpretation of structural relaxation in glass-forming systems, Phys. Rev. E 56 (1997) 730–740.
[204] J.E. Anderson, R. Ullman, Molecular relaxation in a fluctuating environment, J. Chem. Phys. 47 (1967) 2178–2184.
[205] L. Onsager, Electric moments of molecules in liquids, J. Am. Chem. Soc. 58 (1936) 1486–1493.
[206] G. Stell, G.N. Patey, J.S. Høye, Dielectric constants of fluid models: statistical mechanical theory and its quantitative implementation, Adv. Chem. Phys. 48 (1981) 183–328.
[207] D.V. Matyushov, Solvent reorganization energy of electron-transfer reactions in polar solvents, J. Chem. Phys. 120 (2004) 7532–7556.
[208] S.K. Garg, C.P. Smyth, Microwave absorption and molecular structure in liquids. LXII. The three dielectric dispersion regions of the normal primary alcohols, J. Phys. Chem. 69 (1965) 1294–1301.
[209] G. Power, G.P. Johari, J.K. Vij, Effects of ions on the dielectric permittivity and relaxation rate and the decoupling of ionic diffusion from dielectric relaxation in supercooled liquid and glassy 1-propanol, J. Chem. Phys. 116 (2002) 4192–4201.
[210] S. Schildmann, A. Reiser, R. Gainaru, C. Gainaru, R. Böhmer, Nuclear magnetic resonance and dielectric noise study of spectral densities and correlation functions in the glass forming monoalcohol 2-ethyl-1-hexanol, J. Chem. Phys. 135 (2011) 174511.
[211] J. Barthel, K. Bachhuber, R. Buchner, H. Hetzenhauer, Dielectric spectra of some common solvents in the microwave region. Water and lower alcohols, Chem. Phys. Lett. 165 (1990) 369–373.
[212] T. Sato, R. Buchner, Dielectric relaxation spectroscopy of 2-propanol-water mixtures, J. Chem. Phys. 118 (2003) 4606–4613.
[213] T. Sato, R. Buchner, The cooperative dynamics of the H-bond system in 2-propanol/water mixtures: Steric hindrance effects of nonpolar head group, J. Chem. Phys. 119 (2003) 10789–10800.
[214] G.P. Johari, M. Goldstein, Viscous liquids and the glass transition. II. Secondary relaxations in glasses of rigid molecules, J. Chem. Phys. 53 (1970) 2372–2388.
[215] Y. Gao, D. Bi, X. Li, R. Liu, Y. Tian, L.-M. Wang, Debye-type dielectric relaxation in glass-forming 3-methylthio-1-hexanol, J. Chem. Phys. 139 (2013) 024503.
[216] R. Richert, Dynamics of glass-Forming liquids. XIV. A search for ultra-slow dielectric relaxation in glycerol, J. Chem. Phys. 133 (2010) 074502.
[217] D.W. Davidson, Dielectric relaxation in liquids II. Isomeric pentanediols, Can. J. Chem. 39 (1961) 2139–2154.
[218] G. Fytas, Th. Dorfmüller, Depolarized light scattering studies of liquids: 1,5- and 2,4-pentanediol, J. Chem. Phys. 75 (1981) 5232–5238.
[219] G.P. Johari, O.E. Kalinovskaya, J.K. Vij, Effects of induced steric hindrance on the dielectric behavior and H bonding in the supercooled liquid and vitreous alcohol, J. Chem. Phys. 114 (2001) 4634–4642.
[220] S. Bauer, H. Wittkamp, S. Schildmann, M. Frey, W. Hiller, T. Hecksher, N.B. Olsen, C. Gainaru, R. Böhmer, Broadband dynamics in neat 4-methyl-3-heptanol and in mixtures with 2-ethyl-1-hexanol, J. Chem. Phys. 139 (2013) 134503.
[221] Y. Gao, W. Tu, Z. Chen, Y. Tian, R. Liu, L.-M. Wang, Dielectric relaxation of long-chain glass-forming monohydroxy alcohols, J. Chem. Phys. 139 (2013) 164504.
[222] S.P. Bierwirth, T. Büning, C. Gainaru, C. Sternemann, M. Tolan, R. Böhmer, Supramolecular x-ray signature of susceptibility enhancement in hydrogen-bonded liquids, Phys. Rev. E (submitted).
[223] W. Dannhauser, L.W. Bahe, R.Y. Lin, A.F. Flueckinger, Dielectric constant of hydrogen-bonded liquids. IV. Equilibrium and relaxation studies of homologous neoalcohols, J. Chem. Phys. 43 (1965) 257–266.
[224] U. Kaatze, R. Behrends, K. von Roden, Structural aspects in the dielectric properties of pentyl alcohols, J. Chem. Phys. 133 (2010) 094508.
[225] P. Petong, R. Pottel, U. Kaatze, Dielectric relaxation of H-bonded liquids. Mixtures of ethanol and n-hexanol at different compositions and temperatures, J. Phys. Chem. A 103 (1999) 6114–6121.
[226] P.C. Brot, Dispersion ultrahertzienne et liason hydrogene dans quelques alcohols, Ann. Phys. 2 (1957) 714–763.
[227] P. Debye, F. Bueche, Electric moments of polar polymers in relation to their structure, J. Chem. Phys. 19 (1951) 589–594.

[228] S. Bauer, K. Burlafinger, C. Gainaru, P. Lunkenheimer, W. Hiller, A. Loidl, R. Böhmer, Debye relaxation and 250 K anomaly in glass forming monohydroxy alcohols, J. Chem. Phys. 138 (2013) 094505.
[229] V.F. Petrenko, R.W. Whitworth, Physics of Ice, Oxford University Press, New York, 1999.
[230] G.P. Johari, W. Dannhauser, Effect of pressure on dielectric relaxation in isomeric octanols, J. Chem. Phys. 50 (1969) 1862–1876.
[231] S. Pawlus, M. Wikarek, C. Gainaru, M. Paluch, R. Böhmer, How do high pressures change the Debye process of 4-methyl-3-heptanol?, J. Chem. Phys. 139 (2013) 064501.
[232] F. Stickel, E.W. Fischer, R. Richert, Dynamics of glass-forming liquids. II. Detailed comparison of dielectric relaxation, dc-conductivity and viscosity data, J. Chem. Phys. 104 (1996) 2043–2055.
[233] H. Vogel, Das Temperaturabhängigkeitsgesetz der Viskosität von Flüssigkeiten, Phys. Z. 22 (1921) 645–646.
[234] G.S. Fulcher, Analysis of recent measurements of the viscosity of glasses, J. Am. Ceram. Soc. 8 (1925) 339–355.
[235] G. Tammann, W. Hesse, Die Abhängigkeit der Viskosität von der Temperatur bei unterkühlten Flüssigkeiten, Z. Anorg. Allg. Chem. 156 (1926) 245–257.
[236] Y. Takagi, T. Yano, M. Mikami, S. Kojima, Temperature dependence of depolarized spectra in *n*-propanol, Physica B 263–264 (1999) 306–309.
[237] A. Kudlik, C. Tschirwitz, S. Benkhof, T. Blochowicz, E. Rössler, Slow secondary relaxation process in supercooled liquids, Europhys. Lett. 40 (1997) 649–654.
[238] P. Sillrén, A. Matic, M. Karlsson, M. Koza, M. Maccarini, P. Fouquet, M. Götz, T. Bauer, R. Gulich, P. Lunkenheimer, A. Loidl, J. Mattson, C. Gainaru, E. Vynokur, S. Schildmann, S. Bauer, R. Böhmer, Liquid 1-propanol studied by neutron scattering, near-infrared, and dielectric spectroscopy, J. Chem. Phys. 140 (2014) 124501.
[239] W. Kauzmann, Dielectric relaxation as a chemical rate process, Rev. Mod. Phys. 14 (1942) 12–44.
[240] A. Reiser, G. Kasper, C. Gainaru, R. Böhmer, High-pressure dielectric scaling study of a monohydroxy alcohol, J. Chem. Phys. 132 (2010) 181101.
[241] S. Pawlus, M. Paluch, M. Dzida, Molecular dynamics changes induced by hydrostatic pressure in a supercooled primary alcohol, J. Phys. Chem. Lett. 1 (2010) 3249–3253.
[242] S. Pawlus, M. Paluch, M. Nagaraj, J.K. Vij, Effect of high hydrostatic pressure on the dielectric relaxation in a non-crystallizable monohydroxy alcohol in its supercooled liquid and glassy states, J. Chem. Phys. 135 (2011) 084507.
[243] C. Gainaru, M. Wikarek, S. Pawlus, M. Paluch, R. Figuli, M. Wilhelm, T. Hecksher, B. Jakobsen, J.C. Dyre, R. Böhmer, Oscillatory shear and high-pressure dielectric study of 5-methyl-3-heptanol, Colloid Polym. Sci. 292 (2014) 1913–1921.
[244] J. Malecki, Dielectric saturation in aliphatic alcohols, J. Chem. Phys. 36 (1962) 2144–2145.
[245] J. Malecki, Investigations of hexanol-1 multimers and complexes by the method of dielectric polarization in weak and strong electric fields, J. Chem. Phys. 43 (1965) 1351–1355.
[246] A. Piekara, Dielectric saturation and hydrogen bonding, J. Chem. Phys. 36 (1962) 2145–2150.
[247] J. Malecki, The relaxation of the nonlinear dielectric effect, J. Mol. Struct. 436–437 (1997) 595–604.
[248] W. Huang, R. Richert, Reverse dynamic calorimetry of a viscous ionic liquid, J. Chem. Phys. 131 (2009) 184501.
[249] S. Samanta, R. Richert, Limitations of heterogeneous models of liquid dynamics: Very slow rate exchange in the excess wing, J. Chem. Phys. 140 (2014) 054503.
[250] A. Khalife, U. Pathak, R. Richert, Heating liquid dielectrics by time dependent fields, Eur. Phys. J. B 83 (2011) 429–435.
[251] T. Bauer, M. Michl, P. Lunkenheimer, A. Loidl, Nonlinear dielectric response of Debye, α, and β relaxation in 1-propanol, J. Non-Cryst Solids (2014) http://dx.doi.org/10.1016/j.jnoncrysol.2014.07.024.
[252] B. Bagchi, A. Chandra, Collective orientational relaxation in dense dipolar liquids, Adv. Chem. Phys. 80 (1991) 1–126.
[253] I. Rips, J. Klafter, J. Jortner, Solvation dynamics in polar liquids, J. Chem. Phys. 89 (1988) 4288–4299.
[254] E.W. Castner, B. Bagchi, M. Maroncelli, S.P. Webb, A.J. Ruggiero, G.R. Fleming, The dynamics of polar solvation, Ber. Bunsenges. Phys. Chem. 92 (1988) 363–372.
[255] F. Barigelletti, Solvation dynamics in alcoholic solution in the temperature interval 90–190 K, J. Phys. Chem. 92 (1988) 3679–3682.
[256] M.-L. Horng, J.A. Gardecki, M. Maroncelli, Rotational dynamics of coumarin 153: Time-dependent friction, dielectric friction, and other nonhydrodynamic effects, J. Phys. Chem. A 101 (1997) 1030–1047.
[257] R. Richert, Triplet state solvation dynamics: Basics and applications, J. Chem. Phys. 113 (2000) 8404–8429.
[258] L.-M. Wang, R. Richert, Exponential probe rotation in glass-forming liquids, J. Chem. Phys. 120 (2004) 11082–11089.
[259] H. Wendt, R. Richert, Purely mechanical solvation dynamics in supercooled liquids: The $S_0 \leftarrow T_1$ (0-0) transition of naphthalene, J. Phys. Chem. A 102 (1998) 5775–5781.
[260] E.W. Castner, M. Maroncelli, Solvent dynamics derived from optical Kerr effect, dielectric dispersion, and time-resolved stokes shift measurements: an empirical comparison, J. Mol. Liq. 77 (1998) 1–36.
[261] M.S. Beevers, J. Crossley, D.C. Garrington, G. Williams, Consideration of dielectric relaxation and the Kerr-effect relaxation in relation to the reorientational motions of molecules, J. Chem. Soc. Faraday Trans. 2 72 (1976) 1482–1493.
[262] R.H. Cole, Correlation function theory for Kerr-effect relaxation of axially symmetric polar molecules, J. Phys. Chem. 86 (1982) 4700–4704.
[263] J. Emery, S. Gasse, R.A. Pethrick, D.W. Phillips, Ultrasonic studies of molecular relaxation in pure alcohols, Adv. Mol. Relax. Interact. Process. 12 (1978) 47–64.
[264] A. D'Aprano, I.D. Donato, G. D'Arrigo, D. Bertolini, M. Cassettari, G. Salvetti, Molecular association and dynamics in n-pentanol and 2-methyl-2-butanol, Mol. Phys. 55 (1985) 475–488.
[265] R. Kono, T.A. Litovitz, G.E. McDuffie, Comparison of dielectric and mechanical relaxation processes in glycerol *n*-propanol mixtures, J. Chem. Phys. 45 (1966) 1790–1796.
[266] P. Benassi, V. Mazzacurati, M. Nardone, G. Ruocco, G. Signorelli, Low frequency polarized and depolarized light scattering in H-bonded liquids: $CH_3(CH_2)_{n-1}OH$ ($n = 1, \ldots, 5$), J. Chem. Phys. 91 (1989) 6752–6757.
[267] M. Ahart, F. Jiang, M. Mikami, I.-S. Park, S. Kojima, Microscopic Brillouin scattering study of relaxation phenomena in low molecular weight alcohols of ethanol and methanol, Japan. J. Appl. Phys. 38 (1999) 3058–3061.
[268] E. Di Fabrizio, M. Nardone, A. Nucara, P. Gallo, G. Ruocco, Non-Lorentzian depolarized Raman line shapes in n-pentanol, J. Chem. Phys. 97 (1992) 6136–6143.
[269] S. Magazú, D. Majolino, F. Mallamace, P. Migliardo, F. Aliotta, C. Vasi, A. D'Aprano, D.I. Donato, Velocity and damping of thermal phonons in isomeric alcohols, Mol. Phys. 66 (1989) 819–829.
[270] F.J. Bermejo, R. Ramirez, J.L. Martinez, C. Prieto, F. Batallan, M. Garcia-Hernandez, Hypersonic relaxation in liquid methanol, J. Phys.: Condens. Matter 3 (1991) 569–576.
[271] J.-H. Ko, S. Kojima, Fast relaxation dynamics of monohydric alcohols revealed by Brillouin scattering, Japan. J. Appl. Phys. 41 (2002) 3206–3209.
[272] F.J. Bermejo, F. Batallan, E. Enciso, M. Garcia-Hernandez, J. Alonso, J.L. Martinez, Coherent inelastic neutron scattering response from liquid methanol, Europhys. Lett. 12 (1990) 129–134.
[273] J. Alonso, F.J. Bermejo, M. García-Hernández, J.L. Martínez, W.S. Howells, A. Criado, Collective excitations in liquid methanol: A comparison of molecular, lattice dynamics, and neutron scattering results, J. Chem. Phys. 96 (1992) 7696–7709.
[274] K. Yoshida, N. Yamamoto, S. Hosokawa, A.Q.R. Baron, T. Yamaguchi, Collective dynamics of sub- and supercritical methanol by inelastic X-ray scattering, Chem. Phys. Lett. 440 (2007) 210–214.
[275] D.B. Davies, A.J. Matheson, G.M. Glover, Viscoelastic behaviour of some viscous liquids, J. Chem. Soc., Faraday Trans. 2 69 (1973) 305–314. Data on 3-phenyl propanol are presented.
[276] C. Gainaru, R. Böhmer, Coupling of the electrical conductivity to the structural relaxation, absence of physical aging on the time scale of the Debye process, and number of correlated molecules in the supercooled monohydroxy alcohol 2-ethylhexanol, J. Non-Cryst. Solids 356 (2010) 542–546.
[277] G. Harrison, The Dynamic Properties of Supercooled Liquids, Academic Press, London, 1976.

[278] R. Behrends, U. Kaatze, Structural isomerization and molecular motions of liquid n-alkanes. Ultrasonic and high-frequency shear viscosity relaxation, J. Phys. Chem. A 104 (2000) 3269–3275.
[279] A low-frequency feature is absent not only for 1-dodecane but also for several other long-chain alkanes (with $\geq$14 carbon atoms) and for some alkane–alkane mixtures near room temperature. For an *n*-eicosane/*n*-tetradecane mixture an acoustical absorption spectrum was found that resembles the one depicted in Fig. 33(a) for 1-dodecanol [278]. It was argued that the two components of that mixture might display their own ultrasonic relaxation and hence this mixture could constitute a special case.
[280] Data for 1-hexanol are shown in: U. Kaatze, R. Behrends, Hydrogen bond fluctuations and dispersive interactions of alcohol/alkane mixtures. An ultrasonic relaxation study, Chem. Phys. Lett. 510 (2011) 67–72.
[281] M. Iwahashi, Y. Ohbu, T. Kato, Y. Suzuki, K. Yamauchi, Y. Yamaguchi, M. Muramatsu, The dynamical structure of normal alcohols in their liquids as determined by the viscosity and self-diffusion measurements, Bull. Chem. Soc. Jpn. 59 (1986) 3771–3774.
[282] For reviews, see A. Ciferri, Supramolecular Polymers, CRC Press, Boca Raton, FL, 2005;
T.F.A. De Greef, M.M.J. Smulders, M. Wolffs, A.P.H.J. Schenning, R.P. Sijbesma, E.W. Meijer, Supramolecular polymerization, Chem. Rev. 109 (2009) 5687–5754.
[283] S.J. George, A. Ajayaghosh, P. Jonkheijm, A.P.H.J. Schenning, E.W. Meijer, Coiled-coil gel nanostructures of oligo-(p-phenylenevinylene)s: gelation-induced helix transition in a higher-order supramolecular self-assembly of a rigid p-conjugated system, Angew. Chem. 116 (2004) 3504–3507.
[284] A. Ajayaghosh, R. Varghese, V.K. Praveen, S. Mahesh, Evolution of nano- to microsized spherical assemblies of a short oligo(p-phenyleneethynylene) into superstructured organogels, Angew. Chem. 118 (2006) 3339–3342.
[285] N. Lou, Y. Wang, X. Li, H. Li, P. Wang, C. Wesdemiotis, A.P. Sokolov, H. Xiong, Dielectric relaxation and rheological behavior of supramolecular polymeric liquid, Macromolecules 46 (2013) 3160.
[286] M.E. Cates, Reptation of living polymers — dynamics of entangled polymers in the presence of reversible chain-scission reactions, Macromolecules 20 (1987) 2289–2296.
[287] F. Tanaka, S.F. Edwards, Viscoelastic properties of physically cross-linked networks. Transient network theory, Macromolecules 25 (1992) 1516–1523.
[288] R. Granek, M.E. Cates, Stress relaxation in living polymers: Results from a Poisson renewal model, J. Chem. Phys. 96 (1992) 4758–4769.
[289] J.D. Ferry, Viscoelastic Properties of Polymers, Wiley, New York, 1980.
[290] C.M. Roland, Viscoelastic Behavior of Rubbery Materials, University Press, Oxford, 2011.
[291] P. Sassi, M. Paolantoni, A. Morresi, Trans-gauche isomerization in 1-octanol probed by Brillouin scattering spectroscopy, Chem. Phys. Lett. 357 (2002) 293–296.
[292] See, e.g. A.Y. Malkin, A.I. Isayev, Rheology: Concepts, Methods, & Applications, ChemTech Publishing, Toronto, 2006.
[293] G. Strobl, The Physics of Polymers: Concepts for Understanding their Structures and Behaviour, Springer Verlag, Berlin, 1997.
[294] This means that we put $G_\infty = G_{\infty,\mathrm{pol}} + G_{\infty,\alpha}$ which may be permitted within an additive approach, see Eq. 8.8.6 in [293].
[295] D.R. Wheeler, N.G. Fuller, R.L. Rowley, Non-equilibrium molecular dynamics simulation of the shear viscosity of liquid methanol: adaptation of the Ewald sum to Lees–Edwards boundary conditions, Mol. Phys. 92 (1997) 55–62.
[296] J. Petravic, J. Delhommelle, Hydrogen bonding in ethanol under shear, J. Chem. Phys. 122 (2005) 234509.
[297] R.W. Gray, G. Harrison, J. Lamb, Dynamic viscoelastic behaviour of low-molecular-mass polystyrene melts, Proc. R. Soc. Lond. Ser. A 356 (1977) 77–102.
[298] P. Debye, Dielectric properties of pure liquids, Chem. Rev. 19 (1936) 171–182.
[299] M. Maroncelli, The dynamics of solvation in polar liquids, J. Mol. Liq. 57 (1993) 1–37.
[300] R. Richert, F. Stickel, R.S. Fee, M. Maroncelli, Solvation dynamics and the dielectric response in a glass-forming solvent: From picoseconds to seconds, Chem. Phys. Lett. 229 (1994) 302–308.
[301] J.T. Fourkas, A. Benigno, M. Berg, Time-resolved nonpolar solvation dynamics in supercooled and low viscosity n-butylbenzene, J. Chem. Phys. 99 (1993) 8552–8558.
[302] J. Ma, D. Vanden Bout, M. Berg, Transient hole burning of s-tetrazine in propylene carbonate: a comparison of mechanical and dielectric theories of solvation, J. Chem. Phys. 103 (1995) 9146–9160.
[303] M. Berg, Viscoelastic continuum model of nonpolar solvation. 1. Implications for multiple time scales in liquid dynamics, J. Phys. Chem. A 102 (1998) 17–30.
[304] R. Palomar, G. Sesé, Microscopic dynamics of supercooled low weight alcohols, J. Chem. Phys. 133 (2010) 044501. Diffusion coefficients for methanol and ethanol are calculated.
[305] T. Kulschewski, J. Pleiss, A molecular dynamics study of liquid aliphatic alcohols: simulation of density and self-diffusion coefficient using a modified OPLS force field, Mol. Simul. 39 (2013) 754–767.
[306] K.E. Larsson, L. Queroz do Amaral, N. Ivanchev, S. Râpeanu, L. Bergstedt, U. Dahlborg, Proton motions in complex hydrogenous liquids. II. Results gained from some neutron-scattering experiments, Phys. Rev. 151 (1966) 126–132;
K.E. Larsson, Rotational and translational diffusion in complex liquids, Phys. Rev. 167 (1968) 171–182. In these articles it was found that some neutron data tend to overestimate the diffusion coefficient.
[307] F. Aliotta, M.C. Bellissent-Funel, D.I. Donato, P. Migliardo, C. Vasi, Incoherent quasi-elastic neutron scattering in isomeric alcohols, Physica B 180&181 (1990) 861–864.
[308] M.P. Jannelliy, S. Magazù, P. Migliardo, F. Aliotta, E. Tettamanti, Transport properties of liquid alcohols investigated by IQENS, NMR and DLS studies, J. Phys.: Condens. Matter 8 (1996) 8157–8171.
[309] R.E. Rathbun, A.L. Babb, Self-diffusion in liquids. III. Temperature dependence in pure liquids, J. Phys. Chem. 65 (1961) 1072–1074.
[310] J. Jonas, J.A. Akai, Transport processes in compressed liquid methanol, J. Chem. Phys. 66 (1977) 4946–4950.
[311] K.C. Pratt, W.A. Wakeham, Self-diffusion in water and monohydric alcohols, J. Chem. Soc., Faraday Trans. 2 73 (1977) 997–1002.
[312] M. Woznyj, F.X. Prielmeier, H.-D. Lüdemann, Pressure dependence of the melting and self diffusion in 2,2-dimethylpropane, 2,2-dimethylpropionitrile, and 2-methylpropanol-2, Z. Naturforsch. 39a (1984) 800–806.
[313] R.L. Hurle, A.J. Easteal, L.A. Woolf, Self-diffusion in monohydric alcohols under pressure. Methanol, methan(^{2}H)ol and ethanol, J. Chem. Soc., Faraday Trans. 1 81 (1985) 769–779.
[314] S. Meckl, M.D. Zeidler, Self-diffusion measurements of ethanol and propanol, Mol. Phys. 63 (1988) 85–95.
[315] N. Karger, T. Vardag, H.D. Lüdemann, Temperature dependence of self-diffusion in compressed monohydric alcohols, J. Chem. Phys. 93 (1990) 3437–3444.
[316] N. Shaker-Gaafar, N. Karger, S. Wappmann, H.D. Lüdemann, p,T-dependence of self-diffusion in liquid ethanol and the propanols, Ber. Bunsenges. Phys. Chem. 97 (1993) 805–811.
[317] N. Karger, S. Wappmann, N. Shaker-Gaafar, H.D. Lüdemann, The p,T-dependence of self diffusion in liquid 1-, 2- and 3-pentanol, J. Mol. Liq. 64 (1995) 211–219.
[318] U. Sülzner, G. Luft, Effect of hydrogen bonding on the viscosity of alcohols at high pressures, Int. J. Thermophys. 18 (1997) 1355–1367.
[319] M. Iwahashi, Y. Hayashi, N. Hachiya, H. Matsuzawa, H. Kobayashi, Self-association of octan-1-ol in the pure liquid state and in decane solutions as observed by viscosity, self-diffusion, nuclear magnetic resonance and near-infrared spectroscopy measurements, J. Chem. Soc. Faraday Trans. 89 (1993) 707–712.
[320] H. Weingärtner, Chapter 3. NMR studies of self-diffusion in liquids, Annu. Rep. Prog. Chem., Sect. C: Phys. Chem. 91 (1994) 37–69.
[321] D. Kivelson, Rotational dynamics of small and macromolecules, in: T. Dorfmüller, R. Pecora (Eds.), Lecture Notes in Physics, vol. 293, Springer, Berlin, 1987, pp. 1–14.
[322] J.T. Edward, Molecular volumes and the Stokes–Einstein equation, J. Chem. Educ. 47 (1970) 261.
[323] I. Chang, H. Sillescu, Heterogeneity at the glass transition: translational and rotational self-diffusion, J. Phys. Chem. B 101 (1997) 8794–8801.

[324] S.F. Swallen, M.K. Mapes, Y.S. Kim, R.J. McMahon, M.D. Ediger, S. Satija, Neutron reflectivity measurements of the translational motion of tris(naphthylbenzene) at the glass transition temperature, J. Chem. Phys. 124 (2006) 184501.
[325] E.W. Lang, H.-D. Lüdemann, Density dependence of rotational and translational molecular dynamics in liquids studied by high pressure NMR, Prog. Nucl. Magn. Reson. Spectrosc. 25 (1993) 507–633.
[326] J.F. Douglas, D. Leporini, Obstruction model of the fractional Stokes–Einstein relation in glass-forming liquids, J. Non-Cryst. Solids 235 (1998) 137–141.
[327] I. Chang, F. Fujara, B. Geil, G. Heuberger, T. Mangel, H. Sillescu, Translational and rotational motion in supercooled liquids studied by NMR and forced Rayleigh scattering, J. Non-Cryst. Solids 172–174 (1994) 248–255.
[328] S. Pawlus, S. Klotz, M. Paluch, Effect of compression on the relationship between viscosity and dielectric relaxation time in hydrogen-bonded primary alcohols, Phys. Rev. Lett. 110 (2013) 173004.
[329] M. Butsch, H. Sillescu, private communication, March 2006.
[330] F.X. Prielmeier, E.W. Lang, R.J. Speedy, H.-D. Lüdemann, The pressure dependence of self diffusion in supercooled light and heavy water, Ber. Bunsenges. Phys. Chem. 92 (1988) 1111–1117.
[331] W. Weber, Über die Druckabhängigkeit der Viskosität von Alkohol-Wasser-Gemischen, Rheol. Acta 14 (1975) 1012–1025;
A. Anson, R. Garriga, S. Martinez, P. Perez, M. Gracia, Densities and viscosities of binary mixtures of 1-bromobutane with butanol isomers at several temperatures, J. Chem. Eng. Data 50 (2005) 1478–1483.
[332] R. Livingston, H. Zeldes, Paramagnetic resonance study of liquids during photolysis: hydrogen peroxide and alcohols, J. Chem. Phys. 44 (1966) 1245–1259;
D.J. Morantz, R.C. Thompson, Observation of structural effects in liquid and solid alcohols near their solidification temperatures using electron spin resonance, J. Phys. C: Solid State Phys. 3 (1970) 1335–1342.
[333] J.T. Arnold, S.S. Dharmatti, M.E. Packard, Chemical effects on nuclear induction signals from organic compounds, J. Chem. Phys. 19 (1951) 507;
J.T. Arnold, M.E. Packard, Variations in absolute chemical shift of nuclear induction signals of hydroxyl groups of methyl and ethyl alcohol, J. Chem. Phys. 19 (1951) 1608–1609.
[334] D. Gerritzen, H.H. Limbach, Kinetic and equilibrium isotope effects of proton exchange and autoprotolysis of pure methanol studied by dynamic NMR spectroscopy, Ber. Bunsenges. Phys. Chem. 85 (1981) 527–535.
[335] The reference frequency ν_{ref} is here chosen to be that of the methyl group. Otherwise the resonance line of trimethylsilane is typically chosen as a standard.
[336] A.L. Van Geet, Anal. Chem. 42 (1970) 679–680.
[337] M. Hoffmann, M.S. Conradi, Are there hydrogen bonds in supercritical methanol and ethanol?, J. Phys. Chem. B 102 (1998) 263–271.
[338] E. Bich, U. Hensen, M. Michalik, D. Wandschneider, A. Heintz, ^{1}H-NMR spectroscopic and thermodynamic studies of hydrogen bonding in liquid n-butanol + cyclohexane, tert-butanol + cyclohexane, and n-butanol + pyridine mixtures, Phys. Chem. Chem. Phys. 4 (2002) 5827–5832.
[339] J. Barthel, R. Buchner, High frequency permittivity and its use in the investigation of solution properties, Pure & Appl. Chem. 63 (1991) 1473–1482.
[340] J.M. Lopez del Amo, U. Langer, V. Torres, M. Pietrzak, G. Buntkowsky, H.-M. Vieth, M.F. Shibl, O. Kühn, M. Bröring, H.-H. Limbach, Isotope and phase effects on the proton tautomerism in polycrystalline porphycene revealed by NMR, J. Phys. Chem. A 113 (2009) 2193–2206.
[341] M. Huelsekopf, R. Ludwig, Hydrogen bonding in a sterically hindered alcohol, J. Mol. Liq. (2002) 163–171.
[342] M. Huelsekopf, R. Ludwig, Temperature dependence of hydrogen bonding in alcohols, J. Mol. Liq. 85 (2000) 105–125.
[343] R. Ludwig, The structure of liquid methanol, ChemPhysChem 6 (2005) 1369–1375.
[344] R. Ludwig, F. Weinhold, T.C. Farrar, Quantum cluster equilibrium theory of liquids: temperature dependent chemical shifts, quadrupole coupling constants and vibrational frequencies in liquid ethanol, Mol. Phys. 97 (1999) 479–486.
[345] P. Zarzycki, J.R. Rustad, Theoretical determination of the NMR spectrum of liquid ethanol, J. Phys. Chem. A 113 (2009) 291–297.
[346] S. Nagatomo, M. Nobuhira, Y. Yamamura, M. Sumita, K. Saito, Identification of hydrogen-bonded oligomers in associating liquid by ^{1}H-NMR: 1-phenyl-1-cyclohexanol, Bull. Chem. Soc. Jpn. 86 (2013) 569–576.
[347] For additional information on ^{17}O chemical shifts see T. Sugawara, Y. Kawada, H. Iwamura, Oxygen-17 NMR chemical shifts of alcohols, ethers and esters, Chem. Lett. (1978) 1371;
M. Takasuka, Relationship of the ^{17}O chemical shift to the stretching frequency of the hydroxy-group in saturated alcohols, J. Chem. Soc., Perkin Trans. 2 (1981) 1558–1561.
[348] H.Y. Sun, J.W. Bozzelli, Structures, intramolecular rotation barriers, and thermochemical properties: ethanol, monoethanols, dichloroethanols, and corresponding radicals derived from H atom loss, J. Phys. Chem. A 105 (2001) 9543–9552.
[349] H.W. Spiess, Rotation of Molecules and Nuclear Spin Relaxation, in: P. Diehl, E. Fluck, H. Günther, R. Kosfeld, J. Seelig (Eds.), NMR Basic Principles and Progress, vol. 15, Springer, Heidelberg, 1978, pp. 55–214.
[350] D.E. Woessner, Spin relaxation processes in a two-proton system undergoing anisotropic reorientation, J. Chem. Phys. 36 (1962) 1–4;
D.E. Woessner, Nuclear magnetic dipole–dipole relaxation in molecules with internal motion, J. Chem. Phys. 42 (1965) 1855–1859.
[351] P.A. Beckmann, Spectral densities and nuclear spin relaxation in solids, Phys. Rep. 171 (1988) 85–128.
[352] B. Blicharska, H.G. Hertz, H. Versmold, Nuclear magnetic relaxation in the presence of intramolecular rotations, J. Magn. Reson. 33 (1979) 531–540.
[353] R. Ludwig, D.S. Gill, M.D. Zeidler, Molecular reorientation in liquid methanol, Z. Naturforsch. 46a (1991) 89–94.
[354] R. Ludwig, Ch. Rusbüldt, Ph.A. Bopp, M.D. Zeidler, The anisotropy of the molecular reorientational motions in liquid methanol, Z. Naturforsch. 50a (1995) 211–216.
[355] M. Pöschl, H.G. Hertz, Intramolecular thermal motions in liquid *n*-propanol (+ glycerol), a proton magnetic relaxation study, J. Phys. Chem. 98 (1994) 8195–8208.
[356] M. Pöschl, G. Althoff, S. Killie, E. Wenning, H.G. Hertz, Investigation of complex intramolecular motion in supercooled liquids, Ber. Bunsenges. Phys. Chem. 95 (1991) 1084–1091.
[357] H.G. Hertz, The problem of intramolecular rotation in liquids and nuclear magnetic relaxation, Prog. Nucl. Magn. Reson. Spectrosc. 16 (1983) 115–162.
[358] M.S. Ansari, H.G. Hertz, An NMR investigation of internal molecular motion in liquid ethanol, Z. Physik. Chemie NF 140 (1984) 71–105.
[359] T. Frech, H.G. Hertz, Rotational, internal rotational and translational motion of liquid i-propanol, Ber. Bunsenges. Phys. Chem. 89 (1985) 948–958.
[360] See Ref. [45] and also R. Ludwig, M.D. Zeidler, NMR relaxation in ethanol and propanol and in their binary mixtures with carbon-tetrachloride, Mol. Phys. 82 (1994) 313–323.
[361] T. Blochowicz, A. Kudlik, S. Benkhof, J. Senker, E. Rössler, G. Hinze, The spectral density in simple organic glass formers — comparison of dielectric and spin-lattice relaxation, J. Chem. Phys. 110 (1999) 12011–12022.
[362] D. Kruk, A. Herrmann, E.A. Rössler, Field-cycling NMR relaxometry of viscous liquids and polymers, Prog. Nucl. Mag. Reson. Spectrosc. 63 (2012) 33–64.
[363] A useful relationship was recently given in H. Nelson, A. Ihrig, R. Kahlau, P. Kibies, S.M. Kast, R. Böhmer, Deuteron magnetic resonance and dielectric studies of guest reorientation and water dynamics in six clathrate hydrates containing ring-type guests, J. Non-Cryst. Solids (2014) http://dx.doi.org/10.1016/j.jnoncrysol.2014.08.059.
[364] K. Hu, Y. Zhou, J. Shen, Z. Ji, G. Cheng, Microheterogeneous structure of 1-octanol in neat and water-saturated state, J. Phys. Chem. B 111 (2007) 10160–10165.
[365] K. Schmidt-Rohr, H.W. Spiess, Multidimensional Solid State NMR and Polymers, Academic, London, 1994.
[366] R. Böhmer, G. Diezemann, G. Hinze, E. Rössler, Dynamics of supercooled liquids and glassy solids, Prog. Nucl. Mag. Reson. Spectrosc. 39 (2001) 191–267.
[367] K. Schmidt-Rohr, H.W. Spiess, Nature of nonexponential loss of correlation above the glass transition investigated by multidimensional NMR, Phys. Rev. Lett. 66 (1991) 3020–3023.

[368] S.S.N. Murthy, J. Sobhanadri, Gangasharan, The origin of β-relaxation in organic glasses, J. Chem. Phys. 100 (1994) 4601–4606.
[369] T. El Goresy, R. Böhmer, Diluting the hydrogen bonds in mixtures of n-butanol with n-bromobutane: A dielectric study, J. Chem. Phys. 128 (2008) 154520.
[370] S. Bauer, K. Moch, P. Münzner, S. Schildmann, C. Gainaru, R. Böhmer, Mixed Debye-type liquids studied by dielectric, shear mechanical, nuclear magnetic resonance, and near-infrared spectroscopy, J. Non-Cryst. Solids (2014) http://dx.doi.org/10.1016/j.jnoncrysol.2014.07.018.
[371] S. Schildmann, Aufklärung der molekularen Dynamik in glasbildenden Monoalkoholen mithilfe der Kernspinresonanz-Spektroskopie, Dissertation, Dortmund, 2012.
[372] For a general overview, see, e.g., Infrared and Raman Spectroscopy, B. Schrader (Ed.), VCH, Weinheim, 1995.
[373] M. Sokolova, S.J. Barlow, G.V. Bondarenko, Y.E. Gorbaty, M. Poliakoff, Comparison between IR absorption and raman scattering spectra of liquid and supercritical 1-butanol, J. Phys. Chem. A 110 (2006) 3882–3885.
[374] J.H.van der Mass, E.T.G. Lutz, Structural information from OH stretching frequencies monohydric saturated alcohols, Spectrochim. Acta 206 (1974) 2006–2019;
E.T.G. Lutz, J.H. van der Mass, The sensorial potentials of the OH stretching mode, J. Mol. Struct 436-437 (1997) 213–231;
F.A.J. Singelenberg, E.T.G. Lutz, J.H. van der Maas, Structural information from the integrated intensity of the OH-stretching band of saturated alcohols, Appl. Spectrosc. 40 (1986) 1093–1098.
[375] U. Buck, F. Huisken, Infrared spectroscopy of size-selected water and methanol clusters, Chem. Rev. 100 (2000) 3863–3890.
[376] M.A. Suhm, Hydrogen bond dynamics in alcohol clusters, Adv. Chem. Phys. 142 (2009) 1–57.
[377] M.A. Czarnecki, Two-dimensional correlation analysis of hydrogen-bonded systems: basic molecules, Appl. Spectrosc. Rev. 46 (2011) 67–103.
[378] U. Liddel, E.D. Becker, Infrared spectroscopic studies of hydrogen bonding in methanol, ethanol and t-butanol, Spectrochim. Acta 10 (1957) 70–84.
[379] G.W. Pimentel, A.C. McClellan, The Hydrogen Bond, Freeman, San Francisco, 1960.
[380] M. Falk, E. Whalley, Infrared spectra of methanol and deuterated methanols in gas, liquid, and solid phases, J. Chem. Phys. 34 (1961) 1554–1568.
[381] W.A.P. Luck, M. Fritzsche, The OH stretching mode and a 3 species model of liquid methanol, Z. Phys. Chem. 191 (1995) 71–86.
[382] X. Wu, Y. Chen, T. Yamaguchi, Hydrogen bonding in methanol studied by infrared spectroscopy, J. Mol. Spectrosc. 246 (2007) 187–191.
[383] C. Mello, T. Mello, E. Sevéri, L. Coelho, D. Ribeiro, A. Marangoni, R.J. Poppi, I. Noda, Microstructures formation in a seemingly ideal homogeneous mixture of ethanol and methanol: An experimental evidence and two-dimensional correlation spectroscopy approach, J. Chem. Phys. 131 (2009) 084501.
[384] J.E. Bertie, S.L. Zhang, Infrared intensities of liquids XXI: Integrated absorption intensities of CH_3OH, CH_3OD, CD_3OH and CD_3OD and dipole moment derivatives of methanol, J. Mol. Struct. 413 (1997) 333–363.
[385] J.-J. Max, C. Chapados, Infrared spectroscopy of methanol-hexane liquid mixtures. II. The strength of hydrogen bonding, J. Chem. Phys. 130 (2009) 124513.
[386] K. Lin, X. Zhou, Y. Luo, S. Liu, The microscopic structure of liquid methanol from raman spectroscopy, J. Phys. Chem. B 114 (2010) 3567–3573.
[387] A. Arencibia, M. Taravillo, F.J. Pérez, J. Núñez, V.G. Baonza, Effect of pressure on hydrogen bonding in liquid methanol, Phys. Rev. Lett. 89 (2002) 195504.
[388] K. Lin, N. Hu, X. Zhou, S. Liu, Y. Luo, Reorientation dynamics in liquid alcohols from Raman spectroscopy, J. Raman Spectrosc. 43 (2012) 82–88.
[389] J.D. Weibel, C.F. Jackels, R.L. Swofford, Experimental and ab initio investigation of the O–H overtone vibration in ethanol, J. Chem. Phys. 117 (2002) 4245–4254. The experimental data refer to the gas phase.
[390] P. Lalanne, J.M. Andanson, J.-C. Soetens, T. Tassaing, Y. Danten, M. Besnard, Hydrogen bonding in supercritical ethanol assessed by infrared and Raman spectroscopies, J. Phys. Chem. A 108 (2004) 3902–3909.
[391] N. Michniewicz, M.A. Czarnecki, J.P. Hawranek, Near-infrared spectroscopic study of liquid propanols, J. Mol. Struct. 844–845 (2007) 181–185.
[392] J.P. Hawranek, N. Michniewicz, W. Wrzeszcz, M. Pajdowska, Infrared dispersion of liquid 1-propanol, J. Non-Cryst. Solids 353 (2007) 4555–4559.
[393] M.A. Czarnecki, H. Maeda, Y. Ozaki, M. Suzuki, M. Iwahashi, Resolution enhancement and band assignments for the first overtone of oh stretching modes of butanols by two-dimensional near-infrared correlation spectroscopy. 2. Thermal dynamics of hydrogen bonding in n- and tert-butyl alcohol in the pure liquid states, J. Phys. Chem. A 102 (1998) 9117–9123.
[394] M.A. Czarnecki, B. Czarnik-Matusewicz, Y. Ozaki, M. Iwahashi, Resolution enhancement and band assignments for the first overtone of OH(D) stretching modes of butanols by two-dimensional near-infrared correlation spectroscopy. 3. Thermal dynamics of hydrogen bonding in butan-1-(ol-d) and 2-methylpropan-2-(ol-d) in the pure liquid states, J. Phys. Chem. A 104 (2000) 4906–4911.
[395] M.A. Czarnecki, D. Wojtków, K. Haufa, Rotational isomerism of butanols: Infrared, near-infrared and DFT study, Chem. Phys. Lett. 431 (2006) 294–299.
[396] S.J. Barlow, G.V. Bondarenko, Y.E. Gorbaty, T. Yamaguchi, M. Poliakoff, An IR study of hydrogen bonding in liquid and supercritical alcohols, J. Phys. Chem. A 106 (2002) 10452–10460.
[397] P. Sassi, F. Palombo, R.S. Cataliotti, M. Paolantoni, A. Morresi, Distributions of H-bonding aggregates in tert-butyl alcohol: The pure liquid and its alkane mixtures, J. Phys. Chem. A 111 (2007) 6020–6027.
[398] F. Palombo, M. Paolantoni, P. Sassi, A. Morresi, R.S. Cataliotti, Spectroscopic studies of the "free" OH stretching bands in liquid alcohols, J. Mol. Liq. 125 (2006) 139–146.
[399] J.-M. Andanson, J.-C. Soetens, T. Tassaing, M. Besnard, Hydrogen bonding in supercritical tert-butanol assessed by vibrational spectroscopies and molecular-dynamics simulations, J. Chem. Phys. 122 (2005) 174512.
[400] M.A. Czarnecki, Two-dimensional correlation analysis of the second overtone of the ν(OH) mode of octan-I-ol in the pure liquid phase, Appl. Spectrosc. 54 (2000) 1767–1770.
[401] M.A. Czarnecki, Near-infrared spectroscopic study of hydrogen bonding in chiral and racemic octan-2-ol, J. Phys. Chem. A 107 (2003) 1941–1944.
[402] M.A. Czarnecki, K. Orzechowski, Effect of temperature and concentration on self-association of octan-3-ol studied by vibrational spectroscopy and dielectric measurements, J. Phys. Chem. A 107 (2003) 1119–1126.
[403] M. Paolantoni, P. Sassi, A. Morresi, R.S. Cataliotti, Raman noncoincidence effect on OH stretching profiles in liquid alcohols, J. Raman Spectrosc. 37 (2006) 528–537.
[404] M.A. Czarnecki, Study on self-association of octanols by two-dimensional FT-NIR correlation spectroscopy, Vib. Spectrosc. 36 (2004) 237–239.
[405] M. Paolantoni, P. Sassi, A. Morresi, R.S. Cataliotti, Infrared study of 1-octanol liquid structure, Chem. Phys. 310 (2005) 169–178.
[406] F. Palombo, P. Sassi, M. Paolantoni, A. Morresi, R.S. Cataliotti, Comparison of hydrogen bonding in 1-octanol and 2-octanol as probed by spectroscopic techniques, J. Phys. Chem. B 110 (2006) 18017–18025.
[407] P. Bordewijk, F. Gransch, C.J.F. Böttcher, Static dielectric constant, infra-red spectrum, and NMR spectrum of straight-chain heptanols, Trans. Faraday Soc. 66 (1970) 293–299.
[408] A. D'Aprano, D.I. Donato, P. Migliardo, F. Aliotta, C. Vasi, Temperature effects on the structure and dynamics of isomeric pentanols by IR and Raman spectroscopy, Phys. Chem. Liq. 17 (1988) 279–296.
[409] L. Stordrange, A.A. Christy, O.M. Kvalheim, H. Shen, Y. Liang, Study of the self-association of alcohols by near-infrared spectroscopy and multivariate 2d techniques, J. Phys. Chem. A 106 (2002) 8543–8553.
[410] M.A. Czarnecki, Y. Ozaki, The temperature-induced changes in hydrogen bonding of decan-1-ol in the pure liquid phase studied by two-dimensional Fourier transform near-infrared correlation spectroscopy, Phys. Chem. Chem. Phys. 1 (1999) 797–800.
[411] R. Iwamoto, T. Matsuda, Characterization of infrared and near-infrared absorptions of free alcoholic OH groups in hydrocarbon, Appl. Spectrosc. 58 (2004) 1001–1009.
[412] K. Ohno, H. Yoshida, H. Watanabe, T. Fujita, H. Matsuura, Conformational study of 1-butanol by the combined use of vibrational spectroscopy and ab initio molecular orbital calculations, J. Phys. Chem. 98 (1994) 6924–6930.
[413] R. Chelli, S. Ciabatti, G. Cardini, R. Righini, P. Procacci, Calculation of optical spectra in liquid methanol using molecular dynamics and the chemical potential equalization method, J. Chem. Phys. 111 (1999) 4218–4229.

[414] W.O. George, T. Has, M. Fokhray Hossain, B.F. Jones, R. Lewis, Hydrogen-bonded forms of ethanol — IR spectra and ab initio computations, J. Chem. Soc., Faraday Trans. 94 (1998) 2701–2708.
[415] A. Miani, V. Hanninen, M. Horn, L. Halonen, Anharmonic force field for methanol, Mol. Phys. 98 (2000) 1737–1748.
[416] V. Hänninen, L. Halonen, Calculation of spectroscopic parameters and vibrational overtones of methanol, Mol. Phys. 101 (2003) 2907–2916.
[417] A.K. Sum, S.I. Sandler, Ab initio calculations of cooperativity effects on clusters of methanol, ethanol, 1-propanol, and methanethiol, J. Phys. Chem. A 104 (2000) 1121–1129.
[418] K. Ohno, T. Shimoaka, N. Akai, Y. Katsumoto, Relationship between the broad oh stretching band of methanol and hydrogen-bonding patterns in the liquid phase, J. Phys. Chem. A 112 (2008) 7342–7348.
[419] E.E. Fileti, S. Canuto, Calculated infrared spectra of hydrogen-bonded methanol–water, water–methanol, and methanol–methanol complexes, Int. J. Quantum Chem. 104 (2005) 808–815.
[420] D. Wandschneider, M. Michalik, A. Heintz, Spectroscopic and thermodynamic studies of liquid n-butanol + n-hexane and +cyclohexane mixtures based on quantum mechanical ab initio calculations of n-butanol clusters, J. Mol. Liq. 125 (2006) 2–13.
[421] R. Zheng, Y. Sun, Q. Shi, Theoretical study of the infrared and Raman line shapes of liquid methanol, Phys. Chem. Chem. Phys. 13 (2011) 2027–2035.
[422] A. Kivinen, J. Murto, J. Korppi-Tommola, R. Kuopio, Fluoroalcohols, part 15. a near-infrared study of the self-association of trifluoro and hexafluoro substituted tertiary butyl alcohols. a model for the structures of alcohol associates, Acta Chem. Scand. 26 (1972) 904–922.
[423] R. Bicca de Alencastro, C. Sandorfy, A low temperature infrared study of self-association in thiols, Can. J. Chem. 50 (1972) 3594–3600.
[424] S. Woutersen, U. Emmerichs, H.J. Bakker, A femtosecond midinfrared pump–probe study of hydrogen-bonding in ethanol, J. Chem. Phys. 107 (1997) 1483–1490.
[425] H. Graener, T.Q. Ye, A. Laubereau, Ultrafast dynamics of hydrogen bonds directly observed by time resolved infrared spectroscopy, J. Chem. Phys. 90 (1988) 3413.
[426] Sometimes branched bonds are designated as ε species, see, e.g. K. Kwac, E. Geva, A mixed quantum–classical molecular dynamics study of the hydroxyl stretch in methanol/carbon tetrachloride mixtures III: nonequilibrium hydrogen-bond dynamics and infrared pump–probe spectra, J. Phys. Chem. B 117 (2013) 7737–7749.
[427] J.B. Asbury, T. Steinel, C. Stromberg, K.J. Gaffney, I.R. Piletic, M.D. Fayer, Hydrogen bond breaking probed with multidimensional stimulated vibrational echo correlation spectroscopy, J. Chem. Phys. 119 (2003) 12981–12997.
[428] In addition, a Fermi resonance arising from the mixing of the OD stretching vibration with a combination band of the methyl rocking and the valence angle deformation vibration [413] shows up near 2440 cm^{-1}. Such a resonance is not observed for protonated methanol.
[429] See, e.g. C.A. Angell, V. Rodgers, Near-infrared spectra and the disrupted network model of normal and supercooled water, J. Phys. Chem. 80 (1984) 6245–6252;
W.A.P. Luck, Caloric properties of liquid alcohols—H-bonded liquids continuum or spectroscopic determined mixture model, is that really the question, J. Mol. Liq. 32 (1986) 41–51;
P.L. Geissler, Temperature dependence of inhomogeneous broadening: On the meaning of isosbestic points, J. Am. Chem. Soc. 127 (2005) 14930–14935.
[430] G.E. Walrafen, Effects of equilibrium H-bond distance and angle changes on Raman intensities from water, J. Chem. Phys. 120 (2004) 4868–4876.
[431] W.A.P. Luck, The importance of cooperativity for the properties of liquid water, J. Mol. Struct. 448 (1998) 131–142.
[432] L.G. Weyer, S.-C. Lo, Spectra-Structure Correlations in the Near-infrared, in: J.M. Chalmers (Ed.), Sample Characterization Data, in: Handbook of vibrational spectroscopy, vol. 3, Wiley, Weinheim, 2002, pp. 1817–1837.
[433] I. Noda, Y. Ozaki, Two-dimensional Correlation Spectroscopy: Applications in Vibrational and Optical Spectroscopy, Wiley, Weinheim, 2004.
[434] C. Sandorfy, Anharmonicity and hydrogen bonding, in: P. Schuster, G. Zundel, C. Sandorfy (Eds.), The Hydrogen Bond, vol. 2, North-Holland, Amsterdam, 1976, pp. 613–654.
[435] B. Czarnik-Matusewicz, S. Pilorz, L. Ashton, E.W. Blanch, Potential pitfalls concerning visualization of the 2D results, J. Mol. Struct. 799 (2006) 253–258.
[436] X. Wang, G.S. Huang, J.R. Wu, Y.J. Nie, X.J. He, K.W. Xiang, Molecular motions in glass–rubber transition region in polyisobutylene investigated by two-dimensional correlation dielectric relaxation spectroscopy, Appl. Phys. Lett. 99 (2011) 121902.
[437] X.B. Wu, H.G. Wang, Z.G. Zhu, C.S. Liu, Quantifying changes in the low-frequency dynamics of amorphous polymers by 2d correlation mechanical spectroscopy, J. Phys. Chem. B 117 (2013) 467–472.
[438] S. Bauer et al. (unpublished work).
[439] J.D. Worley, I.M. Klotz, Near-infrared spectra of H_2O–D_2O solutions, J. Chem. Phys. 45 (1966) 2868–2871.
[440] A. Barkatt, C.A. Angell, Optical probe studies of relaxation processes in viscous liquids, J. Chem. Phys. 70 (1979) 901–911.
[441] P. Papadopoulos, W. Kossack, F. Kremer, Intra- and inter-molecular dynamics in glass-forming liquids, Soft Matter 9 (2013) 1600–1603.
[442] A. Barkatt, C.A. Angell, Use of structural probe ions for relaxation studies in glasses. 2. Temperature-jump and temperature-ramp studies of cobalt(II) in nitrate glasses, J. Phys. Chem. 82 (1978) 1972–1979.
[443] L.-M. Martinez, C.A. Angell, Chemical order lifetimes in liquids, and a second fictive temperature for glassformers, Physica A 314 (2002) 548–559.
[444] R. Böhmer, E. Sanchez, C.A. Angell, AC technique for simultaneous study of local and global linear responses near the glass transition: The case of doped $Ca^{2+}/K^{+}/NO_3^{-}$, J. Phys. Chem. 96 (1992) 9089–9092.
[445] S.V. Shilov, M. Müller, D. Krüerke, G. Heppke, H. Skupin, F. Kremer, Molecular arrangements and reorientation behavior in a dibenzopyrene-derivative ferroelectric columnar liquid crystal as studied by time-resolved Fourier-transform IR spectroscopy, Phys. Rev. E 65 (2002) 021707.
[446] L. Bokobza, Origin of Near-Infrared Absorption Bands, in: H.W. Siesler, Y. Ozaki, S. Kawata, H.M. Heise (Eds.), Near-Infrared Spectroscopy: Principles, Instruments, Applications, Wiley, Weinheim, 2002, pp. 11–41.
[447] W.A.P. Luck, T. Wess, Semiclassical model calculations of weak, strong, and short O–H · · · OH-bonds, Can. J. Chem. 69 (1991) 1819–1826.
[448] W. Groh, Overtone absorption in macromolecules for polymer optical fibers, Makromol. Chem. 189 (1988) 2861–2874.
[449] C. Bourdéron, C. Sandorfy, Association and the assignment of the OH overtones in hydrogen bonded alcohols, J. Chem. Phys. 59 (1973) 2527–2536.
[450] M. Asselin, C. Sandorfy, A low temperature study of self-associated alcohols in the near-infrared, J. Mol. Struct. 8 (1971) 145–158.
[451] S. Woutersen, Simultaneous photon absorption as a probe of molecular interaction and hydrogen bond cooperativity in liquids, J. Chem. Phys. 127 (2007) 154517.
[452] It should be noted that anharmonicity effects would lead to a negative frequency shift and can therefore not explain these effects.
[453] R.F. Lake, H.W. Thompson, Far infrared studies of hydrogen bonding in alcohols, Proc. R. Soc. Lond. Ser. A 291 (1966) 469–477.
[454] J.K. Vij, F. Hufnagel, Advances in microwave and submillimeter-wave dielectric spectroscopic techniques and their applications, Adv. Chem. Phys. 63 (1985) 775–837.
[455] Y. Yomogida, Y. Sato, K. Yamakawa, R. Nozaki, T. Mishina, J. Nakahara, Comparative dielectric study of pentanol isomers with terahertz time-domain spectroscopy, J. Mol. Struct. 970 (2010) 171–176.
[456] J.K. Vij, C.J. Reid, Submillimetre laser and interferometric spectroscopy of the alkyl alcohols, Chem. Phys. Lett. 92 (1982) 528–532.
[457] J.K. Vij, C.J. Reid, M.W. Evans, Molecular dynamics of methanol: Far infra-red laser spectroscopy, interferometry and computer simulation, Mol. Phys. 50 (1983) 935–947.
[458] Y. Yomogida, Y. Sato, R. Nozaki, T. Mishina, J. Nakahara, Dielectric study of normal alcohols with THz time-domain spectroscopy, J. Mol. Liq. 154 (2010) 31–35.
[459] Y. Yomogida, Y. Sato, R. Nozaki, T. Mishina, J. Nakahara, Comparative dielectric study of monohydric alcohols with terahertz time-domain spectroscopy, J. Mol. Struct. 981 (2010) 173–178.
[460] Y. Yomogida, Y. Sato, R. Nozaki, T. Mishina, J. Nakahara, Comparative study of boson peak in normal and secondary alcohols with terahertz time-domain spectroscopy, Physica B 405 (2010) 2208–2212.
[461] J.T. Kindt, C.A. Schmuttenmaer, Far-infrared dielectric properties of polar liquids probed by femtosecond terahertz pulse spectroscopy, J. Phys. Chem. 100 (1996) 10373–10379.

[462] K.N. Woods, H. Wiedemann, The influence of chain dynamics on the far-infrared spectrum of liquid methanol, J. Chem. Phys. 123 (2005) 134506.
[463] K.N. Woods, H. Wiedemann, The influence of chain dynamics on the far-infrared spectrum of liquid methanol-water mixtures, J. Chem. Phys. 123 (2005) 134507.
[464] T. Fukasawa, T. Sato, J. Watanabe, Y. Hama, W. Kunz, R. Buchner, Relation between dielectric and low-frequency Raman spectra of hydrogen-bond liquids, Phys. Rev. Lett. 95 (2005) 197802.
[465] U. Møller, D.G. Cooke, K. Tanaka, P.U. Jepsen, Terahertz reflection spectroscopy of Debye relaxation in polar liquids, J. Opt. Soc. Amer. B Opt. Phys. 26 (2009) A113–A125.
[466] C.A. Schmuttenmaer, Exploring dynamics in the far-infrared with terahertz spectroscopy, Chem. Rev. 104 (2004) 1759–1779.
[467] M.A. Ramos, S. Vieira, F.J. Bermejo, J. Dawidowski, H.E. Fisher, H. Schober, M.A. González, C.K. Loong, D.L. Price, Quantitative assessment of the effects of orientational and positional disorder on glassy dynamics, Phys. Rev. Lett. 78 (1997) 82–85.
[468] O. Yamamuro, K. Harabe, T. Matsuo, K. Takeda, I. Tsukushi, T. Kanaya, Boson peaks of glassy mono- and polyalcohols studied by inelastic neutron scattering, J. Phys.: Condens. Matter. 12 (2000) 5143–5154;
O. Yamamuro, K. Takeda, I. Tsukushi, T. Matsuo, Boson peaks in hydrogen-bonded molecular glasses, Physica B 311 (2002) 84–89.
[469] F.J. Bermejo, J. Alonso, A. Criado, F.J. Mompeán, J.L. Martínez, Low-frequency excitations in a molecular glass: Single-particle dynamics, Phys. Rev. B 46 (1992) 6173–6186. This article deals with methanol.
[470] I. Natkaniec, K. Holderna-Natkaniec, I. Majerz, K. Parlinski, Neutron spectroscopy of deuterated substitutes and DFT modeling vibrational spectra of methanol clusters, Chem. Phys. 317 (2005) 171–177.
[471] N.V. Surovtsev, S.V. Adichtchev, J. Wiedersich, V.N. Novikov, E.A. Rössler, Fast relaxation in the structural glass and glassy crystal of ethanol and cyano cyclohexane: A quasielastic light scattering study, J. Chem. Phys. 119 (2003) 12399–12408.
[472] P. Sassi, M. Paolantoni, S. Perticaroli, F. Palombo, A. Morresi, A study of collective motions in liquid tert-butanol from low-wavenumber Raman scattering, J. Raman Spectrosc. 40 (2009) 1278–1283.
[473] N.J. Harrison, B.R. Jennings, Optical Kerr-effect measurement for a series of alcohols, J. Appl. Phys. 73 (1993) 8076–8080. This work does not explicitly focus on dynamics aspects. The results can be compared with those in Z. Błaszczak, M. Farhoud, Optical Kerr effect in a series of n-alcohols. J. Chem. Soc., Faraday Trans. 90 (1994) 2455-2457. The anisotropy of the index of refraction of several monohydroxy alcohols was also given by P. Ho, R.R. Alfano, Optical Kerr effect in liquids, Phys. Rev. A 20 (1979) 2170–2187.
[474] M. Cho, M. Du, N.F. Scherer, G.R. Fleming, S. Mukamel, Off-resonant transient birefringence in liquids, J. Chem. Phys. 99 (1993) 2410–2428.
[475] H. Shirota, K. Yoshihara, N.A. Smith, S. Lin, S.R. Meech, Deuterium isotope effects on ultrafast polarisability anisotropy relaxation in methanol, Chem. Phys. Lett. 281 (1997) 27–34.
[476] C.J. Fecko, J.D. Eaves, A. Tokmakoff, Isotropic and anisotropic Raman scattering from molecular liquids measured by spatially masked optical Kerr effect spectroscopy, J. Chem. Phys. 117 (2002) 1139–1154.
[477] In Ref. [476] also the isotropic OKE response of methanol was measured and discussed. The isotropic OKE signal stems from interaction induced effects and provides information on relative orientations between molecules and on distances between (i.e., on density–density fluctuations).
[478] G. Diezemann, R. Böhmer, G. Hinze, H. Sillescu, Reorientational dynamics in simple supercooled liquids, J. Non-Cryst. Solids 235–237 (1998) 121–127.
[479] M.L. Senent, Y.G. Smeyers, R. Dominguez-Gómez, M. Villa, Ab initio determination of the far infrared spectra of some isotopic varieties of ethanol, J. Chem. Phys. 112 (2000) 5809–5819.
[480] G.P. Johari, Molecular inertial effects in liquids: Poley absorption, collision-induced absorption, low-frequency Raman spectrum and boson peaks, J. Non-Cryst. Solids 307–310 (2002) 114–127.
[481] U. Stumper, Dielectric absorption of liquid normal alkanes in the microwave and far infrared regions, Adv. Mol. Relax. Process. 7 (1975) 189–208.
[482] J.P. Laib, D.M. Mittleman, Temperature-dependent terahertz spectroscopy of liquid n-alkanes, Infrared Milli. Terahz. Waves 31 (2010) 1015–1021.
[483] J. Zheng, K. Kwak, M.D. Fayer, Ultrafast 2D IR vibrational echo spectroscopy, Acc. Chem. Res. 40 (2007) 75–83.
[484] M. Cho, Coherent two-dimensional optical spectroscopy, Chem. Rev. 108 (2008) 1331–1418.
[485] P. Hamm, M. Zanni, Concepts and Methods of 2D Infrared Spectroscopy, University Press, Cambridge, 2011.
[486] E.T.J. Nibbering, T. Elsaesser, Ultrafast vibrational dynamics of hydrogen bonds in the condensed phase, Chem. Rev. 104 (2004) 1887–1914. See in particular their Chapter 6.4 on hydrogen bond cleavage.
[487] D. Li, F. Yang, C. Han, J. Zhao, J. Wang, Correlated high-frequency molecular motions in neat liquid probed with ultrafast overtone two-dimensional infrared spectroscopy, J. Phys. Chem. Lett. 3 (2012) 3665–3670.
[488] M.A.F.H. van den Broek, H.K. Nienhuys, H.J. Bakker, Vibrational dynamics of the C–O stretch vibration in alcohols, J. Chem. Phys. 114 (2001) 3182–3186.
[489] R. Laenen, C. Rauscher, K. Simeonidis, Transient spectral hole burning and hydrogen-bond breaking determined in different solutions of ethanol in deuterated ethanol, J. Chem. Phys. 110 (1999) 5814–5820.
[490] R. Laenen, C. Rauscher, Time-resolved infrared spectroscopy of ethanol monomers in liquid solution: molecular reorientation and energy relaxation times, Chem. Phys. Lett. 274 (1997) 63–70.
[491] R. Laenen, K. Simeonidis, Energy relaxation and reorientation of the OH mode of simple alcohol molecules in different solvents monitored by transient IR spectroscopy, Chem. Phys. Lett. 299 (1999) 589–596.
[492] R. Laenen, K. Simeonidis, R. Ludwig, Investigation of an H-bonded dimer: Calculations of bonding structures and temperature dependence of the librational substructure of the OH-stretching band, J. Chem. Phys. 111 (1999) 5897–5904.
[493] A.J. Lock, S. Woutersen, H.J. Bakker, Ultrafast energy equilibration in hydrogen-bonded liquids, J. Phys. Chem. A 105 (2001) 1238–1243.
[494] K.J. Gaffney, I.R. Piletic, M.D. Fayer, Hydrogen bond breaking and reformation in alcohol oligomers following vibrational relaxation of a non-hydrogen-bond donating hydroxyl stretch, J. Phys. Chem. A 106 (2002) 9428–9435.
[495] R. Laenen, C. Rauscher, A structural model for associated liquid ethanol developed from transient spectroscopy, J. Chem. Phys. 107 (1997) 9759–9763.
[496] S.-H. Shim, M.T. Zanni, How to turn your pump–probe instrument into a multidimensional spectrometer: 2D IR and vis spectroscopies via pulse shaping, Phys. Chem. Chem. Phys. 11 (2009) 748–761.
[497] J.B. Asbury, T. Steinel, C. Stromberg, K.J. Gaffney, I.R. Piletic, A. Goun, M.D. Fayer, Ultrafast heterodyne detected infrared multidimensional vibrational stimulated echo studies of hydrogen bond dynamics, Chem. Phys. Lett. 374 (2003) 362–371.
[498] J.B. Asbury, T. Steinel, M.D. Fayer, Vibrational echo correlation spectroscopy probes of hydrogen bond dynamics in water and methanol, J. Lumine. 107 (2004) 271–286.
[499] M.D. Fayer, Watching Ultrafast Molecular Motions with 2D IR Chemical Exchange Spectroscopy, World Scientific, Bangalore, 2011.
[500] V.K. Yadav, A. Karmakar, J.R. Choudhuri, A. Chandra, A first principles molecular dynamics study of vibrational spectral diffusion and hydrogen bond dynamics in liquid methanol, Chem. Phys. 408 (2012) 36–42.
[501] R. Jiang, E.L. Sibert, How do hydrogen bonds break in small alcohol oligomers?, J. Phys. Chem. A 113 (2009) 7275–7285.
[502] A. Loidl, R. Böhmer, Glass transitions and relaxation phenomena in orientational glasses and supercooled plastic crystals, in: R. Richert, A. Blumen (Eds.), Disorder Effects on Relaxational Processes, Springer, Berlin, 1994, pp. 659–696.
[503] The slowest δ relaxation mode is due to rotational fluctuations of the molecule around its short axis. See the references also to pending theoretical work as cited in F. Kremer, A. Schönhals, Molecular and Collective Dynamics of (Polymeric) Liquid Crystals, in: F. Kremer, A. Schönhals (Eds.), Broadband Dielectric Spectroscopy, Springer, Berlin, 2002, pp. 385–432. In analogy to the monohydroxy alcohols, for the δ mode no calorimetric signature could be detected so far, see A.R. Brás, M. Dionísio, H. Huth, C. Schick, A. Schönhals, Origin of glassy dynamics in a liquid crystal studied by broadband dielectric and specific heat spectroscopy, Phys. Rev. E 75 (2007) 061708.
[504] A.C. Legon, The halogen bond: an interim perspective, Phys. Chem. Chem. Phys. 12 (2010) 7736–7747.
[505] P. Politzer, J.S. Murray, T. Clark, Halogen bonding: an electrostatically-driven highly directional noncovalent interaction, Phys. Chem. Chem. Phys. 12 (2010) 7748–7757.

[506] L.-M. Wang, Y. Tian, R. Liu, K.L. Ngai, Anomalous component dynamics of a binary mixture of associating glass-forming liquids, J. Phys. Chem. B 115 (2011) 719–724.
[507] H.-J. Kwon, T.H. Kim, J.-H. Ko, Y.-H. Hwang, Relaxation phenomena in supercooled liquid and glassy acetaminophen studied by dielectric, photon correlation and Brillouin light scattering spectroscopies, Chem. Phys. Lett. 556 (2013) 117–121.
[508] A.R. Brás, J.P. Noronha, A.M.M. Antunes, M.M. Cardoso, A. Schönhals, F. Affouard, M. Dionísio, N.T. Correia, Molecular motions in amorphous ibuprofen as studied by broadband dielectric spectroscopy, J. Phys. Chem. B 112 (2008) 11087–11099.
[509] K. Adrjanowicz, K. Kaminski, M. Dulski, P. Wlodarczyk, G. Bartkowiak, L. Popenda, S. Jurga, J. Kujawski, J. Kruk, M.K. Bernard, M. Paluch, Synperiplanar to antiperiplanar conformation changes as underlying the mechanism of Debye process in supercooled ibuprofen, J. Chem. Phys. 139 (2013) 111103.
[510] F. Affouard, N.T. Correia, Debye Process in ibuprofen glass forming liquid: Insights from MD simulations, J. Phys. Chem. B 114 (2010) 11397–11402.
[511] S. Bauer, M. Storek, H. Zimmermann, R. Böhmer, Dynamics in supercooled, amorphous, and crystalline ibuprofen studied using deuteron magnetic resonance, rheology, and near infrared spectroscopy, J. Chem. Phys. (2014) submitted for publication.
[512] R.-Y. Lin, W. Dannhauser, Dielectric constant of hydrogen-bonded liquids. II. N-monosubstituted acetamides, J. Phys. Chem. 67 (1963) 1805–1810.
[513] S.J. Bass, W.I. Nathan, R.M. Meighan, R.H. Cole, Dielectric properties of alkyl amides. II. Liquid dielectric constant and loss, J. Phys. Chem. 68 (1964) 509–515.
[514] W. Dannhauser, G.P. Johari, Intermolecular association and dielectric relaxation in some liquid amides, Can. J. Chem. 46 (1968) 3143–3149.
[515] J. Barthel, R. Buchner, B. Wurm, The dynamics of liquid formamide, N-methylformamide, N,N-dimethylformamide, and N,N-dimethylacetamide. A dielectric relaxation study, J. Mol. Liq. 98-99 (2002) 51–69.
[516] L.-M. Wang, R. Richert, Identification of dielectric and structural relaxations in glass-forming secondary amides, J. Chem. Phys. 123 (2005) 054516.
[517] C.G. Seipelt, M.D. Zeidler, Correlation times and quadrupole coupling constants in liquid N-methylformamide and N-methylacetamide, Ber. Bunsenges. Phys. Chem. 101 (1997) 1501–1508.
[518] T.W. Whitfield, G.J. Martyna, S. Allison, S.P. Bates, H. Vass, J. Crain, Structure and hydrogen bonding in neat *N*-methylacetamide: classical molecular dynamics and Raman spectroscopy studies of a liquid of peptidic fragments, J. Phys. Chem. B 110 (2006) 3624–3637.
[519] W.A. Herrebout, K. Clou, H.O. Desseyn, Vibrational spectroscopy of N-methylacetamide revisited, J. Phys. Chem. A 105 (2001) 4865–4881.
[520] M.T. Zanni, M.C. Asplund, R.M. Hochstrasser, Two-dimensional heterodyned and stimulated infrared photon echoes of N-methylacetamide-D, J. Chem. Phys. 114 (2001) 4579–4590.
[521] D.A. Turtona, K. Wynne, Structural relaxation in the hydrogen-bonding liquids *N*-methylacetamide and water studied by optical Kerr effect spectroscopy, J. Chem. Phys. 128 (2008) 154516.
[522] S. Trabelsi, F. Hammami, S. Nasr, M.-C. Bellissent-Funel, Neutron and X-ray scattering experiments on fully deuterated liquid N-methylacetamide $CD_3CONDCD_3$ at various temperatures and under pressure, J. Mol. Struct. 891 (2008) 388–395.
[523] R. Ludwig, O. Reis, R. Winter, F. Weinhold, T.C. Farrar, Quantum cluster equilibrium theory of liquids: Temperature dependence of hydrogen bonding in liquid *N*-methyl-acetamide studied by IR spectra, J. Phys. Chem. B 102 (1998) 9312–9318.
[524] M. Huelsekopf, R. Ludwig, Correlations between structural, NMR and IR spectroscopic properties of *N*-methylacetamide, Magn. Reson. Chem 39 (2001) S127–S134.
[525] L. Chen, T. Groß, H.-D. Lüdemann, T, p-dependence of self-diffusion in the lower N-methylsubstituted amides, Z. Phys. Chem. 214 (2000) 239–251.
[526] R.G. Wassink, P. Bordewijk, Dielectric relaxation of some amides in carbon tetrachloride, Adv. Mol. Relax. Interact. Proc. 13 (1978) 299–308.
[527] Y. Wang, P.J. Griffin, A. Holt, F. Fan, A.P. Sokolov, Observation of the slow, Debye-like relaxation in hydrogen-bonded liquids by dynamic light scattering, J. Chem. Phys. 140 (2014) 104510.
[528] P.J. Griffin, A.P. Holt, Y. Wang, V.N. Novikov, J.R. Sangoro, F. Kremer, A.P. Sokolov, Interplay between hydrophobic aggregation and charge transport in the ionic liquid methyltrioctylammonium Bis(trifluoromethylsulfonyl)imide, J. Phys. Chem. B 118 (2014) 783–790.
[529] Similar trends were also inferred from investigation for water in comparisons with other hydrogen bonded substances such as, e.g., oligomeric and polymeric propylene glycols, see, e.g. J. Mattsson, R. Bergman, P. Jacobsson, L. Börjesson, Effects of hydrogen bonding on supercooled liquid dynamics and the implications for supercooled water, Phys. Rev. B 79 (2009) 174205.
[530] See Fig. 3 in S. Schwerdtfeger, F. Köhler, R. Pottel, U. Kaatze, Dielectric relaxation of hydrogen bonded liquids: mixtures of monohydric alcohols with n-alkanes, J. Chem. Phys. 115 (2001) 4186–4194.
[531] See Table 4 in D.P. Fernández, A.R.W. Goodwin, E.W. Lemon, J.M.H. Levelt Sengers, R.C. Williams, A formulation for the static permittivity of water and steam at pressures up to 1200 MPa, including derivatives and Debye–Hückel coefficients, J. Phys. Chem. Ref. Data 26 (1997) 1125–1166.
[532] T. Sato, R. Buchner, Dielectric relaxation processes in ethanol/water mixtures, J. Phys. Chem. A 108 (2004) 5007–5015.
[533] Incidentally, the simplest liquid involves short lived hydrogen-bonded zig-zag chains is HF, see, e.g U. Röthlisberger, M. Parrinello, Ab initio molecular dynamics simulation of liquid hydrogen fluoride, J. Chem. Phys. 106 (1997) 4658–4664;
F. Fernandez-Alonso, F.J. Bermejo, S.E. McLain, J.F.C. Turner, J.J. Molaison, K.W. Herwig, Observation of fractional Stokes–Einstein behavior in the simplest hydrogen-bonded liquid, Phys. Rev. Lett. 98 (2007) 077801.
[534] See, e.g. R. Buchner, J. Barthel, J. Stauber, The dielectric relaxation of water between 0 °C and 35 °C, Chem. Phys. Lett. 306 (1999) 57–63.
[535] O. Conde, J. Teixeira, Hydrogen-bond dynamics in water studied by depolarized rayleigh-scattering, J. Physique 44 (1983) 525–529.
[536] T. Steinel, J.B. Asbury, J. Zheng, M.D. Fayer, Watching hydrogen bonds break, J. Phys. Chem. A 108 (2004) 10957–10964.
[537] H.F.M.C. Martiniano, N. Galamba, Insights on hydrogen-bond lifetimes in liquid and supercooled water, J. Phys. Chem. B 117 (2013) 16188–16195.
[538] M.N. Rodnikova, A new approach to the mechanism of solvophobic interactions, J. Mol. Liq. 136 (2007) 211–213.
[539] W.M. Slie, A.R. Donfor, Jr, T.A. Litovitz, Ultrasonic shear and longitudinal measurements in aqueous glycerol, J. Chem. Phys. 44 (1966) 3712–3718.
[540] C.A. Angell, Supercooled water, Annu. Rev. Phys. Chem. 34 (1983) 593–630.
[541] T. Head-Gordon, M.E. Johnson, Tetrahedral structure or chains for liquid water, Proc. Natl. Acad. Sci. 103 (2006) 7973–7977.
[542] T.D. Kühne, R.Z. Khaliullin, Electronic signature of the instantaneous asymmetry in the first coordination shell of liquid water, Nature Commun. 4 (2013) 1450–1456.
[543] A.H. Narten, H.A. Levy, Liquid water: molecular correlation functions from X-ray diffraction, J. Chem. Phys. 55 (1971) 2263–2269.
[544] For a study in this direction, see G. Power, J.K. Vij, G.P. Johari, Relaxations and nano-phase-separation in ultraviscous heptanol-alkyl halide mixture, J. Chem. Phys. 126 (2007) 034512.